Evolution of competing populations in time-varying environments

Matthew William Asker

Submitted in accordance with the requirements for the degree of

Doctor of Philosophy

University of Leeds

School of Mathematics

July 2025

For my grandparents.

Intellectual Property Statement

I confirm that the work submitted is my own, except where work which has formed part of jointly authored publications has been included. My contribution and the other authors to this work has been explicitly indicated below. I confirm that appropriate credit has been given within the thesis where reference has been made to the work of others.

Contents of Chapters 3, 4, and 5 appear in jointly authored publications:

Hernández-Navarro Ll., **Asker M.**, Rucklidge A. M. and Mobilia M.,
Coupled environmental and demographic fluctuations shape the evolution of cooperative antimicrobial resistance,
J. R. Soc. Interface, **20**, 20230393 (2023).

All authors contributed to the writing of the manuscript and discussion of the results. My specific contributions were: formal analysis (supporting), investigation, software, validation, writing - review and editing (supporting).

Asker M., Hernández-Navarro Ll., A. M. Rucklidge, and Mobilia M.,
Coexistence of Competing Microbial Strains under Twofold Environmental Variability and Demographic Fluctuations,
New J. Phys., **25**, 123010 (2023).

All authors contributed to the writing of the manuscript. My specific contributions were: conceptualisation (supporting), methodology, formal analysis (lead), data curation, software, writing - original draft, writing - review & editing, visualisation, investigation, validation.

Hernández-Navarro Ll., **Asker M.**, and Mobilia M.,
Eco-evolutionary dynamics of cooperative antimicrobial resistance in a population of fluctuating volume and size,
J. Phys. A: Math. Theor., **57**, 265003 (2024).

All authors contributed to the writing of the manuscript and discussion of the results. My specific contributions were: formal analysis, software, writing - original draft, writing - review & editing, visualisation, investigation, validation.

Asker M., Swailem M., Täuber U. C., & Mobilia M.,
Fixation and extinction in time-fluctuating spatially structured metapopulations,
arXiv:2504.08433 (2025). Under review.

All authors contributed to the writing of the manuscript. My specific contributions were: conceptualisation (supporting), formal analysis, data curation, investigation, methodology, software, validation, visualisation, writing - original draft, writing - review & editing.

Contributor roles taxonomy by CRediT (Brand et al., 2015).

Acknowledgements

I would first and foremost like to thank my supervisor, Mauro Mobilia, for his invaluable guidance, steadfast pragmatism, and for embodying a *Doktorvater* in every sense of the word. I am grateful to Alastair Rucklidge and Uwe Täuber for their crucial advice and support throughout my studies, helping me to see the wood for the trees. I would also like to thank Lluís, Kenny, and Swailem for being excellent collaborators and even better friends – our meetings were a source of ideas and respite in equal measure. To everyone in the Mathematics Satellite PGR office – and especially Matt, Lucas, Laura, Marcus, Rob, Matthew, and Adam – thank you for making the days fly by.

I am deeply indebted to my parents, whose unwavering support formed the foundations that have allowed me to pursue this path. To my grandparents, for their unconditional love, a source of strength at every stage of my life. To my siblings, for their absurd belief in me – so absolute it borders on foolish – and for reminding me not to take myself too seriously. To Neha, for her relentless encouragement, endless kindness, and for being the ultimate rubber duck. And finally, to my friends, for the laughter, the pints, the well-timed distractions, and the quiet support that made these years so enjoyable.

Abstract

Populations evolve subject to the conditions of their environment, which vary in time. Changes in the environment directly impact the evolution of the population, making an understanding of population evolution under environmental variability crucial to uncovering the evolutionary dynamics of natural populations. This thesis investigates the effect of the coupling between ecological dynamics, driven by varying environmental conditions, and population evolution. In particular, it considers the combined effect of demographic fluctuations (randomness caused by stochastic births and deaths in a finite population) and environmental variability on four models of competition in two-species microbial populations. These models are inspired by real-world issues such as antimicrobial resistance evolution and the establishment of unwanted mutants in healthy populations. In a constant environment, the behaviour in each model is understood and, in the motivating contexts considered, often leads to undesirable evolutionary outcomes. However, these dynamics change dramatically upon the introduction of environmental variability. The majority of this thesis focuses on environmental variability modelled by a dichotomous Markov noise controlling the carrying capacity of the population (the number of individuals it can typically support). This drives the population size of the community and thus directly impacts the strength of demographic fluctuations, providing a coupling between ecological and evolutionary dynamics. The case where environmental variability impacts both the reproductive capabilities of species and the carrying capacity is also considered. Due to the eco-evolutionary coupling, driven by environmental changes, interesting novel phenomena arise at the evolutionary level. In particular, in each model a preferred evolutionary outcome is motivated, and it is shown how appropriate conditions on environmental variability can promote those outcomes. These behaviours are investigated through extensive stochastic simulations and the development of analytical techniques.

Contents

Abbreviations

DF	demographic fluctuations
EV	environmental variability
DMN	dichotomous Markov noise
ME	master equation
MA	Moran approximation
MFT	mean fixation time
AMR	antimicrobial resistance
PDMP	piecewise-deterministic Markov process
QPSD	quasi-stationary population size distribution
MET	mean extinction time

Chapter 1

Introduction

Natural selection is a key mechanism of evolution, where individuals with advantageous traits are more likely to survive and reproduce. Within a population, natural selection occurs according to the rules set by its environment. Over generations, advantageous mutations accumulate and traits therefore evolve, allowing the population to become increasingly well-adapted to its ecological landscape. Nature provides countless examples of the end product of this process: the long neck of the giraffe allow it to access treetops in the African savannah, the long, strong limbs of the spider monkey allow it to easily navigate the dense rainforest trees, and the thick fur of the snow leopard provides it with insulation in the snowy mountains. While perhaps a less evocative example, the same goes for microscopic organisms such as bacteria, where they too adapt over time to best survive and replicate in their environment. However, the same evolved traits in a different environment may instead be disadvantageous and unlikely to survive – the snow leopard suffers in the heat of the savannah, the spider monkey struggles in the freezing conditions of the snowy mountains, and the giraffe stumbles in the dense canopy of the jungle. Moreover, environmental factors such as temperature and resource availability often vary in natural environments in both space and time. Therefore, a population well-adapted to one environment may be plunged into a new environment to which it is maladapted. This poses serious challenges in understanding the evolution of such natural systems.

Environmental variability (EV) refers to changes in the environmental conditions that directly influence the ecological dynamics of a population. Moreover, EV can lead to significant shifts in the evolutionary landscape of the population, and understanding the subsequent evolution of the population is non-trivial. This scenario of population evolution subject to EV increasingly aligns itself with modern-day issues of importance to society; for example, the survival and adaptation of species under the effects of climate change (Hoffmann & Sgrò, 2011), the emergence of novel pathogens in shifting ecological landscapes (Engering et al., 2013), and the evolution of antimicrobial resistance (AMR) (Lindsey et al., 2013; Coates et al., 2018; Mahrt et al., 2021). A developed understanding of the evolution of populations in changing environments is therefore imperative should we hope to address these key scientific and societal challenges. This thesis advances the

theoretical understanding of such systems by investigating models of AMR and the establishment of an evolutionarily advantageous but pathogenic mutant under EV.

Theoretical models of biological processes, largely developed over the last century, have been crucial in providing insight into the dynamics of such systems. In particular, ideas from evolutionary and population genetics alongside those from population ecology have lead to significant steps forward in our understanding. Historically, these two fields developed largely independently. Population genetics was first given a firm theoretical basis in the early 20th century by Fisher, Haldane, and Wright, who reconciled natural selection and Mendelian genetics by introducing models for gene frequency change in finite populations (Haldane, 1927; Fisher, 1930; S. Wright, 1931). Later, Feller and Moran introduced stochastic models of genetic drift using Markov chain approaches, which captured the randomness of finite populations (Feller, 1939; Moran, 1958, 1962). Feller, Crow, and Kimura extended these insights with diffusion theory, providing approximations of the genetic evolution of a population that allowed for elegant analytical results (Feller, 1951; Crow & Kimura, 1970). Following these developments, evolutionary game theory emerged from the work of Maynard Smith and Price, who applied the strategic thinking of classical game theory to biological interactions of populations (J. M. Smith & Price, 1973). This provided a connection between evolutionary dynamics and game-theoretic reasoning, enabling the study of behavioural strategies. Almost in parallel to the work of Fisher, Haldane, and Wright, theoretical population ecology was aided significantly by progress due to Lotka and Volterra (Lotka, 1925; Volterra, 1926), resulting in the well-known Lotka-Volterra equations. Additionally, empirical evidence suggested that evolutionary timescales were not necessarily much slower than ecological timescales (Tutt, 1896; Berry, 1964; Johnston & Selander, 1964; Bradshaw, 1965; Pimentel, 1968; Kettlewell, 1973), as was often assumed. This was made even clearer in studies of bacterial species, where evolutionary dynamics are particularly fast (Luria & Delbrück, 1943; Lenski et al., 1991; Yoshida et al., 2003). Furthermore, computational methods and computational power advanced significantly during the 20th century. Monte Carlo methods were developed for the simulation of complex stochastic systems with many possible trajectories by von Neumann and Ulam, and the work later published by Metropolis and Ulam (Metropolis & Ulam, 1949) . These methods permitted the exploration of complex evolutionary scenarios via computational means, and were used to test theoretical predictions and investigate systems where analytical progress was unfeasible. Gillespie later developed methods for statistically correct stochastic simulations, eliminating errors caused due to the specific simulation method selected (Gillespie, 1976, 1977).

With these various developments and the efforts of some prominent figures of the time (Levins, 1966, 1968; Lewontin, 1968), the importance of studying the interplay between ecological and evolutionary dynamics was established. Termed *eco-evolutionary dynamics*, this scenario where ecological changes can impact the evolutionary dynamics and evolutionary changes can affect the ecological dynamics combines the theoretical works from population genetics and population ecology to capture the full picture of population evolu-

tion (Pelletier et al., 2009). In this thesis, I chiefly investigate the effect of environmental changes where their direct impact on the ecology of a population affects how it goes on to evolve, thus leading to eco-evolutionary dynamics.

More recently, studies have made significant headway in addressing the eco-evolutionary dynamics of a population whose size is composition-dependent and therefore varies in time (Parsons & Quince, 2007a, 2007b; Parsons et al., 2010; Houchmandzadeh & Vallade, 2012; Y. T. Lin et al., 2012; Chotibut & Nelson, 2015; Houchmandzadeh, 2015; Rogers & McKane, 2015; Constable et al., 2016; Joshi & Guttal, 2018; DeLong & Cressler, 2023; Wang et al., 2023; Bhat, 2025; Bhat & Guttal, 2025). These works represent significant advances in our understanding, but consider only impacts to the population ecology due to the evolution of the population itself, and not the case where it varies due to an externally-driven environment. Thus, despite this progress, eco-evolutionary dynamics remains poorly understood, with many empirical and theoretical studies continuing to consider either ecological or evolutionary dynamics independently, ignoring the coupling between them. This thesis aims to address this knowledge gap by focussing on the distinct scenario where environmental variations drive ecological dynamics that impact the evolutionary behaviour. In some of the models considered here, the evolution of the population also impacts the ecology of the system (see Ch. 3), but the ecological dynamics are generally not affected.

Traditionally, biological processes have been modelled as continuous and deterministic, an approach where quantities such as the population size are approximated as smoothly varying and random fluctuations due to noise are ignored (Hofbauer & Sigmund, 1998; L. J. S. Allen, 2007). This approach often permits a great deal of analytical progress. On the contrary, such processes are, by their very nature, discrete and stochastic. By ignoring the inherent stochasticity and discreteness of biological systems, we are at risk of missing key features of their dynamics (van Kampen, 1992; L. J. S. Allen, 2003), or even finding unphysical results; see the "atto-fox problem" of Lotka-Volterra dynamics (Mollison, 1991). These discrete, stochastic changes are here modelled in terms of a birth-death process where, at the simplest level, each birth and death occurs randomly and changes the population by one. This leads to *demographic fluctuations* (DF) – randomness in a population's evolution caused by stochastic births and deaths. These fluctuations can lead to the *fixation* of a trait in a population (Crow & Kimura, 1970; van Kampen, 1992; L. J. S. Allen, 2003; Ewens, 2004; Gardiner, 2009), the process in which a population becomes homogeneous and consists only of individuals carrying that specific trait (equivalently all individuals with different traits go extinct). This does not occur in continuous, deterministic modelling approaches, where fixation is only approached asymptotically in time. In this thesis, I will consider individuals of two different competing types, representing distinct microbial strains with different traits. Central questions are thus the fixation probability of a given trait, that is the likelihood that it takes over the entire population, and the mean time for fixation to occur (referred to as the mean fixation time (MFT)). These notions are closely related to the probability and mean time to extinction of the

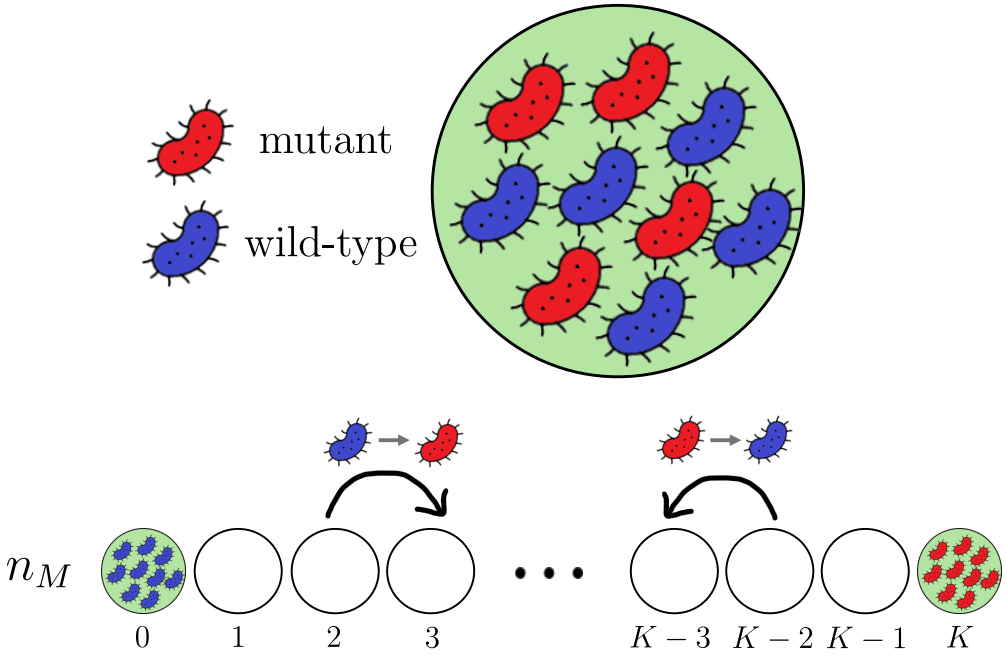

Figure 1.1: Cartoon of the Moran process. A population of mutant (red) and wild-type (blue) cells occupy the same environment. The population is of constant size, equal to its carrying capacity, labelled K. The state of the population is then captured entirely by the number of mutant individuals, labelled n_M. In the example state shown at the top, $K = 9$ and $n_M = 4$. The population evolves, at each step either increasing n_M through the replacement of a wild-type by a mutant (arrow to the right) or decreasing n_M by replacing a mutant by a wild-type (arrow to the left). Therefore, n_M performs a random walk on $\{0, ..., K\}$ until it reaches one of the absorbing states: $n_M = 0$ with all wild-types or $n_M = K$ with all mutants. This process of reaching an absorbing state is called fixation.

other trait initially present.

Mathematically, this process of fixation is often captured using a Markov chain with absorbing boundaries. Several different models are used to describe the behaviour of such systems, but here I focus on the *Moran process* (Moran, 1958, 1962; Antal & Scheuring, 2006; Blythe & McKane, 2007; Traulsen & Haeurt, 2009); see Fig. 1.1 and Ch. 2.2.2. In its classical formulation, the Moran process represents a paradigmatic model of evolution for haploid organisms, where at its simplest there are two species in a population of constant size. At each step of the process, one individual is chosen to replicate, with its offspring replacing an individual of the other species, until fixation of one species occurs. Species which have a higher *fitness* – a quantity directly related to a species' reproductive rate – are more likely to be chosen to replicate; see Ch. 2.2.1. A particularly nice feature of the Moran process is that these rates can generally be density-dependent, i.e. they vary depending on the population composition, behaviour which is also found in experimental settings (Lewontin, 1955; Contois, 1959; Lorenzen & Enberg, 2002). While the Moran process represents a particularly convenient formulation, alternatives such as the Wright-Fisher process could also be used. The conceptual difference between these two approaches is that the Moran model considers overlapping generations in its evolution, while in the

Wright-Fisher model generations are non-overlapping. Quantitatively, this corresponds to a simple rescaling of the population size by a constant factor in results on fixation, so little is lost in selecting one approach over the other.

More generally, the Moran process illustrates a key concept in evolutionary dynamics. This is the impact of *selection* and *diffusion*: selection refers to the process in which a fitter species tends to be favoured in a population, leading to an increase in its abundance; diffusion refers to the randomness of a population's evolution due to DF from the population's finite size, and therefore acts counter to selection. In larger populations, diffusion is weaker, since the typical strength of DF is inversely proportional to the square root of the population size, while the strength of selection is independent of population size (van Kampen, 1992; Ewens, 2004; Gardiner, 2009). Therefore, a small population experiences stronger diffusion in its evolution and requires a large selection strength to ensure the fixation of the fitter species, whereas a large population requires only a small selection strength for the same effect. I will refer throughout this thesis to the strength of selection and diffusion in relation to the evolutionary dynamics of the populations considered. This behaviour is in fact seen in *in vitro* systems, such as in experiments on bacteriophages (Burch & Chao, 1999) and bacteria (Travisano, Mongold, et al., 1995; Travisano, Vasi, & Lenski, 1995). In this context, the Moran process represents a key tool in developing insight into these systems, and I will use it to investigate the evolution of the models described in this thesis.

However, a key assumption of the Moran process is not generally adhered to by biological populations – the constant population size. Ecological factors such as the size of a population can vary dramatically following changes to a population's environment. Thus, EV that leads to changes in the population size also modulate the strength of DF, therefore impacting the strength of diffusion relative to selection and demonstrating the coupling between the ecological and evolutionary dynamics of a population. In fact, this coupling is ubiquitous in real populations but often ignored in theoretical models that, in the absence of suitable theoretical tools, often assume these dynamics are decoupled. An important aspect of this thesis is the consideration of coupled ecological and evolutionary dynamics, where I develop analytical and computational tools to tackle these challenging problems. Without a detailed knowledge of the exact form of EV causing these changes, it is often modelled by allowing the birth and death rates of each species to vary in time. This approach has been used to study a variety of eco-evolutionary phenomena such as phenotypic switching (Balaban et al., 2004; Kussell & Leibler, 2005; Acar et al., 2008; Assaf, Roberts, et al., 2013), cooperation (Assaf, Mobilia, & Roberts, 2013; Melbinger et al., 2015; Wienand et al., 2017, 2018), species coexistence (Chesson & Warner, 1981; Chesson, 1994, 2000a, 2000b; Hidalgo et al., 2017; Ellner et al., 2019; Meyer et al., 2021), and more general fixation and extinction (Ashcroft et al., 2014; Hufton et al., 2016; Danino & Shnerb, 2018; Taitelbaum et al., 2020; Raatz & Traulsen, 2023; Taitelbaum et al., 2023). In this thesis, I shall utilise the dichotomous Markov noise (DMN) process to capture the effects of EV on microbial populations, which I will now introduce.

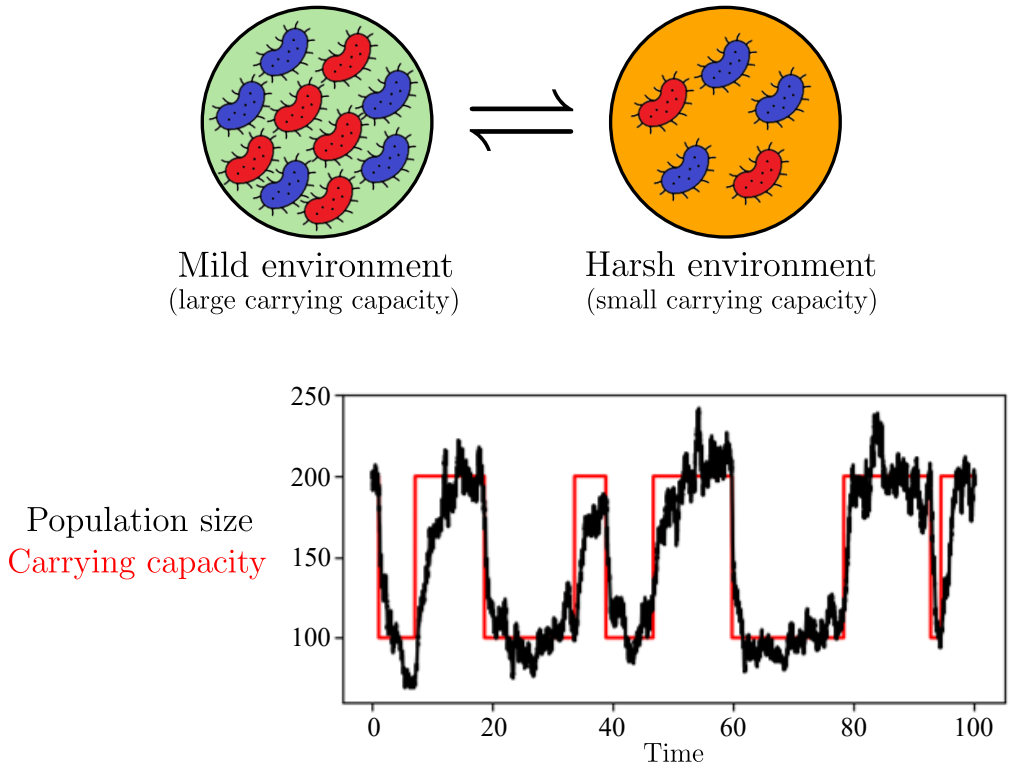

Figure 1.2: Cartoon demonstrating the effect of dichotomous Markov noise driving the carrying capacity of a population. The environment switches stochastically between harsh and mild environmental conditions, corresponding to small and large carrying capacities, respectively. A change in the carrying capacity (red line) drives the evolution of the population size (black line) towards the new carrying capacity. In the example realisation, the carrying capacity switches between values of 100 and 200 with a rate 0.1.

DMN is a two-state Markovian process whereby a random variable defined by a DMN process switches between its two possible values with constant rates (Horsthemke & Lefever, 1984; Bena, 2006; Ridolfi et al., 2011). In the following chapters, I shall use DMN to vary the death rates of the individuals in the population, switching between a high and low value; see Ch. 2.3 and Wienand et al. (2017, 2018). This is done through a time-varying *carrying capacity*, where the carrying capacity gives the number of individuals that can be supported in a population. Biologically, this corresponds to the effect of varying resource availability, where a high death rate/small carrying capacity means few resources (harsh environment) and a low death rate/large carrying capacity means abundant resources (mild environment); see Fig. 1.2. This is particularly relevant to microbial communities where, due to their scale, sharp transitions in nutrient availability in the system can occur or the population can be rapidly and significantly diluted as in many experimental studies (Wahl et al., 2002; Brockhurst, 2007; Patwa & Wahl, 2010; Shade et al., 2012). In fact, due to the instantaneous switches that characterise DMN, its relevance is largely restricted to such natural systems where the changes to the environmental state can be approximated by sudden variations. However, these are systems of particular interest and this approximation allows for significant analytical tractability, as we shall see. In such systems, nutrient shocks, where the amount of available resource suddenly and drastically decreases, lead to population bottlenecks where the population size rapidly shrinks. This produces the coupling between the ecological and evolutionary dynamics, discussed previously. In fact, in most lab-controlled experiments, changing environments are implemented by means of a binary time-varying environment (Acar et al., 2008; Sanchez & Gore, 2013; G. Lambert & Kussell, 2014; Rodríguez-Verdugo et al., 2019; Abdul-Rahman et al., 2021; Nguyen et al., 2021; Shibasaki et al., 2021) that can be well represented by DMN. The models considered in this thesis are inspired by the chemostat set-up, which is a bioreactor with a continuous inflow of fresh medium (typically nutrients) and outflow of cells, and waste products (Novick & Szilard, 1950; James, 1961; Jakiela et al., 2013). This set-up is commonly used in experimental studies to obtain a steady state population. A change to the environment may be implemented in a chemostat through a change to the inflowing medium, for example in the nutrient concentration or toxin level, leading to a different steady state. This contrasts with batch cultures, another common experimental setup, where a population is exposed to an initial fixed amount of resource and there is no flow of medium. As the resources are consumed, growth halts and cell death ensues.

Aside from its physical relevance to microbial communities, DMN has many other positive attributes: (i) it is simple enough that analytical results are possible to obtain for some systems; (ii) it is bounded, i.e. the range of values it can take does not diverge in time; (iii) it is easy to implement in simulations; (iv) it is a *coloured* noise, meaning it generally has non-zero temporal autocorrelation. This final property is particularly attractive when looking to model EV in biological systems, allowing for the capture of correlations in time which occur in natural environments. In such cases where the evolutionary dynamics occur on similar or faster timescales than the ecological dynamics, EV drives the system and shapes the landscape in which it evolves. This is particularly relevant to microbial

communities, where evolutionary timescales are fast and therefore correlations of the EV are important.

To fully appreciate the strengths of DMN, it is instructive to compare it to other forms of noise used in modelling a changing nutrient level in biological systems. Here, I will compare DMN with two common alternatives: the Ornstein-Uhlenbeck (OU) process and periodic dichotomous noise (PDN). Although not explicitly considered in this thesis, these forms of noise are common alternatives in related contexts, with OU processes appropriate for modelling continuously varying environments correlated in time, and PDN suited to environments that vary in a strictly periodic fashion. A system driven by an OU process does not enjoy the attributes (i)-(iii): (i) in general, to obtain analytical results for a system driven by an OU process, it is necessary to resort to limiting regimes where the correlation time of the noise is either much shorter or longer than that of the evolutionary dynamics (Horsthemke & Lefever, 1984); (ii) the Gaussian noise driving the OU process has an unbounded range (i.e. can take any value in $(-\infty, \infty)$), therefore allowing the carrying capacity to take unphysical negative values and being generally unbounded; (iii) the value of the OU process driving the system varies continuously in time, therefore making it impossible to exactly simulate the full system. Further issues arise in simulations due to the carrying capacity including unphysical values in its range, requiring ad-hoc corrections (Bena, 2006). In the case of a system driven by a PDN, we find that attributes (i) and (iii) are not satisfied and DMN provides a good approximation for the dynamics of a system driven by PDN, making it the more attractive modelling approach (Taitelbaum et al., 2020). Throughout this thesis, a common theme is the finding of suitable methods to combine analytical results of DMN (see Ch. 2.3) with the analytical results of the Moran process (see Ch. 2.2.2) to capture the joint eco-evolutionary dynamics of the system. In this thesis I combine these results to develop an understanding of fixation and coexistence in populations with cooperative AMR under a time-varying volume (see Ch. 3.4.2) (Hernández-Navarro, Asker, & Mobilia, 2024) and populations with resistant species subject to twofold environmental variability (see Ch. 4.3) (Asker et al., 2023), as well as to investigate fixation of an advantageous mutant species on spatially structured populations (see Ch. 5.3) (Asker et al., 2025).

Spatial structure is another key aspect of realistic microbial populations that is often beyond mathematical analysis and is dealt with almost exclusively by computational means. In this thesis, spatial structure refers specifically to the spatial distribution of cells, rather than environmental inhomogeneities across space which is neglected. Microbial populations typically occupy complex spatial structures, across which the distribution of microbes fluctuates. For instance, many organisms live in densely packed aggregates on surface-attached biofilms (Widder et al., 2016), numerous commensal bacteria are distributed throughout the gastrointestinal tract (Engel & Moran, 2013; Garud et al., 2019), and patients' organs are spatial environments between which bacteria can migrate (She et al., 2024). Following on from the population ecology developments of Lotka and Volterra, several theoretical advancements were made in the consideration of spatially

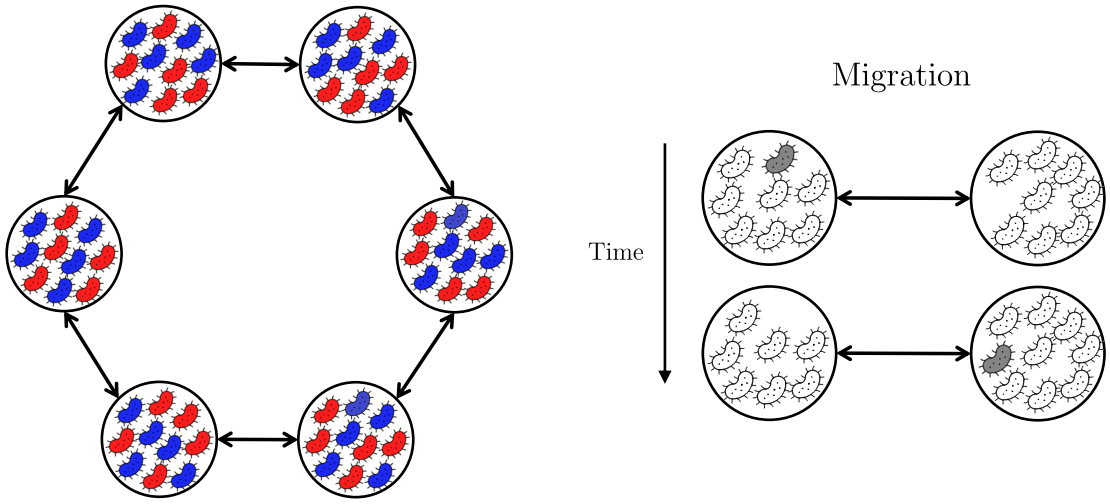

Figure 1.3: Cartoon of a metapopulation containing two species and an example migration of an individual between two adjacent deme in a metapopulation. Individuals interact only with those occupying the same subpopulation, but may also migrate along the arrows connecting deme. An example of such a migration event is depicted, with the grey cell migrating from the left subpopulation to the right one.

structured ecological communities, termed *metapopulations* (S. Wright, 1931; Kimura & Weiss, 1964; MacArthur & Wilson, 1967; Levins, 1969; Maruyama, 1970; Slatkin, 1981). These metapopulations consist of several demes (subpopulations) representing different spatial niches in a population. Individuals interact within these demes, and may migrate to neighbouring demes; see Fig. 1.3. While this simplifies the spatial structure of natural systems by representing space as discrete, interacting demes, it nonetheless captures essential features of microbial populations such as migration and competition. Furthermore, models considering continuous space are often intractable and require numerical simulations. Due to their relevance to natural systems and analytical tractability, the use of metapopulation models in the study of spatially structured populations remains a common approach (Whitlock, 2003; Constable & McKane, 2014; Hauert et al., 2014; Szczesny et al., 2014; Marrec et al., 2021; Yagoobi & Traulsen, 2021; Abbara & Bitbol, 2023; Marrec, 2023; Abbara et al., 2024; Hernández-Navarro, Distefano, et al., 2024; Moawad et al., 2024; Asker et al., 2025).

In microbial systems, mutations frequently arise through errors in DNA replication during reproduction, and occasionally one of these may provide a reproductive advantage to the mutant daughter cell over the resident population (Barrick et al., 2009; Tenaillon et al., 2016; Good et al., 2017). As such, the population then consists of the individuals without the mutation denoted the wild-type, and the individual with the advantageous mutation, denoted the mutant. These mutations are often rare, and so this population will then evolve and eventually consist of all mutants or all wild-types through fixation of either strain. The dynamics of such a population is well understood in the absence of spatial structure, as discussed. An interesting question to ask is then: how is the fixation of a mutant strain impacted by spatial structure?

Several theoretical studies have probed this question on metapopulations in constant environments where cell migration is symmetric (cells have no preference in where they migrate). Maruyama (1970) notably showed that, under some additional simple and physically relevant conditions, the fixation probability of a mutant is independent of the spatial structure and migration rate. Furthermore, many works have investigated how random extinction (the process where all individuals within a subpopulation die) and recolonisation (the process whereby an extinct subpopulation has an individual migrate to it and restore the population) of demes affect mutant fixation within metapopulations (Levins, 1969; Barton, 1993; Lande et al., 1998; Hanski, 1999). Recently, Marrec et al. (2021) studied the the influence of slow migration on the fate of mutants, and demonstrated that asymmetric migration can dramatically affect the fixation probability on certain spatial structures. Chiefly, these theoretical studies into metapopulation dynamics have focussed on the influence of spatial structure on evolution *without* EV, with experimental studies following suit (Kryazhimskiy et al., 2012; Nahum et al., 2015; Chakraborty et al., 2023; Kreger et al., 2023). Moreover, the natural environments of spatially structured populations are also generally not static. One example is the gut microbiome, which is exposed to large fluctuations across several timescales, affecting the diversity of the microbiota (Smits et al., 2017; Cignarella et al., 2018). Therefore, to achieve a full understanding of these biological systems, we must consider their evolution taking into account the effects of EV and spatial structure. This thesis thus also investigates the eco-evolutionary dynamics on spatially structured metapopulations in the presence of EV to understand how a changing environment coupled to DF interacts with spatial structure to shape evolutionary outcomes; see Ch. 5. By doing so, it extends classical models to more realistic settings and provides theoretical insights into evolutionary outcomes in natural, dynamic landscapes such as the gut microbiome.

After having set the scene and motivated the research undertaken in this thesis, I now provide a brief outline of the following chapters. In this thesis, I investigate four distinct models of microbial populations subject to EV: two focussed on cooperative AMR, one on the coexistence of resistant and sensitive species, and one on spatially structured populations. Specifically, I ask:

- What mechanisms enable eradication of AMR under EV?
- How does EV govern fixation versus long-lived species coexistence in competing microbial species?
- How does EV affect the fixation probability of an advantageous mutant in a spatial metapopulation?

In Ch. 2, I will develop the mathematical techniques and computational methods used throughout the rest of this thesis. In Ch. 3, I address the first question, introducing two models of cooperative AMR, where resistant cells pay a metabolic cost for resistance. The resistance is shared among all cells if they exceed a certain threshold in resistant cell abundance, and kept private if they do not (Hernández-Navarro et al., 2023; Hernández-

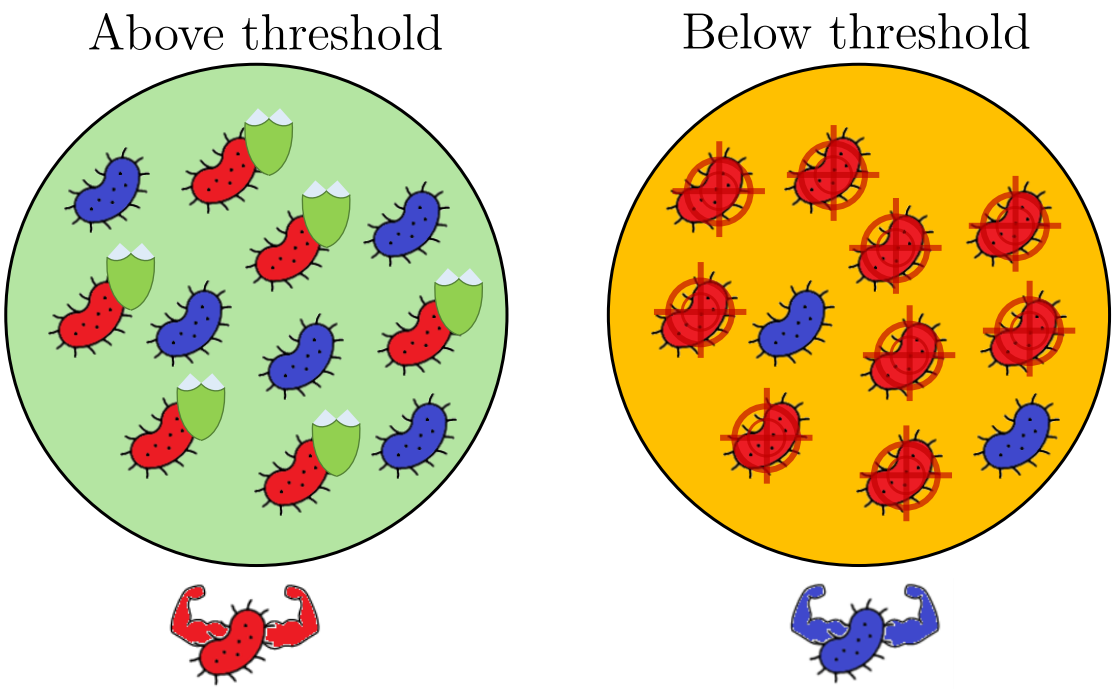

Figure 1.4: Cartoon of cooperative AMR. When the resistant (blue) cells exceed their threshold in abundance for shared resistance, the sensitive (red) cells are protected. The resistant cells have paid a metabolic cost to produce the resistance enzyme, while the sensitive cells have not. Therefore, the sensitive cells are better off and will increase in abundance. When the resistant cells are below the threshold, the resistant cells maintain resistance to the antimicrobial, while the sensitive cells suffer a metabolic cost larger than that paid by the resistant cells for resistance. Therefore, the resistant cells are better off and will increase in abundance. This leads to the population being driven towards the threshold; see Ch. 3.

Navarro, Asker, & Mobilia, 2024); see Fig. 1.4. I investigate the fixation and coexistence properties of both strains under constant antimicrobial concentration, determining under which EV fixation or long-lived coexistence occurs. Moreover, I am able to identify and fully characterise a novel *EV-driven* resistance-eradication mechanism; see Ch. 3.3.1. I also show more generally that the picture of cooperative AMR evolution can be greatly altered by the joint effect of EV and DF; see Chs. 3.3.1 and 3.4.2. In Ch. 4, I consider the second question in a distinct model of AMR, where the resistance remains private to the resistant cells (Asker et al., 2023). Here, the antimicrobial is not always supplied at a concentration sufficient to impede sensitive cells. Its concentration is instead driven by another independent DMN process, varying between a high toxin level and a low toxin level, impacting the birth rate of the sensitive strain. The distinctive feature of this study is therefore the *twofold environmental variability* accounting for variation of the toxin level and the switches of the nutrient level, impacting both the birth rates and death rates, respectively. I determine the environmental conditions under which long-lived coexistence of the strains is possible or certain, and those in which one strain dominates the other. The coexistence mechanism is induced by environmental changes that are sufficiently large and frequent, and so is closely related to bet-hedging strategies and the storage effect (Chesson

& Warner, 1981; Frank & Slatkin, 1990; Gaál et al., 2010; Xue & Leibler, 2017; Bhat & Guttal, 2025). I also analyse the make-up of the population when the strains coexist, and their average abundance. In Ch. 5, I cover the final proposed question. I study a class of time-varying microbial metapopulation models consisting of demes in which wild-type and mutant cells evolve in a time-varying environment represented by a time-varying carrying capacity. I use coarse-grained descriptions of the dynamics to study the joint influence of EV, DF, migration, and spatial structure on the evolution of the metapopulation; see Figs. 1.2 and 1.3. I demonstrate that the coupling of EV and DF in spatially structured populations leads to qualitatively distinct outcomes compared to the case of a static environment, and notably determine how the probability of mutant fixation depends explicitly on migration and EV. Viewing this through the lens of an unwanted mutant arising and attempting to spread through an otherwise healthy system, I determine optimal conditions to eradicate mutants without risking metapopulation extinction. I am able to capture this behaviour through novel analytic approaches and extensive stochastic simulations.

Collectively, the findings of this thesis demonstrate that EV impacting the ecology of a population couple directly to its evolution and can unveil qualitatively distinct behaviour that is not found when this interplay is neglected. Importantly, this unveils dynamical scenarios that are relevant to modern-day societal issues, such as the evolution of AMR, the emergence of novel pathogens, and the spread of cancer. In considering this interplay, I find novel mechanisms for the eradication of AMR and unwanted mutants that have implications for these issues. These findings suggest that the dynamics of microbial communities cannot be fully understood without considering the joint eco-evolutionary effects of coupled EV and DF. In this thesis, I develop a suite of mathematical tools, combined with efficient computational methods, to analyse in detail several models of population evolution in time-varying environments.

Chapter 2

Mathematical preliminaries

In this chapter, I will introduce logistic growth dynamics for well-mixed populations consisting of a single species. Starting with the microscopic dynamics underlying the birth-death processes at the individual level, I will demonstrate how the mean-field (MF) approximation, where DF (and hence correlations) are neglected, can be obtained from the full microscopic description in the large population size limit. Furthermore, I will show how the dynamics change under considerations of finite population size, notably considering the mean time to extinction and the quasi-stationary population size distribution (QPSD) when the extinction time is long; see later. Following this, I present the concept of competition for shared resources between two species, first determining the microscopic processes underlying such a model, and considering the MF approximation for the evolution of its composition. Subsequently, I present the Moran process, and demonstrate its utility in modelling the evolution of a population under logistic growth, particularly in the capturing of stochastic effects that the MF approximation neglects. I will then introduce the concept of dichotomous Markov noise (DMN), and demonstrate some of the properties it possesses that make it useful both for modelling EV and obtaining analytical results. I continue by showing how I utilise DMN to vary the resources available to the populations considered in the following chapters, and discuss properties of this form of noise. Furthermore, I will demonstrate that we can capture an analytic approximate expression for the QPSD of the population under this noise, and demonstrate the practicality of this expression using an illustrative example case in which I capture the fixation properties of the population under environmental variability.

2.1 Logistic growth of a single-species population

We will start by considering the simple case of logistic growth in a population with a single species. Here, and throughout the rest of this thesis, we neglect mutations on the timescale of the population dynamics considered. Logistic growth is a prototypical example of population growth under a finite resource restriction, and the models considered in this thesis are assumed to follow such growth. Other models of population growth exist and are

active areas of interesting research, e.g. exponential phase, predator-prey interactions, the Allee-effect, and range expansions (Allee & Bowen, 1932; Mollison, 1977; Chesson, 1978; Sun, 2016; R. J. Allen & Waclaw, 2018; Diz-Pita & Otero-Espinar, 2021). Logistic growth is arguably the simplest example of a model of growth dynamics with finite resources and, given the analytical progress this simplicity allows when introducing DMN (as we shall see later), it presents a key step towards understanding the impact of EV on evolutionary dynamics. I note here that all models considered in this thesis are in continuous-time, capturing the asynchronous births and deaths of individuals in microbial populations.

2.1.1 Master equation and the mean-field approximation

To begin, we consider the microscopic processes underlying the dynamics. The population is comprised of n individuals, existing in a well-mixed environment, i.e. there is no spatial structure to the population. We denote the probability of finding this system with n individuals at time t as $P(n,t)$. The rates at which the system transitions from $P(n,t) \to P(n\pm1,t)$ are given by $T^{\pm}(n)$, where $P(n,t) \to P(n+1,t)$ represents a birth event and $P(n,t) \to P(n-1,t)$ represents a death event. From these microscopic rates, we can write a master equation (ME) for $P(n,t)$ describing its time evolution, given by

$$\partial_t P(n,t) = \underbrace{T^+(n-1)P(n-1,t) + T^-(n+1)P(n+1,t)}_{\text{inflow to } P(n,t)} - \underbrace{[T^+(n) + T^-(n)]P(n,t)}_{\text{outflow from } P(n,t)}, \tag{2.1}$$

where $T^{\pm}(n) = 0$ for $n \leq 0$ and $P(n) = 0$ for $n < 0$, such that the system population size remains physical (i.e. $n \geq 0$) and $n = 0$ is the only absorbing state. This equation wholly determines the evolution of the system but is too complicated to solve directly if either of the transitions rates $T^{\pm}(n)$ is non-linear in n, as is typical for many systems. Despite this apparent pitfall, we can still derive much understanding from various approximations of this equation. Here, we start by investigating the evolution of the mean population size, $\langle n \rangle = \sum_n nP(n,t)$. Multiplying Eq. (2.1) by n and summing over all n we have

$$\begin{aligned}\frac{\mathrm{d}}{\mathrm{d}t}\langle n\rangle &= \sum_n n\partial_t P(n,t),\\ &= \sum_n n\left[T^+(n-1)P(n-1,t) + T^-(n+1)P(n+1,t) - [T^+(n)+T^-(n)]P(n,t)\right].\end{aligned}$$

Shifting the indices of summation and carrying out the averaging procedure yields

$$\frac{\mathrm{d}}{\mathrm{d}t}\langle n\rangle = \left\langle T^+(n)\right\rangle - \left\langle T^-(n)\right\rangle.$$

So far, this equation is exact and independent of the form of $T^{\pm}(n)$. To proceed further, we must now choose the forms of these rates. Here, we focus on the case of logistic growth. Resources are limited, so the population does not grow indefinitely, and this is introduced via a carrying capacity $K > 0$. Each individual gives birth with a per-capita rate b and dies with a per-capita rate $d\frac{n}{K}$, where both $b, d > 0$. Therefore, the rates of birth and

death for the total population are given by $T^+(n) = bn$ and $T^-(n) = d\frac{n^2}{K}$, respectively. This leaves us with (L. J. S. Allen, 2003; Gardiner, 2009)

$$\frac{\mathrm{d}}{\mathrm{d}t}\langle n\rangle = b\langle n\rangle - \frac{d}{K}\langle n^2\rangle .$$

This equation is not closed with respect to the moment hierarchy in n, i.e. the evolution of $\langle n\rangle$ depends on the behaviour of a higher order moment, $\langle n^2\rangle$, and so we must make a suitable approximation to proceed. Here, we adopt the simplest form of moment closure approximation, assuming $\langle n^2\rangle = \langle n\rangle^2$ in order to close the equations. This approximation equates to the assumption that the variance of n is small and therefore fluctuations in n are negligible compared to its mean. For increasing population sizes this approximation improves as the ratio between the size of fluctuations and the population size scales like $n^{-\frac{1}{2}}$ (van Kampen, 1992; Gardiner, 2009). This is known as the *mean-field* (MF) approximation, and while here it is an uncontrolled approximation (we have made no guarantee here that fluctuations will indeed be small), the same result is reached using approaches that are controlled but typically more involved; see Ch. 2.2.1. Therefore, we now have

$$\frac{\mathrm{d}}{\mathrm{d}t}\langle n\rangle = b\langle n\rangle - \frac{d}{K}\langle n\rangle^2 , \tag{2.2}$$

which can be solved to give

$$\langle n\rangle = \frac{n_0 e^{bt}}{1 + \frac{n_0}{K}\frac{d}{b}(e^{bt} - 1)}, \tag{2.3}$$

where n_0 is the number of individuals at time $t = 0$. We see that $\lim_{t\to\infty}\langle n\rangle = K\frac{b}{d}$. Alternatively, this can be easily seen from simple stability analysis of the fixed points of Eq. (2.2). Therefore, under logistic growth, the MF approximation predicts that the population size will tend towards an equilibrium value at $\langle n\rangle = K\frac{b}{d}$, and does so exponentially quickly. For simplicity and without loss of generality, we herein consider that $b = d = 1$. Therefore, the typical interpretation of the carrying capacity K is that it gives the number of individuals the system can typically sustain. This behaviour is particularly useful when considering more complex dynamics within the population, as it allows us to treat the population size as approximately constant at $n = K$. We will use this later.

2.1.2 Stochasticity and the quasi-stationary population size distribution

While the MF approximation is useful, particularly in large populations, it gives no information on the distribution of n except the mean. For smaller populations, the variance of n increases and DF can be of comparable order to the mean. This can have dramatic effects on the dynamics within the population, in extreme cases leading to extinction of the population (as we shall see in Ch. 5). To gain a better understanding of the distribution of n, we look to calculate its approximate QPSD. Concretely, a population undergoing logistic growth dynamics as described previously will inevitably reach population extinction at the absorbing state $n = 0$ as $t \to \infty$, since the population is driven to $n = K$ and the probability of reaching the state $n = 0$ from $n = K$ is non-zero (L. J. S. Allen, 2003; Assaf

& Meerson, 2010). However, the time for extinction can be exceedingly long – far longer than the timescale of the dynamics that we are interested in. In such cases, it is useful to consider the distribution of the population size neglecting extinction. The QPSD for n can be approximated by assuming that $T^-(1) = 0$, i.e. extinction does not occur due to a reflecting boundary at $n = 1$. We denote this approximate QPSD by $\pi(n)$. Assuming stationarity as we are in equilibrium, we can then say that $\pi(1)T^+(1) = \pi(2)T^-(2)$. Proceeding similarly, we can then say $\pi(2)T^+(2) = \pi(3)T^-(3)$, and so on where this equates the probability flow between adjacent states such that the approximate QPSD satisfies detailed balance (Gardiner, 2009). Therefore, we can write (L. J. S. Allen, 2003)

$$\pi(n) = \pi(1) \prod_{i=1}^{n-1} \frac{T^+(i)}{T^-(i+1)}.$$

Using the condition that $\sum_j \pi(j) = 1$ we determine $\pi(1)$ as

$$\pi(1) = \frac{1}{\sum_j \prod_{i=1}^{j-1} \frac{T^+(i)}{T^-(i+1)}},$$

and hence,

$$\pi(n) = \frac{\prod_{i=1}^{n-1} \frac{T^+(i)}{T^-(i+1)}}{\sum_j \prod_{i=1}^{j-1} \frac{T^+(i)}{T^-(i+1)}}.$$

For the case of logistic growth, we have $T^+(i)/T^-(i+1) = Ki/(i+1)^2$ and so, the numerator is given by

$$\prod_{i=1}^{n-1} \frac{Ki}{(i+1)^2} = K^n \frac{(n-1)!}{n! \cdot n!} = \frac{K^n}{n \cdot n!}.$$

A similar calculation applies in the denominator and we thus have

$$\begin{aligned} \pi(n) &= \frac{K^n/(n \cdot n!)}{\sum_j K^j/(j \cdot j!)}, \\ &= \frac{1}{\mathrm{Ei}(K) - \ln(K) - \gamma_{\mathrm{EM}}} \frac{K^n}{n \cdot n!}, \end{aligned} \tag{2.4}$$

where $\mathrm{Ei}(x) = -\int_{-x}^{\infty} \frac{e^{-t}}{t}\,\mathrm{d}t$ is the exponential integral and $\gamma_{\mathrm{EM}} = 0.577...$ is the Euler-Mascheroni constant. The latter representation is useful when implementing the QPSD in computer code. We can then calculate the mean population size of the approximate QPSD as $\langle n \rangle = \sum_{n=1}^{\infty} n\pi(n)$ giving

$$\langle n \rangle = \frac{\exp(K) - 1}{\mathrm{Ei}(K) - \ln(K) - \gamma_{\mathrm{EM}}}.$$

This can be seen by noting that multiplying Eq. (2.4) by n and summing over all n gives precisely the power series of the exponential function minus the $n = 0$ term. Taking the limit of large population size, i.e. assuming that $K \gg 1$, we expand the terms in our expression. First, we have asymptotically that $\mathrm{Ei}(x) \sim \frac{e^x}{x} \sum_{k=0}^{\infty} \frac{k!}{x^k}$ (O'Malley, 2014). Truncating at the first term, this gives $\mathrm{Ei}(x) \approx \frac{e^x}{x}$ and this is dominant over the other terms

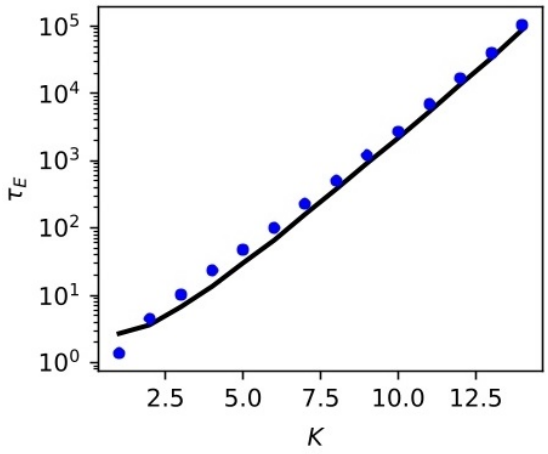

Figure 2.1: Mean extinction time of a population under logistic growth, τ_E, against carrying capacity K, initialised at $n = K$. Blue circles are simulation data, black line shows the predictions of Eq. (2.6).

in the denominator. Furthermore, the exponential in the numerator dominates. Therefore, this leaves us with $\langle n \rangle \approx K$, as in the MF approximation, showing that for large K the MF approach provides a good approximation to the true dynamics. However, as mentioned previously, due to DF extinction is inevitable since $n = 0$ is the sole absorbing state. This extinction occurs after a time which scales with the population size. To understand when we can reasonably ignore extinction or when we must consider it, I now will estimate that time.

The mean extinction time (MET) for a population with carrying capacity K, initialised with K individuals, denoted $\tau_E(K)$, is given by (L. J. S. Allen, 2003)

$$\tau_E(K) = \sum_{n=0}^{K-1} \left(\frac{n!}{K^n} \sum_{i=n+1}^{\infty} \frac{1}{i} \frac{K^i}{i!} \right). \tag{2.5}$$

The leading contribution to this expression arises from the term $n = 0$ term, and so $\tau_E(K) \approx \sum_{i=1}^{\infty} K^i/(i \cdot i!)$. This expression, corresponding to the MET for a population initialised with a single individual, is a good approximation of Eq. (2.5) which indicates that the MET is independent of initial condition (to leading order in τ_E). We have already seen this expression in the normalisation of $\pi(n)$ in Eq. (2.4), and thus have $\tau_E(K) \approx \mathrm{Ei}(K) - \ln(K) - \gamma_{\mathrm{EM}}$. Using the asymptotic expression for $\mathrm{Ei}(x)$ to first order again, we find

$$\tau_E(K) \approx \frac{e^K}{K}. \tag{2.6}$$

The MET hence increases almost exponentially with K and is essentially independent of the initial state. This approximation matches well to simulation results as seen in Fig. 2.1. For larger populations as considered previously, this time can thus be very long, far exceeding the timescale of the dynamics of interest. In this case, the population is characterised by the approximate QPSD of Eq. (2.4), where extinction can be ignored. In smaller populations however, this time is comparable to the timescale of the dynamics of

interest and extinction must be explicitly considered. Chs. 3 and 4 will consider only cases of large populations and so extinction is irrelevant, while Ch. 5 will explicitly consider the possibility of extinction.

I shall now look at competition between species, where the logistic growth dynamics are recovered in the population size.

2.2 Competition for shared resources

Typically, several species occupy a given environment. These species make use of the resources available in the environment, such as glucose, to replicate (Fuhrer et al., 2005; Nannipieri et al., 2017; Van den Bergh et al., 2018; Grilli, 2020). It is common for different species to utilise the same resource for replication. This leads to a competition between species, where they each compete for the same resource and those that can do so more effectively are more likely to survive and replicate. This type of competition involves no direct interactions between members of different species, such as is typical in predatory reproduction under predator-prey interactions where individuals consume members of other species to reproduce. Here, I shall consider solely the case of competition for shared resources, ignoring any direct inter-species interactions. Specifically, I consider competition between two species for a constant supply of resources held at a limited level. Under these restrictions, analytical progress can be made. Furthermore, restricting our attention to two species is less limiting than it might initially seem. In environments where multiple species are present, if differences among them in replication rates and resource usage are negligible, they may be treated as effectively equivalent for modelling purposes. This simplification allows us to reduce a complex community to a two-species system without significant loss of generality. In any case, the two-species case provides a clear and analytically tractable example, which will serve as a useful tool in subsequent analysis.

Here, I will start from the ME for competition between two species, where one is assumed to be a mutant, denoted M, competing with the wild-type species, denoted W. This arbitrary labelling will vary in the chapters following this to suit the context of the model considered. I will show that in the MF limit, we retrieve an equation for the evolution of the composition of the population, capturing the change in relative abundance of the species in time. I will then consider the Moran process (Moran, 1958, 1962; Ewens, 2004), demonstrating its utility in considering the evolution of a population under the logistic growth dynamics considered in Ch. 2.1.

2.2.1 Master equation and the van Kampen expansion

Again, we begin by considering the underlying microscopic processes of the dynamics. The population contains $n = n_M + n_W$ individuals, where n_M and n_W denotes the mutant and wild-type components of the population, respectively. We again consider no spatial structure, and so the system is well-mixed. The probability of finding the system with n_M mu-

tant individuals and n_W wild-type individuals at a time t is denoted $P(n_M, n_W, t)$. Birth and death events are independent for each species. Therefore, the rates at which the system transitions from $P(n_M, n_W, t) \to P(n_M \pm 1, n_W, t)$ and $P(n_M, n_W, t) \to P(n_M, n_W \pm 1, t)$, are given by $T_M^{\pm}(n_M, n_W)$ and $T_W^{\pm}(n_M, n_W)$, respectively. The ME describing this system is then given by

$$\begin{aligned}\partial_t P(n_M, n_W, t) = \sum_{\alpha=\{M,W\}} \big[&\left(\mathbb{E}_\alpha^- - 1\right) T_\alpha^+(n_M, n_W) P(n_W, n_M, t) \\ &+ \left(\mathbb{E}_\alpha^+ - 1\right) T_\alpha^-(n_M, n_W) P(n_M, n_W, t)\big],\end{aligned} \tag{2.7}$$

where the operators $\mathbb{E}_\alpha^{\pm}$ act on a general function $f(n_M, n_W, t)$ to give $\mathbb{E}_M^{\pm} f(n_M, n_W, t) = f(n_M \pm 1, n_W, t)$ and $\mathbb{E}_W^{\pm} f(n_M, n_W, t) = f(n_M, n_W \pm 1, t)$. Furthermore, we set $P(n_M, n_W, t) = 0$ whenever $n_M < 0$ or $n_W < 0$ to avoid unphysical population sizes, a condition we shall apply throughout this thesis. It is important to note that we generally consider $T_\alpha^+ = 0$ for $n_\alpha = 0$, meaning once a species has reached extinction it cannot return and the system has entered an absorbing state. To proceed, we perform a van Kampen system size expansion (van Kampen, 1992). We assume a large parameter K (here the carrying capacity), where $n_M, n_W \sim K$, and define the variables $x = n_M/K$, $y = n_W/K$, which become continuous in the limit of $K \to \infty$. We then also write $P(x, y, t) \equiv P(n_M = Kx, n_W = Ky, t)$. Furthermore, we assume that the rates $T_\alpha^{\pm}$ can be written as $T_\alpha^{\pm} = K\Xi_\alpha^{\pm}(x, y)$, where $\Xi_\alpha^{\pm}$ remain finite as $K \to \infty$.

The impact of the operators $\mathbb{E}_\alpha^{\pm}$ on a general function $f(n_M, n_W, t) \equiv f(Kx, Ky, t)$ can then be expanded in K, giving[1]

$$\begin{aligned}\mathbb{E}_M^{\pm} f(Kx, Ky, t) &\approx f(Kx, Ky, t) \pm \frac{1}{K}\partial_x f(Kx, Ky, t), \\ \mathbb{E}_W^{\pm} f(Kx, Ky, t) &\approx f(Kx, Ky, t) \pm \frac{1}{K}\partial_y f(Kx, Ky, t).\end{aligned}$$

Substituting the above into Eq. (2.7) yields

$$\partial_t P(x, y, t) = \partial_x \left[(\Xi_M^+(x, y) - \Xi_M^-(x, y))P(x, y, t)\right] + \partial_y \left[(\Xi_W^+(x, y) - \Xi_W^-(x, y))P(x, y, t)\right].$$

We note that this equation can be simply rearranged to give a continuity equation $\partial_t P(x, y) + \nabla \cdot [\vec{v}(x, y)P(x, y, t)] = 0$ with $\vec{v}(x, y) = (\Xi_M^-(x, y) - \Xi_M^+(x, y), \Xi_W^-(x, y) - \Xi_W^+(x, y))$, and so demonstrates the conservation of probability where $\vec{v}(x, y)$ describes the flow of probability at each point in phase space (x, y). Using the method of characteristics (Riley et al., 2006), we obtain

$$\begin{aligned}\frac{\mathrm{d}}{\mathrm{d}t}x &= \Xi_M^+(x, y) - \Xi_M^-(x, y), \\ \frac{\mathrm{d}}{\mathrm{d}t}y &= \Xi_W^+(x, y) - \Xi_W^-(x, y).\end{aligned} \tag{2.8}$$

[1] In cutting the expansion of $\mathbb{E}_\alpha^{\pm}$ at first-order, I have implicitly assumed that the size of the relative fluctuations scales as $K^{-\frac{1}{2}}$ and therefore goes to zero as $K \to \infty$. Therefore, we consider averaged quantities from this point, i.e. $\langle x \rangle, \langle y \rangle, \langle n_M \rangle$, and $\langle n_W \rangle$, though do not change the notation for clarity.

Finally, multiplying through by K yields,

$$\begin{aligned}\frac{\mathrm{d}}{\mathrm{d}t}n_M &= T_M^+(n_M, n_W) - T_M^-(n_M, n_W),\\ \frac{\mathrm{d}}{\mathrm{d}t}n_W &= T_W^+(n_M, n_W) - T_W^-(n_M, n_W).\end{aligned} \tag{2.9}$$

Typically, Eqs. (2.9) can not be solved exactly for $n_M(t)$ and $n_W(t)$ since the rates are commonly non-linear functions of n_M and n_W. Let us consider now the specific case of interest to us. Here, the rates of increase and decrease of individuals of species $\alpha \in \{M, W\}$ are given by (Melbinger et al., 2010; Cremer et al., 2011; Wienand et al., 2017, 2018)

$$T_\alpha^+ = \frac{f_\alpha}{\overline{f}} n_\alpha \quad \text{and} \quad T_\alpha^- = \frac{n}{K} n_\alpha, \tag{2.10}$$

where f_α denotes the *fitness* of species α, and $\overline{f} = \frac{n_M f_M + n_W f_W}{n_M + n_W}$ denotes the average fitness of the entire population. Fitness, as briefly mentioned in Ch. 1, is a value assigned to a species denoting the reproductive capabilities of an individual of that species – a species with a higher fitness will reproduce more often. This is seen in the form of the birth rates of Eq. (2.10). The choice to rescale T_α^+ by the average fitness of the entire population is common for a broad range of evolutionary processes, though alternatives have been proposed (Traulsen et al., 2005). The convenience of this choice becomes clear when considering the evolution of the total population size n under these rates. Summing Eqs. (2.10) over α gives the overall rates for increase and decrease of the population size n. We find that we retrieve the logistic growth rates of Ch. 2.1 and therefore this system also undergoes logistic growth dynamics, seen directly by substituting these rates into the sum of Eqs. (2.9). Therefore, Eq. (2.2) has been obtained under a controlled approximation, unlike the method of Ch. 2.1.1. This is particularly useful, as it allows us to consider that the population size of this system is approximately constant at $n = K$ and independent of its composition, which will allow us to use the Moran process later. This reduces the dimensionality of the problem in the population composition evolution, as we need only consider the evolution of $n_M = K - n_W$. Then, the evolution of the composition, now given by $x \equiv n_M/n = n_M/K$ alone (with $y = 1 - x$), follows the first of Eqs. (2.8) with the rates of Eq. (2.10), giving

$$\begin{aligned}\frac{\mathrm{d}}{\mathrm{d}t}x &= x\left(\frac{f_M}{\overline{f}} - 1\right),\\ &= x(1-x)\frac{f_M - f_W}{\overline{f}},\end{aligned} \tag{2.11}$$

which is the adjusted replicator equation; see J. M. Smith (1982). Therefore, if $f_M > f_W$ then $x \to 1$ (and thus $y \to 0$), and if $f_M < f_W$ then $x \to 0$ (and thus $y \to 1$). This gives a clear qualitative understanding of the composition evolution at the MF level: if one species is fitter than the other, then its relative abundance increases.

A further useful consideration is that of *weak selection*, where there is only a small selective advantage to one of the species (Hofbauer & Sigmund, 1998; Wild & Traulsen, 2007). Let

us assume $f_W = 1$ and $f_M = 1 + s$ with $0 < s \ll 1$, therefore allowing the mutant species a small selective advantage. Eq. (2.11) is then approximated by

$$\frac{\mathrm{d}}{\mathrm{d}t}x \approx sx(1-x). \tag{2.12}$$

Therefore, at the MF level we expect an increase in the fraction of M in the population on a timescale of order $\mathcal{O}(1/s)$. Since $0 < s \ll 1$, this is typically far slower than the timescale on which the population size n evolves, where from Eq. (2.23) we expect this to occur on a timescale of order $\mathcal{O}(1)$. There is then a *timescale separation* between n and x, where n relaxes quickly while x relaxes slowly. We will make use of this relevant regime later; see Chs. 3 and 5. We now continue, and consider where this MF approximation breaks down.

2.2.2 Stochasticity and the impact of finite size

We again find that, while useful in large populations, the MF description fails to capture some crucial aspects of the dynamics in finite populations. For example, Eq. (2.11) predicts that the fitter species is certain to grow in abundance and get arbitrarily close to taking over the population, but will never fixate, i.e. reach $x = 0, 1$. Fixation, as introduced in Ch. 1, only occurs in finite populations as a stochastic effect due to DF. We now look to capture this process of fixation.

In systems such as those described in Ch. 2.1, we can make use of the approximately constant population size under logistic growth for $K \gg 1$, through the Moran process (Moran, 1958, 1962). Therefore, we approximate our system using a Moran process, which we term the Moran approximation (MA) of the system. In the MA we couple the processes of birth and death and define effective rates, such that the population size remains constant at $n = K$, i.e. each M birth is accompanied by a W death, and each W birth is accompanied by an M death. This allows the population to evolve in its composition, while maintaining a constant population size where $n_M = K - n_W$. The reactions

$$\begin{aligned}(n_M, n_W) &\xrightarrow{T^+_{\mathrm{MA}}} (n_M + 1, n_W - 1),\\ (n_M, n_W) &\xrightarrow{T^-_{\mathrm{MA}}} (n_M - 1, n_W + 1),\end{aligned} \tag{2.13}$$

maintaining the constant population size but allowing the composition of the population to evolve, occur at effective rates $T^{\pm}_{\mathrm{MA}}$. To obtain expressions for these rates we start by noting that changes in x in the MA according to Eq. (2.13) are of size $\Delta x = 1/K$. Taking the MF approximation for the first two moments of the ME of Eq. (2.7), we find

the evolution of x and the evolution of its variance σ_x^2 are given by[1]

$$\begin{aligned}\frac{\mathrm{d}}{\mathrm{d}t}x &= \frac{1-x}{K}(T_M^+ - T_M^-) - \frac{x}{K}(T_W^+ - T_W^-),\\ \frac{\mathrm{d}}{\mathrm{d}t}\sigma_x^2 &= \left(\frac{1-x}{K}\right)^2 (T_M^+ + T_M^-) + \left(\frac{x}{K}\right)^2 (T_W^+ + T_W^-).\end{aligned} \tag{2.14}$$

The effective rates T_{MA}^+ and T_{MA}^- correspond to an increase or decrease in x by an amount Δx, respectively. Therefore, separately (but obtained similarly), we have for the evolution of x and σ_x^2 in the MA that

$$\begin{aligned}\frac{\mathrm{d}}{\mathrm{d}t}x &= (T_{\mathrm{MA}}^+ - T_{\mathrm{MA}}^-)\Delta x,\\ \frac{\mathrm{d}}{\mathrm{d}t}\sigma_x^2 &= (T_{\mathrm{MA}}^+ + T_{\mathrm{MA}}^-)(\Delta x)^2.\end{aligned} \tag{2.15}$$

Thus, we can combine Eqs. (2.14) and (2.15) to find general expressions for the effective rates, $T_{\mathrm{MA}}^{\pm}$, leading to the same evolution of the mean and variance of x as the true microscopic rates. Therefore, the population evolution given by Eq. (2.2.1) and the effective process are equivalent at the level of the Fokker-Planck approximation (van Kampen, 1992; Gardiner, 2009). These effective rates are given by

$$T_{\mathrm{MA}}^{\pm} = \frac{1}{2\Delta x}\left(\frac{\frac{\mathrm{d}}{\mathrm{d}t}\sigma_x^2}{\Delta x} \pm \frac{\mathrm{d}}{\mathrm{d}t}x\right). \tag{2.16}$$

Substituting Eqs. (2.14) into Eq. (2.16), this simplifies to (Wienand et al., 2017, 2018)

$$\begin{aligned}T_{\mathrm{MA}}^+(n_M) &= \frac{T_M^+(n_M)\,T_W^-(n_M)}{K},\\ T_{\mathrm{MA}}^-(n_M) &= \frac{T_W^+(n_M)\,T_M^-(n_M)}{K}.\end{aligned}$$

Noting that the MA of the system also has absorbing boundaries at $n_M = 0, K$, we see that in this approximation we have obtained a one-dimensional random walk with state-dependent rates and two absorbing boundaries. If the $n_M = K$ state is reached, then the mutant has fixated the population, whereas if $n_M = 0$ is reached, the wild-type has fixated the population. In such a case, we can define *first-step equations* (difference equations) for the fixation probability of the mutant, $\phi_{\mathrm{MA}}(n_M)$, and the mean fixation time (MFT), $\tau_{\mathrm{MA}}(n_M)$, assuming initially n_M mutant individuals (Gardiner, 2009; Ashcroft et al., 2014). Note that in this thesis we always consider the unconditional MFT, i.e. the

[1] Alternatively, we could have carried out our van Kampen expansion of the ME to second order in the previous section to obtain a Fokker-Planck equation. From this, the expressions for the evolution of the mean and variance can be read off directly (van Kampen, 1992; Gardiner, 2009).

mean time to fixation regardless of which species fixates. These are given by

$$\begin{aligned}\left[T^{+}_{\mathrm{MA}}(n_M)+T^{-}_{\mathrm{MA}}(n_M)\right]\phi_{\mathrm{MA}}(n_M) &= \underbrace{T^{+}_{\mathrm{MA}}(n_M)\phi_{\mathrm{MA}}(n_M+1)}_{\text{fixation from } n_M+1}+\underbrace{T^{-}_{\mathrm{MA}}(n_M)\phi_{\mathrm{MA}}(n_M-1)}_{\text{fixation from } n_M-1},\\ \left[T^{+}_{\mathrm{MA}}(n_M)+T^{-}_{\mathrm{MA}}(n_M)\right]\tau_{\mathrm{MA}}(n_M) &= \underbrace{T^{+}_{\mathrm{MA}}(n_M)\tau_{\mathrm{MA}}(n_M+1)}_{\text{fixation from } n_M+1}+\underbrace{T^{-}_{\mathrm{MA}}(n_M)\tau_{\mathrm{MA}}(n_M-1)}_{\text{fixation from } n_M-1}+1,\end{aligned} \tag{2.17}$$

where the motivation is to look one "step" into the future and consider the subsequent evolution of the system, and the $+1$ on the right hand side of the first-step equation for τ_{MA} is a time increment. These are classical results, and can be solved exactly to give (Antal & Scheuring, 2006; Traulsen & Haeurt, 2009)

$$\phi_{\mathrm{MA}}(n_M) = \frac{1+\sum_{k=1}^{n_M-1}\prod_{i=1}^{k}\gamma_{\mathrm{MA}}(i)}{1+\sum_{k=1}^{K-1}\prod_{i=1}^{k}\gamma_{\mathrm{MA}}(i)}, \tag{2.18}$$

$$\begin{aligned}\tau_{\mathrm{MA}}(n_M) = \phi_{\mathrm{MA}}(n_M)&\sum_{k=n_M}^{K-1}\sum_{i=1}^{k}\frac{\prod_{m=i+1}^{k}\gamma_{\mathrm{MA}}(m)}{T^{+}_{\mathrm{MA}}(i)}\\ &-\left[1-\phi_{\mathrm{MA}}(n_M)\right]\sum_{k=1}^{n_M-1}\sum_{i=1}^{k}\frac{\prod_{m=i+1}^{k}\gamma_{\mathrm{MA}}(m)}{T^{+}_{\mathrm{MA}}(i)},\end{aligned} \tag{2.19}$$

where $\gamma_{\mathrm{MA}}(i) = \frac{T^{-}_{\mathrm{MA}}(i)}{T^{+}_{\mathrm{MA}}(i)}$. For the specific rates given by Eq. (2.10), we find $\gamma_{\mathrm{MA}}(i) = \gamma_{\mathrm{MA}} = \frac{f_W}{f_M}$. This simplifies the expression for the fixation probability significantly, giving

$$\phi_{\mathrm{MA}}(n_M) = \frac{1-\left(\frac{f_W}{f_M}\right)^{n_M}}{1-\left(\frac{f_W}{f_M}\right)^{K}}, \tag{2.20}$$

while the expression for $\tau_{\mathrm{MA}}(n_M)$ remains unwieldy. Therefore, we are able to capture the evolution of the population size and its composition in a constant environment.

Consider again the weak selection limit used to obtain Eq. (2.12), with $f_M = 1+s$ and $f_W = 1$ where $0 < s \ll 1$. In this limit, assuming $K \gg 1$, we have

$$\phi_{\mathrm{MA}}(n_M) \approx \frac{1-\exp(-n_M s)}{1-\exp(-Ks)},$$

which demonstrates the impact and interplay of selection through the selective advantage, s, and diffusion through the population size, K. For $Ks \gg 1$ selection is the dominating factor and $\phi_{\mathrm{MA}}(n_M) \approx 1$, while for $Ks \ll 1$, diffusion drives fixation and $\phi_{\mathrm{MA}} \approx n_M/K$, with a transition around $Ks \sim 1$. These parameters define the environment of the population. Should this environment change, which as discussed previously is ubiquitous across natural systems, these parameters are liable to change. This will therefore directly affect

the fixation probability of the mutant, and the MFT. Capturing the effect of EV on such processes is typically non-trivial, but is crucial if we hope to understand the behaviour of the real biological systems.

I now look to introduce environmental variability, showing how it is modelled here, and concretely how we capture its effects through an illustrative example.

2.3 Dichotomous Markov noise

Dichotomous Markov noise (DMN), as discussed in Ch. 1, is a simple form of noise, where two states are switched between with constant rates. Defining a time-varying random variable $\xi(t)$ that evolves according to DMN, we have $\xi \in \{\xi_-, \xi_+\}$ and

$$\xi = \xi_+ \xrightarrow{\nu_+} \xi_- \text{ and } \xi = \xi_- \xrightarrow{\nu_-} \xi_+. \tag{2.21}$$

where $\nu_\pm$ are the switching rates of the DMN. It is useful to define the average switching rate ν and the switching bias δ as

$$\nu \equiv \frac{\nu_- + \nu_+}{2} \text{ and } \delta \equiv \frac{\nu_- - \nu_+}{2\nu},$$

such that $\nu_\pm = \nu(1 \mp \delta)$. This means that $\delta > 0$ corresponds to a bias towards time spent in the $\xi(t) = \xi_+$ state, while $\delta < 0$ indicates more time in the $\xi(t) = \xi_-$ state. Herein, I initialise the DMN from its stationary distribution (i.e. the probability distribution of ξ attained at long times), giving $\xi(0) = \xi_\pm$ with probabilities $(1 \pm \delta)/2$, and I choose $\xi_\pm = \pm 1$ for simplicity and without loss of generality. Thus, for $\xi(t)$ we find the average over its stationary distribution $\langle \xi(t) \rangle = \delta$ and autocovariance (autocorrelation up to a constant) $\langle \xi(t)\xi(t') \rangle - \langle \xi(t) \rangle \langle \xi(t') \rangle = (1 - \delta^2) \exp(-2\nu|t - t'|)$, where $\langle . \rangle$ here denotes the ensemble average. The correlation time of the DMN, $1/(2\nu)$, is half of the inverse of the average switching rate of ξ.

I will now show how DMN is implemented to model EV through a carrying capacity that changes in time.

2.3.1 Stochastically switching carrying capacity

Using the DMN, I look to introduce EV through sudden changes in available resources, such as in cycles of feast and famine (Hengge-Aronis, 1993; Srinivasan & Kjelleberg, 1998; Merritt & Kuehn, 2018; Himeoka & Mitarai, 2020). This is implemented by allowing the carrying capacity to fluctuate in time between two values, such that we have $K(t) \in \{K_-, K_+\}$, with $K_+ > K_-$, mimicking the effect of a varying nutrient availability. We denote K_+ the large carrying capacity, associated with mild environmental conditions (high nutrient availability) and K_- the small carrying capacity, associated with harsh environmental conditions (low nutrient availability). As motivated in Ch. 1, this allows us to simply model sudden extreme changes in the population size, particularly the formation of population bottlenecks (Wahl et al., 2002; Brockhurst, 2007; Patwa & Wahl, 2010; G.

Lambert & Kussell, 2014; Wienand et al., 2017, 2018; Mahrt et al., 2021; Shibasaki et al., 2021), and make analytical progress in capturing their effects. To achieve this, $K(t)$ is driven by the DMN $\xi(t) = \{-1, 1\}$ that randomly switches between -1 and 1 as given in Eq. (2.21). Concretely, we then have (Wienand et al., 2017, 2018; Taitelbaum et al., 2020, 2023)

$$K(t) = \frac{1}{2}\left[K_+ + K_- + \xi(t)(K_+ - K_-)\right], \tag{2.22}$$

which, with $K_0 \equiv \frac{K_+ + K_-}{2}$ and $\gamma \equiv \frac{K_+ - K_-}{2K_0}$, can conveniently be written as

$$K(t) = K_0[1 + \gamma\xi(t)].$$

Through analogy with the constant environment case, this suggests that, at the MF level, the population size now denoted N evolves according to the stochastic differential equation

$$\dot{N} = N\left(1 - \frac{N}{K(t)}\right) = \begin{cases} N\left(1 - \frac{N}{K_-}\right) & \text{if } \xi = -1, \\ N\left(1 - \frac{N}{K_+}\right) & \text{if } \xi = +1, \end{cases} \tag{2.23}$$

where a dot denotes the time derivative here and throughout this thesis. This defines a *piecewise-deterministic Markov process* (PDMP), consisting of deterministic evolution interspersed with stochastic switches (Davis, 1984). Therefore, N will stochastically be driven out of equilibrium and generally vary significantly. It is useful to consider the QPSD of N under this PDMP description, where we consider only fluctuations due to the environment as given by Eq. (2.23), i.e. ignoring DF, as we will be able to obtain its analytical form and see that it approximates qualitatively well the true QPSD of the system (Wienand et al., 2017, 2018).

To do so, following the derivations of Horsthemke and Lefever (1984) and Ridolfi et al. (2011), we start by defining the pair process (N, ξ). In what follows we abuse notation slightly by using ξ to denote both the DMN process and its instantaneous state in a given realisation. Here, ξ fluctuates independently of N, according to Eq. (2.21) and N evolves according to the stochastic differential equation defined in Eq. (2.23). Concretely, I define that $\dot{N} = \mathcal{F}_\xi(N)$ where $\mathcal{F}_\xi(N) = N\left(1 - \frac{N}{K_0(1+\gamma\xi)}\right)$. The Chapman-Kolmogorov equation for the pair process (N, ξ) is given by

$$p(n, \xi, t + \delta t | n_0, \xi_0, 0) = \sum_{\alpha \in \{\xi_-, \xi_+\}} \int \mathrm{d}m \; p(n, \xi, t + \delta t | m, \alpha, t) p(m, \alpha, t | n_0, \xi_0, 0),$$

where $p(n, \xi, t | n', \xi', t')$ denotes the probability of being in state (n, ξ) at time t given the system was in state (n', ξ') at time t', n_0 and ξ_0 denote the values of the respective variables at $t = 0$, and δt is a small time increment. This simply states that, by the Markov property, the probability to go from the state (n_0, ξ_0) at time 0 to the state (n, ξ) at time $t + \delta t$ can be captured by summing (and integrating) over all possible intermediate states (m, α) occurring at a time t (van Kampen, 1992; Gardiner, 2009). For brevity we will introduce $p(n, \xi, t|0) \equiv p(n, \xi, t | n_0, \xi_0, 0)$ and show this derivation for the case only

of $\xi = \xi_+$ as the derivation for $\xi = \xi_-$ is almost identical. Furthermore, we will use $\xi_\pm$ to denote the environmental states explicitly for clarity. Allow $f(n)$ to be a sufficiently smooth real-valued function with compact support. Then we have that

$$\int \mathrm{d}n\ f(n)p(n,\xi_+,t+\delta t|0) = \sum_\alpha \int \mathrm{d}m\ p(m,\alpha,t|0)\left[\int \mathrm{d}n\ f(n)p(n,\xi_+,t+\delta t|m,\alpha,t)\right].$$

We can now subtract $\int \mathrm{d}n\ f(n)p(n,\xi_+,t|0)$ from each side, divide by δt and take the limit as $\delta t \to 0$ to obtain on the left-hand side

$$\lim_{\delta t\to 0} \frac{\int \mathrm{d}n\ f(n)\left[p(n,\xi_+,t+\delta t|0) - p(n,\xi_+,t|0)\right]}{\delta t} = \int \mathrm{d}n\ f(n)\partial_t p(n,\xi_+,t|0), \tag{2.24}$$

where we can exchange the integral and the limit as $\partial_t p(n,\xi_+,t|0)$ is assumed to exist and be continuous. Now to evaluate the right-hand side we must find expressions for $p(n,\xi_+,t+\delta t|m,\alpha,t)$ for $\alpha \in \{\xi_-,\xi_+\}$ in the limit as $\delta t \to 0$. To do this we start by considering the transition rates for the possible transitions of ξ in a time δt. The transition probability for no jump $\xi_+ \to \xi_+$ is $1-\nu_+\delta t + o(\delta t)$ and for one jump $\xi_- \to \xi_+$ is $\nu_-\delta t + o(\delta t)$. The probability for two or more jumps is of order $o(\delta t)$ and thus in our limit these need not be considered. If ξ does not jump then $N = m$ at time t and we have $n = m + \mathcal{F}_{\xi_+}(m)\delta t + o(\delta t)$ at time $t+\delta t$. Thus we have that

$$p(n,\xi_+,t+\delta t|m,\xi_+,t) = \delta(n - [m + \mathcal{F}_{\xi_+}(m)\delta t])(1-\nu_+\delta t) + o(\delta t)$$

where $\delta(x)$ denotes the Dirac-delta function. If we now consider the case of a single jump occurring in the interval $[t, t+\delta t)$, and denote the fraction of time passed prior to a jump as τ whereby this fraction is uniformly distributed on $[0,1]$, then (starting at $N = m$ at time t) we find that N at a time $t+\delta t$ takes the value

$$n = m + \tau\mathcal{F}_{\xi_-}(m)\delta t + (1-\tau)\mathcal{F}_{\xi_+}(m)\delta t + o(\delta t)$$

giving us

$$p(n,\xi_+,t+\delta t|m,\xi_-,t) = \delta(n - [m + \tau\mathcal{F}_{\xi_-}(m)\delta t + (1-\tau)\mathcal{F}_{\xi_+}(m)\delta t])\nu_-\delta t + o(\delta t).$$

Substituting these expressions for $p(n,\xi_+,t+\delta t|m,\xi_+,t)$ and $p(n,\xi_+,t+\delta t|m,\xi_-,t)$ into the right-hand side of Equation (2.24) and neglecting terms of order $o(\delta t)$ we get

$$\begin{aligned}\int \mathrm{d}n\ f(n)\partial_t p(n,\xi_+,t|0) = \lim_{\delta t\to 0}\frac{1}{\delta t}\Bigg[&\int \mathrm{d}n\ p(n,\xi_+,t|0)f(n+\mathcal{F}_{\xi_+}(n)\delta t)(1-\nu_+\delta t)\\ &+ \int \mathrm{d}n\ p(n,\xi_-,t|0)f(n+\tau\mathcal{F}_{\xi_-}(n)\delta t + (1-\tau)\mathcal{F}_{\xi_+}(n)\delta t)\nu_-\delta t\\ &- \int \mathrm{d}n\ f(n)p(n,\xi_+,t|0)\Bigg].\end{aligned}$$

We can now take a Taylor expansion of $f(n)$ to first order, neglect terms of order $o(\delta t)$

and integrate by parts using the compact support of $f(n)$ to obtain

$$\int \mathrm{d}n\ f(n)\partial_t p(n,\xi_+,t|0) = \int \mathrm{d}n\ f(n)\{-\partial_n[\mathcal{F}_{\xi_+}(n)p(n,\xi_+,t|0)] \\ -\nu_+ p(n,\xi_+,t|0)+\nu_- p(n,\xi_-,t|0)\}.$$

Since $f(n)$ was chosen as an arbitrary function, we have

$$\partial_t p(n,\xi_+,t) = -\partial_n(\mathcal{F}_{\xi_+}(n)p(n,\xi_+,t)) - \nu_- p(n,\xi_+,t) + \nu_+ p(n,\xi_-,t),$$

and a similar result holds if we first consider $\xi = \xi_-$. Denoting $p(n,\xi,t)$ as p_ξ for convenience, we therefore have

$$\begin{aligned}\partial_t p_\xi &= -\partial_n(\mathcal{F}_\xi(n)p_\xi) - \nu_{-\xi}p_\xi + \nu_\xi p_{-\xi}, \\ &= -\partial_n J_\xi \text{ where } J_\xi = \mathcal{F}_\xi p_\xi + \int^n \mathrm{d}n'(\nu_{-\xi}p_\xi - \nu_\xi p_{-\xi}).\end{aligned} \tag{2.25}$$

If we now consider p_ξ and J_ξ at stationarity, denoted p^*_ξ and J^*_ξ, we have

$$\partial_t p^*_\xi = -\partial_n J^*_\xi = 0.$$

This implies that $\partial_n(J^*_+ + J^*_-) = 0$ and so, taking the natural boundary conditions, i.e. there is no probability current at the boundaries (Gardiner, 2009), gives $J^*_+ + J^*_- = 0$. We thus find that

$$p^*_\xi = -\frac{\mathcal{F}_{-\xi}}{\mathcal{F}_\xi}p^*_{-\xi}.$$

Using this in conjunction with Eq. (2.25) gives

$$\partial_n(\mathcal{F}_\xi p^*_\xi) + \left(\frac{\nu_+}{\mathcal{F}_{\xi_-}} + \frac{\nu_-}{\mathcal{F}_{\xi_+}}\right)\mathcal{F}_\xi p^*_\xi = 0,$$

which we can rewrite by dividing through by $\mathcal{F}_\xi p^*_\xi$, integrating, and exponentiating to give

$$\mathcal{F}_\xi p^*_\xi = \xi\mathcal{Z}\exp\left[-\int\left(\frac{\nu_+}{\mathcal{F}_{\xi_-}} + \frac{\nu_-}{\mathcal{F}_{\xi_+}}\right)\mathrm{d}n\right],$$

where $\mathcal{Z}$ is a normalisation constant ensuring $\int p_\xi\ \mathrm{d}n = 1$. Therefore, the stationary distributions conditioned on the environmental state are given by

$$p^*_\xi(n) = \begin{cases} \frac{\mathcal{Z}}{n^2}\left(\frac{K_+-n}{n}\right)^{\nu_--1}\left(\frac{n-K_-}{n}\right)^{\nu_+} & \text{if } \xi=\xi_+=+1, \\ \frac{\mathcal{Z}}{n^2}\left(\frac{K_+-n}{n}\right)^{\nu_-}\left(\frac{n-K_-}{n}\right)^{\nu_+-1} & \text{if } \xi=\xi_-=-1, \end{cases} \tag{2.26}$$

where the $p^*_\xi(n)$ have support $[K_-,K_+]$. Furthermore, we can construct the joint stationary distribution $p^*(n) = [(1+\delta)p^*_+(n) + (1-\delta)p^*_-(n)]/2$ giving

$$p^*(n) = \frac{\mathcal{Z}}{n^2}\left(\frac{K_+-n}{n}\right)^{\nu_--1}\left(\frac{n-K_-}{n}\right)^{\nu_+-1}, \tag{2.27}$$

where $\mathcal{Z}$ has been redefined to absorb a constant factor and the approximate QPSD has support $[K_-, K_+]$. Herein, we shall refer to $p^*(n)$ and $p^*_\xi(n)$ as simply $p(n)$ and $p_\xi(n)$ for notational clarity. Intuitively, these distributions can be understood through the lens of a histogram where population sizes are binned through time. The histogram for $p_+(n)$ is binned while $\xi = \xi_+$, for $p_-(n)$ while $\xi = \xi_-$, and $p(n)$ is always binned regardless of ξ.

This distribution has a particularly simple form and captures well many aspects of the distribution, while neglecting the width of its peaks since we have ignored DF. It is possible to capture the width of the peaks using the linear noise approximation, where it is seen that the true distribution is captured more accurately. However, it is far more complex and computationally expensive to use, and little is gained over using the analytically tractable QPSD of the PDMP (Wienand et al., 2018).

2.3.2 Illustrative example

To illustrate the utility of the approximate QPSD of Eq. (2.27), I will demonstrate how it can be used in a simple case, considered in Wienand et al. (2017). Consider a two-species population governed by the birth and death rates defined in Eq. (2.10), where we again denote the species as either mutant (M) or wild-type (W). We also now allow $K \to K(t)$ in the death rates to vary according to Eq. (2.22), driven between $K = K_+$ and $K = K_-$ by a DMN process labelled ξ. For simplicity, we will consider symmetric switching in the environment, i.e. $\nu_+ = \nu_- = \nu$ and $\delta = 0$. The ME for this system is thus given by

$$\partial_t P(n_M, n_W, \xi, t) = \sum_{\alpha \in \{M,W\}} \left[\left(\mathbb{E}_\alpha^- - 1\right) \frac{f_\alpha}{\overline{f}} n_\alpha + \left(\mathbb{E}_\alpha^+ - 1\right) \frac{n}{K} n_\alpha \right] P(n_M, n_W, \xi, t) + \nu \left[P(n_M, n_W, -\xi, t) - P(n_M, n_W, \xi, t) \right],$$

with $P(n_M, n_W, \xi, t) = 0$ for $n_M < 0$ or $n_W < 0$, where the operators $\mathbb{E}_\alpha^\pm$ are defined as in Eq. (2.7). The top row of the right-hand side gives the birth and death dynamics already discussed in Ch. 2.2.1, while the bottom row makes explicit the switching environment through the DMN variable ξ.

It is first useful to consider the population size distribution and how this depends on the switching rate ν. Herein I simply write N for both the stochastic process N and its instantaneous value n. We will consider how the approximate QPSD compares to the true distribution, both through qualitative comparison of the distributions and quantitative comparison of the average population size of the distributions, denoted $\langle N \rangle$. We see from Fig. 2.2(a) that for slow switching rate, $\nu \ll 1$, the distribution is bimodal, sharply peaked around each of $K_\pm$. Here, the population is initialised with a carrying capacity $K(0) = K_\pm$, each with a probability 1/2 due to symmetric switching, and does not switch for long periods of time. In this limit, the QPSD given by Eq. (2.27) becomes approximately a sum of delta functions, $p(N) = \frac{1}{2}\delta(N - K_+) + \frac{1}{2}\delta(N - K_-)$, one for each of the possible starting states. Therefore, the average population size is given by $\langle N \rangle = \frac{K_+}{2} + \frac{K_-}{2} = K_0$.

On the other hand, for fast switching rate, $\nu \gg 1$, the environment switches on a faster

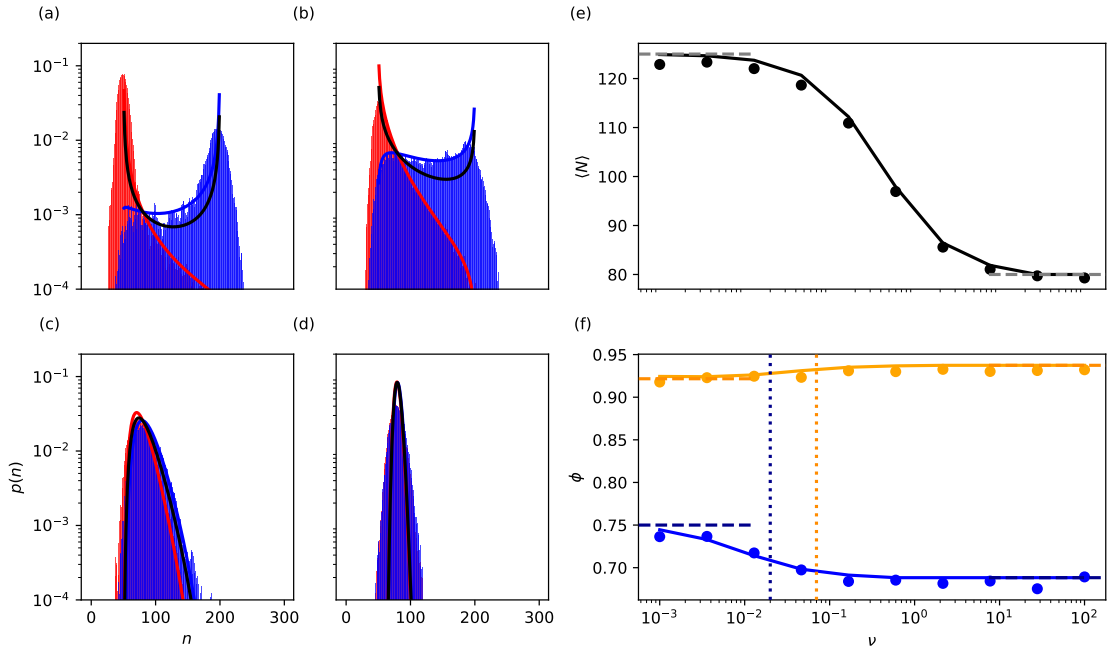

Figure 2.2: QPSD and fixation dynamics for the illustrative example. (a-d): the QPSD for (a) $\nu = 0.05$, (b) 0.5, (c) 5, and (d) 50. The red and blue lines correspond to $p_\xi(n)$ given by Eq. (2.26) for $\xi = -1$ and $\xi = 1$, respectively. The black line corresponds to $p(n)$ given by Eq. (2.27). The red and blue bars correspond to simulation data for the QPSD conditioned on $\xi = -1$ and $\xi = 1$, respectively, with their overlapping regions appearing purple. (e): average population size $\langle N \rangle$ against switching rate ν. Solid line is theory given by Eq. (2.28) while simulation data are plotted as circles. Horizontal dashed grey lines are from the slow and fast switching limits given by $\langle N \rangle = K_0$ and $\langle N \rangle = \mathcal{K}$, respectively. (f): fixation probability of mutant in a switching environment ϕ against ν for $s = 0.02$ (blue) and $s = 0.07$ (orange). Solid lines calculated using Eq. (2.29) and simulation data plotted as circles. Horizontal dashed lines for each s (with matching colour) are the slow and fast switching limits given by $\phi(n_M) \approx \frac{1}{2}(\phi_{\mathrm{MA}}(n_M, K_+) + \phi_{\mathrm{MA}}(n_M, K_-))$ and $\phi(n_M) \approx \phi_{\mathrm{MA}}(n_M, \mathcal{K})$, respectively. The vertical dotted lines give the point $\nu = s$, indicating the transition point between slow and fast switching for each s (with matching colour). In each case, $K_+ = 200$, $K_- = 50$, $\delta = 0$, and initial composition $x = 0.5$.

timescale than that of the relaxation dynamics of the population size which relaxes on a timescale $\sim \mathcal{O}(1)$; see Eq. (2.23). Therefore, the population feels an 'effective environment', given by an effective carrying capacity which the distribution becomes unimodal around. This is seen in Fig. 2.2(d), both in the analytic approximation of the QPSD and the results from simulations; see Appendix D. The effective carrying capacity in this limit, denoted $\mathcal{K}$, is due to the self-averaging of the DMN. Its expression is obtained from considering (Wienand et al., 2017, 2018)

$$\dot{N} = \mathcal{F}_\xi = N\left(1 - \frac{N}{K_0(1+\xi\gamma)}\right),$$

which can be rewritten, using $\xi^2 = 1$, as

$$\mathcal{F}_\xi = N\left(1 - \frac{N(1-\xi\gamma)}{K_0(1-\gamma^2)}\right),$$

and averaged over the stationary distribution of ξ, giving

$$\begin{aligned}\langle\mathcal{F}\rangle &= N\left(1 - \frac{N(1-\delta\gamma)}{K_0(1-\gamma^2)}\right), \\ &= N\left(1 - \frac{N}{\mathcal{K}}\right),\end{aligned}$$

where $\langle\xi\rangle = \delta$ and $\mathcal{K} = K_0(1-\gamma^2)/(1-\delta\gamma)$, simplifying to $\mathcal{K} = K_0(1-\gamma^2)$ in the case of symmetric switching. Hence, sufficiently fast environmental switching reproduces an effectively constant environment, which is also captured by the approximate QPSD with $p(N) \approx \delta(N-\mathcal{K})$. The average population size $\langle N\rangle = \mathcal{K}$ is then also adequately captured in this limit; see Fig. 2.2(e).

When not in the limits of fast or slow switching, we consider intermediate switching where $\nu \sim 1$. In fact, it is at $\nu = 1$ where $p(N)$ undergoes a noise-induced transition: increasing ν from below to above 1, the approximate QPSD transitions from a bimodal to unimodal distribution. Remarkably, we find that $p(N)$ is still able to capture key features of the true distribution; see Fig. 2.2(b,c). Furthermore, now defining

$$\langle N\rangle = \int_{K_-}^{K_+} N p(N)\, \mathrm{d}N, \tag{2.28}$$

we see in Fig. 2.2(e) that across all ν, using our approximate expression for the QPSD excellently captures $\langle N\rangle$ from simulations. Due to the population size following logistic growth dynamics as in Eq. (2.23), N takes longer to grow than it does to decay following an environmental switch. This is because, assuming $K_+ \gg K_-$, immediately following a switch from K_- to K_+ we have $\dot{N} \approx K_-\left(1 - \frac{K_-}{K_+}\right) \approx K_-$, while following a switch from K_+ to K_- we have $\dot{N} \approx K_+\left(1 - \frac{K_+}{K_-}\right) \approx -K_+^2/K_-$, where $K_+^2/K_- \gg K_-$. This means that for $\nu < 1$, the peak at $N = K_-$ is larger than the peak at $N = K_+$. The peaks are most similar for $\nu \to 0$, with the peak around $N = K_+$ decreasing as ν increases and approaches 1. For larger ν, the population becomes unimodal around $\mathcal{K}$. This explains

the behaviour of $\langle N \rangle$ with ν, where we see it smoothly decreases as ν increases. Having determined that $p(N)$ adequately captures the ecological dynamics of the population, we now look to how we may utilise $p(N)$ in capturing its impact on fixation.

Concretely, we will consider the case of a small selective advantage to the mutant, such that $f_W = 1$ and $f_M = 1 + s$ where $0 < s \ll 1$, and assume that the population is initially composed of mutants and wild-types in equal measure, i.e. $n_M = K(0)/2$ and $n_W = K(0)/2$. As seen in Eq. (B.1), we then have a timescale separation between the composition evolution x, given by Eq. (2.12), evolving on a timescale of order $\mathcal{O}(1/s)$, while the evolution of the population size N, given by Eq. (2.23), evolves on a timescale of order $\mathcal{O}(1)$. Therefore, while N relaxes rapidly, x does so slowly. Therefore, during the evolution of x towards fixation, we expect N to explore the entire QPSD. This suggests a way to proceed, where $p(N)$ captures the variation in N due to EV, and ϕ_{MA} given by Eq. (2.20) captures the probability of fixation for each N in the QPSD. We therefore seek to combine these results in such a way that their combination captures fixation under an EV-driven population size. To do so, we must ensure that the timescales on which ϕ_{MA} and $p(N)$ evolve are matched. Hence, we rescale the switching rate ν in $p(N)$, such that $\nu \to \nu/s$, where the average number of environmental switches prior to fixation scales as ν/s, so that the timescale of environmental switching is mapped onto that of fixation. We denote this rescaled $p(N)$ as $p_{\nu/s}(N)$ for clarity. We can then combine these quantities for the fixation probability in a switching environment, ϕ, to give (Wienand et al., 2017, 2018; Taitelbaum et al., 2020, 2023)

$$\phi(n_M) = \int_{K_-}^{K_+} \phi_{\mathrm{MA}}(n_M, N)\; p_{\nu/s}(N)\; \mathrm{d}N, \tag{2.29}$$

where we have explicitly included the dependence on population size N of ϕ_{MA}. Similarly, the mean fixation time in a switching environment, τ, can be captured through

$$\tau(n_M) = \int_{K_-}^{K_+} \tau_{\mathrm{MA}}(n_M, N)\; p_{\nu/s}(N)\; \mathrm{d}N,$$

though we focus on the fixation probability in this example for simplicity. We see from Fig. 2.2(f) that, similar to the analysis of $\langle N \rangle$, in the slow ($\nu \ll s$) and fast ($\nu \gg s$) switching limits, we have $\phi(n_M) \approx \frac{1}{2}(\phi_{\mathrm{MA}}(n_M, K_+) + \phi_{\mathrm{MA}}(n_M, K_-))$ and $\phi(n_M) \approx \phi_{\mathrm{MA}}(n_M, \mathcal{K})$, respectively. This can be understood as follows: should the switching be far slower than the timescale of fixation, the population is initialised with a given carrying capacity and will fixate in that carrying capacity prior to a switch; should the switching be much faster, the carrying capacity rapidly switches between its two values, and fixation occurs with an effective population size of $N \approx \mathcal{K}$. Remarkably, the predictions of Eq. (2.29) also quantitatively capture the behaviour in the intermediate switching regime. Furthermore, we see that increasing the switching rate of the environment can act to either increase or decrease the probability of mutant fixation, depending on s. This example demonstrates the power of using Eq. (2.27) in incorporating the environment-driven ecological dynamics into the analysis of population evolution and fixation, and the impact that EV can have

on the evolution of a population. In the following chapters, we shall similarly utilise our approximation for the QPSD on more complex systems of interest.

Chapter 3

Cooperative antimicrobial resistance

The rise of AMR is a pressing global issue (Eliopoulos et al., 2003; Gothwal & Shashidhar, 2015; O'Neill, 2016; Dadgostar, 2019; Murray et al., 2022). O'Neill (2016) estimated that 700,000 deaths each year are directly attributable to AMR, with this projected to rise to 10 million by 2050 without intervention. Not only is this an enormous human cost, but this is economically crippling, with costs estimated at 100 trillion USD over the same time frame in terms of losses in global production. It is therefore of the utmost importance to develop our understanding of how AMR evolves (Bottery et al., 2021), with the hope that we uncover mechanisms for preventing and eradicating it.

One common mechanism for AMR involves the production by resistant cells of an enzyme which can inactivate antimicrobial drugs (Davies, 1994; Brook, 2004; G. D. Wright, 2005; Brook, 2009; Shahid et al., 2009; Yurtsev et al., 2013). This enzyme production process has some associated metabolic cost to the resistant cell, i.e. the resistant cells divert some of their energy away from replication and towards enzyme production. This provides the resistant cells with protection in the presence of an antimicrobial drug. Also present are sensitive cells, which pay no metabolic cost but are impeded heavily by antimicrobial if it is present. The enzyme produced by the resistant cells may be either intracellular or extracellular. An intracellular enzyme only breaks down the antimicrobial within the cell, making resistance private to the resistant cells. In this case, the problem considered here reduces to that of Ch. 2.3.2 and Wienand et al. (2017, 2018) and the resistance is not cooperative. If the enzyme is extracellular, it breaks down antimicrobial in the medium itself around the resistant cell. Therefore, when the abundance of resistant cells exceeds some threshold, the enzyme is sufficiently abundant in the medium to also break down the antimicrobial present there. This provides resistance to the sensitive cells which have paid no metabolic cost. Below this threshold, there is insufficient enzyme in the medium and sensitive cells suffer the effects of the antimicrobial. The concentration of antimicrobial above which it inhibits the sensitive cells is known as the *minimum inhibitory concentration* (MIC). This behaviour may then be viewed as the antimicrobial concentration being raised

above or brought below its MIC, depending on the abundance of resistant cells which acts as a proxy for the abundance of resistance enzyme.

In this case, AMR can be viewed as a thresholded cooperative behaviour where inactivation of the antimicrobial throughout the medium is considered a public good. Therefore, below the threshold the resistant cells are better off, increasing in abundance, while when above this threshold the sensitive cells are better off, meaning resistant cells decrease in abundance as was illustrated previously in Fig. 1.4 (see also Figs. 3.3(a) and 3.6(a)). In static environments where the population is large, the population is then driven towards the threshold, which leads to a long-lived coexistence of sensitive and resistant strains during antimicrobial treatment, where neither species is eradicated (Yurtsev et al., 2013; Vega & Gore, 2014; Meredith et al., 2015; Bottery et al., 2016). How this picture changes when the environment varies in time is not well understood, and thus is the focus of this chapter.

In this chapter, I will investigate two models of cooperative AMR, where a cooperator resistant strain, R, competes with a defector sensitive strain, S, to fixate the population. Here, I assume that the cooperative resistance mechanism is mediated by the cooperator strain, which pays some metabolic cost to produce an extracellular enzyme. This enzyme hydrolises antimicrobial in the medium. Furthermore, I assume that the medium (composed of antimicrobial and nutrients) is being continuously replenished. This mimics the chemostat setup of experimental investigations, described in Ch. 1, where environmental factors can be held constant, allowing the ecological dynamics to reach a steady state (Novick & Szilard, 1950; James, 1961). Cooperators are always resistant to the antimicrobial, since the enzyme they produce is able to break it down. Defectors are not generally protected against the antimicrobial by the enzyme. However, if the cooperators exceed some threshold in either absolute or relative abundance (each choice requiring its own investigation; see later), there is sufficient enzyme in the medium for the antimicrobial to be brought below its MIC and defectors are also protected from the antimicrobial without having paid the metabolic cost to produce the enzyme, as described previously.

The two choices for the cooperation threshold (in absolute or relative abundance) are entirely equivalent when the environment stays constant and $N(0) = K(0)$, but under a time-varying environment implemented as in Ch. 2.3.1 a threshold in absolute abundance corresponds to a *time-varying resource concentration* in a fixed volume, whereas a threshold in relative abundance corresponds to a *time-varying volume of resource* at fixed concentration; see Fig. 3.1.

Contents of this chapter appear in Hernández-Navarro et al. (2023) and Hernández-Navarro, Asker, and Mobilia (2024).

3.1 Model description

In the model, I consider a population of size N, comprised of N_R resistant cells and $N_S = N - N_R$ sensitive cells. The composition of the population $x = N_R/N$ gives the

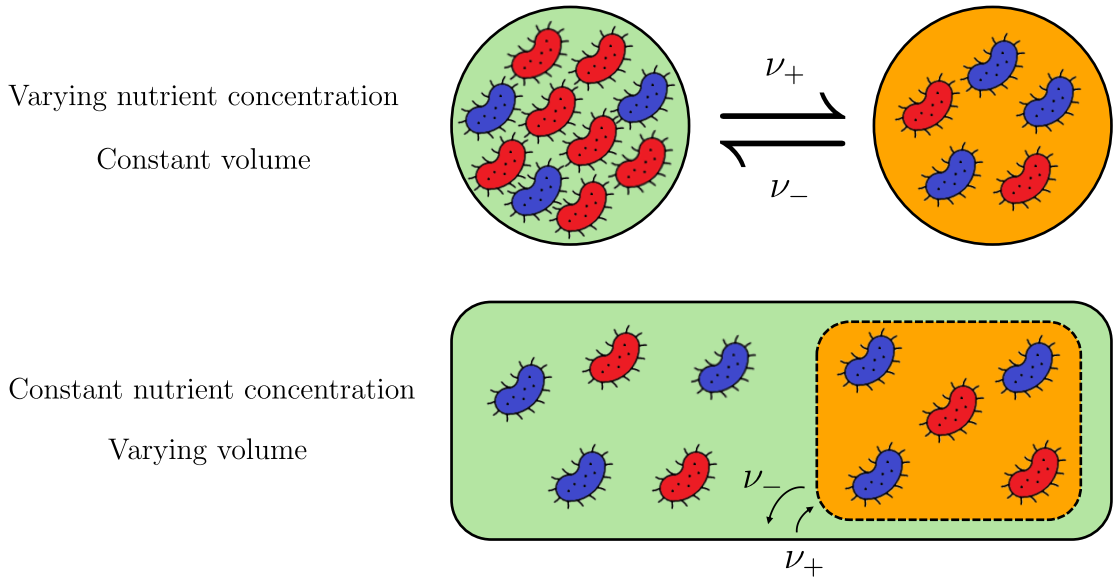

Figure 3.1: Cartoon depicting the difference between the two choices of threshold in the thresholded shared resistance mechanism. Resistant cells (blue) compete with sensitive cells (red). A green background indicates mild environmental conditions, while an orange background indicates harsh environmental conditions which are switched between with rates $\nu_\pm$ as shown. Top: threshold in the absolute abundance of resistant cells. Regardless of the nutrient concentration, which allows for a larger total population, the volume remains constant and therefore the same number of resistant cells produce sufficient resistance enzyme to provide resistance across the whole volume. In this example, the threshold is $N_{\text{th}} = 3$. Bottom: threshold in the relative abundance of resistant cells. While the nutrient concentration does not vary, the volume increases providing more nutrient overall to the population, and therefore allowing for a larger population size. To produce enough resistance enzyme to cover the larger volume requires more resistant cells. In this example, the threshold is $x_{\text{th}} = 0.6$

relative abundance of resistant cells. Here, R cells have a constant fitness $f_R = 1 - s$, where $0 < s < 1$ denotes the metabolic cost to R to produce the resistance enzyme. The fitness of S however depends on if there is sufficient enzyme in the population. If there is, S pays no cost and feels no effect of the antimicrobial, and has fitness $f_S = 1$. If there is not, S pays a significant cost due to the effects of the antimicrobial on its replication, and has fitness $f_S = 1 - a$ with $s < a < 1$. Note that here we focus on the effect of a biostatic antimicrobial which only acts to slow the growth of bacteria (Pankey & Sabath, 2004; Bernatová et al., 2013; Nemeth et al., 2015). The effect of a biocidal antimicrobial, increasing the death rates of bacteria, is an interesting problem not studied here, though typically the effect of a drug can be either biostatic or biocidal depending on its concentration (Pankey & Sabath, 2004; Bernatová et al., 2013; Nemeth et al., 2015). In the case of a threshold in the absolute abundance of R cells for shared resistance with S (varying nutrient concentration, fixed volume), we denote this threshold number N_{th}. For a threshold in the relative abundance of R cells (fixed nutrient concentration, varying volume), we denote the threshold composition x_{th}. For convenience, we define

$H_N = H[N_{\text{th}} - N_R]$ and $H_x = H[x_{\text{th}} - x]$, where $H[z]$ is the Heaviside step function, defined as $H[z] = 1$ if $z > 0$ and $H[z] = 0$ otherwise. Therefore, we have that the fitness of f_S is given by

$$f_S = \begin{cases} 1 - aH_N & \text{for a fixed volume,} \\ 1 - aH_x & \text{for a fixed concentration.} \end{cases}$$

Herein, I will use H to denote both H_N and H_x for simplicity, and only differentiate between the two choices where it becomes important in the time-varying environment. Thus, we use $f_S = 1 - aH$, where $H = 0$ when resistance is shared, and $H = 1$ when it is not. The average population fitness is then given by $\overline{f} = f_R N_R/N + f_S N_S/N$. The population evolves according to the birth-death process defined by the reactions

$$N_{R/S} \xrightarrow{T^+_{R/S}} N_{R/S} + 1,$$
$$N_{R/S} \xrightarrow{T^-_{R/S}} N_{R/S} - 1,$$

with transition rates

$$\begin{aligned} T^+_R &= \frac{f_R}{\overline{f}} N_R = \frac{(1-s)x}{1 - aH + (aH - s)x} N, \quad T^-_R = \frac{N}{K} N_R, \\ T^+_S &= \frac{f_S}{\overline{f}} N_S = \frac{(1-aH)(1-x)}{1 - aH + (aH - s)x} N, \quad T^-_S = \frac{N}{K} N_S, \end{aligned} \tag{3.1}$$

where K denotes the carrying capacity, assumed to be time-varying as in Ch. 2.3.1. The ME giving the time evolution of the probability $P(N_R, N_S, \xi, t)$ for the population to consist of N_R and N_S cells in the environmental state ξ at time t is (Gardiner, 2009)

$$\begin{aligned} \partial_t P(N_R, N_S, \xi, t) = \sum_{\alpha \in \{R,S\}} & \left[\left(\mathbb{E}^-_\alpha - 1 \right) T^+_\alpha + \left(\mathbb{E}^+_\alpha - 1 \right) T^-_\alpha \right] P(N_R, N_S, \xi, t) \\ & + \nu_{-\xi} P(N_R, N_S, -\xi, t) - \nu_\xi P(N_R, N_S, \xi, t), \end{aligned} \tag{3.2}$$

where $\mathbb{E}^\pm_{R/S}$ are shift operators such that $\mathbb{E}^\pm_R f(N_R, N_S, t) = f(N_R \pm 1, N_S, t)$ and $\mathbb{E}^\pm_S f(N_R, N_S, t) = f(N_R, N_S \pm 1, t)$. Furthermore, we assume the system is always initialised at stationarity with $N(0) = K(0)$ and $N_R(0) = N_{\text{th}}$ or $N_R(0) = N(0)x_{\text{th}}$, depending on the modelling choice for the abundance threshold. The last line on the right-hand-side of Eq. (3.2) accounts for the random environmental switching as defined in Ch. 2.3. To recover the ME in the case of a constant environment, we set $\nu_+ = \nu_- = 0$, K = constant, and remove the ξ dependence in Eq. (3.2).

3.2 Constant environment

To develop an understanding of this system, it is instructive to consider and analyse the case of a constant environment, with $K(t) = K$ = constant. As mentioned before, the dynamics under a constant environment do not depend on the choice of cooperation threshold assuming we start at stationarity. However, the threshold must still be specified

in the analytical expressions. We make the arbitrary choice to use N_{th} here, which can be equivalently expressed as $N_{\text{th}} = N x_{\text{th}}$ to find the expressions in terms of x_{th}.

Mean-field analysis leads to long-lived coexistence

It is useful to start with the case of a very large population with carrying capacity $K \gg 1$. The rates of Eq. (3.1) are identical in form to Eqs. (2.10). Therefore, in the MF limit the population's dynamics is aptly described by Eqs. (2.2) and (2.11) upon substituting in the rates of Eq. (3.1), giving (Hernández-Navarro et al., 2023; Hernández-Navarro, Asker, & Mobilia, 2024)

$$\dot{N} = N\left(1 - \frac{N}{K}\right), \tag{3.3}$$

and

$$\dot{x} = \frac{(aH - s)\, x(1-x)}{(1 - aH) + (aH - s)\, x}. \tag{3.4}$$

Eqs. (3.3) and (3.4) show that the dynamics of N and x are coupled for $H = H_N$ or decoupled for $H = H_x$ at the MF level. However, given we start at stationarity and the environment is constant, N remains at $N = K$ for all time, and only x changes. Hence, the dynamics are entirely equivalent. Furthermore, we see that N evolves on a timescale of order $\mathcal{O}(1)$, where $N \to K$, while x has a stable equilibrium at $x = N_{\text{th}}/N$ that it reaches on a timescale of order $\mathcal{O}(1/s)$ when $x > N_{\text{th}}/N$ and $\mathcal{O}(1/(a-s))$ when $x \leq N_{\text{th}}/N$. Moreover, when $s < a \ll 1$ there is a timescale separation between N and x. N relaxes to K on a fast timescale, while x relaxes on a slower timescale to N_{th}/N. Due to the fast relaxation of $N \to K$, should N be initialised out of equilibrium, it would rapidly attain $N = K$ causing a short transient in x in the $H = H_N$ case, and x would subsequently evolve while effectively experiencing $N = K =$ constant at the MF level.

This behaviour implies that, at the MF level, the two species will experience coexistence: excluding the boundaries at $x = 0, 1$, we have $\dot{x} > 0$ for $x \leq N_{\text{th}}/N$ and $\dot{x} < 0$ for $x > N_{\text{th}}/N$, and thus $x \to N_{\text{th}}/N$. As we have seen before, in finite populations fixation will always eventually occur. However, when the coexistence state is stable this can take a very long time, far longer than the timescale of the dynamics of interest in the system, similar to the case of population extinction seen in Ch. 2.1.2. In such cases, we say that the two species experience a long-lived coexistence, which I will define concretely later. The key here is that we must consider three qualitatively distinct behaviours of the system: fixation of R, fixation of S, and long-lived coexistence of R and S.

Large populations in static environments: fixation or long-lived coexistence

To continue we consider a population that is large but now finite in a constant environment. As in Ch. 2.2.2, in this setting the dynamics are characterised by eventual fixation of one of the strains, though now this may be preceded by a long-lived coexistence in which case fixation is not seen over the timescales we are interested in. Similarly to Ch. 2.3.2, the population undergoes logistic growth dynamics and so we may define a suitable Moran process giving a MA of the system; see Ch. 2.2.2. Thus, despite the coexistence state

expected from Eq. (3.4), when the population size is finite, DF are present and can therefore prevent the long-lived coexistence of both species by leading to fixation. Here, we are interested in characterising these scenarios of dominance by one strain or long-lived coexistence. As in Ch. 2.2.2 we define the reactions in the MA

$$N_R + N_S \xrightarrow{\widetilde{T}_R^+} (N_R + 1) + (N_S - 1),$$
$$N_R + N_S \xrightarrow{\widetilde{T}_R^-} (N_R - 1) + (N_S + 1),$$

with effective transition rates

$$\widetilde{T}_R^+ = \frac{(1-s)x(1-x)}{1 - aH + (aH - s)x} K,$$
$$\widetilde{T}_R^- = \frac{(1-aH)x(1-x)}{1 - aH + (aH - s)x} K,$$

which define the MA of the dynamics in a constant environment. I will now show results for the fixation probability and MFT, obtained from approximations of the exact expressions for the fixation probability and MFT given in Ch. 2.2.2 adapted to this specific system, as well as the long-lived coexistence probability of this system.

Fixation probability. Here, the fixation probability of the strain R when the population initially consists of N_R^0 resistant individuals (and $N_S^0 = N - N_R^0$ sensitive cells) is denoted by $\phi_N\left(N_R^0\right)$, where the subscript signifies that the expression is for a population of constant size N.

From Eqs. (3.3) and (3.4), we can predict that the make-up of a large population in a static environment reaches its coexistence equilibrium, i.e. $N_R \to N_{\text{th}}$, for any initial condition N_R^0 well separated from the absorbing boundaries at $N_R = 0$ and $N_R = N$, such that DF are not too strong and the MF description is a reasonable approximation. However, since the population is finite, we infer that N_R will linger around N_{th} until fixation occurs driven by DF. When N_R^0 is not too close to 0 or N, we can thus assume $\phi_N(N_R^0) \approx \phi_N\left(N_R^0 = N_{\text{th}}\right) \equiv \phi_N$, yielding

$$\phi_N \approx \frac{1}{1 + (1-a)^{N_{\text{th}} - N^*}}, \tag{3.5}$$

with $N^* \approx N\frac{\ln(1-s)}{\ln(1-a)}$. This approximate expression is derived from the full expression Eq. (A.2) in Appendix A.1.1. Here, N^* is defined as the critical value of the cooperation threshold for which both strains have probability $1/2$ of fixation, i.e. $\phi_N = 1/2$. This is an important quantity, as it defines the critical value where for $N_{\text{th}} > N^*$ the resistant species is more likely to fixate. Equivalently, substituting $x_{\text{th}} = N_{\text{th}}/N$ gives the analogous result for a threshold in the relative abundance, where we have $x^* \equiv N^*/N \approx \ln(1-s)/\ln(1-a)$. For biologically plausible values, e.g. $0 < s < a \lesssim 10^{-1}$ and $N > 25$, Eq. (3.5) is a good approximation for the fixation probability and matches up well with the exact solution and simulation data; see Fig. 3.2(a).

Therefore, when a large amount of R is required to inactivate the drug ($N_{\text{th}} \gg N^*$) we find $\phi_N \to 1$, while when only a small amount of R can inactivate the drug ($N_{\text{th}} \ll N^*$) we find $\phi_N \to 0$, as confirmed by simulations in Fig. 3.2(a). Interestingly, this shows that the less efficient R cells are at producing the enzyme at fixed metabolic cost s, i.e. the higher N_{th} is, the more likely they are to fixate, the opposite being true for more efficient R cells.

Mean fixation time. The MFT given the population initially consists of N_R^0 resistant individuals is denoted $\tau_N(N_R^0)$, with the subscript again denoting a constant population size N. This is the mean of a distribution from which the random variable ζ, representing the fixation time of a given realisation, is drawn from. As before, since fixation generally arises from excursions from the coexistence equilibrium $N_R \approx N_{\text{th}}$ driven by DF, then $\tau_N\left(N_R^0\right) \approx \tau_N\left(N_R^0 = N_{\text{th}}\right) \equiv \tau_N$ when N_R^0 is not too close to 0 or N, and we obtain

$$\tau_N \approx \phi_N \frac{a(1-s)}{s^2(a-s)} \frac{N}{N_{\text{th}}} \frac{\left(\frac{1}{1-s}\right)^{N-N_{\text{th}}} - 1}{N - N_{\text{th}}}, \tag{3.6}$$

see Appendix A.1.2 for the full derivation. This simple expression matches well the simulation results of Fig. 3.2(b) and the exact expression given by Eq. (2.19) where the MFT is sufficiently large, around $\tau_N > 50$. Note that τ_N is much larger for $N_{\text{th}} \approx N^*$, exponentially decreasing for N_{th} either side of N^*. Thus, for a given s, a, and N, resistant strains that are either very efficient or very inefficient in producing resistance enzyme (N_{th} very small or large) lead to a rapid dominance of one strain, whereas resistant strains with an intermediate efficiency promote a long-lived coexistence of the two species.

Long-lived coexistence probability. As we have mentioned several times now, though in a finite population DF will unavoidably cause the fixation of one strain (hence the extinction of the other), this fixation may only occur after a long-lived coexistence of the two species. In this case, the coexistence state is effectively metastable, and the population is at quasi-stationarity. Here, the MFT generally scales super-linearly with the population size N, and the fixation time of a given realisation of the system, denoted ζ, is generally exponentially distributed with a cumulative distribution given by $1 - \exp(-\zeta/\tau_N)$; see e.g. Assaf and Mobilia (2010), Mobilia and Assaf (2010), Assaf and Mobilia (2011), and Assaf and Meerson (2017). In the case of species dominance the scaling with N is generally sub-linear (Antal & Scheuring, 2006; Reichenbach et al., 2007; Cremer et al., 2009; Assaf & Mobilia, 2010, 2011; He et al., 2011; Asker et al., 2023). These two regimes are separated by an intermediate regime where the MFT scales linearly with N, often found under neutral dynamics (Reichenbach et al., 2007; Cremer et al., 2009). With these considerations, we then determine that a coexistence is long-lived when ζ exceeds $2N$, where the factor of 2 is chosen for convenience. It should be noted that quantitative details change upon the use of a different factor, but this is not relevant for the discussion here. We may then concretely define our probability of coexistence in a population of size N as

$$\eta_N \equiv \text{Prob.}\left(\zeta > 2N\right) = \exp(-2N/\tau_N). \tag{3.7}$$

Under the assumption that the fixation probability of a strain and the probability of a long-lived coexistence state are independent, we may use Eqs. (3.5), (3.6), and (3.7) to estimate the probability of fast fixation (i.e. in time less than $2N$) by either R or S in a population of constant size N. These quantities are given by

$$\phi_N(1-\eta_N) \quad \text{and} \quad (1-\phi_N)(1-\eta_N), \tag{3.8}$$

respectively, where we remind ourselves that ϕ_N is the fixation probability of the resistant strain regardless of long-lived coexistence, η_N is the probability of long-lived coexistence, and τ_N is the mean time for fixation to occur, each for a population of constant size N. The three quantities defined by Eqs. (3.7) and (3.8) then fully determine the long-time behaviour of this system in static environments. Looking again to Fig. 3.2, we therefore see that for N_{th} sufficiently close to the boundaries at 0 and N, i.e. $\min(N_{\text{th}}, N-N_{\text{th}}) \lesssim \sqrt{N}$, DF are sufficiently large to cause a fast fixation (fixation prior to long-lived coexistence, i.e. in a time less than $2N$) and the type of fixation is fully determined by the value of N_{th} relative to N^*. For $N_{\text{th}} < N^*$, the sensitive defectors are more likely to fixate, while for $N_{\text{th}} > N^*$, the resistant cooperators are more likely to fixate. For N_{th} far from the boundaries, i.e. $\min(N_{\text{th}}, N-N_{\text{th}}) \gg \sqrt{N}$, DF are weak and a long-lived coexistence state is reached. Interestingly, we see from Fig. 3.2 that increasing the constant population size for a given N_{th} increases the MFT exponentially, and the fixation probability approaches a step function, transitioning at $N_{\text{th}} = N^*$. Considering how the resistant species may be eradicated, we see that this requires $N_{\text{th}} < N^*$. While increasing the population size for $N_{\text{th}} < N^*$ will increase the likelihood of S fixation, i.e. R eradication, the time for this to occur becomes much longer for larger populations and there is instead a long-lived coexistence, except for N_{th} very close to zero. Therefore, it is difficult to see how one may eradicate the resistant species in a reasonable time more generally in a static environment.

This leads us to the conclusion that in a static environment AMR either dominates or survives in a long-lived coexistence state, so long as N_{th} is not close to zero. We shall now investigate how EV changes this picture, first in the case where the concentration of resources change in time in a fixed volume, and then in the case of a constant resource concentration and time-varying volume.

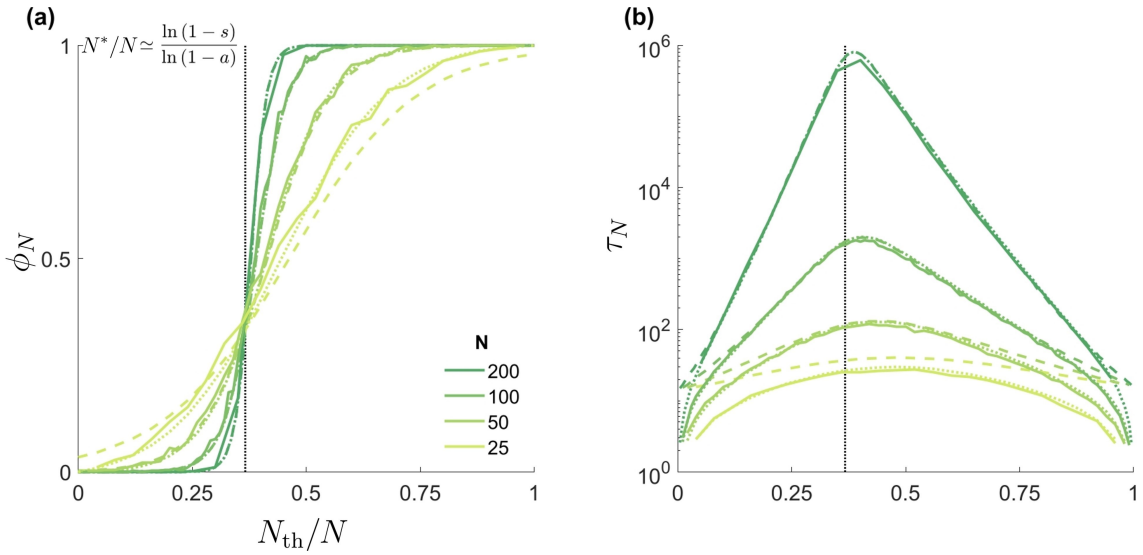

Figure 3.2: R fixation probability and mean fixation time (MFT) in static environments. (a) R fixation probability ϕ_N against the scaled cooperation threshold $N_{\rm th}/N \equiv x_{\rm th}$ for $s = 0.1$, $a = 0.25$, and for five examples of total population size, from $N = 25$ (yellow green) to 200 (dark green); the starting microbial composition is set at the coexistence equilibrium $N_R^0 = N_{\rm th}$; dotted and dashed lines show the exact and approximated Moran predictions of Eq. (3.5), respectively, which are only distinguishable for the smallest population size; noisy solid lines are from simulation data (10^3 realisations for each data point) and match with dotted lines. The vertical black dashed line shows the value of N^*/N for which each strain has a probability $1/2$ to fixate when $N \gg 1$. (b) Mean fixation time τ_N against $N_{\rm th}/N$ in log-linear scale; the simplified formula of Eq. (3.6) (dashed lines), approximates well (for $\tau_N > 50$) the exact MFT (2.19) (dotted lines) and simulation results for the MFT (solid lines); legend and line styles as in panel (a).

3.3 Time-varying resource concentration

In the case of a time-varying environment, implemented through a time-varying capacity as introduced in Ch. 2.3.1, the choice of the cooperation threshold, H, being in the absolute or relative abundance of R, i.e. $H = H_N$ or $H = H_x$, no longer leads to equivalent dynamics. In this section, we look to model a fixed volume with time-varying resource concentration and so use the former choice, reinstating $H = H_N$. This can be understood by assuming that the fixed-volume population is well-mixed with R cells homogeneously distributed throughout the population; see Fig. 3.1. For a constant antimicrobial concentration supplied to the medium, N_{th} resistant cells are required to bring the concentration below the MIC, regardless of the total number of cells. In the chemostat setup mentioned previously, where a constant inflow of fresh medium into a population at constant concentration (nutrients, antimicrobial, etc.) allows the ecological dynamics of the population to reach a stationary state, instead here the nutrient concentration flowing into the chemostat is stochastically switched between two values.

3.3.1 Fixation and coexistence: a novel resistance-eradication mechanism

In this section we analyse how the coupling of EV and DF shape the evolution of cooperative AMR (Coates et al., 2018; Bottery et al., 2021). The main goal is to determine under which conditions does this coupling lead to the eradication of resistance (fixation of sensitive cells such that no resistant cells remain), and reduce the size of the population which we assume to be pathogenic.

Coupled environmental variability and demographic fluctuations induce regimes of coexistence and dominance

As in Ch. 3.2, the long-time behaviour of the population is captured by the probability of fast fixation of either strain and the probability of long-lived coexistence. In the case of a switching carrying capacity, and denoting the MFT in the switching environment τ, long-lived coexistence requires $\zeta > 2\langle N\rangle$, where ζ is again the fixation time of a given realisation and $\langle N\rangle$ is the average population size as in Eq. (2.28). Continuing, under time-varying environments we denote the fixation probability of R as ϕ, and the probability of long-lived coexistence η, where we have now dropped the subscript to indicate that the population size fluctuates. Therefore, the three quantities defined in Eqs. (3.7) and (3.8) have their analogue in the time-varying environment given by

$$\eta \equiv \text{Prob.}\left(\zeta > 2\langle N\rangle\right) = \exp(-2\langle N\rangle/\tau),$$

and

$$\phi(1-\eta) \quad \text{and} \quad (1-\phi)(1-\eta).$$

We compute ϕ and η using statistically correct stochastic simulations (see Appendix D.1), when the external conditions fluctuate between harsh ($K_- = 120$, scarce resources) and

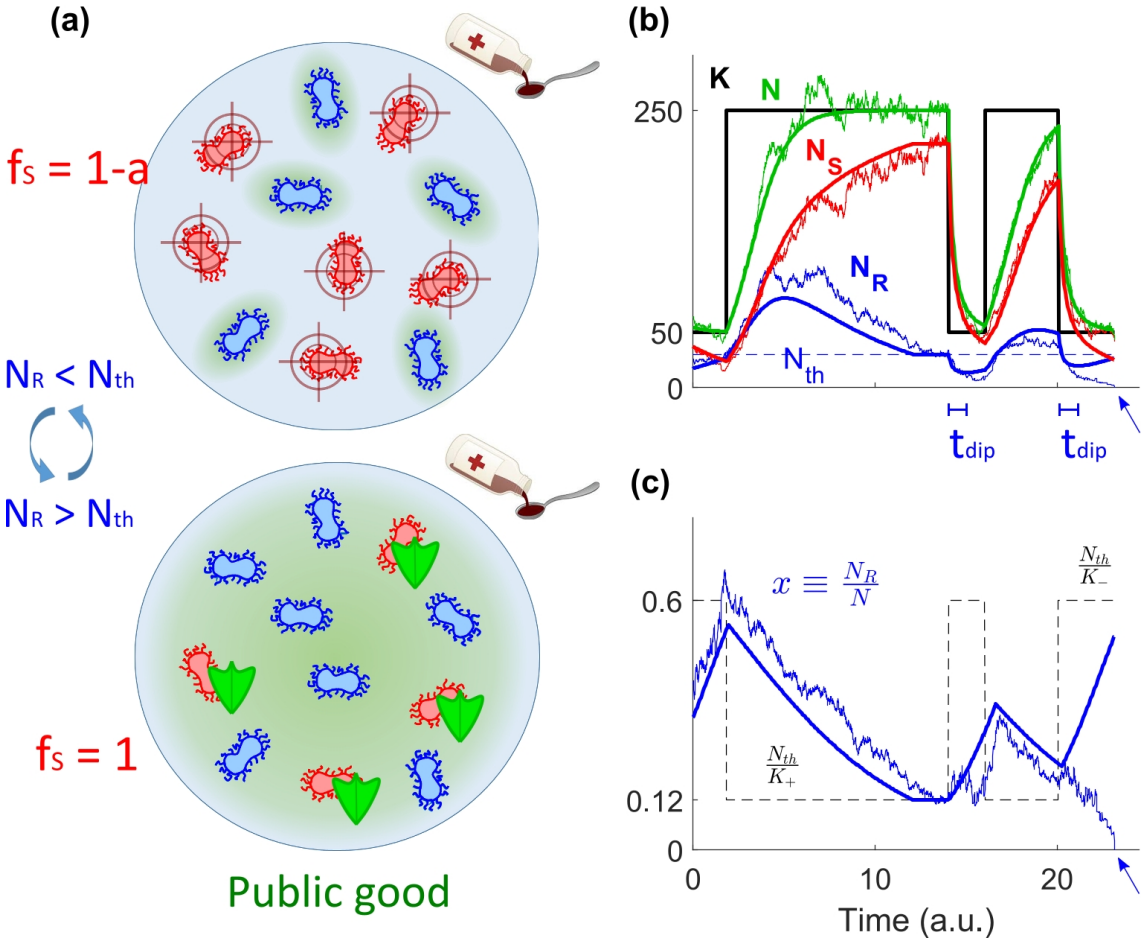

Figure 3.3: Microbial community model. (a) Top: When the abundance of R (blue microbes) is below the cooperation threshold N_{th}, antimicrobial drug hinders the growth rate of S (red microbes) and R cells have a growth advantage. Bottom: AMR becomes cooperative when the number of R exceeds N_{th} and these generate enough *resistance enzyme* (public good in green shade) to hydrolyse the antimicrobial drug below the MIC for the whole medium, so that protection against the drug is shared with S (with green shields). (b) Dynamics of the microbial community for example parameters $s = 0.2$, $a = 0.5$, $K_- = 50$, $K_+ = 250$, $\nu = 0.2$, and $\delta = 0.6$; thick black line shows the sample path of the time-switching carrying capacity $K(t)$, with a cooperation threshold $N_{\text{th}} = 30$ (dashed blue line); thick solid lines depict the $N \to \infty$ PDMP defined by Eqs. (2.23) and (3.4) for the total microbial population (N, green), number of R ($N_R = Nx$, blue), and number of S ($N_S = N(1-x)$, red); noisy lines show an example stochastic realisation of the full model under the joint effect of DF and EV. In the absence of DF, R can experience bumps and dips (thick blue line), and t_{dip} indicates the mean time to reach the bottom of a dip from its inception; see Ch. 3.3.1. In the presence of DF, fluctuations about the dip can lead to the extinction of R (blue arrow). (c) R fraction $x = N_R/N$ for the same sample path of varying environment as in (b); line styles as in panel (b); the dashed black line shows the stable R fraction in each environment as $K(t)$, driven by $\xi(t)$, switches in time.

mild ($K_+ = 1000$, abundant resources). In our simulations, we consider a wide range of switching rates ν and environmental biases δ, while also varying the cooperation threshold, though maintaining $N_{\text{th}} \sim 10^2 < K_-$. Furthermore, we use $s \in [0.1, 0.2]$ and $a \in [0.25, 0.5]$ as plausible values for the metabolic cost of producing resistance enzyme and the impact of the drug on S, respectively (van der Horst et al., 2011; Melnyk et al., 2015). Our choice of $K_\pm$ ensures that the dynamics is not dominated mainly by DF or EV, but by the interplay of DF and EV, and the choice of $N_{\text{th}} < K_-$ guarantees that long periods of time in K_- are not purely characterised by R dominance. Note that here we simulate systems which are small compared to most microbial communities for computational tractability. However, as discussed in Ch. 3.3.2, the behaviour reported here is also expected to be observed in large populations of more realistic size, i.e. $N > 10^6$.

The behaviour in ν-δ space is shown in Fig. 3.4(a-c), obtained from simulations. We see across cooperation thresholds N_{th}, fixation of either strain or long-lived coexistence can occur. In particular, for $N_{\text{th}} \lesssim 10K_+/K_-$ ($N_{\text{th}} \lesssim 83$ for our parameter choices) we find that S fixates quickly with a high probability (red region) where switching occurs at intermediate rate and the bias is not too extreme, meaning the eradication of resistant cells. Furthermore, for slow and fast switching where the bias is not too close to -1, we find black regions where long-lived coexistence of the strains is likely. As N_{th} increases, we find the parameter regime where R is likely to fixate (blue region) grows, particularly where the environmental bias is towards the harsh state; see Fig. 3.4(c). This occurs due to the advantage of R in the harsh state: N_{th} approaches K_-, leaving $K_- - N_{\text{th}}$ sensitive cells vulnerable to DF since $K_- - N_{\text{th}} < N_{\text{th}}$ in our example.

We now analyse the various regimes of Fig. 3.4(a-c), with a focus on the red area, where resistant cells are eradicated. This allows us to determine the optimal environmental conditions for the eradication of resistant cells and the reduction of the overall size of the population, two issues of great biological and practical relevance.

Weak demographic fluctuations promote coexistence

For an intuitive understanding of the eco-evolutionary dynamics under environmental switching, here we discuss the sample paths of Figs. 3.3(b,c) and 3.4(d-f) in terms of N and x.

When the population is large enough for DF to be negligible ($1/\sqrt{N} \to 0$) we may use the PDMP description as defined in Ch. 2.3.1 to capture the evolution of the population size. Hence, N follows the evolution of Eq. (2.23) and x is coupled to this evolution through $H = H_N$ in Eq. (3.4). Sample paths of the PDMP are shown as solid lines in Figs. 3.3(b,c). The realisations of Fig. 3.3(b,c) illustrate the coupling of x to N, where N tracks the switching carrying capacity K independently of x, while x evolves towards the coexistence equilibrium at the cooperation threshold $x_{\text{th}} = N_{\text{th}}/N$, which changes in time as N varies. Hence, x increases when $N_R \leq N_{\text{th}}$, and it decreases when $N_R > N_{\text{th}}$. For extremely slow or fast environmental switching rate (i.e. $\nu \to 0$ or $\nu \to \infty$ as in Fig. 3.4(d,f)), since the dynamics of N under the rates given by Eq. (3.1) are identical

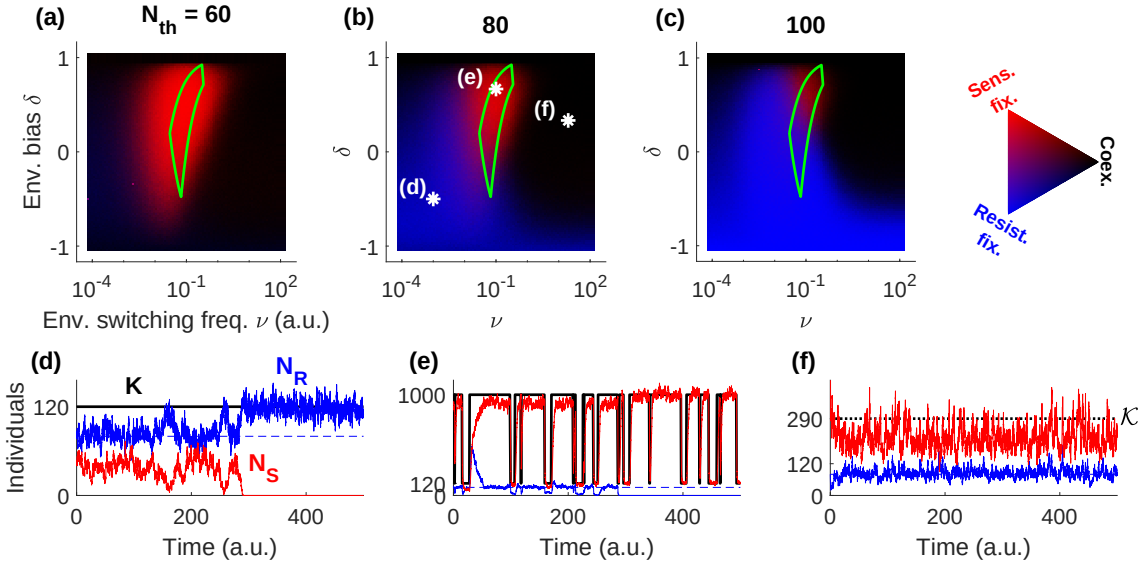

Figure 3.4: Eco-evolutionary dynamics in the phase diagram of the joint fixation and coexistence probability. (a-c) Fixation and coexistence joint probability from simulations at a given environmental bias δ and mean switching frequency ν for $s = 0.1$, $a = 0.25$, $K_- = 120$, and $K_+ = 1000$ at resistant cooperation thresholds $N_{\rm th} = 60,\ 80$, and 100; see the discussion in Ch. 3.3.2 for the behaviour at much larger populations and thresholds. Stronger blue (red) depicts a higher fixation probability of R (S). Darker colour indicates higher coexistence probability, defined as the probability to not reach any fixation by $t = 2\langle N\rangle$, where we take the average total population in its stationary state. The area enclosed within the green solid line indicates the optimal regime for the eradication of R; see Eq. (3.12) in Ch. 3.3.1. The white asterisks in (b) depict the environmental statistics for each of the bottom panels. (d-f) Sample paths for the carrying capacity (K, black), number of R (N_R, blue), number of S (N_S, red), and fixed cooperation threshold $N_{\rm th} = 80$ (dashed blue) for the environmental parameters (ν, δ) depicted by the corresponding white asterisk in (b). The high environmental switching frequency in (f) results in an effectively constant carrying capacity ($K = \mathcal{K}$, dotted line); see Ch. 3.3.1.

in form to that considered in Ch. 2.3.2, we see the same behaviour of N. Therefore, under slow switching the system has two behaviours: it is initialised at $N = K_+$ and remains there for long times with $N_R = N_{\text{th}}$ and $N_S = K_+ - N_{\text{th}}$, leading to a long-lived coexistence provided $\min(N_{\text{th}}, K_+ - N_{\text{th}})$ is not too small or it is initialised at $N = K_-$, leading to $N_R = N_{\text{th}}$ and $N_S = K_- - N_{\text{th}}$, where fixation is expected provided that $\min(N_{\text{th}}, K_- - N_{\text{th}})$ is small, and the most likely type of fixation is given by which of N_R and N_S is largest at equilibrium. Under fast switching, we again see that the effective carrying capacity attains $N = \mathcal{K}$. Hence, provided that δ is not too close to -1 (i.e. $\mathcal{K}$ not too small), long-lived coexistence of both strains is likely (with abundances $N_R \approx N_{\text{th}}$ and $N_S \approx \mathcal{K} - N_{\text{th}}$), as shown in Fig. 3.4(f).

Demographic fluctuations can eradicate antimicrobial resistance in time-varying environments

Under slow and fast environmental switching rates, the population takes effectively constant size at $K_\pm$ and $\mathcal{K}$, respectively. Under slow switching, η and ϕ are given by $\eta = (1+\delta)\eta_{K_+}/2 + (1-\delta)\eta_{K_-}/2$ and $\phi = (1+\delta)\phi_{K_+}/2 + (1-\delta)\phi_{K_-}/2$, and under fast switching we find $\eta = \eta_{\mathcal{K}}$ and $\phi = \phi_{\mathcal{K}}$, similar to the results discussed in Ch. 2.3.2. At intermediate switching rates where several switches occur prior to fixation, the dynamical behaviour is far richer, as seen by the red regions in Fig. 3.4(a-c) for $\nu \in [10^{-2}, 10^{0}]$. In this regime, we cannot simply express ϕ and η in terms of their effectively static counterparts ϕ_N and η_N. Here, environmental switches lead to transient "dips" and "bumps" in N_R following the carrying capacity switches $K_+ \to K_-$ and $K_- \to K_+$, respectively as in Fig. 3.3(b) and 3.4(e). Of prime importance here are the transient dips in N_R, and so that is where we direct our focus. For sufficiently strong transient dips, N_R becomes small enough that DF, which are amplified in the harsh environment due to the smaller population size, can lead to the eradication of R (fixation of S), giving rise to the red regions of Fig. 3.4(a-c). Each dip has some non-negligible probability of R eradication and so drastically reduces the MFT compared to the static case. To have this fast R eradication then requires three things: intermediate switching, such that the population size N is given sufficient time to track $K(t)$ following environmental changes; timescale separation between the population composition x and size N, where the composition evolves more slowly, allowing for the transient behaviour following an environmental switch; and a small number of resistant cells at the bottom of the transient dip, allowing DF to eradicate them. Concretely, we require $N_R \sim \mathcal{O}(1)$ for R to be prone to extinction by DF during the transient dip; see later.

Here, we are interested in characterising the transient dips in N_R, since it forms the backbone of the EV-driven resistance-eradication mechanism we uncover here. To investigate their behaviour further, we consider the PDMP description of N_R, assuming large

populations, giving

$$\dot{N}_R = T_R^+ - T_R^- = \frac{(a-s)\,N_R(\alpha_R - \frac{N_R}{K})}{(1-a)+(a-s)\,N_R/N}, \quad \text{with } \alpha_R \equiv \frac{(1-s)K-(1-a)N}{(a-s)K}, \tag{3.9}$$

where we have assumed $N_R \leq N_{\text{th}}$ since the equivalent description for $N_R > N_{\text{th}}$ gives $\dot{N}_R < 0$ leading to $N_R \leq N_{\text{th}}$. Following a bottleneck of the population size, in the absence of DF, resistant cells will inevitably survive and recover to their equilibrium number at $N_R = N_{\text{th}}$. However, in finite populations where $K_- \ll K_+$, the minimum of the transient dip of N_R predicted by the PDMP description may reach values small enough that DF from the finite size of the population causes R eradication. The strength of DF in this transient increases as the minimum of the dip decreases.

In order to adequately characterise the behaviour in the red region of the ν-δ phase diagram, we seek to estimate the value N_R reaches at its minimum in this transient dip and the time it takes to reach this minimum. We have that N_R evolves according to Eq. (3.9) and so setting $\dot{N}_R = 0$ allows us to determine its equilibrium; see Fig. 3.3(b). To find t_{dip} from Eq. (3.9) we require $\dot{N}_R(t_{\text{dip}}) = 0$ which requires $\alpha_R = N_R/K_-$. Assuming $s < a \ll 1$, yields $N(t_{\text{dip}}) \approx K_-(1-s)/(1-a)$. From the solution of Eq. (3.3) with the initial condition $N(t=0) \approx K_+$ (see Eq. (2.3) of Ch. 2.1.1), we find

$$\begin{aligned} t_{\text{dip}} &\approx \ln\left[\frac{1-s}{a-s}\left(1-\frac{K_-}{K_+}\right)\right], \\ &\approx \ln\left(\frac{1}{a-s}\right), \end{aligned}$$

where in the approximation of the second line we assume $K_+ \gg K_-$ and $s \ll 1$. To determine the value of N_R at the dip, denoted N_R^{dip}, we use the timescale separation in the evolution of x and N since $s < a \ll 1$. In the low relative abundance limit of R, i.e. $x \to 0$, Eq. (3.4) simplifies, giving

$$\dot{x} \approx (a-s)x. \tag{3.10}$$

Thus, x evolves on a timescale of order $\mathcal{O}(1/(a-s))$ which is a *slow timescale* relative to the evolution of N. Therefore, assuming $x(t=0) = \frac{N_{\text{th}}}{K_+}$, where $t=0$ is the time at the $K_+ \to K_-$ environmental switch, we obtain that at short times

$$x(t) \approx x(0) = \frac{N_{\text{th}}}{K_+}.$$

For $s < a \ll 1$, we have that $t_{\text{dip}} \sim \mathcal{O}(\ln(\frac{1}{a-s}))$ whereas the timescale of x relaxation is $\sim \mathcal{O}(\frac{1}{a-s})$, meaning the predicted dip can occur on these short, transient timescales. The total population follows the logistic dynamics of Eq. (3.3) in the harsh environment after the switch, and so rapidly attains $N = K_-$ in a time of order $\mathcal{O}(1)$. Therefore,

multiplying both expressions provides the final estimate of the number of R at the bottom of the transient dip, N_R^{dip}, giving

$$N_R^{\text{dip}} = x\left(t_{\text{dip}}\right) N\left(t_{\text{dip}}\right) \approx \frac{N_{\text{th}} K_-}{K_+}, \tag{3.11}$$

occurring at time $t \approx t_{\text{dip}}$, where we assumed that R started from $N_R(t=0) = N_{\text{th}}$. DF at the bottom of a dip are of the order $\sqrt{N_R^{\text{dip}}}$. For DF to possibly drive R to extinction, and the EV-driven eradication scenario to hold, it is necessary that $\sqrt{N_R^{\text{dip}}} \sim N_R^{\text{dip}}$, which requires small N_R^{dip}, i.e. $N_R^{\text{dip}} \lesssim 10$. This condition is certainly satisfied when K_- and N_{th} are of comparable size (with $K_- > N_{\text{th}}$), and each of order $\sqrt{K_+}$, which can also hold for realistically large populations of $N > 10^6$; see Ch. 3.3.2 for further discussion of large population sizes. Furthermore, we note that while we have assumed $s < a \ll 1$, the timescale separation for the eradication mechanism only requires $a - s \ll 1$ (see Eq. (3.10)), allowing for the eradication to work at larger values of a and s, so long as their difference is small. However, $a - s \ll 1$ is naturally satisfied for $s < a \ll 1$ and so we continue under this assumption.

Having characterised the eradication mechanism, we then note that each bottleneck is thus seen as an attempt to eradicate resistant cells. Therefore, after finitely many bottlenecks arising at a frequency $\sim \nu$ we expect R eradication, allowing fixation to occur prior to $t = 2\langle N \rangle$. With these requirements, the parameter regime to effectively and quickly eradicate R in large, populations under EV can be estimated. Firstly, R must be allowed to evolve to its equilibrium position $N_R = N_{\text{th}}$ following a switch to K_+, requiring $\nu_+ \lesssim s$, where $1/s$ is the evolutionary timescale. Secondly, following a bottleneck of the population, R should be allowed sufficient time to reach the bottom of the transient dip and experience the enhanced DF there, giving $\nu_- \lesssim t_{\text{dip}}^{-1}$. Thirdly, should R not be eradicated in a transient dip, the environment should recover to the mild state as soon as possible to eliminate the possibility of R fixation in this state. Therefore, we require $\nu_- \gtrsim (a-s)/(2\ln(\frac{K_+}{K_-}))$, where the expression on the right hand side is the inverse of twice the expected time to reach equilibrium in the harsh state following a switch, obtained from Eq. (3.10). Finally, we also require that these repeated bottlenecks are as frequent as possible while satisfying all previous conditions (i.e. that we do not wait for too long after x relaxation in the mild state), giving $\nu_+ \gtrsim s/(2\ln(\frac{K_+}{K_-}))$, where similarly the expression on the right hand side here is the inverse of twice the expected time to reach equilibrium in the mild state following a switch. We therefore find that

$$\begin{aligned} \frac{s}{2\ln\frac{K_+}{K_-}} &\lesssim \nu_{\text{opt}}\left(1-\delta_{\text{opt}}\right) \lesssim s, \\ \frac{a-s}{2\ln\frac{K_+}{K_-}} &\lesssim \nu_{\text{opt}}\left(1+\delta_{\text{opt}}\right) \lesssim t_{\text{dip}}^{-1}, \end{aligned} \tag{3.12}$$

where ν_{opt} and δ_{opt} denote the optimal values for the environmental parameters ν and δ, respectively. To summarise, the top line of Eq. (3.12) allows sufficient time for N_R

relaxation following a switch to the mild state, but not too long, while the bottom line allows for sufficient time for transient dips following a switch to the harsh state, but not too long. The green contour lines in Fig. 3.4(a-c) enclose the predicted optimal region for the fast eradication of R under $s = 0.1$, $a = 0.25$, $K_- = 120$ and $K_- = 1000$, and fall in the red areas observed in simulations. The green lines with positive slope correspond to the top line of Eq. (3.12) while those with negative slope correspond to the bottom line. The true borders of these regions from the simulation data depend on N_{th}. This stems from the dependence of ϕ and the MFT on N_{th} (see Fig. 3.2) and the criterion for long-lived coexistence ($\zeta > 2\langle N \rangle$). The prediction of Eq. (3.12) ignores any dependence on N_{th} and thus fail to capture this effect.

In summary, DF can eradicate AMR in time-varying environments when the population composition x evolves on a much slower timescale than the population size N, satisfied for $s < a \ll 1$. Moreover, the magnitude of the bottleneck K_+/K_- is required to be of the order of the cooperation threshold N_{th} or larger, the threshold has to fall below the lowest value of the carrying capacity, i.e. $N_{\text{th}} < K_-$, and the switching rate ν should be of order s and hence comparable to the rate of relaxation of the population composition.

Impact of environmental variability on the strains fraction and abundance

Having characterised the long-term population composition under environmental switches in our region of interest, we additionally look to understand the non-trivial impact of EV on the size and composition of the population outside of this regime, particularly where coexistence is likely.

As seen in Ch. 2.3.1, the average size of the population $\langle N \rangle$ is a decreasing function of the switching rate ν for fixed δ. Furthermore, for fixed ν, $\langle N \rangle$ is an increasing function of δ, where in particular we see $\langle N \rangle \to K_\pm$ as $\delta \to \pm 1$. As a consequence of this behaviour, the surviving pathogenic population can be reduced generally by increasing the environmental switching rate ν and/or the time spent in the harsh environmental state, $\delta \to -1$. Moreover, since the R fraction x is directly coupled to N through the cooperation threshold N_{th} (see Eq. (3.4)) EV non-trivially shapes the R fraction in the coexistence regime (coloured areas in Fig. 3.5(f)).

Under slow environmental switching rate relative to the evolutionary dynamics of the system (i.e. $\nu \ll s$), the population is likely to not switch prior to $t = 2\langle N \rangle$. Therefore, if the environment is initially mild, the R cells will relax to $N_R = N_{\text{th}}$, with the S cells at $N_S = K_+ - N_{\text{th}}$, and a long-lived coexistence will remain. However, if the initial environment is harsh, (and $N_{\text{th}} \sim K_-$), DF will rapidly eradicate S, and hence not allow coexistence of the species. Therefore, the distributions of N_R, N_S, and N are each approximately bimodal as we average over the behaviours in each starting environment. In the mild environment, we have $N_R = N_{\text{th}}$, $N_S = K_+ - N_{\text{th}}$, and $N = K_+$, and in the harsh environment, we have $N_R = K_-$, $N_S = 0$, and $N = K_-$; see Fig. 3.5(a). As ν is increased to $\nu \lesssim s$, and we approach the regime detailed in the previous section, fixation again dominates the dynamics, and the distributions of N_R and N_S become trimodal, with $N_{R/S}$

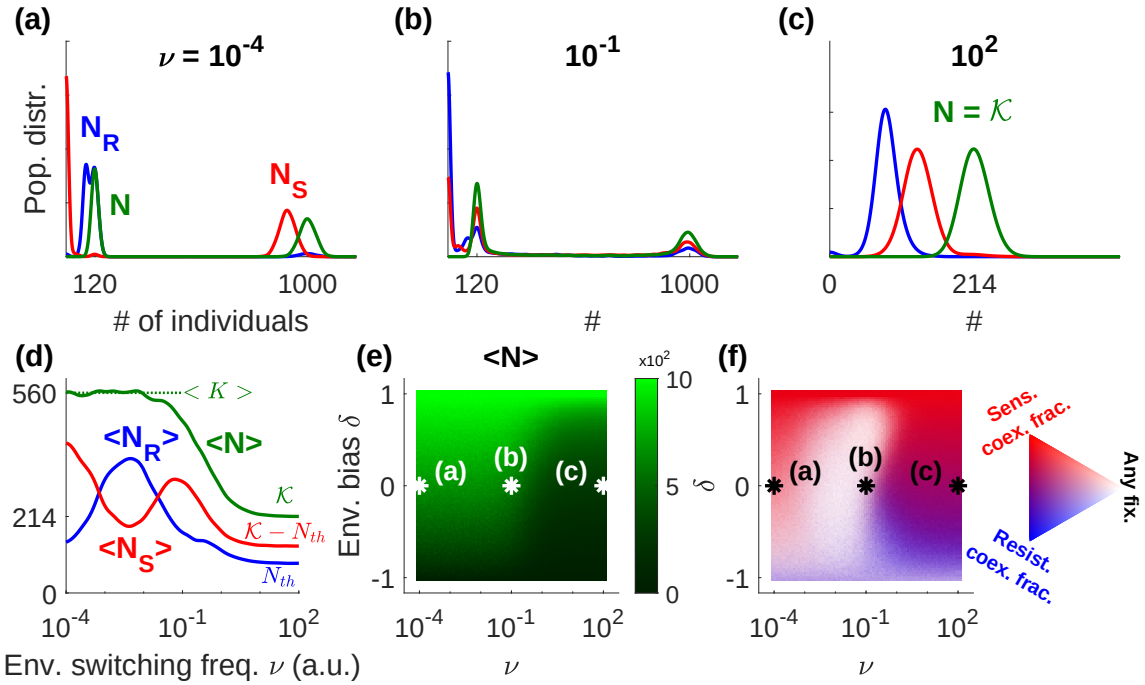

Figure 3.5: Total population, strain abundance, and coexistence composition in time-varying environments. (a-c) Probability distributions of the total population (N, green), number of R (N_R, blue), and number of S (N_S, red), from simulations with parameters $s = 0.1$, $a = 0.25$, $K_- = 120$, $K_+ = 1000$, and $N_{\text{th}} = 80$, under no environmental bias ($\delta = 0$) and for mean switching rates in (a) slow $\nu = 10^{-4}$, (b) intermediate $\nu = 10^{-1}$, and (c) fast $\nu = 10^2$ conditions. Histograms are smoothed by a Gaussian filter of width $\sigma = 10$ in cell number. (d) Average overall population (number of individuals on the vertical axis) and strain abundances under no bias, i.e., $\delta = 0$, as a function of switching rate ν; colours as in (a-c). Lines are smoothed by a log-scale Gaussian filter of width $\sigma = 10$, i.e., one frequency decade. (e) Average overall population size in dynamic environments. (f) Coexistence composition and fixation probability (of any strain) in dynamic environments. Stronger blue (red) depicts a higher coexistence fraction of R (S). Lighter colour indicates lower coexistence probability, defined as the probability for no fixation event to occur by $t = 2\langle N \rangle$. The white and black asterisks in (e,f) depict the environmental statistics for each of the top panels. All panels are computed at quasi-stationarity reached after a time $t > 2\langle N \rangle$, ensuring that N reaches its (quasi-)stationary state.

peaks at 0, K_-, and K_+; see Fig. 3.5(b). The relative weights of the peaks at $N_{R/S} = 0$ compared to those at $N_{R/S} = K_\pm$ is set by the fixation probabilities of the species. The total population size N remains bimodal around $K_\pm$. As ν is increased further, such that $\nu \gg 1$, we enter the coexistence regime where $K \to \mathcal{K}$, and the distributions become unimodal around the coexistence equilibrium $N_R = N_{\text{th}}$, $N_S = \mathcal{K} - N_{\text{th}}$, and $N = \mathcal{K}$; see Fig. 3.5(c).

As a consequence, if R is eradicated, imposing fast environmental switching ($\nu \gg 1$) and harsh conditions $\delta \to -1$ would considerably reduce the abundance of the surviving community of pathogenic S cells; see Fig. 3.5(d) (green solid line) and Fig. 3.5(e). However, if R survives, imposing $\nu \gg 1$ and $\delta < 0$ would not only decrease the abundance of both strains but it would also increase the R fraction, and risk further AMR spreading; see Fig. 3.5(f) (magenta area). In the case that the environment is externally controlled, following R eradication the best course of action is to remain in K_- forever ($\delta = -1$), reducing the size of the remaining pathogenic population of S.

3.3.2 Review of the modelling assumptions

In studying an idealised model of a microbial system, we make several assumptions that it is important to review and contrast with realistic experimental conditions achievable in a laboratory. The first assumption we shall address here is that of the cooperation threshold, based on a number of experimental observations of microbial cooperation; see Davies (1994), G. D. Wright (2005), Sanchez and Gore (2013), and Yurtsev et al. (2013). As explained before, here setting this threshold in the number of resistant microbes, N_{th}, allows us to assume that the nutrient concentration changes at constant volume with environmental changes (Sanchez & Gore, 2013). It is this choice that leads to the transient bumps and dips in N_R, which lead to the EV-induced eradication mechanism detailed previously. In the next section, we shall consider the complementary scenario, where the cooperation threshold is set by a fixed R fraction x_{th}, relevant to a different set of microbial systems. Furthermore, in some cases the resistant species are able to regulate the production of the resistance enzyme through quorum sensing (Pai et al., 2012), but its impact on cooperative AMR remains an open problem. We also note that certain resistance mechanisms exhibit an anti-cooperative behaviour, such as efflux pumps, which may result in enhanced metabolic costs to the sensitive cells (Poole, 2007; Soto, 2013). Here, we have assumed that the enzyme breaking down the antimicrobial is public and shared throughout the population. In the case that this resistance is private, i.e. only available to the resistant cells that produce the enzyme, the model reduces to that of Ch. 2.3.2, and those studied in Wienand et al. (2017, 2018). Further analytical results where resistance is not shared are discussed in Uecker and Hermisson (2011) in a variable environment, and in A. Lambert (2006), Parsons and Quince (2007a), and Patwa and Wahl (2008) in the case of a static environment.

The second assumption we review here is that of the system size considered in our simulations, with $K_- \gtrsim N_{\text{th}} \sim 10^2$ and $K_+ \sim 10^3$. These parameters are chosen for computa-

tional efficiency, but correspond to small populations biologically. Therefore, it is right to consider if the interesting behaviour, particularly the EV-driven eradication mechanism, is also present in systems of more biologically realistic size. Typical microbiology laboratory experiments study total microbial populations of size $N \sim 10^6$ or larger (Sanchez & Gore, 2013). These studies model real-life microbial communities that are usually a few orders of magnitude larger still, such as in case studies of mature or chronic clinical infections with $N \gtrsim 10^8$ (Canetti, 1956; M. R. Smith & Wood Jr, 1956; Feldman, 1976; Palaci et al., 2007; Coates et al., 2018).

Communities of microbes of realistic size in the presence of antimicrobials could consist of populations of $N = K_+ \sim 10^{12}$ cells under mild, nutrient abundant conditions. Furthermore, as used throughout our analysis, biologically reasonable values for the metabolic cost of producing the resistance enzyme, s, and the metabolic cost of replicating without resistance in the antimicrobial, a, are plausibly around 10% and 25%, respectively, i.e. $s = 0.1$, $a = 0.25$ (van der Horst et al., 2011; Melnyk et al., 2015). Moreover, a fixed volume may require $N_{\text{th}} = 2 \times 10^6$ resistant cells for the sensitive cells to be protected from the antimicrobial. A sudden and drastic bottleneck to the population via a nutrient shock (or addition of an additional toxin) may cause the population to be reduced greatly, to say $N = K_- \sim 5 \times 10^6$ cells, i.e. five in every million cells survives. Under these plausible parameters, the conditions detailed in Eq. (3.12) can be satisfied. Furthermore, Eq. (3.11) then predicts that $N_R^{\text{dip}} \approx 10$, meaning DF may still lead to eradication of R, even in these larger, realistic system sizes. A recent study considering a spatial extension of this model considers larger population sizes, though spatially structured, and determines that the resistance-eradication mechanism uncovered here remains and can be enhanced under slow migration (Hernández-Navarro, Distefano, et al., 2024).

Finally we note that, as shown previously, the relative magnitude of the population bottleneck K_+/K_- is critical to enhance the eradication of R during transient dips. An increase in this leads to a smaller expected number of R cells at the minimum of the transient dip, and thus stronger DF possibly leading to the eradication of resistance. Introducing an intermediate environmental step between harsh and mild regimes would reduce the population bottleneck at each stage and may promote coexistence (Sanchez & Gore, 2013).

A specific choice of this model is the focus on *biostatic* antimicrobials, i.e. those decreasing birth rates and not increasing death rates (Pankey & Sabath, 2004; Bernatová et al., 2013; Nemeth et al., 2015). Most antimicrobials, however, act biostatically at low concentrations, becoming biocidal at higher concentrations (Andersson et al., 2007; Hughes & Andersson, 2012; San Millan & Maclean, 2017). Therefore, our approach captures the case of a constant low concentration of antimicrobial. Through this choice and the normalisation of the strain birth rates by the average fitness of the population (see Eq. (3.1) (Ewens, 2004; Blythe & McKane, 2007)) the population size N does not depend on the composition x. A simpler model has been investigated in the scenario where this decoupling is not present, and N depends on x (Wienand et al., 2017, 2018).

Finally, we note that the mechanisms by which resistance can be eradicated, along with the other interesting behaviours due to the eco-evolutionary dynamics of the model, all present themselves at biologically reasonable and clinically relevant environmental switching rates. Though we do not explicitly set a timescale in our model, a crude approximation assuming replication of a single cell takes ~ 1 hour sets the timescale, and we see that for environmental switches occurring at $\nu \sim s$ leading to the resistance-eradication mechanism mean periods of ~ 10 hours in each environmental state. This timescale is feasible for laboratory experiments, where typically bottlenecks occur periodically on the order of hours.

3.4 Time-varying volume

We now look to the case of the threshold for shared resistance in the relative abundance of R. This corresponds to a system with a time-varying volume at fixed nutrient concentration, now with $H = H_x$; see Figs. 3.1 and 3.6(a). This can again be understood by assuming that the fixed nutrient concentration population is always well-mixed with R cells homogeneously distributed throughout the population, including immediately following an environmental switch. In a larger volume, where the concentration of antimicrobial is also maintained, more R cells will be required as there is, in total, more antimicrobial present. Therefore, x_{th} is now constant while N_{th} depends on N; see Fig. 3.6(b,c).

3.4.1 Insight into fixation and coexistence via sample paths

It is useful to first consider the trajectories of Figs. 3.6(b,c) to gain some insight into the dynamics. Clearly, the long-time dynamics leading to a long-lived coexistence or fixation (and the type of fixation) are chiefly controlled by x_{th}. Since $H = H_x$, x is now decoupled from N and the transients of Ch. 3.3 do not occur. For fixation to occur in a time less than $2\langle N\rangle$, our condition for long-time coexistence, we require that x_{th} is sufficiently close to the boundaries at 0 and 1, allowing DF to drive the system to fixation. Similarly to the constant environment case, the most likely type of strain fixation is determined by whether $x_{\text{th}} > x^* \approx \ln\left(\frac{1-s}{1-a}\right)$ or $x_{\text{th}} < x^*$; see Figs. 3.2(a) and 3.7. Furthermore, fixation occurs prior to the condition for long-lived coexistence when x is close to the absorbing boundaries; see Figs. 3.2(b) and 3.7. In Fig. 3.7(a,e,i), we have $x_{\text{th}} = 0.1 < x^* \approx 0.37$, therefore leading to a fast fixation of S, whereas in Fig. 3.7(d,h,l), we see a fast R fixation since $x_{\text{th}} = 0.9 > x^*$. In these same two sets of panels we see the impact of slow and fast environmental switching rate ν. In Figs. 3.7(a,e,i), the switching rate is particularly slow, and so the population remains in its initial harsh environmental state at $K(t) = K(0) = K_-$ until fixation. In Figs. 3.7(d,h,l), the switching rate is very fast, and the carrying capacity attains its effective value $\mathcal{K}$. In the remaining panels of Figs. 3.7(b,f,j) and Figs. 3.7(c,g,k) we see that in the case in which x_{th} is close to x^*, with x_{th} far from the boundaries at 0 and 1, we find a long-lived coexistence. Environmental switches, and in particular time in the harsh environmental state, lead to periods where DF are enhanced due to the smaller population size. This is seen in Fig. 3.7(b,c), where

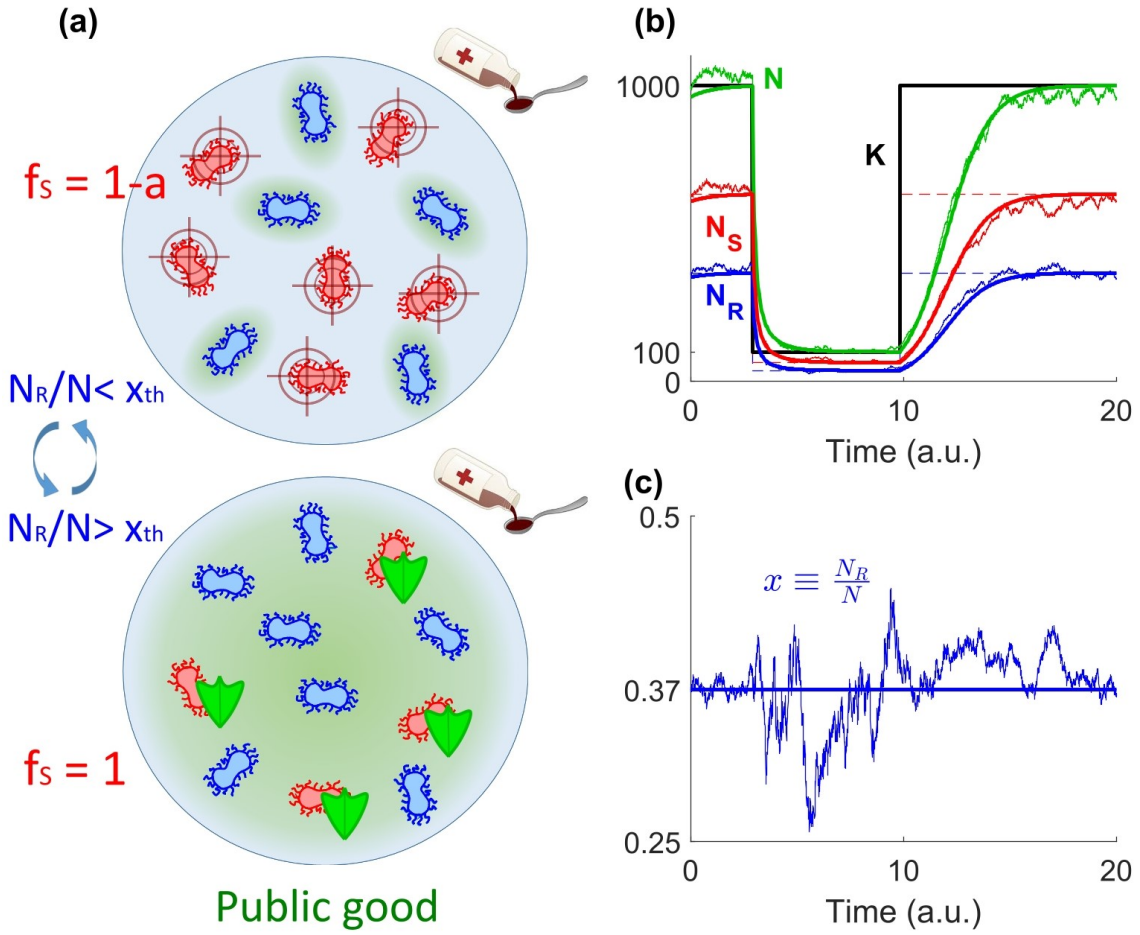

Figure 3.6: Model cartoon and example realisations. (a) Top: when the fraction of R (blue microbes) is below the concentration cooperation threshold $x_{\rm th}$, antimicrobial drug hinders the growth rate of S (red microbes) and R has a growth advantage. Bottom: in a cooperative scenario arising above the concentration cooperation threshold, resistance becomes shared (green shields) as the fraction of R exceeds $x_{\rm th}$ and these generate enough *resistance enzyme* (public good, green shade) to break down the drug and bring its concentration below the MIC for the whole community. (b) Eco-evolutionary dynamics of the microbial community for parameters $x_{\rm th} = 0.37$, $s = 0.1$, $a = 0.25$, $K_- = 100$, $K_+ = 1000$, $\nu = 0.1$, $\delta = 0.5$, and for initial conditions $K(t=0) = K_+$, $N_R(t=0) = x_{\rm th}K_+$, and $N_S(t=0) = (1-x_{\rm th})\,K_+$; thick black line shows the sample path of the time-switching carrying capacity $K(t)$, thick solid coloured lines correspond to a realisation of the PDMP that ignores DF and is defined by Eqs. (2.23) and (3.4) (see Ch. 3.4.1), for the total population (N, green), number of R ($N_R = xN$, blue), and number of S ($N_S = (1-x)N$, red); noisy lines are the corresponding stochastic realisation of the full model under the joint effect of DF and EV; dashed lines show the piecewise (meta-)stable equilibrium $N_R = x_{\rm th}K(t)$ (blue) and $N_R = (1-x_{\rm th})K(t)$ (red). (c) R fraction $x = N_R/N$ for the same sample path of varying environment as in (b); line styles as in panel (b).

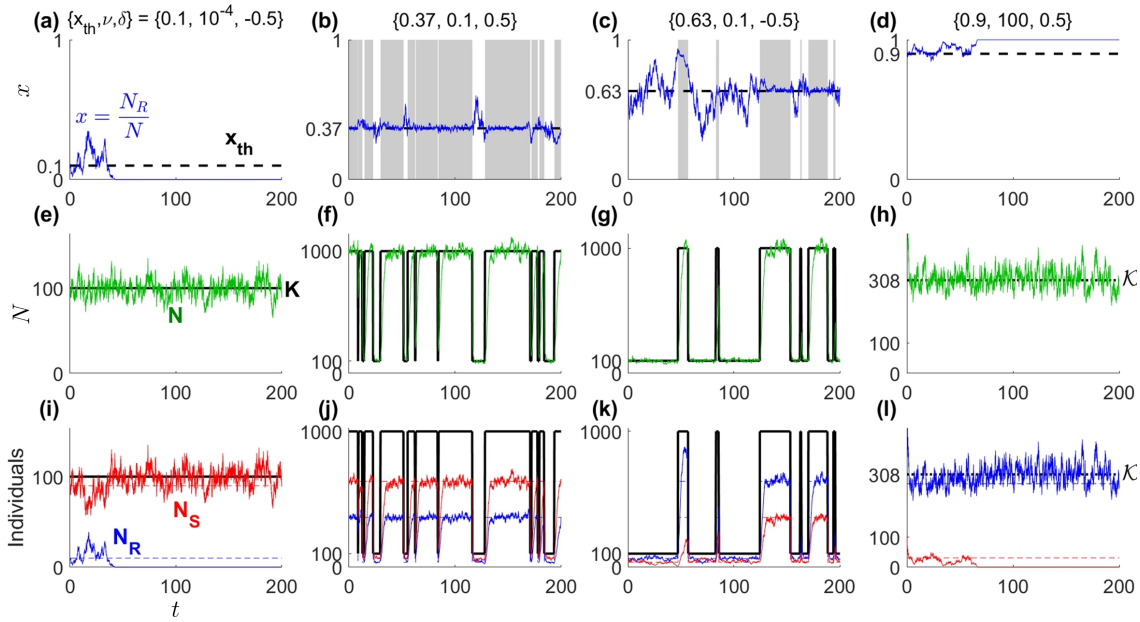

Figure 3.7: Eco-evolutionary dynamics sample paths. (a-d) Examples of R fraction sample paths from simulations (blue lines) for four concentration cooperation thresholds x_{th} (dashed black lines), three average switching rates ν, and two environmental biases δ, for $s = 0.1$, $a = 0.25$, $K_- = 100$, and $K_+ = 1000$, with initial conditions $N_R(t=0) = x_{\text{th}}K(t=0)$ and $N_S(t=0) = (1-x_{\text{th}})\,K(t=0)$. Shaded and white areas in panels (b-c) encode periods of abundance ($K(t) = K_+$) and scarcity (K_-), respectively. Note the larger amplitude of DF for the latter since $N \to K_- \ll K_+$. (e-h) Same example paths as in the corresponding panels (a-d) for the population size N (green lines); black lines show example path for the carrying capacity K. The very high environmental switching rate ν in panel (h) provides the effectively constant carrying capacity $\mathcal{K}$ (black dashed line). (i-l) Same example paths as in the previous panels for the number of R (blue lines) and S (red lines). Dashed lines show the corresponding (meta-)stable coexistence equilibrium $N_R = x_{\text{th}}K$ (blue) and $N_S = (1-x_{\text{th}})K$ (red). The DF and low value of $x_{\text{th}} = 0.1$ in panels (a,e,i) lead to fast extinction of R, whereas the high threshold $x_{\text{th}} = 0.9$ and DF in panels (d,h,l) lead to an early fixation of R and extinction of S.

$x_{\text{th}} = 0.37$ and $x_{\text{th}} = 0.63$ with $\nu = 10^{-1}$ and the bottlenecks where $N \approx K_-$ are given by periods with white background. We see that following an environmental switch, in this intermediate switching range the switches are slow enough that N can relax to $K(t)$. The distribution of N is similarly well captured by Eq. (2.27) as the dynamics of N remain the same.

These features are essentially in line with the discussion of Ch. 3.2, and hence similar to the behaviour found in static environments. In the next section, we will see that, in a dynamic environment, fixation of either strain is also possible when $x_{\text{th}} \approx x^*$ and that there can be long-lived coexistence also when $x_{\text{th}} \approx 0, 1$. These are distinctive effects of EV that are analysed in detail in what follows.

3.4.2 Theory for the fixation-coexistence diagrams

In this section we develop the analytical methods for time-varying environments allowing us to predict when one of the strains will fixate, and when both strains will coexist for long-periods. The theory that we have devised and discuss here is used to analytically reproduce the fixation-coexistence diagrams; see Fig. 3.8(e-h), of Fig. 3.8(a-d) obtained from simulations.

We identify and distinguish between two environmental switching regimes in which the dynamics of fixation and long-lived coexistence are captured by distinct approaches. These regimes are denoted the *quenched* (Q) and *annealed* (A) regimes. These regimes are distinguished by whether or not an environmental switch is expected before the coexistence time $2\langle N\rangle$, respectively. In the Q regime, this therefore requires the environmental switching be so slow, $\nu \ll 1$, and/or so biased $\delta \approx \pm 1$, that no switch occurs before $2\langle N\rangle$ regardless of the initial condition. Conversely, in the A regime we require at least one environmental switch prior to $2\langle N\rangle$. In each case, the analogy is made with quenched and annealed disorder from statistical physics, where for a given realisation the random variable (here the carrying capacity) is either constant or time-varying, respectively (Goldenfeld, 1992; Nishimori & Ortiz, 2010). Similar Q and A environmental regimes have been identified elsewhere (Meyer et al., 2023; Mobilia, 2023). It is worth noting that the annealed regime in similar settings corresponds to the limit of $\nu \to \infty$, where the EV self-averages as seen in Ch. 2.3.2 (Wienand et al., 2017, 2018; Taitelbaum et al., 2020; Meyer et al., 2023; Mobilia, 2023; Taitelbaum et al., 2023). While the A regime is typically used to capture behaviour in this limit, here we also use it to capture the case of intermediate switching where we expect only a finite number of switches prior to fixation or the long-lived coexistence condition. In fact, we find qualitative similarities between these two regimes. The border between Q and A regimes is determined by

$$\max\left(1/\nu_{\pm}\right) \equiv 1/(\nu(1-|\delta|)) = 2\langle N\rangle,$$

splitting the fixation-coexistence ν-δ diagrams of Fig. 3.8 into two distinct regions separated by green/yellow lines where areas to the left of these lines are the Q regime and

areas to the right are the A regime.

Quenched environmental regime. In Q, environmental switches are particularly slow. The environment is initialised in the state $K(0) = K_+$ with probability $(1+\delta)/2$ or $K(0) = K_-$ with probability $(1-\delta)/2$, and the carrying capacity remains at this initial value, $K(t) = K(0)$, at least until time $2\langle N\rangle$. Therefore, the joint probability for a realisation to undergo R fixation and to do so in a time $\zeta \leq 2\langle N\rangle$ (i.e. fast fixation) in the regime Q, denoted by Φ^{Q}, is

$$\begin{aligned}\Phi^{\mathrm{Q}} &\equiv \text{Prob.}(R \text{ fixation},\ \zeta \leq 2\langle N\rangle \mid \text{regime Q}) \\ &= \frac{1+\delta}{2}\,\phi_{K_+}\left(1-\eta^Q_{K_+}\right) + \frac{1-\delta}{2}\,\phi_{K_-}\left(1-\eta^Q_{K_-}\right),\end{aligned}$$

where ϕ_N is the R fixation probability in a population of fixed size N, given by Eq. (3.5), and

$$\eta^Q_N \equiv \text{Prob.}\,(\zeta > 2N) = \exp\left(-\frac{2N}{\tau_N}\right)$$

is the probability of long-lived coexistence in the Q regime, at a constant total population N, with MFT τ_N, as in Eq. (3.7).

Annealed environmental regime. In A, environmental switches are fast enough that at least one switch occurs prior to time $2\langle N\rangle$ regardless of the initial condition. This allows N to experience the full range of values from its quasi-stationary distribution, approximated by $p(N)$ of Eq. (2.27), prior to fixation or long-lived coexistence. Similarly to Wienand et al. (2017, 2018), we assume that fixation occurs in such a system occurs at a population size N where the probability density of N is given by $p(N)$. Following Assaf and Mobilia (2010) and Mobilia and Assaf (2010), we know the MFT τ_N in a population of constant size N where fixation occurs due to deviations from a coexistence state are given by the inverse of the flux towards the absorbing boundaries, and thus the fixation probability ϕ_N is given by the relative flux into the state $N_R = N$ compared to the total flux into the absorbing states. Therefore, ϕ_N/τ_N gives the "rate of R fixation" in a population of size N. Similarly, the "rate of S fixation" is given by $(1-\phi_N)/\tau_N$. In analogy to the constant N case, we define the rates to each fixation in the varying environment by averaging these quantities over $p(N)$ to account for the varying population size. This gives *effective rates* of fixation for each type in the A regime, given by

$$\mathcal{T}_R = \int_{K_-}^{K_+} \frac{\phi_N}{\tau_N} p(N)\ \mathrm{d}N \quad \text{and} \quad \mathcal{T}_S = \int_{K_-}^{K_+} \frac{1-\phi_N}{\tau_N} p(N)\ \mathrm{d}N.$$

Since $\tau_{K_+} \gg \tau_{K_-}$, the main contributions to $\mathcal{T}_{R/S}$, and hence to fixation, arise where N is smallest. For $\nu \ll 1$ this occurs chiefly around $N \approx K_-$, whereas for $\nu \gg 1$ we find that $p(N)$ is unimodal around $N \approx \mathcal{K}$ and each environment contributes similarly. With $\mathcal{T}_{R/S}$, we obtain the R fixation probability and MFT, ϕ^{A} and τ^{A}, respectively, in formal analogy

with the static environment case (Assaf & Mobilia, 2010; Mobilia & Assaf, 2010), giving

$$\phi^{\mathrm{A}} = \frac{\mathcal{T}_R}{\mathcal{T}_R + \mathcal{T}_S} \quad \text{and} \quad \tau^{\mathrm{A}} = \frac{1}{\mathcal{T}_R + \mathcal{T}_S}. \tag{3.13}$$

Furthermore, the long-lived coexistence probability in regime A is given by

$$\eta^{\mathrm{A}} = \exp\left(-\frac{2\langle N\rangle}{\tau^{\mathrm{A}}}\right). \tag{3.14}$$

Eqs. (3.13) and (3.14) allow us to find the joint probability of R fixation and fast fixation in a time $\zeta \leq 2\langle N\rangle$ in the regime A, denoted by Φ^{A}, as

$$\Phi^{\mathrm{A}} \equiv \text{Prob.}(R \text{ fixation},\ \zeta \leq 2\langle N\rangle \mid \text{regime A}) = \phi^{\mathrm{A}}(1-\eta^{\mathrm{A}}),$$

where we have again assumed that strain fixation type and long-lived coexistence are completely uncorrelated.

Crossover regime and general results. Having obtained the fixation and coexistence probabilities in regimes Q and A, we can superpose their expressions to obtain predictions applicable in the crossover regime (about the green/yellow line in Fig. (3.8)), as well as in regimes Q and A. This provides us with general results, that are valid for the entire range of environmental parameters $\{\nu, \delta\}$. Since the probability that no switches occur by time $2\langle N\rangle$ is

$$\Pi \equiv \exp\left[-2\langle N\rangle\nu\,(1-|\delta|)\right],$$

and the probability that at least one switch has occurred by $2\langle N\rangle$ is $1-\Pi$, the overall joint probability of R fixation and fast fixation is

$$\Phi = \Pi\Phi^{\mathrm{Q}} + (1-\Pi)\Phi^{\mathrm{A}}. \tag{3.15}$$

The overall probability of long-lived coexistence is obtained by a similar superposition of η^{Q} and η^{A}, yielding

$$\eta = \Pi\eta^{\mathrm{Q}} + (1-\Pi)\eta^{\mathrm{A}}. \tag{3.16}$$

Equations (3.15) and (3.16) used in the theoretical predictions of Figs. 3.8 and 3.9.

3.4.3 Comparison of theory and simulations

Here, we compare the results of computer simulations and theoretical predictions of Ch. 3.4.2, fully characterising the long-time eco-evolutionary dynamics of the population in a time-varying environment.

The fixation-coexistence diagrams in Fig. 3.8(a-d) show simulation results for the probability of fast R fixation (blue), fast S fixation (red), or long-lived coexistence (black), for different values of the concentration cooperation threshold x_{th}. The main features of these diagrams can be understood in terms of the analysis carried out in Ch. 3.2 and the critical cooperation threshold value $x^* \approx \frac{\ln(1-s)}{\ln(1-a)}$, which to this level of approximation

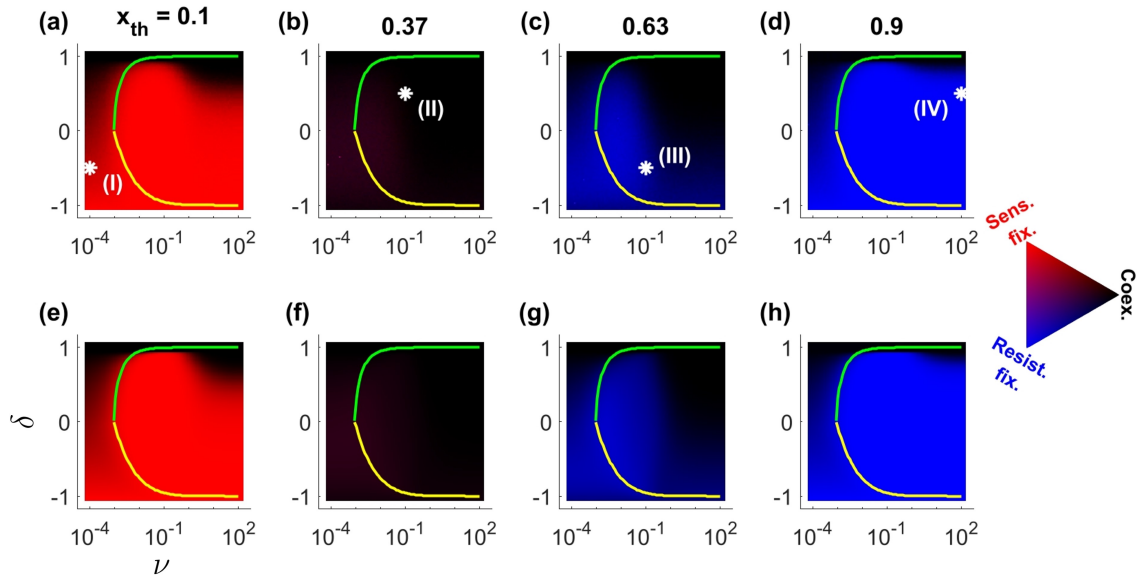

Figure 3.8: Characterisation of the long-time eco-evolutionary dynamics by the fixation-coexistence diagrams. (a-d) Fixation type and fast fixation joint probability from simulations for EV parameters ν (average environmental switching rate) and δ (environmental switching bias), $s = 0.1$, $a = 0.25$, $K_- = 100$, $K_+ = 1000$, and the concentration cooperation thresholds $x_{\rm th} = 0.1,\ 0.37,\ 0.63$, and 0.9. Here, $x^* \approx 0.366$, and the total population is initialised at quasi-stationarity, with $N_R(t=0) = x_{\rm th}K(t=0)$ and $N_S(0) = (1-x_{\rm th})\,K(0)$. Stronger blue (red) corresponds to a higher fixation probability of R (S). Darker colour indicates a higher long-coexistence probability, defined as the probability to have no fixation event by time $2\langle N\rangle$, where we take twice the average total population in its stationary state (average across 10^3 realisations). The green/yellow lines separate the environmental regimes Q and A (respectively on the left and right of the lines); see Ch. 3.4.2. The white asterisks in (a-d) refer to the values of ν and δ used for each of the panel columns in Fig. 3.7. (e-h) Theoretical fixation-coexistence diagrams: same as in panels (a-d) for the theoretical predictions of the fixation-coexistence joint probability given by Eqs. (3.15) and (3.16), where $2\langle N\rangle$ is computed as twice the average over the distribution of Eq. (2.27). Analytical results reproduce remarkably the features of those from simulations.

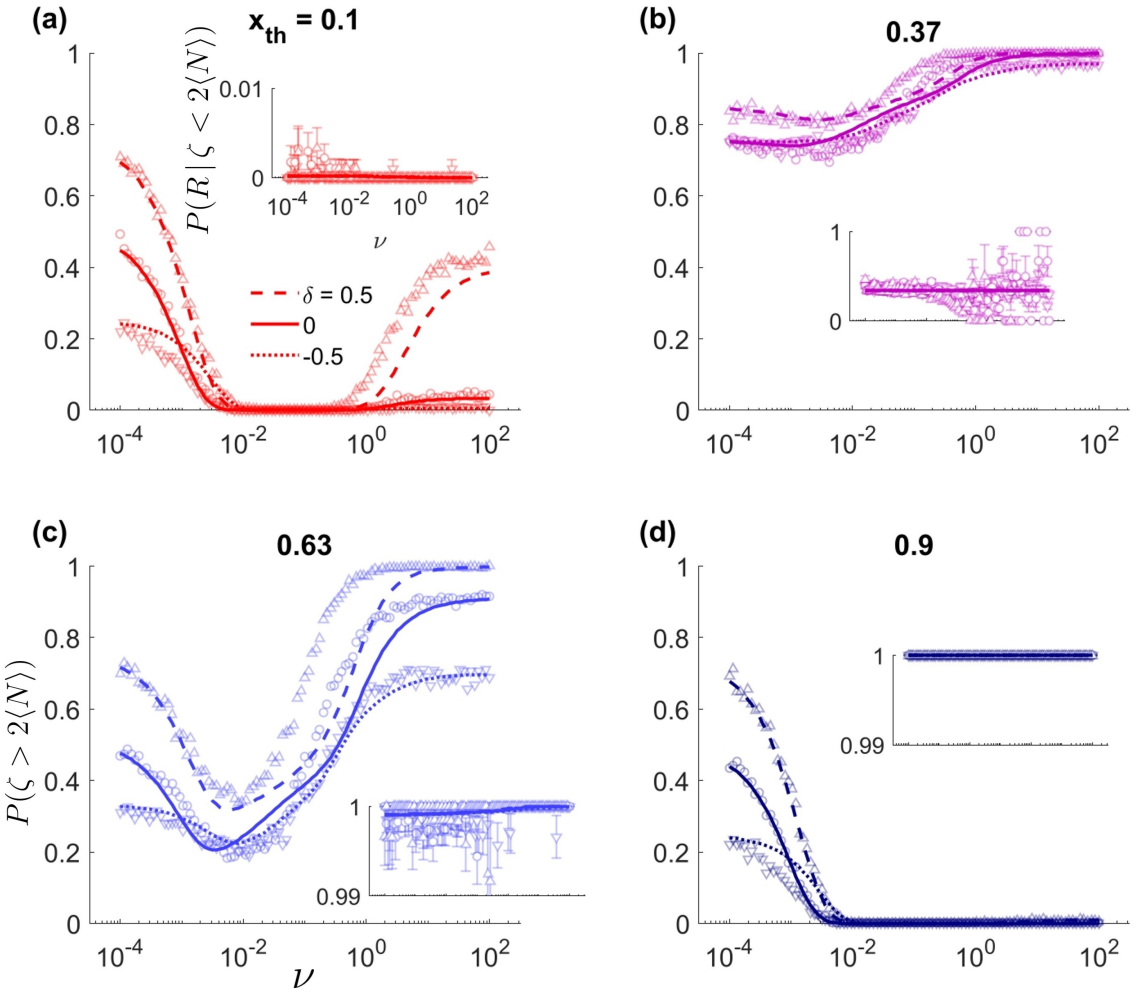

Figure 3.9: Eco-evolutionary probabilities of long-coexistence and fast R fixation. (a) Long coexistence probability at quasi-stationarity $P\left(\zeta > 2\langle N\rangle\right)$, defined as no fixation occurring by $2\langle N\rangle$, as a function of the average environmental switching rate ν for a concentration cooperation threshold of $x_{\text{th}} = 0.1$ and different values of the environmental bias δ. By $t = 2\langle N\rangle$, we assume that N has already reached its quasi-stationary distribution, which we approximate as Eq. (2.27) in the theoretical predictions. Dotted lines (downward triangles), solid lines (circles), and dashed lines (upward triangles) show results for $\delta = -0.5$, 0, and 0.5, respectively. Lines are theoretical predictions from η in Eq. (3.16), and markers are simulation data. Other parameters are: $s = 0.1$, $a = 0.25$, $K_- = 100$ and $K_+ = 1000$, as in Fig. 3.8. Inset: R fixation probability conditioned on fast fixation $P\left(R|\zeta \leq 2\langle N\rangle\right)$ as function of ν; lines are theoretical predictions from $\Phi/(1-\eta)$ (see Eqs. (3.15) and (3.16)); all three theoretical lines for each δ are indistinguishable. Error bars show the binomial standard error of the mean. (b-d) Same as in (a) for $x_{\text{th}} = 0.37$, 0.63, and 0.9. Note that simulation data presents larger error bars for $\nu > 10^{-1}$ in the inset of panel (c) due to the limited proportion of fast fixations in this regime.

is independent of N. When $x_{\rm th} < x^*$ (and $x_{\rm th} \lesssim 1/\sqrt{\langle N\rangle}$), the most likely outcome is the fast fixation of S, while fast fixation of R is the most probable outcome when $x_{\rm th} > x^*$ (and $1 - x_{\rm th} \lesssim 1/\sqrt{\langle N\rangle}$). Long-lived coexistence of R and S is expected when $\min(x_{\rm th}, 1 - x_{\rm th}) \gg 1/\sqrt{\langle N\rangle}$), with the composition determined by $x_{\rm th}$. For the parameters of Fig. 3.8, $x^* \approx 0.37$, and we indeed notice that most of Fig. 3.8(a) appears in red, Fig. 3.8(c,d) are mostly coded in blue, and most of Fig. 3.8(b) appears in black.

We notice however that each panel of Fig. 3.8 is coded in two colours, indicating either fast fixation or long-lived coexistence. In fact, due to EV, long-lived coexistence is possible even when fast fixation of S and R is most likely. In Fig. 3.8(a,d) this leads to the red and blue dominated diagrams to also contain a dark/black area for δ close to 1 (bias of $K(t)$ towards K_+). This can be qualitatively explained by noting that, as $K(t)$ is biased towards K_+, the population size is essentially constant and large, $N \approx K_+$, and does not admit fast fixation of either strain. Similarly, EV can allow for fast fixation even when long-lived coexistence is expected, as found in Fig. 3.8(b), where the black-dominated diagram (due to $x_{\rm th} \approx x^*$) contains a dark coloured "cloud". Here, fast fixation events occur for low values of ν and $\delta \leq 0$, when $N \approx K_-$ for long periods, and the small population size ($K_- = 100$) facilitates early extinction of either R or S; see Fig. 3.9.

In general, the colour-coding of the fixation-coexistence ν-δ diagrams of Fig. 3.8 can be qualitatively understood by noting on the one hand that, as δ is increased from -1 to 1 (at fixed ν), the EV bias moves from K_- (small population) to K_+ (large population), and hence favours long-lived coexistence. On the other hand, increasing the environmental switching rate from slow ($\nu \ll 1$) to intermediate ($\nu \sim 1$) hinders strain coexistence since, under intermediate switching, irrespective of the starting environment, the microbial community experiences long population bottlenecks ($N \approx K_-$) that enhance DF and thus favour fast fixation. However, further increasing the rate to fast switching ($\nu \gg 1$) increases the probability of long-lasting coexistence: the duration of population bottlenecks is reduced, and the community effectively experiences the effective carrying capacity $\mathcal{K} > K_-$, with lower DF and enhanced coexistence. Note that, for extreme values of $x_{\rm th}$, which are closer to extinction/fixation of one strain ($x = 0, 1$), the latter does not hold, as weak DF suffice to prevent coexistence.

With the aim of understanding the evolution of AMR, we are particularly interested in finding the conditions favouring the early extinction of R, and hence the fast fixation of S, since this corresponds to the most favourable environmental conditions for the *eradication of AMR*, as in Ch. 3.3. Here, the best conditions for AMR eradication appear as red areas in the diagrams of Fig. 3.8: these are low values of $x_{\rm th}$ and δ not too close to 1; see Fig. 3.8(a). Moreover, as a signature of the influence of EV, discussed previously, we find that AMR eradication is also possible for intermediate values of $x_{\rm th} \gtrsim x^*$; see dark red/purple area in Fig. 3.8(b) for $\nu < 10^{-1}$ and inset of Fig. 3.9(b).

In summary, a high positive EV bias δ (at fixed ν) and a moderate cooperation threshold ($x_{\rm th} \approx x^*$) favours long-lived coexistence; while intermediate EV switching rates ν (at

fixed δ), and more extreme cooperation thresholds, favour fast fixation of either R (for $x_{\text{th}} \gg x^*$) or S (for $x_{\text{th}} \ll x^*$). This qualitatively explains the boundaries between the coloured and black regions in the fixation-coexistence diagrams of Fig. 3.8; and, notably, it captures the long-lived coexistence in the top/right-half and fast R fixation in the bottom/left-half of Fig. 3.8(c). Critically, the location of the boundaries between the phases of long-lived coexistence and fast fixation are accurately predicted by the theory presented in Ch. 3.4.2, as shown in Fig. 3.8(e-h) where the fixation-coexistence diagrams are reproduced remarkably well by the predictions of Eqs. (3.15) and (3.16). However, we do not find environmental conditions in which we can generally eradicate AMR. This suggests that, in trying to eradicate AMR through bottlenecks, introducing them through restricting nutrient concentration and maintaining a constant volume (as in Ch. 3.3) is the more effective approach.

Fig. 3.9 provides a more quantitative comparison between the fixation-coexistence diagrams obtained from simulations in Fig. 3.8 (top row) and from the theory of Ch. 3.4.2 (bottom row), for three different values of environmental bias (high/low δ and $\delta = 0$). In each panel we find that the ν-dependence of the long-lived coexistence probability, that is, the probability that $\zeta > 2\langle N \rangle$ for a realisation, is well captured by the theoretical prediction of η given by Eq. (3.16). The agreement between simulations and η is quantitatively remarkable at low and high values of ν. For intermediate values of ν, the predictions of η are able to reproduce the main qualitative features of the simulation data, including the non-monotonic behaviour arising in Fig. 3.9(a,c). The values of ν for which the probability of long-lived coexistence is low correspond to regions coloured in red/blue in Fig. 3.8. The main deviations between theory and simulations arise in the regime of intermediate ν and high δ. We attribute these deviations to the assumptions made in the annealed regime (approximation of the actual fixation rates), leading to an underestimate of the long-lived coexistence probability. The inset of each panel of Fig. 3.9 illustrates the R fixation probability, conditioned on fast fixation, which determines the relative red-to-blue colour levels in Fig. 3.8. Consistently with the fixation-coexistence diagrams of Fig. 3.8, fast R fixation is found to be essentially independent of switching rate ν and bias δ, a feature that is well reproduced by the theoretical predictions (lines in Fig. 3.9), obtained from Eqs. (3.15) and (3.16) as

$$\Phi/(1-\eta) \equiv \mathrm{P}\left(R \,|\, \zeta \leq 2\langle N \rangle\right).$$

The inset of Fig. 3.9(b) indicates that the probability of fast S fixation is more likely than fast R fixation (whose probability is less than 1/2), which explains the dark red/purple "cloud" in Fig. 3.8(b).

Chapter 4

Twofold environmental variability

So far, in this thesis we have considered only EV impacting the death rates of the species, where the death rates switch between larger and smaller values, corresponding in our motivating example to lower or higher nutrient availability; see Ch. 2.3.2. However, the (per capita) birth rates remain unaffected. Naturally, one may then ask the following question: what happens if the stochastic switching is not limited to the death rates, but also impacts the birth rates of the species? Such a setup where both the birth and death rates vary stochastically in time captures the dynamics of various microbial communities of interest. Considering an extension on the simple example of Ch. 2.3.2, an additional EV impacting birth rates could be seen as a variation in toxin level (i.e. an antimicrobial above or below MIC) where one species is resistant to the toxin and the other is sensitive. Alternatively, one may envisage a population undergoing stochastic nutrient variations, with competition for shared resources between a wild-type species with constant birth rate and a mutant *bet-hedging* species (Gaál et al., 2010; Xue & Leibler, 2017; Barabás et al., 2018), which stochastically switches between periods of high and low birth rate. In any case, we consider that this additional stochastic switching changes the *direction* of selection, i.e. which species is fittest and therefore predicted to increase in relative abundance at the MF level. Under these dynamics, the population experiences EV that drives the population size impacting both species in an identical manner, and EV that changes the direction of selection such that each environmental switch benefits only one of the species.

In this chapter, motivated by evidence showing that microbial communities generally evolve in volatile environments (Thattai & Van Oudenaarden, 2004; Fux et al., 2005; Hooper et al., 2005; Caporaso et al., 2011; Rescan et al., 2020; Murugan et al., 2021), I shall consider a toxin level in the environment that switches stochastically impacting species birth rates in addition to the previously introduced stochastically varying nutrient level affecting species death rates, reflecting additional EV in the system, i.e. *twofold environmental variability*. I will characterise the behaviour of the population first under only toxin-level switches, demonstrating that a long-lived coexistence between species is possible under sufficiently strong and frequent toxin EV. I will then investigate how this

picture changes under additional EV in the nutrient level. We will see that stronger toxin-level EV promotes coexistence, while stronger nutrient-level EV jeopardises it, therefore demonstrating the non-trivial impact of EV on the coexistence of species - a topic of particular interest in biology and ecology (Chesson & Warner, 1981; Chesson, 1994, 2000a, 2000b; Barabás et al., 2018; Ellner et al., 2019; Abdul-Rahman et al., 2021) with applications to problems of great societal concern such as the maintenance of biodiversity (Kalyuzhny et al., 2015; Ghoul & Mitri, 2016; Leibold et al., 2019; M. L. Pinsky, 2019; Grilli, 2020; Meyer & Shnerb, 2020; Meyer et al., 2021; Hu et al., 2022; R. West & Shnerb, 2022) and the evolution of AMR (Balaban et al., 2004; Yurtsev et al., 2013; W.-H. Lin & Kussell, 2016; Raymond et al., 2016; Lopatkin et al., 2017; Coates et al., 2018).

Contents of this chapter appear in Asker et al. (2023).

4.1 Model description

I consider a well-mixed population consisting of $N(t) = N_R(t) + N_S(t)$ individuals which, at time t, consists of N_R resistant cells labelled R and N_S sensitive cells labelled S, which compete for the same resources. Though named the same as the previous chapter, these species differ to those defined there. The resistant R species has paid a metabolic cost for resistance to a toxin that is private to the resistant species, while the sensitive strain pays no metabolic cost and is sensitive to the toxin; see Fig. 4.1. For concreteness, we again assume a biostatic toxin as in Ch. 3 (Hernández-Navarro et al., 2023; Hernández-Navarro, Asker, & Mobilia, 2024). In this setting, resistant R bacteria have a constant fitness f_R, whereas the sensitive S bacteria have an environment-dependent fitness $f_S(\xi_T)$, where $\xi_T(t) \in \{-1, 1\}$ is a DMN variable encoding the toxin level: $\xi_T = 1$ for the low toxin level and $\xi_T = -1$ for the high toxin level. DMN again adequately captures sudden and drastic variations in the environment of the population; see Ch. 2.3. We here consider

$$f_R = 1 \qquad \text{and} \qquad f_S = \exp(s\xi_T),$$

where $s > 0$ denotes the selection bias favouring the strain S when $\xi_T = 1$, and strain R when $\xi_T = -1$. The parameter s therefore encodes both selection and the strength of the EV associated with the changes in toxin level (T-EV); see Appendix B.1. An exponential is chosen for f_S to allow for a greater range of s and an equivalent multiplicative effect on the fitness in each state compared to R. The average fitness of the population, $\overline{f}$, is therefore given by

$$\overline{f} = N_R/N + N_S \exp(\xi_T s)/N,$$

and thus also depends on the T-EV. The environmental effect on the level of nutrients (K-EV), varying between scarcity and abundance, is modelled as before with the carrying capacity, $K(t)$, evolving according to Eq. (2.22), where we now denote the DMN driving the carrying capacity $\xi_K \in \{-1, 1\}$. This again captures the sharp and sudden variations in the environment which occur, particularly in microbial populations; see Ch. 2.3.

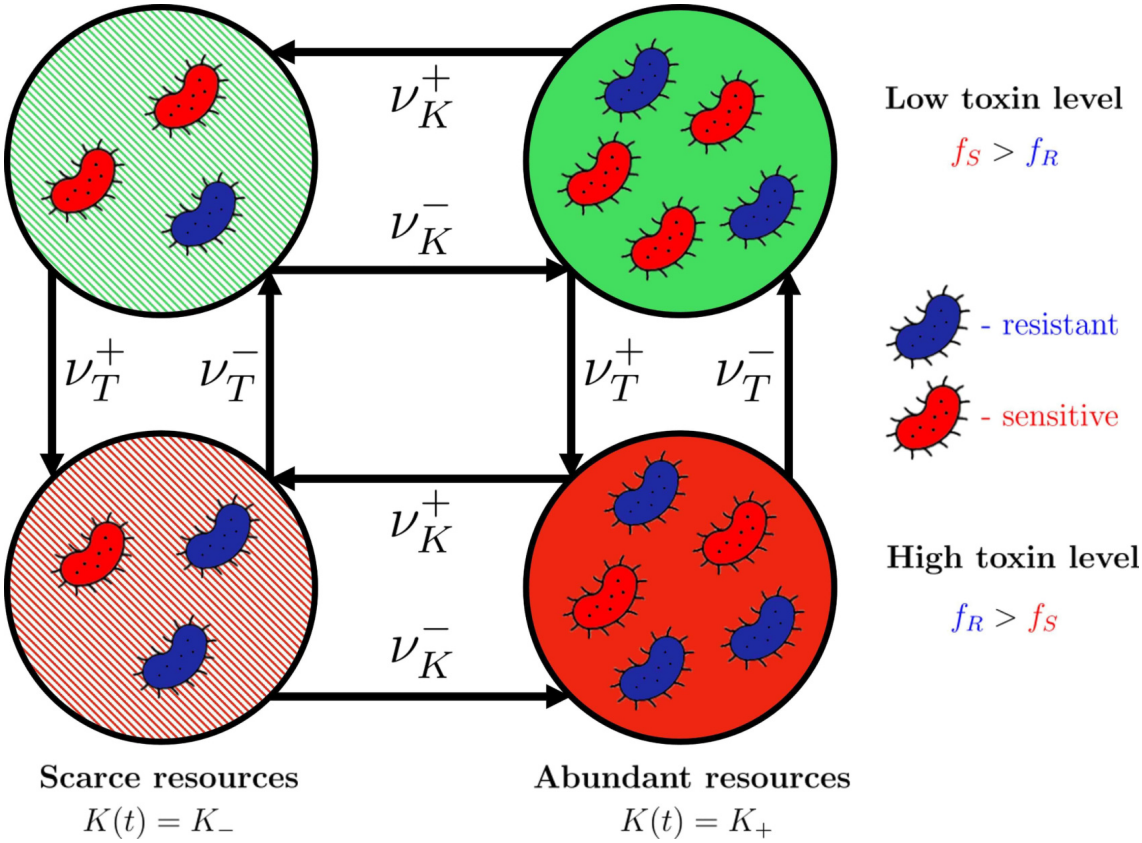

Figure 4.1: Cartoon of the model characterised by twofold EV. A microbial community consisting of two strains, denoted by R (resistant, blue , fitness f_R) and S (sensitive, red, fitness f_S), evolves in a time-varying environment, as illustrated by the arrows: the level of toxin, ξ_T, stochastically switches with rates $\nu_T^\pm$ (vertical arrows) between low ($\xi_T = +1$) and high ($\xi_T = -1$), and the amount of available resources, modelled by the carrying capacity $K(t)$, stochastically switches with rates $\nu_K^\pm$ (horizontal arrows) between scarce and abundant. The strain R fares better than S under high toxin level ($f_R > f_S$), while S grows faster under low toxin level ($f_R < f_S$). The carrying capacity $K(t) = K_+$ when there are abundant resources, while $K(t) = K_- < K_+$ when available nutrients are scarce. The four environmental states characterising the twofold EV are indicated by their background: striped / solid refers to scarce / abundant resources, while green / red shows low / high toxin level.

The population therefore evolves under twofold EV encoded in the environmental states ξ_T, ξ_K (see Fig. 4.1) by the reactions

$$\xi_\alpha = +1 \xrightarrow{\nu_\alpha^+} -1, \quad \text{and} \quad \xi_\alpha = -1 \xrightarrow{\nu_\alpha^-} +1,$$

where $\nu_\alpha^\pm$ are the switching rates of the α-DMN, with $\alpha \in \{T, K\}$ indicating the relevant EV. We similarly define the average switching rate ν_α and switching bias δ_α for each α-DMN as

$$\nu_\alpha \equiv \frac{\nu_\alpha^- + \nu_\alpha^+}{2} \quad \text{and} \quad \delta_\alpha \equiv \frac{\nu_\alpha^- - \nu_\alpha^+}{2\nu_\alpha},$$

such that $\nu_\alpha^\pm \equiv \nu_\alpha(1 \mp \delta_\alpha)$. Hence, $\delta_T > 0$ corresponds to a bias towards low toxin level (mild T state, $\xi_T = +1$) favouring the S strain, whereas $\delta_T < 0$ indicates a bias towards

high toxin level (harsh T state, $\xi_T = -1$) where the growth of S is hampered and the R is better off; see Fig. 4.1. Similarly, $\delta_K > 0$ corresponds to bias towards the environmental state rich in nutrients (where $K = K_+$), while $\delta_K < 0$ is associated with a bias towards an environment where nutrients are scarce ($K = K_-$), identically to that considered in the previous chapters. We also similarly define $K_0 = (K_+ + K_-)/2$ and $\gamma = (K_+ - K_-)/(2K_0)$.

We make the plausible assumption that ξ_K and ξ_T are totally uncorrelated here. Considering the motivating example, this assumption implies that the toxin and nutrient levels vary independently. The case where ξ_T and ξ_K are fully correlated or fully anti-correlated, with $\xi_T = \xi_K = \xi$ or $\xi_T = -\xi_K = \xi$, where ξ is a single DMN process, is briefly discussed in Appendix B.4.

A chemostat setup, as discussed in Ch. 3, closely resembles the model considered here, whereby toxin and nutrient levels can be maintained at constant levels and switched via a modification of the concentration of incoming medium into the system (Abdul-Rahman et al., 2021; Shibasaki et al., 2021). The switch $\xi_T \to -\xi_T$ with $\xi_T = -1$ can be seen as switching the concentration of an antibiotic drug in the incoming medium from above the MIC, where R is better off since it is resistant, to a concentration below the MIC where the S strain is better off as it pays no metabolic cost (Yurtsev et al., 2013; W.-H. Lin & Kussell, 2016; Marrec & Bitbol, 2020). Similarly to the before, the switch $\xi_K \to -\xi_K$ can be seen as a change in the nutrient concentration in the incoming medium.

At time t, the fraction of R-types in the system is $x \equiv \frac{N_R}{N}$, giving the population composition. As before (see Eqs. (2.10) and (3.1)), the population size and composition evolve according to the birth-death process (van Kampen, 1992; Gardiner, 2009)

$$N_{R/S} \xrightarrow{T^+_{R/S}} N_{R/S} + 1 \quad \text{and} \quad N_{R/S} \xrightarrow{T^-_{R/S}} N_{R/S} - 1, \tag{4.1}$$

where the birth and death transition rates are

$$T^+_{R/S} = \frac{f_{R/S}}{\overline{f}} N_{R/S} \quad \text{and} \quad T^-_{R/S} = \frac{N}{K} N_{R/S}. \tag{4.2}$$

The differences of the model here compared to the previous chapters appear via the fitnesses through the factor $f_{R/S}/\overline{f}$. The per-capita birth rates $f_{R/S}/\overline{f}$ thus vary with the toxin level and population composition, while the logistic per-capita death rate N/K varies with nutrient level and population size. With $\mathbf{N} \equiv (N_R, N_S)$, the ME giving the probability $P(\mathbf{N}, \xi_T, \xi_K, t)$ for the population to consist of N_R and N_S bacteria of type R and S, respectively, in the environmental state (ξ_T, ξ_K) at time t is

$$\begin{aligned} \frac{\partial P(\mathbf{N}, \xi_T, \xi_K, t)}{\partial t} = \sum_{\alpha \in \{R,S\}} & \left\{ \left(\mathbb{E}^-_\alpha - 1\right) \left[T^+_\alpha P(\mathbf{N}, \xi_T, \xi_K, t)\right] \right. \\ & \left. + \left(\mathbb{E}^+_\alpha - 1\right) \left[T^-_\alpha P(\mathbf{N}, \xi_T, \xi_K, t)\right] \right\} \\ & + \nu_T^{-\xi_T} P(\mathbf{N}, -\xi_T, \xi_K, t) - \nu_T^{\xi_T} P(\mathbf{N}, \xi_T, \xi_K, t) \\ & + \nu_K^{-\xi_K} P(\mathbf{N}, \xi_T, -\xi_K, t) - \nu_K^{\xi_K} P(\mathbf{N}, \xi_T, \xi_K, t), \end{aligned} \tag{4.3}$$

where $\mathbb{E}^{\pm}_{R/S}$ are shift operators such that $\mathbb{E}^{\pm}_{R} f(N_R, N_S, \xi_T, \xi_K, t) = f(N_R \pm 1, N_S, \xi_T, \xi_K, t)$ and $\mathbb{E}^{\pm}_{S} f(N_R, N_S, \xi_T, \xi_K, t) = f(N_R, N_S \pm 1, \xi_T, \xi_K, t)$, and we have $\nu^{\xi_\alpha}_{\alpha} \equiv \nu^{\pm}_{\alpha}$ when $\xi_\alpha = \pm 1$. We note that the last two lines on the right-hand-side of Eq. (4.3) account for the random environmental switching of the toxin level ($\xi_T \to -\xi_T$) and the nutrient level ($\xi_K \to -\xi_K$). The stochastic simulation method set out in Appendix D.1 generates statistically correct trajectories and thus exactly reproduces the dynamics encoded in Eq. (4.3). As we have already discussed, fixation of one strain and extinction of the other is expected when strains compete for the same resources, and always occurs in a finite population (Wienand et al., 2017, 2018; Taitelbaum et al., 2020). In stark contrast, here we show that T-EV can lead to the long-lived coexistence of competing species where the dynamics under a static environment does not allow coexistence, unlike in Ch. 3 (Hernández-Navarro et al., 2023; Hernández-Navarro, Asker, & Mobilia, 2024). Furthermore, we find that K-EV jeopardises this long-lived coexistence. I characterise this behaviour and develop the necessary theoretical tools which accurately capture the long-time population evolution under twofold EV. Moreover, I demonstrate how the abundance of each species can be captured under twofold EV, showing that there exists an intermediate region of switching rates in the T-EV where a species abundance reaches its maximum or minimum. The understanding of coexistence in biology and ecology is a topic of much interest (Chesson & Warner, 1981; Chesson, 1994, 2000a, 2000b; Barabás et al., 2018; Abdul-Rahman et al., 2021), and thus demonstrating the contrasting effects of different forms of EV on coexistence is of particular relevance.

4.2 Time-varying fitness and constant carrying capacity

Given that ξ_T and ξ_K are independent random variables, it is useful to initially consider only the EV due to the varying toxin level, impacting the birth rates of Eq. (4.2), and maintain a constant carrying capacity. Therefore, in this section, we assume that the carrying capacity is constant and large, with $K(t) = K \gg 1$.

4.2.1 Mean-field analysis

In this section, we consider the case where $N = K \to \infty$, and thus ignore DF as these fluctuations become negligible with increasing population size; see Ch. 2.2.1. In this case, the population composition evolves according to the MF equation (Gardiner, 2009)

$$\dot{x} = \frac{T^{+}_{R} - T^{-}_{R}}{N} = x(1-x)\left(\frac{1 - e^{s\xi_T}}{x + (1-x)e^{s\xi_T}}\right). \tag{4.4}$$

Due to ξ_T, Eq. (4.4) is a MF *stochastic* differential equation that defines a PDMP, similarly to the PDMP considered in Ch. 2.3.1 for the population size N. Therefore, the evolution of x following the PDMP consists of periods of deterministic evolution according to Eq. (4.4) with a fixed value of ξ_T, interspersed with random switches in ξ_T which changes the deterministic evolution followed by x.

We consider Eq. (4.4) in the regimes of (i) low, (ii) high, and (iii) intermediate switching rate ν_T:

(i) Under low switching rate, $\nu_T \to 0$, the population reaches its final state without experiencing any T-switches and therefore maintains its initial toxin level $\xi_T(0)$, i.e. $\xi_T(0) = \xi_T(\infty) = \pm 1$ with probability $(1 \pm \delta_T)/2$. In this regime, Eq. (4.4) boils down to

$$\dot{x} = \begin{cases} -\frac{x(1-x)(e^s-1)}{x+(1-x)e^s} & \text{with probability } \frac{1+\delta_T}{2}, \\ \frac{x(1-x)(1-e^{-s})}{x+(1-x)e^{-s}} & \text{with probability } \frac{1-\delta_T}{2}. \end{cases}$$

Since $s > 0$, with a probability $(1 + \delta_T)/2$ we have $\xi_T(0) = \xi_T(\infty) = +1$ and $x \to 0$ (S fixates), while with a probability $(1 - \delta_T)/2$ we have $\xi_T(0) = \xi_T(\infty) = -1$ and $x \to 1$ (R fixates). Though under MF dynamics, x only reaches 0 or 1 as $t \to \infty$ and thus S or R fixation never occurs, the scenarios are still characterised by the dominance of either one of the strains in a sufficiently large population. Therefore, in the absence of DF, the MF dynamics predict that R and S cannot coexist for long periods under a low switching rate in the toxin level.

(ii) Under high switching rate, $\nu_T \gg 1$, the population experiences a large number of T-switches before relaxing into its final state; see later. In this case the T-EV *self-averages*, similar to the case of K-EV seen in Ch. 2.3.1. We are left with a process defined by the effective rates $T_R^{\pm} \to \langle T_R^{\pm} \rangle$ obtained by averaging ξ_T over its stationary distribution, yielding

$$\begin{aligned} \langle T_R^+ \rangle &= \frac{Nx}{2}\left(\frac{1+\delta_T}{x+(1-x)e^s} + \frac{1-\delta_T}{x+(1-x)e^{-s}}\right), \\ \langle T_R^- \rangle &= Nx. \end{aligned} \tag{4.5}$$

When $N \to \infty$, the MF equation associated with the effective process reads (van Kampen, 1992; Blythe & McKane, 2007; Gardiner, 2009)

$$\begin{aligned} \dot{x} &= \frac{\langle T_R^+ \rangle - \langle T_R^- \rangle}{N}, \\ &= \frac{x(1-x)}{2}\left[\frac{(1+\delta_T)(1-e^s)}{x+(1-x)e^s} + \frac{(1-\delta_T)(1-e^{-s})}{x+(1-x)e^{-s}}\right], \end{aligned} \tag{4.6}$$

where the right-hand-side can be interpreted as the right-hand side of Eq. (4.4) averaged over the stationary distribution of ξ_T. In addition to the trivial fixed points $x = 0$ and $x = 1$, Eq. (4.6) admits a *coexistence equilibrium*

$$x^* = \frac{1}{2} - \frac{\delta_T}{2}\coth\frac{s}{2}, \tag{4.7}$$

when $-\tanh\frac{s}{2} < \delta_T < \tanh\frac{s}{2}$. This equilibrium emerges from the T-DMN and thus is an *EV-induced coexistence point*. In the case of large s, we have that $\coth\frac{s}{2} \to 1$ and x^* exists ($0 < x^* < 1$) for all values of δ_T. Since $\frac{\mathrm{d}}{\mathrm{d}x}\dot{x}\big|_{x^*} = -\frac{4}{1-\delta_T^2}\tanh^2\left(\frac{s}{2}\right)(1-x^*) < 0$, linear stability analysis reveals that x^* is the sole asymptotically stable equilibrium of Eq. (4.6) when it exists ($x = 0, 1$ are thus unstable). When $s \ll 1$, $\coth\frac{s}{2} \to \frac{2}{s}$, and x^* exists only

for $-\frac{s}{2} < \delta_T < \frac{s}{2}$. This means that for $s \ll 1$, coexistence is essentially possible only under symmetric switching ($\delta_T = 0$); see Appendix B.1. In what follows, we focus on the less restrictive case $s = \mathcal{O}(1)$, for which coexistence is possible for a broad range of parameters (ν_T, δ_T).

(iii) In the regime of intermediate switching rate, where $\nu_T \sim 1$, the population experiences a finite number of T-switches prior to settling in its final state. Depending on the number of switches, as well as the selection strength s and the population size, the dynamics may be closer to either the slow or fast switching ν_T regimes, with dominance or coexistence possible but, in general, not certain; see Fig. 4.3 later.

4.2.2 Stochastic effects: fixation and long-lived coexistence

From the MF analysis, we have found that when $N \to \infty$ species coexistence is possible under fast T-EV switching, whereas only R or S dominance occurs under slow switching. We now study how these results change when the population size is fixed but finite.

Carrying out the MA to capture the evolution according to Eqs. (4.1) and (4.2) (as seen in Ch. 2.2.2 and 3.2) we find the effective reactions

$$\begin{aligned}(N_R, N_S) &\xrightarrow{\widetilde{T}_R^+} (N_R + 1, N_S - 1),\\ (N_R, N_S) &\xrightarrow{\widetilde{T}_R^-} (N_R - 1, N_S + 1),\end{aligned}$$

corresponding, respectively, to the simultaneous birth of an R and death of an S with rate $\widetilde{T}_R^+$, and death of an R and birth of an S with rate $\widetilde{T}_R^-$, where

$$\begin{aligned}\widetilde{T}_R^+ &\equiv \frac{T_R^+ T_S^-}{N} = Nx(1-x)\frac{f_R}{\overline{f}(t)},\\ \widetilde{T}_R^- &\equiv \frac{T_R^- T_S^+}{N} = Nx(1-x)\frac{f_S(t)}{\overline{f}(t)},\end{aligned} \tag{4.8}$$

The impact of the time-varying toxin level can be seen in the time-dependence of f_S and $\overline{f}$ through ξ_T, which is specific to the model considered here.

The model dynamics is therefore captured by a suitable MA and its final state unavoidably corresponds to the fixation of one strain, i.e. the population eventually ends up in either the state $(N_R, N_S) = (N, 0)$ or $(N_R, N_S) = (0, N)$ (Ewens, 2004; Antal & Scheuring, 2006; Blythe & McKane, 2007; M. A. Pinsky & Karlin, 2011). This means that, strictly, the finite population does not admit stable coexistence: when it exists, x^* is metastable, i.e. the MFT of the population scales exponentially with the population size (Assaf & Mobilia, 2010; Mobilia & Assaf, 2010; Assaf & Meerson, 2017), as seen in Ch. 3.2. Therefore, we again see that while fixation is guaranteed, this may take a very long time following a long-lived coexistence, as suggested by the MF analysis of the regime with $\nu_T \gg 1$. It is thus relevant to study under which circumstances there is long-lived coexistence of the strains.

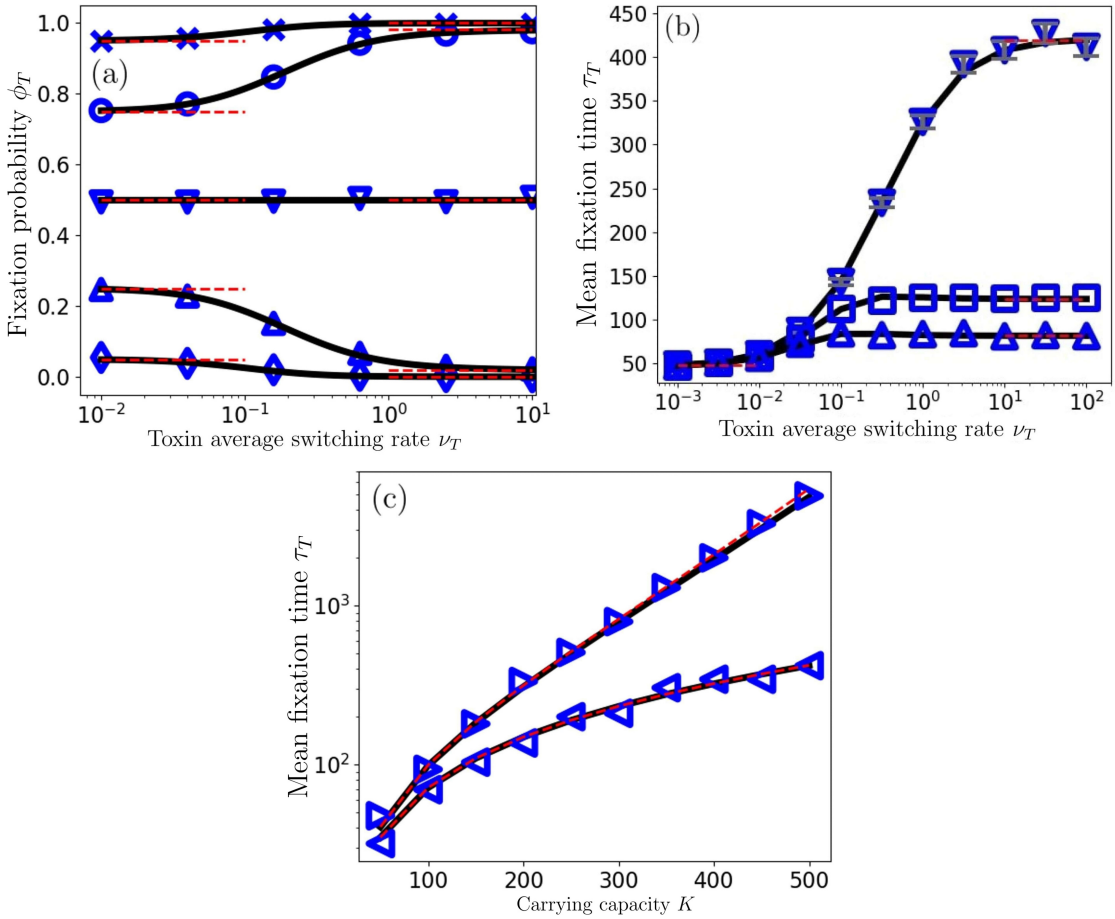

Figure 4.2: R fixation probability ϕ_T and MFT τ_T under constant carrying capacity and T-EV. Symbols are from stochastic simulations (10^3 realisations) with carrying capacity K (and non-constant N), and full black lines are for the Moran approximation with $N = K$, based on Eq. (4.12) (a) and Eq. (4.13) (b,c). (a) ϕ_T against ν_T, for $\delta_T = -0.9$ ($\times$), -0.5 ($\bigcirc$), 0 ($\triangledown$), 0.5 ($\triangle$), 0.9 ($\Diamond$), from top to bottom, with $s = 0.3$ and $K = 50$. Red dashed lines are predictions of Eq. (4.9) and Eq. (4.11). (b) τ_T against ν_T, for $\delta_T = 0$ ($\triangledown$), 0.3 ($\square$), 0.5 ($\triangle$) from top to bottom, with $s = 0.1$ and $K = 500$. Any bias $\delta_T \neq 0$, reduces τ_T. Error bars are overlaid for the case $\delta_T = 0$ and are almost indistinguishable from the symbols. Red dashed lines are analytical predictions in the limiting regimes $\nu_T \to 0, \infty$. (c) τ_T against K under fast T-EV in the coexistence regime for $\delta_T = 0$, $s = 0.1$ ($\triangleleft$) and $s = 0.3$ ($\triangleright$). Here, there is long-lived coexistence of the strains at the (meta-)stable equilibrium $x^* = x_0 = 0.5$ prior to fixation. The MFT grows exponentially when $Ks^2 \gg 1$; see Appendix B.1. Red dashed lines show the analytical predictions for the MFT when $\nu_T \to \infty$, compared with the predictions of Eq. (4.13) (black lines) and simulation results (markers) for $\nu_T = 100$.

The evolutionary dynamics under T-EV is characterised by the fixation probability of the strain R, denoted by ϕ_T, and the MFT, here denoted by τ_T. To this end, we therefore study how ϕ_T and τ_T are impacted by varying ν_T for different choices of K, δ_T, and s. We investigate where there is long-lived coexistence, defined similarly to Ch. 3 (Hernández-Navarro et al., 2023; Hernández-Navarro, Asker, & Mobilia, 2024), and characterise the fixation dynamics when they occur prior to long-lived coexistence. As in the previous chapter, we assume the population is always initialised at $x_0 = 0.5$, such that the population initially consists of resistant and sensitive cells in equal number.

In the limits $\nu_T \to 0, \infty$, we can use the results of the Moran process to obtain $\phi_T(\nu_T)$ and $\tau_T(\nu_T)$ from their MA counterparts ϕ_{MA} and τ_{MA} as in Eqs. (2.18) and (2.19). The fixation probability in the slow-switching regime, $\phi_T(\nu_T \to 0)$ is obtained by averaging $\phi_{\mathrm{MA}}|_{\xi_T}$, denoting the R fixation probability of the MA of the system in static environment ξ_T, over the stationary distribution of ξ_T (Wienand et al., 2017, 2018; Taitelbaum et al., 2020, 2023), giving

$$\begin{aligned}\phi_T(\nu_T \to 0) = &\left(\frac{1+\delta_T}{2}\right)\phi_{\mathrm{MA}}|_{\xi_T=+1} \\ &+ \left(\frac{1-\delta_T}{2}\right)\phi_{\mathrm{MA}}|_{\xi_T=-1}.\end{aligned} \tag{4.9}$$

When $N \gg 1$ and $\xi_T = +1$ (under sufficient s) the strain S is always favoured and $\phi_{\mathrm{MA}}|_{\xi_T=+1} \approx 0$, whereas R is favoured when $\xi_T = -1$ and in this case $\phi_{\mathrm{MA}}|_{\xi_T=-1} \approx 1$. Since $\xi_T(0) = -1$ with probability $(1-\delta_T)/2$, this coincides with the R fixation probability, given by $\phi(\nu_T \to 0) \approx (1-\delta_T)/2$. The probability that S fixates when $\nu_T \to 0$ is thus $1 - \phi(\nu_T \to 0) \approx (1+\delta_T)/2$.

In the fast-switching regime the fixation probability is that of the Moran process defined by the effective rates

$$\begin{aligned}\left\langle \widetilde{T}_R^+ \right\rangle &= \frac{Nx(1-x)}{2}\left(\frac{1+\delta_T}{x+(1-x)e^s} + \frac{1-\delta_T}{x+(1-x)e^{-s}}\right), \\ \left\langle \widetilde{T}_R^- \right\rangle &= \frac{Nx(1-x)}{2}\left(\frac{(1+\delta_T)e^s}{x+(1-x)e^s} + \frac{(1-\delta_T)e^{-s}}{x+(1-x)e^{-s}}\right).\end{aligned} \tag{4.10}$$

Using Eq. (4.10) with $x = n/N$ and substituting into Eq. (2.18), we thus find (Ewens, 2004; Antal & Scheuring, 2006; Traulsen & Haeurt, 2009)

$$\phi_T(\nu_T \to \infty) = \frac{1 + \sum_{k=1}^{Nx_0-1}\prod_{n=1}^{k}\frac{\langle \widetilde{T}_R^- \rangle(n/N)}{\langle \widetilde{T}_R^+ \rangle(n/N)}}{1 + \sum_{k=1}^{N-1}\prod_{n=1}^{k}\frac{\langle \widetilde{T}_R^- \rangle(n/N)}{\langle \widetilde{T}_R^+ \rangle(n/N)}}. \tag{4.11}$$

A similar analysis can also be carried out for τ_T. The result of this approach, shown as red dashed lines in Fig. 4.2, accurately capture the behaviour in the limiting regimes for ϕ_T and τ_T where $\nu_T \to 0, \infty$. Fig. 4.2(b) in particular demonstrates the presence of a long-lived coexistence state as $\nu_T \to \infty$, with a much larger MFT under high ν_T than under low ν_T (at fixed δ_T). In Fig. 4.2(b), the MFT when $\nu_T \gg 1$ for $\delta_T = 0$ is

significantly larger than under $\delta_T \neq 0$. This is because $x^* = 1/2$ is the stable fixed point of Eq. (4.6) when $\delta_T = 0$, whereas as $|\delta_T| \to 1$ the equilibrium point moves closer to the boundaries, making it more prone to DF causing fixation. Fig. 4.2(a,b) also illustrate the excellent agreement between the predictions of the MA with $N = K$ and those obtained from stochastic simulations with $K =$ constant and $N \approx K$.

Therefore, the MF analysis and results of Fig. 4.2 suggest that under sufficiently high switching rate ν_T there is long-lived coexistence of the strains. Hence, similarly to Ch. 3, we consider a long-lived coexistence of the R and S strains to exist when the MFT exceeds $2\langle N\rangle$, i.e. $\tau_T > 2\langle N\rangle$, approximately capturing the region where τ_T scales superlinearly with population size. Note that this differs slightly from Ch. 3, as we now do not assume that the fixation time of realisations, ζ, is exponentially distributed with MFT τ_T. Instead, we elect to use a simple binary outcome, where there is coexistence for $\tau_T > 2\langle N\rangle$ and no coexistence otherwise. This simplification allows us to more easily capture the coexistence probability under K-EV later, though neglects smooth transitions between regimes of coexistence and fixation; see Ch. 4.3.1. When, as in this section, N fluctuates about the constant carrying capacity K ($N \approx K$), we simply have $\langle N\rangle = K$.

Our analysis of the MF equations, seen in Eqs. (4.5)-(4.7), allow us to estimate under which conditions the long-lived coexistence state occurs. We expect coexistence when ξ_T self-averages, which requires a switching rate ν_T that is sufficiently high, seen from averaging the rates giving Eq. (4.5) and leading to Eq. (4.6). To self-average, the toxin level switches have to occur at least on the order of the demographic processes of the cells, i.e. births and deaths. These events take place for each individual on a timescale $\sim \mathcal{O}(1)$. Therefore, $\nu_T > 1$ indicates fast T-switching. To ensure long-lived coexistence, we see from Eq. (4.7) that the necessary condition $\nu_T > 1$ is supplemented by the requirement that $s \sim 1$ to allow a broad range of δ_T to lead to coexistence. This condition therefore ensures that T-EV is also sufficiently strong and a regime of coexistence where the MFT generally scales exponentially with population size when $s = \mathcal{O}(1)$ (Crow & Kimura, 1970; Ewens, 2004; Antal & Scheuring, 2006; Cremer et al., 2009; Assaf & Mobilia, 2010; Mobilia & Assaf, 2010; Assaf & Mobilia, 2011) guaranteeing long-lived coexistence. Hence, the expected conditions for long-lived coexistence are $\nu_T > 1$ (fast T-switching) and $s \gtrsim \mathcal{O}(1)$ (enough EV), which are satisfied in the examples considered here when $\nu_T > 1$ and $s = 1, 10$.

We have studied the influence of T-EV on the fixation and coexistence properties of the model with constant carrying capacity $K =$ constant and selection strength s by running a large number of computer simulations until $t > 2K$ across the ν_T-δ_T parameter space. If after $t = 2K$ both species are present, we label a given run for (ν_T, δ_T, s) as being characterised by long-lived coexistence which is RGB coded $(0, 1, 0)$. There is no long-lived coexistence for the run (ν_T, δ_T) if one of the species fixates by $t \leq 2K$: either the strain R, which is RGB coded $(1, 0, 0)$, or the strain S, which is coded by $(0, 0, 1)$, fixates the population. This procedure is repeated for 10^3 realisations for different (ν_T, δ_T) and, after sample averaging, yields the RGB-diagram of Fig. 4.3(a-c).

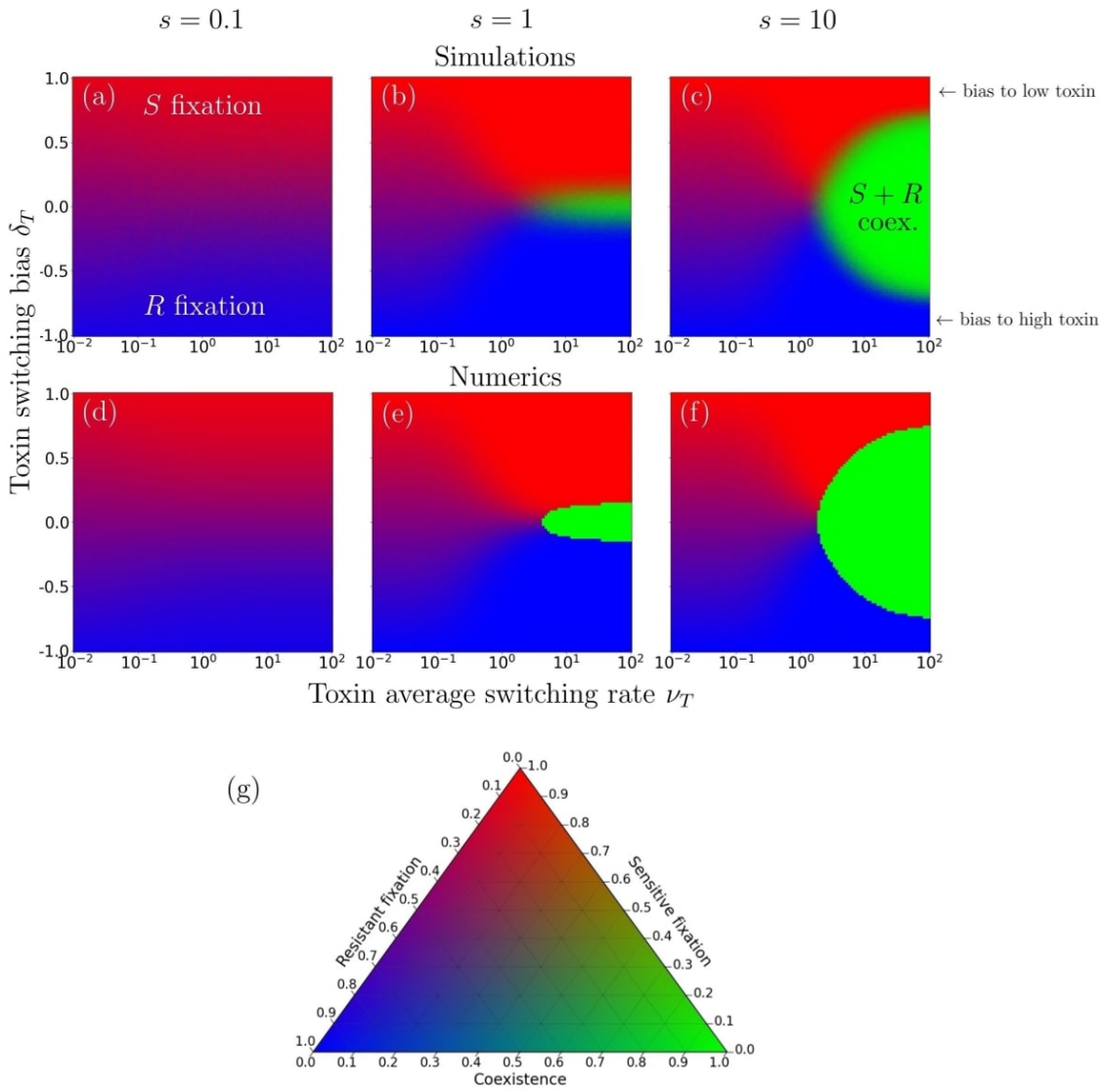

Figure 4.3: Fixation/coexistence diagrams under T-EV in the (ν_T, δ_T) parameter space for a small system of constant carrying capacity $K = 50$, with selection bias $s = 0.1$ (a,d), $s = 1$ (b,e), and $s = 10$ (c,f), after a time $t = 2K$. (a)-(c): phase diagrams obtained from stochastic simulations of the model with a constant K (N fluctuates about K) over 10^3 realisations and coded according to the RGB colourmap of panel (g): red / blue corresponds to the likely fixation of S/R (red: S dominance; blue: R dominance), regions indicated as "S/R fixation" in panel (a); magenta indicates where fixation of R or S is likely, area between "S/R fixation" regions in panel (a); green indicates where long-lived coexistence is most likely, area highlighted as "$S + R$ coex." in panel (c). (d)-(f): same as in (a)-(c) but from numerical solutions obtained from solving Eq. (4.14) computationally for the corresponding Moran process with a constant population size $N = K$.

It is also useful to study the effect of the T-EV and obtain the fixation-coexistence diagrams in the realm of the MA using numerical results. For this, we set up first-step equations for the fixation probability and MFT with the transition rates Eq. (4.8), for a constant population size, $N = K$. Denoting the R fixation probability from the state with n cells of type R in environmental state ξ_T as $\phi_n^{\xi_T}$, we have (Gardiner, 2009; Ashcroft et al., 2014)

$$(\widetilde{T}_R^+(n) + \widetilde{T}_R^-(n) + \nu_T^{\xi_T})\phi_n^{\xi_T} = \widetilde{T}_R^+(n)\phi_{n+1}^{\xi_T} + \widetilde{T}_R^-\phi_{n-1}^{\xi_T} + \nu_T^{\xi_T}\phi_n^{-\xi_T}, \tag{4.12}$$

subject to the boundary conditions $\phi_0^{\xi_T} = 0$ and $\phi_N^{\xi_T} = 1$. Similarly, the mean fixation time in the environmental state ξ_T, $\tau_n^{\xi_T}$, satisfies

$$(\widetilde{T}_R^+(n) + \widetilde{T}_R^-(n) + \nu_T^{\xi_T})\tau_n^{\xi_T} = 1 + \widetilde{T}_R^+(n)\tau_{n+1}^{\xi_T} + \widetilde{T}_R^-(n)\tau_{n-1}^{\xi_T} + \nu_T^{\xi_T}\tau_n^{-\xi_T}, \tag{4.13}$$

with boundary conditions $\tau_0^{\xi_T} = \tau_N^{\xi_T} = 0$. These resemble the first-step equations of Ch. 2.2.2, where there are now additional terms for the T-switching making a closed-form solution unfeasible. Eqs. (4.12) and (4.13) are thus linear difference equations that can be solved numerically. The fixation probability and MFT are obtained after averaging over the stationary distribution of ξ_T, yielding

$$\begin{aligned} \phi_n &= \left(\frac{1+\delta_T}{2}\right)\phi_n^+ + \left(\frac{1-\delta_T}{2}\right)\phi_n^-, \\ \tau_n &= \left(\frac{1+\delta_T}{2}\right)\tau_n^+ + \left(\frac{1-\delta_T}{2}\right)\tau_n^-. \end{aligned} \tag{4.14}$$

Since we always consider $x_0 = 1/2$, we henceforth write $\phi_T \equiv \phi_{N/2}$ for the R-fixation probability and $\tau_T \equiv \tau_{N/2}$ for the MFT in the realm of the MA under T-EV. For each triple (ν_T, δ_T, s), we numerically solve Eqs. (4.13) and (4.14) computationally. In the region of the parameter space where $\tau_T > 2K$, there is long-lived coexistence, which is coded by $(0, 1, 0)$ in the RGB-diagram of Fig. 4.3(d-f). When $\tau_T \leq 2K$, there is dominance of one of the species, characterised by the fixation probabilities ϕ_T and $1 - \phi_T$ of R and S, respectively, obtained from Eq. (4.12) and coded by $(\phi_T, 0, 1 - \phi_T)$ in Fig. 4.3(d-f).

Numerical results obtained from solving Eq. (4.14) computationally for the MA with $N = K$ in Fig. 4.3(d-f) are in excellent agreement with those of simulations obtained for $N \approx K =$ constant in Fig. 4.3(a-c). As expected from the MF analysis, the long-lived coexistence, occurs for T-EV of sufficiently large magnitude, i.e. $s \gtrsim 1$, and under high enough switching rate, i.e. $\nu_T \gtrsim 1$, shown as green areas in Fig. 4.3. The region of coexistence separates regimes dominated by either species, especially at high ν_T when $\phi_T \approx 0$ when $\delta_T > 0$ while $\phi_T \approx 1$ when $\delta_T < 0$. In Fig. 4.3, the boundaries between the regimes of R/S dominance, coded in blue / red, and coexistence, areas in green, are interspersed by crossover regimes where both species are likely to fixate (magenta in Fig. 4.3), or coexist with probability between 0 and 1 (faint green in Fig. 4.3), as coded in Fig. 4.3(g). In Fig. 4.3(d-f), we have used that coexistence is achieved where $\tau_T > 2\langle N \rangle$. The use of the binary choice for coexistence leads to the sharp transition between fixation

and coexistence which is not seen in the simulation results of Fig. 4.3(d-f) which instead assigns each realisation to be either coexistence or fixation, giving the smoother transition.

4.3 Time-varying fitness *and* carrying capacity

Having characterised the behaviour under T-EV only, we have seen that long-lived coexistence of the R and S can occur if s and ν_T are order 1 or higher, i.e. the magnitude and frequency of T-EV is sufficiently large. We now look to understand how this picture changes when the time-varying carrying capacity representing changes in the nutrient availability the population, defined as in Eq. (2.22), is reintroduced and drives the fluctuating population size N. EV is thus twofold, and the population evolves under the joint effect of T-EV and K-EV. As previously discussed, microbial communities often evolve in varying environments in which several aspects of the environment change in time. The introduction of twofold EV therefore captures a more realistic view of microbial population evolution, and is typically non-trivial to capture due to the distinct impacts of the EVs.

At the MF level the population evolves according to Eqs. (2.23) and (4.4) where the population size, N, is independent of s and affected only by K-EV via ξ_K in $K(t)$ (see Eq. (2.22)), while the evolution of x is impacted by ξ_K, ξ_T, and s via $x = N_R/N$, $f_S = \exp(s\xi_T)$, and $\overline{f}(t) = x + (1-x)\exp(s\xi_T)$. We therefore have a pair of coupled PDMPs which capture the evolution of N and x, where the population composition is coupled to the evolution of the population size, leading to eco-evolutionary dynamics.

4.3.1 Theory for fixation and coexistence

Following the simple case of Ch. 2.3.2, we notice that the population undergoes identical dynamics in N, and therefore the approximate QPSD defined by Eq. (2.27) captures the variations in population due to the K-EV here and approximates the true population size distribution. We therefore will utilise this useful tool to explore the fixation properties of the population. As in the simple example of Ch. 2.3.2, fixation typically occurs after N has been allowed sufficient time to explore its full QPSD. Hence, where the timescales of the N evolution and fixation are separated, the R fixation probability (with $x_0 = 1/2$) under T-EV and K-EV, denoted ϕ, can be suitably approximated by averaging $\phi_T(N)$ over the approximate QPSD given by $p(N)$ as (Wienand et al., 2017, 2018)

$$\phi \approx \int_{K_-}^{K_+} \phi_T(N) p(N)\, \mathrm{d}N. \tag{4.15}$$

We can use $p(N)$, given by Eq. (2.27), and the results for the MFT $\tau_T(N)$, obtained from solving Eq. (4.13), to determine the probability of coexistence under the N-PDMP approximation. For this, we first numerically solve Eq. (4.13) for $\tau_T(N^*) = 2\langle N\rangle$ to obtain N^*, where $\langle N\rangle$ is given by Eq. (2.28). Since τ_T is an increasing function of N (see Fig. 4.2(c)) we have $\tau_T(N) > 2\langle N\rangle$ for all $N > N^*$, which is the long-lived coexistence condition. Within the N-PDMP approximation, the lowest possible value of N^* is K_-

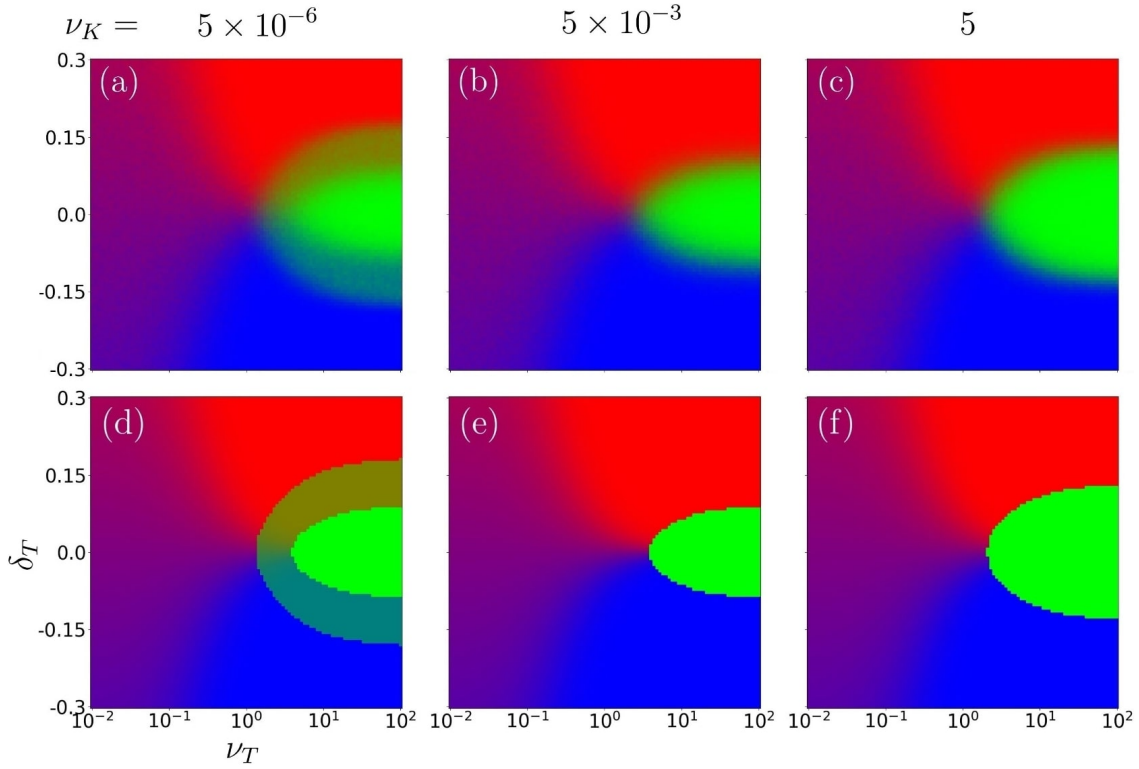

Figure 4.4: Fixation/coexistence diagrams under T-EV and K-EV in the (ν_T, δ_T) parameter space showing the influence of the K-switching rate ν_K on the fixation and coexistence probabilities, for $\nu_K = 5 \times 10^{-6}$ (a,d), $\nu_K = 5 \times 10^{-3}$ (b,e), and $\nu_K = 5$ (c,f). Other parameters are $K_0 = 1200$, $s = 0.5$, $\gamma = 2/3$, $\delta_K = 0$. (a)-(c): phase diagrams obtained from stochastic simulations data collected immediately following $t = 2\langle N \rangle$ over 10^3 realisations. (d)-(f): same as in (a)-(c) but from the theoretical predictions based on Eqs. (4.15) and (4.16). All diagrams are colour-coded as in Fig. 4.3.

since $N \in [K_-, K_+]$. We then determine the probability η that this condition is satisfied by integrating $p(N)$ over $[N^*, K_+]$, giving

$$\eta \equiv \text{Prob.}\left\{\tau_T(N) > 2\langle N \rangle\right\} = \int_{N^*}^{K_+} p(N)\, \mathrm{d}N, \tag{4.16}$$

where N^* depends on both T-EV and K-EV, while the integrand depends only on K-EV. We thus have that $\eta \to 1$ when $N^* \to K_-$. We therefore see that long-lived coexistence is almost certain when $N^* \approx K_-$, i.e. whenever the MFT of a population of fixed size $N = K_-$ exceeds $2\langle N \rangle$. Furthermore, the results of Ch. 4.2.2 indicate that η will increase with ν_T and s. For sufficiently large ν_T and s (and $|\delta_T|$ small enough to keep the stable coexistence point far from the boundaries), we expect $N^* \to K_-$ and $\eta \to 1$.

4.3.2 Fixation-coexistence diagrams

The fixation-coexistence diagrams under joint effect of T-EV and K-EV are obtained as in Ch. 4.2.2, with the difference being that long-lived coexistence arises when $t > 2\langle N \rangle$, a condition that depends on (ν_K, δ_K). This is exactly the condition for long-lived coexistence considered in Ch. 3 under a time-varying carrying capacity (Hernández-Navarro et al.,

2023; Hernández-Navarro, Asker, & Mobilia, 2024). In our simulations, we considered different values of ν_K (assuming symmetric switching, i.e. $\delta_K = 0$, for simplicity), and ran simulations until $t > 2\langle N\rangle$. Each run in which both species still coexist after $t = 2\langle N\rangle$ are RGB coded $(0, 1, 0)$, whereas those in which R or S fixates by $t \leq 2\langle N\rangle$ are respectively RGB coded $(1, 0, 0)$ or $(0, 0, 1)$. The RGB fixation-coexistence diagrams of Fig. 4.4(a-c) are obtained after sample-averaging the outcome of this procedure, repeated 10^3 times for each pair (ν_T, δ_T) and different values of ν_K.

Theoretical RGB diagrams are obtained from the N-PDMP based approximation using Eqs. (4.15) and (4.16): for a given ν_K, we allocate the RGB value $((1-\eta)(1-\phi), \eta, (1-\eta)\phi)$ obtained for each pair (ν_T, δ_T) of the diagram; see Fig. 4.4(d-f). This triple corresponds to the probability of having either no long-lived coexistence (with probability $1-\eta$) and fixation of R or S (with respective probabilities ϕ and $1-\phi$), or long-lived coexistence (with probability η).

Comparison of the top and bottom rows of Fig. 4.4 show that the N-PDMP based approximation quantitatively reproduces the fixation and coexistence dynamics of the statistically correct stochastic simulations. We again see that the theoretical predictions have sharper boundaries between the fixation and coexistence regions than simulation results. This is due to the use of the MFT in the analytic calculations of the coexistence probability compared to the sample averaged case of simulations, as discussed in Ch. 4.2.2. The regions of Fig. 4.4 where $|\delta_T| \to 1$ are characterised by dominance of one of the strains, and essentially reduces to the model studied in Ch. 2.3.2, as well as in Wienand et al. (2017, 2018). We now focus on characterising the novel coexistence phase, emerging due to T-EV and inhibited by K-EV, and investigate how it is impacted by each of these EVs.

When K_0 is large, under sufficient EV as in Fig. 4.4, the joint effect of T-EV and K-EV on the phase of long-lived coexistence in the RGB diagrams of Fig. 4.4 can be summarised as follows: (i) when $\nu_K \to 0$, a (bright green) region where $\eta \approx 1$ and coexistence is almost certain is surrounded by a faint green "outer shell" where coexistence is possible but not certain $(0 < \eta < 1)$ (see Fig. 4.4(a,d)); (ii) at low, but non-vanishingly small, values of ν_K, the outer-shell where $0 < \eta < 1$ disappears, and the remaining coexistence region has $\eta \approx 1$ (see Fig. 4.4(b,e)); (iii) when $\nu_K \gg 1$, the coexistence region similarly consists only of points where $\eta \approx 1$ (bright green), but it is broader than under low ν_K (see Fig. 4.4(c,f)). In all scenarios (i)-(iii), η increases with $\nu_T \gtrsim 1$ (for not too large δ_T) and hence all the green coexistence phases in Fig. 4.4) become brighter as ν_T is raised and $\eta \to 1$.

These different scenarios can be explained by the dependence of the QPSD on ν_K, well captured by Eq. (2.27). In regime (i) where $\nu_K \ll 1/K_0$, the QPSD and $p(N)$ are bimodal. Therefore, $N \approx K_\pm$ with probability $(1 \pm \delta_K)/2$, and any K-switches by $t = 2\langle N\rangle \sim K_0$ are unlikely, yielding the faint green outer shell of Fig. 4.4(a,d) corresponding to long-lived coexistence arising only when $N \approx K_+$, with a probability $\eta \approx (1 + \delta_K)/2$. In regime (ii), where $1/K_0 \ll \nu_K \ll 1$, the QPSD and $p(N)$ are still bimodal but some K-switches occur

by $t \sim K_0$, resulting in long-lived coexistence arising only when ν_T is high enough to ensure $\eta \approx 1$ when $N \approx K_-$. In regime (iii), where $\nu_K \gg 1$ the QPSD and $p(N)$ are unimodal with average $\langle N \rangle \approx \mathcal{K} \geq K_-$, which results in a long-lived coexistence region where $\eta \approx 1$ that is broader than in (i) and (ii); see Fig. 4.4(c,f). The size of the coexistence region in regime (iii) depends non-trivially on ν_K, as revealed by the modal value of Eq. (2.27) when $\nu_K(1 - |\delta_K|) > 1$, which reads

$$\begin{aligned} \hat{N} = & \frac{K_0}{2}\left[1 + \nu_K(1 - \gamma\delta_K)\right] \\ & - \frac{K_0}{2}\sqrt{(1 + \nu_K(1 - \gamma\delta_K))^2 - 4\nu_K(1 - \gamma^2)}, \end{aligned} \tag{4.17}$$

with $\lim_{\nu_K \to \infty} \hat{N} = \langle N \rangle = \mathcal{K}$. This expression captures well the modal value of the QPSD from simulations; see Fig. B.3 in Appendix B.3. The MFT depends strongly on the population size, particularly near/in the coexistence regime and so capturing the size the population truly takes is important. Under fast switching, the QPSD typically has broad asymmetric tails (as seen in Fig. 2.2 of Ch. 2.3.2), and so $\langle N \rangle$ may differ significantly from $\hat{N}$. The modal value thus allows for the capturing of this most likely size and therefore provides an improved measure for determining coexistence or fixation for a given population. We notice that $\hat{N}$ is an increasing function of ν_K when $\gamma > \delta_K$, and it decreases if $\gamma < \delta_K$ (remaining constant when $\gamma = \delta_K$). As a consequence, the long-lived coexistence region under high K switching rate grows with ν_K when $\gamma > \delta_K$, as in Fig. 4.4(c,f), and, when $\gamma < \delta_K$, shrinks as ν_K is increased; see Appendix B.3.

4.3.3 Impact of the amplitude of carrying capacity variations on coexistence

We have seen that increasing the selection bias, s, increases the amplitude of the T-EV and gives rise to a broader regime of long-lived coexistence. Here, by keeping K_0 constant, we investigate the influence of the parameter γ, which controls the amplitude of K-EV, on the fixation-coexistence diagrams. When $\gamma \to 1$ and $K_0 \gg 1$, the amplitude of K-EV is larger and the population is subject to harsher bottlenecks ($K_- \to 0$), where DF are amplified. Therefore, the K-EV works directly counter to the T-EV: the amplified DF introduced during population bottlenecks due to the smaller population size increase the likelihood of fixation from the coexistence state, while the T-EV acts to restore the system to the coexistence equilibrium following a deviation due to DF and thus maintain the coexistence. Fig. 4.5 illustrates the influence of γ under low and high K-switching rate ($\delta_K = 0$):

- Under low ν_K, the probability of long-lived coexistence η decreases with $K_- = K_0(1 - \gamma)$ when γ is increased. The bright green region in Fig. 4.5(a) where long-lived coexistence is almost certain ($\eta \approx 1$) therefore shrinks with γ and is gradually replaced by a faint green area where coexistence occurs with a lower probability ($\eta = (1 + \delta_K)/2 < 1$); see Fig. 4.5(b,c).

- Under high ν_K, we have $N \approx \mathcal{K} = K_0(1 - \gamma^2)/(1 - \gamma\delta_K)$ which shows the impact of

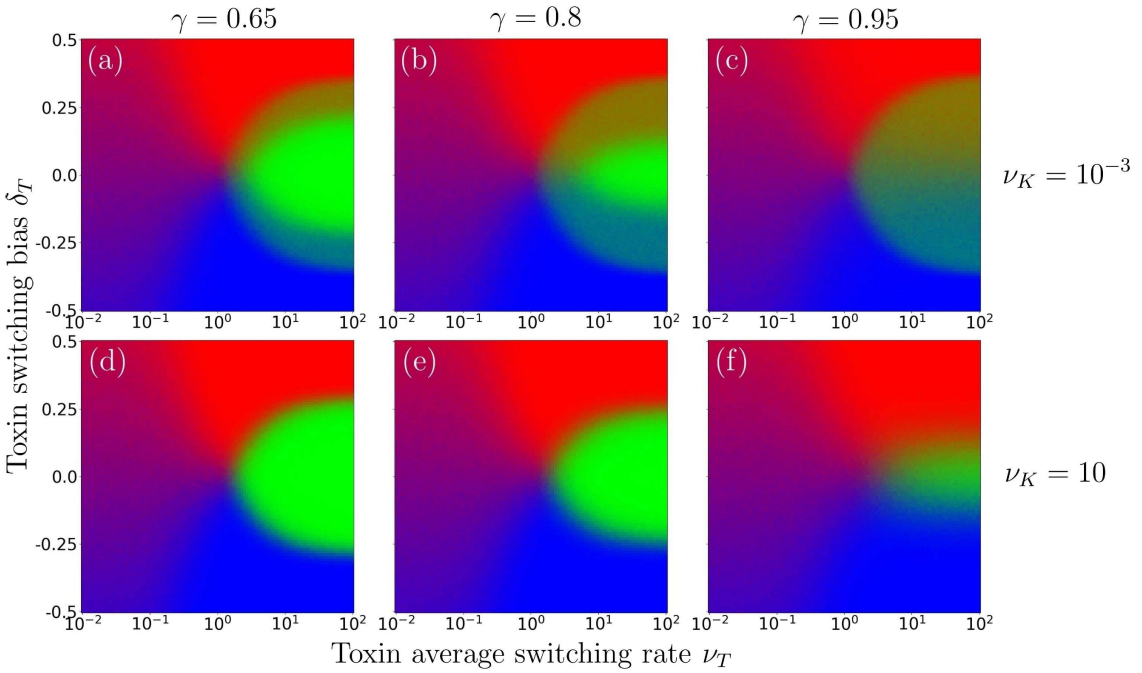

Figure 4.5: Fixation/coexistence diagrams under T-EV and K-EV in the (ν_T, δ_T) parameter space showing the effect of the amplitude of K-EV γ on the fixation and coexistence probabilities when $K_0 = 500$ is kept fixed, for $\gamma = 0.65$ ($K_- = 175$, $K_+ = 825$) (a,d), $\gamma = 0.8$ ($K_- = 100$, $K_+ = 900$) (b,e), and $\gamma = 0.95$ ($K_- = 25$, $K_+ = 975$) (c,f). Other parameters are $s = 1.0$, $\delta_K = 0$, $\nu_K = 10^{-3}$ in (a)-(c) and $\nu_K = 10$ in (d)-(f). Phase diagrams obtained from stochastic simulations data collected just after $t = 2\langle N \rangle$ over 10^3 realisations. All diagrams are colour-coded as in Fig. 4.3.

γ on the coexistence region. When $\delta_K \leq 0$, $\mathcal{K}$ and η decrease with γ, and as a result the bright green region in Fig. 4.5(d) shrinks; see Fig. 4.5(e,f). When $\delta_K > 0$, there is a bias towards $K = K_+$ and $\mathcal{K}$ increases with γ until $\gamma = \bar{\gamma} \equiv (1 - \sqrt{1 - \delta_K^2})/\delta_K$ and then decreases, with $\mathcal{K} < K_0$, when $\gamma > \delta_K$. This results in a non-monotonic dependence of the coexistence region where $\eta \approx 1$: under $\nu_K \gg 1$ and $\delta_K > 0$, the long-lived (bright-green) coexistence region grows with γ up to $\bar{\gamma}$ and shrinks when $\gamma > \bar{\gamma}$.

It is interesting to note that, while under low ν_K the overall coexistence region, i.e. the region where $\eta > 1$, is larger than under high ν_K, but the bright coexistence region where $\eta \approx 1$ is smaller than when under high ν_K. This is due to the fact that under slow switching for $\eta \approx 1$, we require coexistence under long periods in both K_+ and K_-, whereas under fast switching we require coexistence under long periods in $\mathcal{K}$. Since $\mathcal{K} \geq K_-$, DF are weaker under $\mathcal{K}$ and the bright coexistence regime is larger. Under symmetric K-switching case, we have that $K_- = K_0(1-\gamma)$ and $\mathcal{K} = K_0(1-\gamma^2)$, where $\gamma < 1$, clearly demonstration this effect.

We have thus found that the two forms of EV have opposite effects on the species coexistence: increasing the amplitude of T-EV (by raising s) prolongs the coexistence of the strains and expands the coexistence region, but raising the amplitude of K-EV (by raising

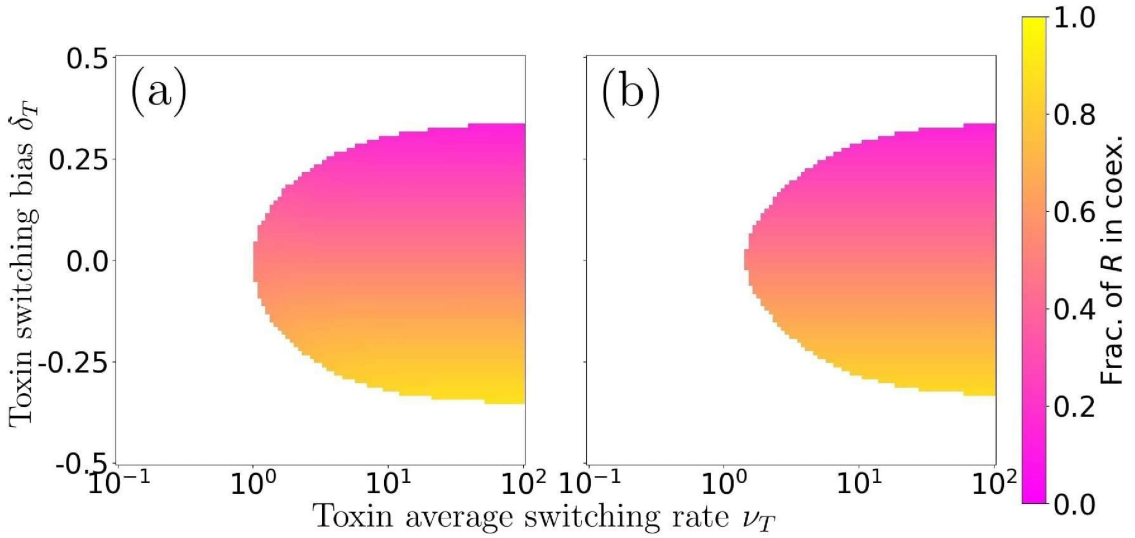

Figure 4.6: Composition of the coexistence state: fraction of the resistant strain R in the coexistence phase as a function of ν_T and δ_T; from simulation results (a) and predictions of Eqs. (4.7) and (4.16) in (b), respectively for x^* and η. The colourbar (brightness bar) gives the characteristic fraction of the R strain in the region of the ν_T-δ_T parameter space where $\eta > 0.01$. Simulation results have been obtained just after $t = 2\langle N\rangle$ and averaged over 10^4 realisations. Parameters are $K_0 = 500$, $\gamma = 0.5$, $\nu_K = 100$, and $s = 1$.

γ) can significantly reduce the probability of long-lived coexistence for all values of ν_K.

4.4 Composition of the coexistence phase and strain average abundance

Having characterised in detail the conditions under which long-lived coexistence and fixation occur, we now study the composition of the coexistence phase and then use this result to determine the stationary average abundance of each strain.

4.4.1 Coexistence phase composition

In the coexistence region, we are interested in characterising the fraction of resistant strain composing the population, denoted x^*. This is the fraction of R expected, given that we have coexistence just after $t = 2\,\langle N\rangle$. According to the MF theory, the fraction of the strain R in the coexistence phase is given by Eq. (4.7). Despite the approximations made to obtain the MF results, deep into the coexistence region where $\eta \approx 1$ and ν_T is sufficiently high, there is good agreement between theory and simulations; see Fig. 4.6(a,b). In addition, even when $\eta < 1$, the MF prediction for x^* remains remarkably close to the value of fraction of R measured in the coexistence state obtained in simulations, with small deviations arising as η approaches 0. We notice that the characteristic fraction of R, for given δ_T, is almost independent of ν_T. This can be understood by noting that the T-EV must self-average through fast switching to allow for coexistence. Once ν_T reaches a value sufficient to prevent chance fixation events for long times, any increase in ν_T serves little purpose as the T-EV is already switching quickly enough to self-average.

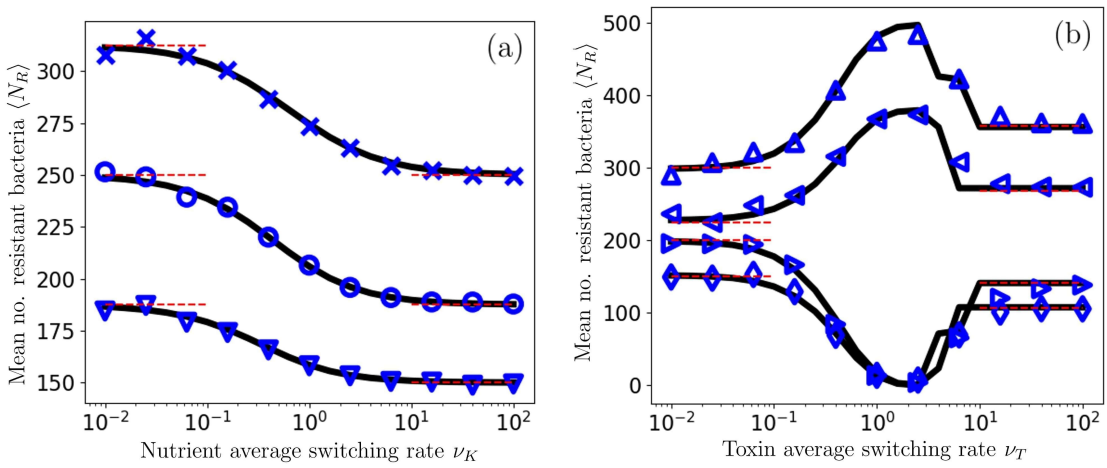

Figure 4.7: Long-time average R abundance $\langle N_R \rangle$ as a function of the average switching rate of the T/K-EV. Solid lines are theoretical predictions of Eq. (4.19) with x^*, $\langle N \rangle$, ϕ and η given by Eqs. (4.7), (2.28), (4.15), and (4.16); symbols are from simulation data. (a) $\langle N_R \rangle$ versus ν_K for $\delta_K = 0.5$ ($\times$), $\delta_K = 0$ ($\bigcirc$) and $\delta_K = -0.5$ ($\bigtriangledown$). Limiting values are plotted for $\nu_K \to 0, \infty$ as dotted lines. Other parameters are: $K_0 = 500$, $\gamma = 0.5$, $s = 1.0$, $\nu_T = 10$, and $\delta_T = 0.0$. (b) $\langle N_R \rangle$ versus ν_T for $(\delta_T, \nu_K) = (-0.2, 0.01)$ ($\bigtriangleup$), $(\delta_T, \nu_K) = (-0.2, 10)$ ($\lhd$), $(\delta_T, \nu_K) = (0.2, 0.01)$ ($\rhd$), $(\delta_T, \nu_K) = (0.2, 10)$ ($\Diamond$). Limiting value are plotted for $\nu_T \to 0, \infty$ as dotted lines. Other parameters are: $K_0 = 500$, $\gamma = 0.5$, $s = 1.0$, and $\delta_K = 0.0$. Simulations data have been collected and sample-averaged after $t = 2\langle K \rangle$ over 10^2 realisations.

Having characterised the behaviour under fixation and coexistence, we can then predict the fraction of R regardless of coexistence or fixation, here denoted by $\langle x \rangle$. The quantity $\langle x \rangle$ thus characterises the fraction of R in the coexistence, fixation, and crossover regime where both coexistence and fixation are possible, with respective probabilities η and ϕ, but neither is certain. Making use of Eqs. (4.7), (4.15), and (4.16) we thus define $\langle x \rangle$ as

$$\langle x \rangle = \eta x^* + (1 - \eta)\phi. \tag{4.18}$$

The dependence of $\langle x \rangle$ on ν_T is captured accurately by this expression. We see that it reduces to the fraction of R in the coexistence phase, $\langle x \rangle = x^*$, when $\eta \approx 1$ and long-lived coexistence is almost certain. Similarly, as fixation becomes more likely, coexistence becomes less likely and so $\eta \to 0$, leading to $\langle x \rangle \to \phi$, as expected – $x = 1$ with probability ϕ or $x = 0$ with probability $1 - \phi$. As shown in Appendix B.2, a closed-form alternative to $\langle x \rangle$ is provided by the modal value of the QPSD of the x-PDMP defined by Eq. (4.4), which, while less accurate than $\langle x \rangle$ in general, captures the qualitative behaviour as η approaches zero more accurately.

4.4.2 Strain average abundance

In this section, we study the ν_T and ν_K dependence of the (quasi-)stationary average abundance of the strains R and S, respectively denoted by $\langle N_R \rangle$ and $\langle N_S \rangle$. Since $\langle N_S \rangle = \langle N \rangle - \langle N_R \rangle$, and $\langle N \rangle$ is well described by Eq. (2.28) (see Fig. 2.2(e)) we only need to focus

on studying $\langle N_R \rangle$.

In fact, while the evolution of N is governed by K-EV and is well-captured by the stochastic logistic equation Eq. (2.23) and the corresponding N-PDMP, the dynamics of the abundance of the R strain depends on both T-EV and K-EV. In the MF limit, where DF are neglected, we have (Gardiner, 2009)

$$\begin{aligned}\frac{\mathrm{d}}{\mathrm{d}t}\langle N_R \rangle = T_R^+ - T_R^- &= \left(\frac{1}{\overline{f}(t)} - \frac{\langle N \rangle}{K(t)}\right)\langle N_R \rangle \\ &= \left(\frac{1}{x + (1-x)e^{s\xi_T}} - \frac{\langle N \rangle}{K_0(1+\gamma\xi_K)}\right)\langle N_R \rangle\,,\end{aligned}$$

which is a stochastic differential equation depending on both ξ_K and ξ_T, and coupled to the N- and x-PDMPs defined respectively by Eqs. (2.23) and (4.4). In the dominance regimes, $\langle N_R \rangle \approx 0$ (S dominance) or $\langle N_R \rangle \approx \langle N \rangle$ (R dominance), which can be obtained from Eq. (2.28). Similarly, finding $\langle N_R \rangle$ in the coexistence phase is straightforward, where $\langle N_R \rangle \approx \langle N \rangle x^*$. However, generally capturing the behaviour is a non-trivial task. Progress can be made by remembering that ξ_K and ξ_T are independent, and so we can approximate $\langle N_R \rangle$ by

$$\langle N_R \rangle \approx \langle N \rangle \langle x \rangle \equiv \langle N \rangle (\eta x^* + (1-\eta)\phi), \tag{4.19}$$

where $\langle N \rangle \eta x^*$ is the contribution to $\langle N_R \rangle$ when there is coexistence (with probability η), and $\langle N \rangle (1-\eta)\phi$ is the contribution arising when there is fixation of the strain R (with probability $(1-\eta)\phi$). In our theoretical analysis $\langle N \rangle$, x^*, ϕ, and η are obtained from Eqs. (2.27), (4.7), (4.15), and (4.16), respectively. Eq. (4.19) thus captures the behaviour of $\langle N_R \rangle$ in each regime: the dominance regime where $\eta \approx 0$ and we have $\langle N_R \rangle \approx \langle N \rangle \phi$, deep in the coexistence phase where we have $\eta \approx 1$ and $\langle N_R \rangle \approx \langle N \rangle x^*$, and where $0 < \eta < 1$ and coexistence is possible but not certain where we have $\langle N_R \rangle \approx \langle N \rangle \langle x \rangle$.

In Fig. 4.7, we see that Eq. (4.19) captures well the results found from simulations over a broad range of ν_K and ν_T, and for different values of δ_K and δ_T. The dependence of $\langle N_R \rangle$ on ν_K reflects that of $\langle N \rangle$ shown in Fig. 2.2(e): $\langle N_R \rangle$ decreases with ν_K at fixed δ_K (see Fig. 4.7(a)) and we have $\langle N \rangle \approx \mathcal{K}$ when $\nu_K \to \infty$ yielding $\langle N_R \rangle \approx \mathcal{K}x^*$ deep in the coexistence phase where $\nu_T \gg 1$, and similarly $\langle N \rangle \approx K_0(1+\gamma\delta_K)$ when $\nu_K \to 0$ yields $\langle N_R \rangle \approx K_0(1+\gamma\delta_K)x^*$. Not shown in Fig. 4.7(a) is the case of $\nu_T \ll 1$, where only dominance occurs such that $\langle N_R \rangle \approx \langle N \rangle (1-\delta_T)/2$. Fig. 4.7(b) shows that the dependence of $\langle N_R \rangle$ on ν_T can be non-monotonic and exhibit an extreme dip ($\delta_T > 0$) or peak ($\delta_T < 0$) at intermediate T-switching rate, $\nu_T \sim 1$. This behaviour can be understood by referring to the diagrams of Fig. 4.5: as ν_T is raised from $\nu_T = 0$ with $\delta_T < 0$ kept fixed, the R fixation probability first slowly increases in the magenta region where there is a small bias towards R fixation and coexistence does not occur ($\eta \approx 0$), giving $\langle N_R \rangle \approx \langle N \rangle \phi$. Increasing ν_T further, R becomes the dominant species (blue phases in Fig. 4.5), with $\phi \approx 1$ and $\langle N_R \rangle \approx \langle N \rangle$ reaching its maximum; as ν_T continues to increase, coexistence becomes possible ($0 < \eta < 1$, faint green in Fig. 4.5) and then almost certain ($\eta \approx 1$, bright green in Fig. 4.5) when ν_T is increased further, which results in a reduction of the

R abundance to $\langle N_R \rangle \approx \langle N \rangle x^* < \langle N \rangle$. A similar reasoning holds for the S strain when $\delta_T > 0$ and results in a maximal value $\langle N_S \rangle \approx \langle N \rangle$ and therefore a dip of the R abundance, with a minimal value $\langle N_R \rangle \approx 0$, when $\nu_T \sim 1$.

The results of this section hence show that the twofold EV has non-trivial effects on the composition of the coexistence phase, and on the average number of cells of each strain, as shown by Fig. 4.6 and the non-monotonic dependence of $\langle N_R \rangle$ on ν_T in Fig. 4.7.

In this chapter, we have found that long-lived coexistence can be sustained in populations under sufficient variation of the toxin level. We have then seen that resource variability can inhibit this coexistence when strong K-EV leads to population bottlenecks, amplifying DF and leading to fixation. More generally, our analysis has allowed us to assess the influence of the population size distribution, whose shape changes greatly with the rate of K-EV, on the fixation-coexistence phase diagram. We have also determined how the composition of the coexistence phase and average abundance of each strain depend on the rates of environmental change. These findings therefore demonstrate the influence of EV on biodiversity in microbial communities and provide insight into a number of potential applications. One such application is that discussed previously of the evolution of AMR in a chemostat setup. In this context, the model is able to predict the environmental conditions under which the number of resistant cells can be minimised, and the composition of the population under coexistence. Another potential application is that of adaptive therapy used in cancer treatment, where drug levels are varied in order to prevent resistance of the cancerous cells to the drug (J. West et al., 2023).

Chapter 5

Fixation and extinction in metapopulations

Spatial structure is ubiquitous in natural microbial communities and its impact on evolutionary dynamics is a topic of great interest. In Ch. 1, I gave an overview of the existing literature and motivation relating to the evolution of spatially structured populations which I will briefly summarise here. Experimental studies have made progress in elucidating the effects of spatial structure on population evolution (Habets et al., 2006; Kryazhimskiy et al., 2012; Engel & Moran, 2013; Nahum et al., 2015; Widder et al., 2016; Garud et al., 2019; Chakraborty et al., 2023; Kreger et al., 2023; She et al., 2024), but it generally remains poorly understood. More recently, with improvements to micro-fluidic techniques, it has become possible to experimentally probe such systems with a far greater level of precision and control (Keymer et al., 2006; Hsu et al., 2019; Totlani et al., 2020). To improve our understanding of the impact of spatial structure on biological systems, it is therefore important to also develop the theoretical tools required to capture the evolution of these populations. However, this is typically a non-trivial task due to the formation of correlations across the spatially structured population over time from the migration of individuals; see Figs. 1.3 and 5.2. To understand realistic microbial communities, relevant tools must therefore be developed to capture the dynamics of models considering the spatial structure of such populations. Furthermore, I have motivated throughout this thesis the importance of EV and its impact on stochastic population evolution. Indeed, on spatially structured microbial communities the same applies, where EV can cause sharp and sudden population bottlenecks, though most theoretical developments thus far have considered a constant environment (Hauert et al., 2014; Marrec et al., 2021; Yagoobi & Traulsen, 2021). Therefore, here we are interested in incorporating both spatial structure and EV to a simple model of population evolution (a spatially extended version of the model considered in Ch. 2.3.2) to understand their joint effect on the system dynamics.

In this chapter, motivated by the relevance of spatial structure and EV to microbial communities, I study a class of metapopulation models. These metapopulations, representing spatially structured biological populations (see Figs. 1.3 and 5.5(a)), consist of many demes

(subpopulations) in which wild-type and mutant cells evolve in a time-varying environment represented by a time-switching carrying capacity as introduced in Ch. 2.3.1. Each of the demes thus resembles the population considered in Ch. 2.3.2. I consider the behaviour of these metapopulations under slow migration, whereby the intra-deme dynamics (birth and death events) occur much faster than the inter-deme dynamics (migrations between demes), which is both biologically relevant and permits analytical progress (S. Wright, 1943, 1949; Keymer et al., 2006; Marrec et al., 2021; Moawad et al., 2024). I will first consider the behaviour of the metapopulations under a static environment, demonstrating that the dynamics is either dominated by competition between wild-type and mutant cells or extinction of demes (and eventually the metapopulation) depending on the environmental conditions and migration of cells (with a small intermediate regime). I will therefore show that, under a static environment, a mutant with a selective advantage either goes extinct with the entire population under extinction-dominated dynamics, or is likely to fixate the population under competition-dominated dynamics. In either case, the resident wild-type population is likely to reach extinction. I will then investigate how the metapopulation evolution changes under population bottlenecks, implemented via the time-varying carrying capacity as before, varying simultaneously on each deme across the metapopulation. We will see that, when bottlenecks are weak such that deme extinction is not expected in the harsh environmental state, there is an optimal switching rate of the environment that maximises the likelihood of mutant fixation. Moreover, the probability of mutant fixation depends on the migration rate of cells in the metapopulation, which is in stark contrast with the case of static environments (Marrec et al., 2021). When bottlenecks are strong such that deme extinction is likely in the harsh environmental state, I will characterise the behaviour of the metapopulation, and uncover a mechanism for the removal of an initially rare mutant which does not risk metapopulation extinction, behaviour not found under static environments.

Contents of this chapter appear in Asker et al. (2025).

5.1 Model description

The spatially explicit metapopulation models which we consider here consist of Ω demes labelled by $x \in \{1, ..., \Omega\}$. Each of these demes is independently identical to the model considered in Ch. 2.3.2. Therefore, at time t, each deme x consists of a well-mixed subpopulation of $n(x) = n_M(x) + n_W(x)$ cells composed of $n_M(x)$ mutant cells and $n_W(x)$ wild-type cells. The number of W/M individuals across the metapopulation is therefore $N_{M/W} \equiv \sum_x n_{M/W}(x)$ and $N \equiv N_W + N_M$ is the total number of individuals in the whole graph. Again, the wild-type cells have a fitness $f_W = 1$, while the mutant cells have a slight selective advantage with fitness $f_M = 1 + s$ and $0 < s \ll 1$.

The metapopulation may then be envisioned as a graph with nodes $x \in \{1, \ldots, \Omega\}$ where each node is a deme containing a well-mixed subpopulation. Here, we focus on fully-connected graphs (as in the island model (S. Wright, 1931; Kimura & Weiss, 1964)) called cliques, and periodic one- and two-dimensional lattices called cycles and grids, respectively;

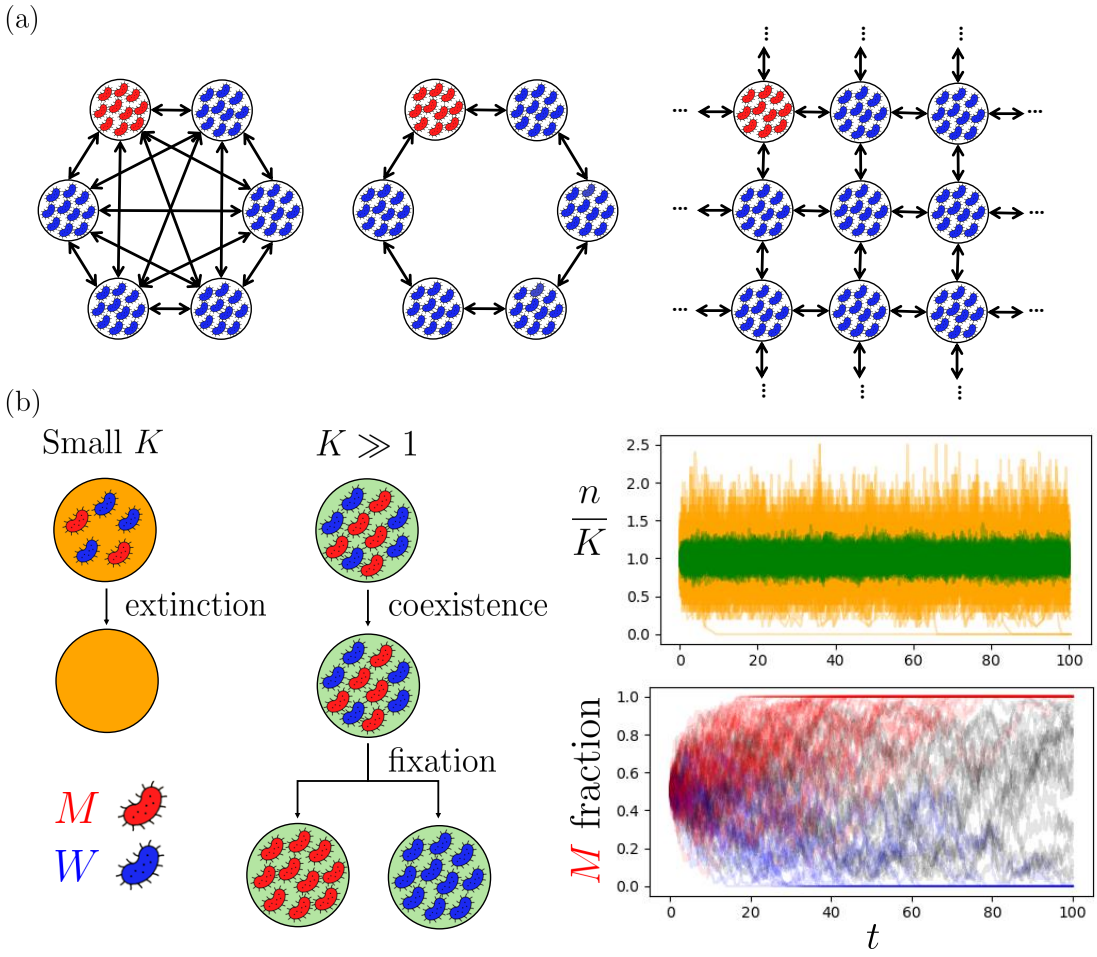

Figure 5.1: Examples of metapopulations and single-deme dynamics. (a) Examples of metapopulation graphs: a clique, cycle, and grid (from left to right). Neighbouring demes are connected by migration (double arrows). Initially, there is one mutant deme (red/light) and $\Omega - 1$ wild-type demes (blue / dark), and all demes have the same constant carrying capacity K. (b) Dynamics in a single deme. Left: Wild-type W cells (blue / dark) compete with mutants of type M (red / light). When K is small, the deme is prone to extinction. When K is large, both types coexist prior to W or M fixation. Top right: Realisations of the rescaled deme size n/K against time t for $K = 5$ (orange/light) and $K = 100$ (green/dark) illustrating how n fluctuates about K. Bottom right: Fraction of M cells against t in a deme with $K = 100$. Deme extinction is not observed. Transient coexistence of W and M is followed by the fixation of W (blue traces) or M (red traces). Here $s = 0.01$.

see Fig. 5.1(a). These are regular graphs, generally denoted by $\mathrm{G} = \{\text{clique}, \text{cycle}, \text{grid}\}$, of Ω demes connected by edges to their q_{G} nearest neighbours via cell migration at per capita rate m (independently from birth and death) (S. Wright, 1931; Kimura & Weiss, 1964; Maruyama, 1970; Marrec et al., 2021; Fruet et al., 2024; Moawad et al., 2024); see Figs. 5.1 and 5.2(a). Furthermore, the graphs considered here are all *circulations*: there is the same incoming and outgoing migration flow at each deme. I define this more concretely later; see Eq. (5.3). This property is crucial for some important known results which we will discuss later (Maruyama, 1970; Lieberman et al., 2005; Marrec et al., 2021). We study the eco-evolutionary dynamics of the metapopulation in the biologically relevant regime of slow migration (whereby intra-deme dynamics occur much faster than inter-deme dynamics; see Ch. 5.2) (S. Wright, 1943, 1949; Keymer et al., 2006; Marrec et al., 2021; Moawad et al., 2024) and consider that initially one deme is occupied entirely by mutants (M deme), while the other $\Omega - 1$ demes (W demes) are all populated by W cells; see Ch. 5.4. This therefore represents the scenario of an advantageous mutant arising, and attempting to take over the population. All demes are assumed to have the same carrying capacity K, which again encodes the EV. In Ch. 5.2, we assume that K is constant in order to understand the impact of spatial structure and migration on metapopulation evolution, similarly to previous works (Barton, 1993; Lande et al., 1998; Lieberman et al., 2005; Marrec et al., 2021), and in Ch. 5.3 we let the carrying capacity switch as in Ch. 2.3.1 to ascertain how EV affects this evolution.

The intra-deme dynamics in a deme x, consisting of competition between mutant and wild-type cells on deme x for the local resources, is thus represented by the simple example birth-death process considered in Ch. 2.3.2 (as in Wienand et al. (2017, 2018)), with reactions

$$n_\alpha \xrightarrow{T_\alpha^+} n_\alpha + 1 \quad \text{and} \quad n_\alpha \xrightarrow{T_\alpha^-} n_\alpha - 1, \tag{5.1}$$

and the rates $T_\alpha^\pm$ defined as in Eq. (2.10). The inter-deme dynamics arise due to migration of cells of type $\alpha \in \{W, M\}$ from the deme x to one of its q_{G} neighbouring demes denoted by y at a per-capita migration rate m. Here, for the sake of simplicity, we assume that the migration rate is the same in all directions and for both species, denoted symmetric migration; see Ch. 5.4 for a discussion of these assumptions. The inter-deme dynamics for all cells at deme x with its neighbouring demes labelled y is therefore implemented according to the reaction

$$[n_\alpha(x), n_\alpha(y)] \xrightarrow{T_\alpha^{m,\mathrm{G}}} [n_\alpha(x) - 1, n_\alpha(y) + 1],$$

occurring at the migration transition rate

$$T_\alpha^{m,\mathrm{G}}(x) = \frac{m n_\alpha}{q_{\mathrm{G}}}. \tag{5.2}$$

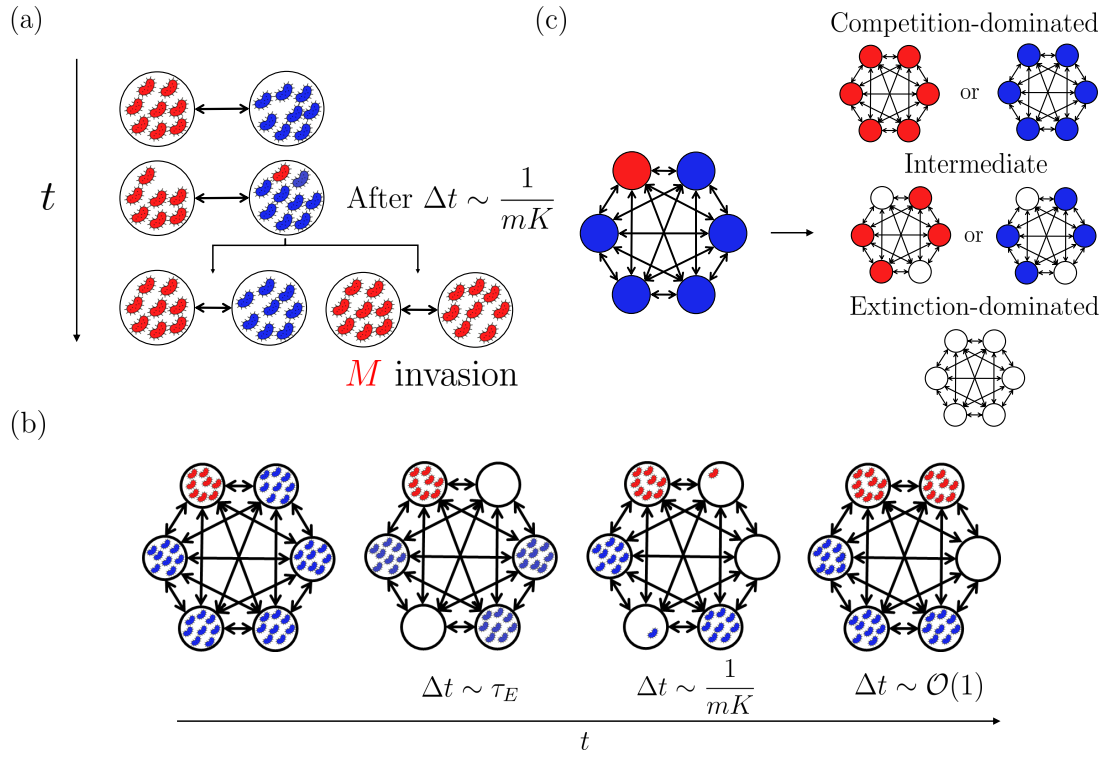

Figure 5.2: Metapopulation dynamics in a static environment. (a) Invasion of W deme by an M cell: Any M cell migrates to a neighbouring W deme with migration rate m after a mean time $\Delta t \sim 1/(mK)$, and then either quickly fixates, producing a new M deme (right), or does not fixate leaving the pair of M and W demes unchanged (left). The same picture holds for the invasion of an M deme by a W cell; see text. (b) Intermediate regime (here for the clique): The dynamics is characterised by deme extinction and W/M competition (see text). Deme extinction occurs after a mean time τ_E, and empty demes are then recolonised by an invader from a neighbouring surviving deme after $\Delta t \sim 1/(mK)$. A recolonised deme is rapidly taken over (in $\Delta t \sim \mathcal{O}(1)$). (c) Coarse-grained description of the metapopulation dynamics: Each deme is always either fully W (blue / dark) or M (red / light) or empty (white). In this description, different scenarios arise, shown for the clique. Competition-dominated regime: all demes are occupied and there is always fixation of W or M. Intermediate regime: eventually W or M take over all occupied demes, resulting in a dynamic equilibrium of empty demes and W or M demes; see text. Extinction-dominated regime: there are frequent deme extinctions and the metapopulation quickly goes extinct.

With this, the condition for a metapopulation to be a circulation is given by

$$\sum_{y \text{ n.n. } x} \sum_{\alpha} T_{\alpha}^{m,\mathrm{G}}(x) = \sum_{y \text{ n.n. } x} \sum_{\alpha} T_{\alpha}^{m,\mathrm{G}}(y) \quad \text{for all } x, \tag{5.3}$$

where y n.n. x denotes the sum over the q_G neighbours y of the deme x. In our case, this simplifies considerably to give $n(x) = \sum_{y \text{ n.n. } x} n(y)/q_G$ for all x. Intuitively, this means that for our setup, if each deme has the same population size, then the metapopulation is a circulation. This will indeed be the case under sufficiently large carrying capacity (such that DF are not so large as to cause deme extinction) due to the logistic growth dynamics on each deme; see Ch. 2.1.

EV is again concretely implemented via the time-varying carrying capacity, $K(t)$, defined by Eq. (2.22). Similarly to Ch. 2.3.2, we also consider symmetric DMN here for simplicity, though the results are easily generalised to asymmetric switching; see Ch. 5.4 and Appendix C.5.

The full individual-based model is therefore a continuous-time multivariate Markov process defined by the reactions of Eqs. (5.1) and (5.2) with transition rates given by Eqs. (2.10) and (5.2) that satisfies the ME given by Eq. (C.1) discussed in Appendix C.1.1. The microscopic intra- and inter-deme dynamics encoded in the ME has been simulated using the Monte Carlo method described in Appendix D.2. While the eco-evolutionary dynamics of a single deme has already been discussed in Ch. 2.3.2, we additionally consider the impact on the dynamics due to migration in Appendix C.1.2. Concretely, each of n, n_W, and n_M fluctuate in time and depend on the deme x, and environmental state defined by ξ in a time-varying environment. However, for notational simplicity, we often drop the explicit dependence of n, n_W, and n_M on some or all of the variables x, t, and ξ. In what follows, I combine coarse-grained analytical approximations viable under slow migration and individual-based stochastic simulations to study the impact of spatial structure, migration, and DF on the fixation and extinction properties of the metapopulation.

5.2 Static environments

It is again initially useful to start by considering the case of a static environment where EV is not present and the carrying capacity K of each deme is constant. This will help to build the tools and understanding required to study the population under EV in Ch. 5.3. The dynamics on each deme follow logistic growth defined as in Eq. (2.2), and therefore the size n of each deme rapidly reaches and fluctuates about K, with $n \approx K$ when $K \gg 1$; see Fig. 5.1(b, top right). I will thus refer to K as "small" where the intra-deme dynamics of fixation occur slower than those of deme extinction. Similarly, K is referred to as large (alternatively, $K \gg 1$) where intra-deme fixation occurs faster than deme extinction. The expected number of migrants per unit time and deme is thus mK. The number of migration events, alongside the strength of selection relative to diffusion in each deme, increases with K. Cell migration and selection are however limited when K is small:

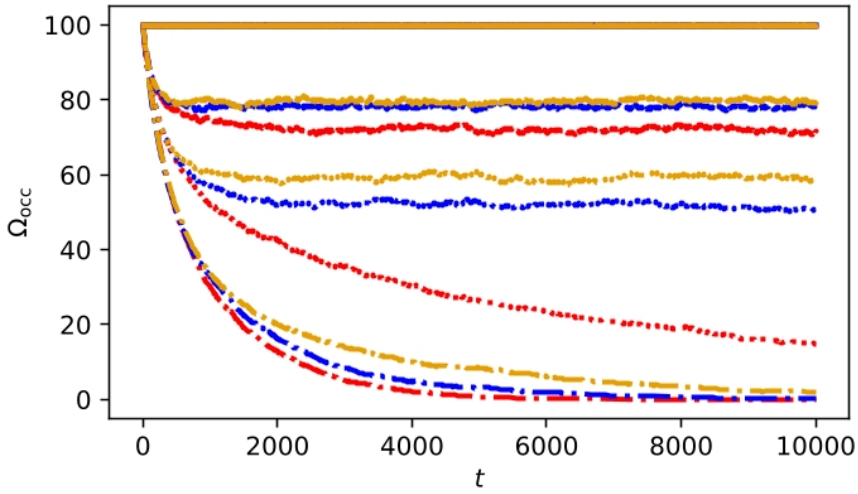

Figure 5.3: Metapopulation occupancy: Ω_{occ} against t for cliques (yellow), cycles (red), and grids (blue), with $\Omega = 100$ and $K = 8$. Simulation results averaged on 100 realisations for the stationary number Ω_{occ} of occupied demes for $\psi = 100$ (solid lines), $\psi = 5$ (dashed lines), $\psi = 2.5$ (dotted lines), and $\psi < 1$ (dash-dotted lines). Eq. (5.6) predicts $\Omega_{\text{occ}} = 100, 80, 60, 0$ for $\psi = 100, 5, 2.5$ and $\psi < 1$, respectively.

regardless of their type, demes of small size are prone to extinction in a mean time τ_E; see Ch. 2.1.2 and Figs. 2.1, 5.1(b), and 5.2(b). In our analysis, we distinguish between different dynamical scenarios through the quantity

$$\psi(m, K) \equiv mK\tau_E, \tag{5.4}$$

giving the average number of migration events during the typical deme extinction time. With the approximate expression for τ_E given by Eq. (2.6), we have $\psi(m, K) \approx me^K$ when $K \gg 1$. In the regime where $\psi \gg 1$, many migration events occur prior to deme extinction, making deme extinction exceedingly unlikely. The dynamics in this regime is therefore dominated by M/W competition. When $\psi(m, K) < 1$, migration does not occur sufficiently often to prevent deme extinction, and all demes quickly go extinct. An intermediate regime where some demes are empty and others occupied by W or M arises when $\psi(m, K) \gtrsim 1$. To rationalise this picture, it is useful to track the number of occupied demes $j = 0, 1, \ldots, \Omega$ (by either W or M cells) as in the coarse-grained description of Lande et al. (1998). Here we consider the clique metapopulation and thus, in this description, residents (of either W or M type) of the j occupied demes can (instantaneously) recolonise a neighbouring empty deme at a rate $B(j)$ or go extinct at a rate $D(j)$ (see Fig. 5.2(b)), given by

$$\begin{aligned} B(j) &= mKj(1 - j/\Omega), \\ D(j) &= j/\tau_E. \end{aligned} \tag{5.5}$$

These rates are obtained by considering that, for recolonisation, the mKj expected migrants per unit time each have a probability $1 - j/\Omega$ to migrate to an empty deme and recolonise it, while for deme extinction, each of the j demes go extinct in a time assumed

to be exponentially distributed with mean given by τ_E. With this we can estimate the number of occupied demes Ω_{occ} in the metapopulation when the environment is static (constant carrying capacity K). At the MF level, we can write the following balance equation (Levins, 1969)

$$\begin{aligned}\frac{\mathrm{d}}{\mathrm{d}t}\Omega_{\text{occ}} &= B(\Omega_{\text{occ}}) - D(\Omega_{\text{occ}}),\\ &= mK\Omega_{\text{occ}}\left(1 - \frac{1}{\psi} - \frac{\Omega_{\text{occ}}}{\Omega}\right).\end{aligned}$$

The equilibria of this equation are $\Omega_{\text{occ}} = 0$ and $\Omega_{\text{occ}} = \Omega\frac{\psi-1}{\psi}$ when $\psi > 1$. The equilibrium $\Omega_{\text{occ}} = 0$ is asymptotically stable when $\psi < 1$ and unstable otherwise. This means that all demes go extinct, and there is extinction of the entire metapopulation when $\psi < 1$. When $\psi > 1$, the equilibrium $\Omega_{\text{occ}} = \Omega\frac{\psi-1}{\psi}$ is asymptotically stable. This corresponds to a fraction $1 - 1/\psi$ of the demes being entirely occupied, and there is a fraction $1/\psi$ of empty demes. In the limit where $\psi \gg 1$, we have $\Omega_{\text{occ}} \to \Omega$ and all demes and hence the metapopulation are fully occupied. Putting everything together, we obtain

$$\frac{j}{\Omega} \to \frac{\Omega_{\text{occ}}(m,K)}{\Omega} \approx \begin{cases} 1 & \text{if } \psi \gg 1,\\ \frac{\psi-1}{\psi} & \text{if } \psi \gtrsim 1,\\ 0 & \text{if } \psi < 1.\end{cases} \tag{5.6}$$

This MF derivation of Ω_{occ} is accurate for large clique metapopulations but, as it ignores spatial correlations, it is a crude approximation for cycles and grids; see Fig. 5.3. In particular, Ω_{occ} overestimates the number of occupied demes in cycles when ψ is not much larger than 1. However, ψ allows us to efficiently distinguish between different the regimes dominated by M/W competition, deme extinction, and the intermediate regime.

Henceforth, we refer to "invasion" when a cell of type M/W migrates to and fixates in a W/M deme, and to "recolonisation" when a cell of either type migrates into an empty deme and repopulates it; see Fig. 5.2(a,b). Accordingly, the competition-dominated and intermediate regimes are respectively characterised by invasions and recolonisations; see Fig. 5.2(a,b).

Extinction-dominated dynamics

In the extinction-dominated regime we have $\psi < 1$ with $m \ll 1$ (for slow migration; see below), and we do not expect any deme invasions in a time τ_E, enabling us to adopt a suitable coarse-grained description. Deme invasions being negligible under slow migration, the timescale of extinction dynamics is much shorter than that of M/W competition, and deme extinction dominates over deme invasion; see Fig. 5.2(c). Continuing with the coarse-grained description of Lande et al. (1998), we have that demes may be regarded as being either occupied (by either W or M cells) or empty with rates of recolonisation and extinction given by Eq. (5.5). Spatial structure may only influence the dynamics

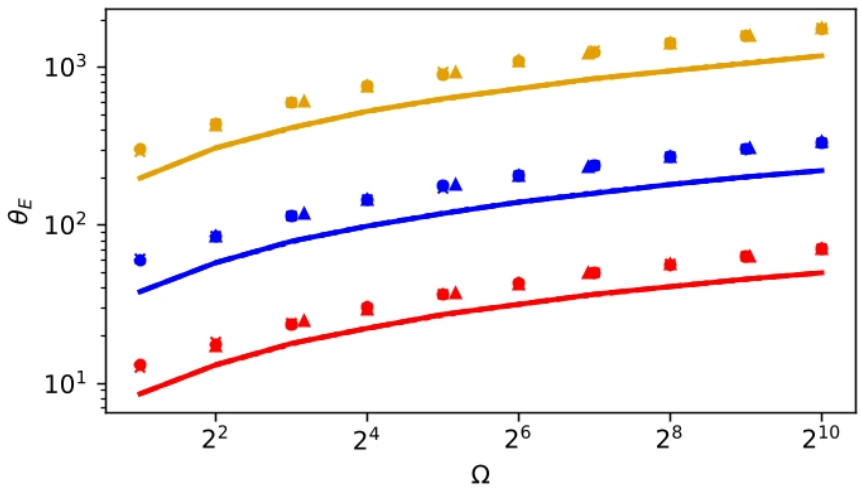

Figure 5.4: θ_E against metapopulation size Ω for $K = 3$ (red), $K = 5$ (blue), $K = 7$ (yellow), and $m = 10^{-4}$. Markers are simulation results and lines are predictions of Eq. (5.9) for cliques (solid lines / crosses), cycles (dashed lines / circles), and grids (dotted lines / triangles). Markers of the same colour are almost indistinguishable. Deviations occur due to the approximation of $\tau_E(K)$ in Eq. (2.6). Selection plays no role in this regime, so results have been obtained with $s = 0$.

via migrations (which occur rarely compared to extinctions here), and thus the coarse-grained dynamics is largely independent of the spatial structure, and can be represented by a birth-death process for the number of occupied demes. Again, we describe the metapopulation dynamics in terms of the number $j = 0, 1, \ldots, \Omega$ of entirely occupied demes. This coarse-grained description of the metapopulation dynamics is therefore a birth-death process with an absorbing state $j = 0$ corresponding to the eventual extinction of the metapopulation, and a reflecting boundary at $j = \Omega$ (all demes are occupied). In this picture, the metapopulation MET, denoted θ_E, i.e. the mean time it takes for every deme on the metapopulation to be empty given they are all initially occupied (at $n = K$), reads (L. J. S. Allen, 2003)

$$\theta_E(K, \Omega) = \sum_{n=1}^{\Omega-1} \left[\left(\prod_{m=1}^{n-1} \frac{B(m)}{D(m)} \right) \sum_{j=n}^{\Omega} \frac{\prod_{l=1}^{j} \frac{B(l)}{D(l)}}{D(j)} \right]. \tag{5.7}$$

With $\psi = mK\tau_E$, and using $\prod_{l=n}^{j-1}(1 - \frac{l}{\Omega}) = \frac{1}{\Omega^{j-n}} \frac{(\Omega-n)!}{(\Omega-j)!}$, Eq. (5.7) can be rewritten as

$$\theta_E(K, \Omega) = \tau_E(K) \sum_{n=1}^{\Omega} \sum_{j=n}^{\Omega} \frac{1}{j} \left(\frac{\psi}{\Omega} \right)^{j-n} \frac{(\Omega - n)!}{(\Omega - j)!}. \tag{5.8}$$

In the extinction-dominated regime $\psi \ll 1$, the main contribution to the inner sum stems

from $j = n$, and the leading contribution to the metapopulation MET is therefore

$$\theta_E(K, \Omega) \approx \tau_E(K) \sum_{n=1}^{\Omega} \frac{1}{n} = \tau_E(K) H_\Omega,$$

where H_Ω is the Ω-th harmonic number. We have $H_\Omega = \ln(\Omega) + \gamma_{\text{EM}} + \mathcal{O}(\Omega^{-1})$ where $\gamma_{\text{EM}} \approx 0.577...$ is the Euler-Mascheroni constant. This expression is independent of selection and, to leading order, generally does not depend on the initial state of the metapopulation. In the limit of a large metapopulation, $\Omega \gg 1$, the metapopulation MET in the regime $\psi(m, K) \ll 1$, is asymptotically given by the simple expression

$$\theta_E(K, \Omega) \approx \tau_E(\ln(\Omega) + \gamma_{\text{EM}}). \tag{5.9}$$

Therefore, for $\psi < 1$ and $\Omega \gg 1$, as ψ increases with K the metapopulation MET grows almost exponentially with K and logarithmically with Ω, and we find $\theta_E \approx e^K \ln(\Omega)/K$; see Figs. 2.1 and 5.4. For $\psi > 1$, Eq. (5.8) predicts a rapid growth of the metapopulation MET, as seen in the simulation results of Fig. 5.5(e), which it captures qualitatively. Furthermore, while $\theta_E(K, \Omega)$ has been explicitly derived for cliques (island model), we see that spatial structure has little impact due to the dominance of extinctions, and thus it also provides insight into the extinction dynamics for cycles and grids.

Competition-dominated dynamics

When $\psi \gg 1$ and $m \ll 1$ (meaning slow migration and permitting a coarse-grained description), the carrying capacity is large enough for many migrations to occur on the timescale of deme extinction, τ_E. Since every deme expects many incoming cells in time τ_E, deme extinction is unlikely and can be neglected. In this regime, the dynamics is dominated by local M/W competition: W and M cells compete in each deme to fixate the local subpopulation; see Figs. 5.1(b) and 5.2(a,c).

As in Marrec et al. (2021), Marrec (2023), and Moawad et al. (2024), we adopt a coarse-grained description of the metapopulation dynamics. Here, each deme is treated as a single entity of type W or M. For this description to accurately capture the dynamics on the metapopulation, we require that migration is slow such that the mean time for an M or W invader to fixate in a deme is negligible compared to $1/(mK)$, the expected time between migrations; see Eq. (5.12) for full definition. In this regime, each sequential migration of an individual into a deme of opposite type is an invasion attempt, with a cell from an M/W deme trying to invade a neighbouring W/M deme; see Fig. 5.2(a). Here, an M/W invasion is the fixation of a single M/W mutant in a deme consisting of $K - 1$ cells of type W/M.

Within the coarse-grained description, the state of the metapopulation is denoted by i, where $i = 0, 1, \ldots, \Omega$ is the number of demes of type M leaving $\Omega - i$ demes of type W. The probability $\rho_{M/W}$ of invasion by an M/W migrant is here given by the classical result for the probability that a single M/W cell takes over a population of constant size K in a

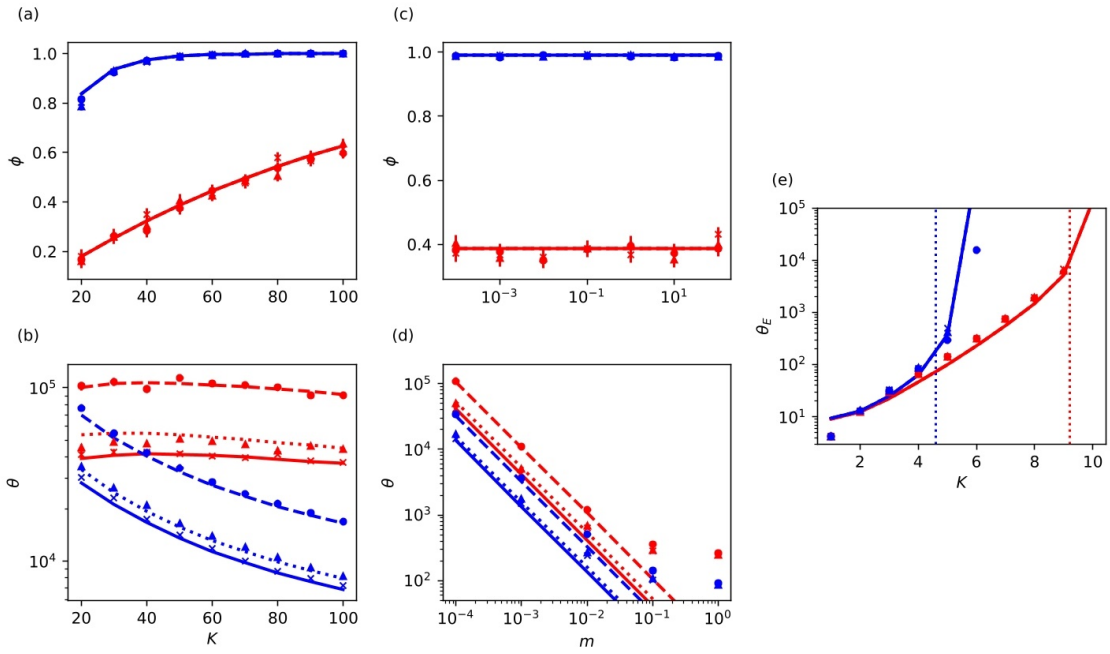

Figure 5.5: (a-d): Competition-dominated dynamics, $\psi \gg 1$. (a) M fixation probability ϕ against constant carrying capacity K; (b) unconditional mean fixation time θ against K; (c) ϕ against per capita migration rate m; (d) θ against m. Markers are simulation results and lines are predictions of Eq. (5.14) for $s = 0.1$ (blue) and $s = 0.01$ (red) on a clique (solid lines / crosses), cycle (dashed lines / circles), and grid (dotted lines / triangles). In (a,b), $m = 10^{-4}, \Omega = 16$, and in (c,d), $K = 50, \Omega = 16$. In (a,c), markers for the same s are almost indistinguishable indicating independence of the spatial structure. (e): Extinction-dominated dynamics, $\psi < 1$. Metapopulation MET θ_E against K for $\Omega = 16$ and $m = 10^{-2}$ (blue) and 10^{-4} (red). Markers are simulation results and thick lines are predictions of Eq. (5.8) for cliques (solid lines / crosses), cycles (dashed lines / circles), and grids (dotted lines / triangles). Thin dashed vertical lines are guides to the eye showing $\psi = 1$ for $m = 10^{-2}$ (blue) and 10^{-4} (red). Selection plays no role in this regime, so panel (e) has been obtained with $s = 0$. In panels (a,c,e), dashed lines overlap with solid lines and so are not visible. In all panels, there is initially one M deme and $\Omega - 1$ demes occupied by W.

Moran process as in Ch. 2.2.2 (Moran, 1958, 1962; Antal & Scheuring, 2006; Traulsen & Haeurt, 2009), and thus reads

$$\begin{aligned}\rho_M &\equiv \phi_{\rm MA}(1) = \frac{s}{1+s}\left[\frac{1}{1-(1+s)^{-K}}\right],\\ \rho_W &\equiv 1-\phi_{\rm MA}(K-1) = \frac{s}{(1+s)^K}\left[\frac{1}{1-(1+s)^{-K}}\right],\end{aligned} \tag{5.10}$$

where $\phi_{\rm MA}(n_M)$ is given by Eq. (2.20). In each time unit, a deme receives from and sends to its neighbours an average of mK cells. Importantly, only edges connecting M and W demes can lead to invasions; see Fig. 5.2(a). These are "active edges" and their number in state i on graph G is denoted by $E_{\rm G}(i)$, where here we consider ${\rm G}\in\{\text{clique},\text{cycle},\text{grid}\}$. Migration is equally likely from a deme to any one of its $q_{\rm G}$ neighbours, where $q_{\rm clique}=\Omega-1$, $q_{\rm cycle}=2$, $q_{\rm grid}=4$, and $q_{d-\rm dim}=2d$ for a d-dimensional regular lattice. It is generally difficult to determine the number of active edges, which varies with the metapopulation state and spatial structure. However, analytical progress is possible in certain spatial structures. In the clique, the i demes of type M are connected to the $\Omega-i$ demes of type W, yielding $E_{\rm clique}(i)=i(\Omega-i)$. The M demes form a single unbreakable cluster since all demes are connected. For a cycle, if the initial state is $i=1$ under slow migration, the initial M deme is exactly connected to two W demes. This property is conserved by the coarse-grained dynamics, with an unbreakable cluster of M demes always connected to a cluster of W demes by two active edges until W or M fixates the metapopulation, yielding $E_{\rm cycle}(i)=2$ for $i\neq 0,\Omega$; see Figs. 5.1(a) and 5.2(a). The unbreakable nature of the M cluster in these two cases alongside the symmetric nature of the specific graphs, means there is only one possible metapopulations state for a given size of M cluster. This is what permits explicit expressions for $E_{\rm G}(i)$, The number of active edges in the grid metapopulation is difficult to obtain because the cluster is not unbreakable and the metapopulation has many possible states for a given number of M demes, but may be approximated. In the case of a large ($\Omega\gg 1$) metapopulation structured as a grid with unit spacing between neighbours, we assume that the mutant spreads outwards from the initial M deme approximately forming an M-cluster with a circular front. If this circular M-cluster has a radius r, it has an area πr^2 containing a number i of M demes. The boundary of the circular M-cluster is of length $2\pi r$. Assuming that this length is equal to the number of M demes on the boundary, we find that $r=\sqrt{i/\pi}$ and there are $2\sqrt{i\pi}$ boundary demes given i demes of type M. We therefore estimate that the average number active edges for a grid is $E_{\rm grid}(i)\approx 2\sqrt{\pi i}$ for $i\neq 0,\Omega$. When $i=0,\Omega$, one strain fixates the entire metapopulation, where all demes are M if $i=\Omega$ and all demes are W when $i=0$, and hence $E_{\rm G}(0)=E_{\rm G}(\Omega)=0$ for all G.

In the coarse-grained description of the competition-dominated dynamics, starting from a single M deme ($i=1$), there are $mKE_{\rm G}(i)/q_{\rm G}$ expected attempts per unit time to grow the number of M demes by invading neighbouring W demes. Each of these attempts is an invasion with probability ρ_M, given by Eq. (5.10), and therefore the number of M demes grows at a rate $mKE_{\rm G}(i)\rho_M/q_{\rm G}$. The number of W demes attempts to grow by sending

migrants into neighbouring M demes, which invade with probability ρ_W. The number of M demes is therefore reduced at a rate $mKE_{\mathrm{G}}(i)\rho_W/q_{\mathrm{G}}$. In this representation, M and W invasions therefore act at the interface of M and W demes by increasing or decreasing the number of M demes, i, at respective rates (Marrec et al., 2021; Fruet et al., 2024; Moawad et al., 2024),

$$\begin{aligned} T_i^+(m,\mathrm{G},K) &= mK\frac{E_{\mathrm{G}}(i)}{q_{\mathrm{G}}}\rho_M, \\ T_i^-(m,\mathrm{G},K) &= mK\frac{E_{\mathrm{G}}(i)}{q_{\mathrm{G}}}\rho_W. \end{aligned} \tag{5.11}$$

With this, we can concretely define slow migration in this setting, which we have so far assumed without explicit consideration. In the competition-dominated regime, $1/s$ sets the timescale of deme dynamics, representing the timescale for fixation of a single isolated deme; see Eq. (2.12) of Ch. 2.2.1. The growth of the number of mutant demes, i, in time $1/s$ is $T_i^+(m,\mathrm{G},K)/s = mKE_{\mathrm{G}}(i)\rho_M/(q_{\mathrm{G}}s)$.[1] In the adopted coarse-grained description, slow migration is the regime where the invasion can be regarded as being instantaneous, with fixation of a successful M invader occurring before the next invasion. This requires that the average number of successful M invaders in the time for the intra-deme dynamics be less than one, i.e. $T_i^+(m,\mathrm{G},K)/s < 1$. Therefore, slow migration is satisfied for

$$m < \frac{sq_{\mathrm{G}}}{K\rho_M E_{\mathrm{G}}(i)} \leq \frac{s}{K\rho_M}, \tag{5.12}$$

where we have used $q_{\mathrm{G}}/E_{\mathrm{G}}(i) \leq 1$. When $s \ll 1$ and $Ks \gg 1$, we have $\rho_M \sim s$ and therefore simply $m < 1/K$. For typical values used in this chapter, e.g. $\Omega = 16, K = 100$ and $s = 0.1$, we can estimate that there is slow migration if $m \lesssim 10^{-2}$, which is in line with the values of $m \in [10^{-5}, 10^{-2}]$ used in our examples, and matches where we see deviations in Fig. 5.5(d).

We have therefore obtained a birth-death process for the number of M demes, i, with absorbing boundaries at $i = \Omega$ (M fixation) and $i = 0$ (W fixation) which is valid under slow migration and competition-dominated dynamics (i.e. $\psi \gg 1$). This very closely resembles the Moran process discussed in Ch. 2.2.2, and this system is in fact amenable to the same techniques introduced in that section. In this representation, the M fixation probability in a metapopulation of size Ω, spatially structured as a graph G, consisting initially of i mutant demes is denoted ϕ_i^{G}, and the MFT denoted θ_i^{G}. These quantities therefore satisfy the first-step equations (L. J. S. Allen, 2003; Ewens, 2004; Antal & Scheuring, 2006; Traulsen & Haeurt, 2009)

$$\begin{aligned} (T_i^+ + T_i^-)\phi_i^{\mathrm{G}} &= T_i^+\phi_{i+1}^{\mathrm{G}} + T_i^-\phi_{i-1}^{\mathrm{G}}, \\ (T_i^+ + T_i^-)\theta_i^{\mathrm{G}} &= 1 + T_i^+\theta_{i+1}^{\mathrm{G}} + T_i^-\theta_{i-1}^{\mathrm{G}}, \end{aligned} \tag{5.13}$$

for $i = 1, \ldots, \Omega - 1$, with boundary conditions $\phi_0^{\mathrm{G}} = 1 - \phi_\Omega^{\mathrm{G}} = 0$ and $\theta_0^{\mathrm{G}} = \theta_\Omega^{\mathrm{G}} = 0$. These are identical in form to Eqs. (2.17) and therefore Eqs. (5.13) can be solved exactly (Antal &

[1] We use the growth of the number of M demes to define slow migration as the mutant has a fitness advantage. Therefore, $\rho_M > \rho_W$ and $T_i^+(m,\mathrm{G},K) > T_i^-(m,\mathrm{G},K)$ in general.

Scheuring, 2006; Traulsen & Haeurt, 2009). Here, we are chiefly interested in the fixation of a single initial M deme, $i = 1$, and simply write $\phi^{\mathrm{G}} \equiv \phi_1^{\mathrm{G}}$ and $\theta^{\mathrm{G}} \equiv \theta_1^{\mathrm{G}}$, finding

$$\begin{aligned} \phi^{\mathrm{G}}(K) &= \phi(K) = \frac{1-\gamma}{1-\gamma^{\Omega}}, \\ \theta^{\mathrm{G}}(m, \mathrm{G}, K) &= \frac{1-\gamma}{1-\gamma^{\Omega}} \sum_{k=1}^{\Omega-1} \sum_{n=1}^{k} \frac{\gamma^{k-n}}{T_n^+(m, \mathrm{G}, K)}, \end{aligned} \tag{5.14}$$

where $\gamma \equiv T_i^-/T_i^+ = \rho_W/\rho_M \approx \exp(-Ks)$ is a quantity independent of m and G. As noted in Marrec et al. (2021), Abbara and Bitbol (2023), and Moawad et al. (2024) the fixation probability $\phi^{\mathrm{G}} = \phi$ is therefore independent of the migration rate and spatial structure. This non-trivial result is due to the graphs considered being circulations; see Eq. (5.3). In *static environments*, a generalised circulation theorem shows that the fixation probability is independent of m and G for circulations (Lieberman et al., 2005; Marrec et al., 2021; Moawad et al., 2024), a feature displayed in Fig. 5.5(a,c). We find that the ϕ increases almost exponentially and $\phi \approx 1$ when $Ks \gg 1$; see Fig. 5.5(a,c). This stems from the invasion of W demes becoming increasingly likely and the invasion of M demes exponentially less likely due to the increase in the strength of selection over diffusion as K increases. When $Ks \ll 1$, the competition is effectively neutral as diffusion dominates over selection for deme fixation. In this case, $\phi \approx 1/\Omega$ since the metapopulation is initialised with one mutant deme, giving an identical result to that obtained from neutral competition (Ewens, 2004). Eqs. (5.14) also predict that the MFT decreases with the migration rate $\theta^{\mathrm{G}} \sim 1/m$. This is seen in the simulation results of Fig. 5.5(b,d). Furthermore, we see that for given parameters, the MFT is shortest on cliques, while it is larger on cycles than on grids. Intuitively, for higher m and more connected graphs, migrants spread faster leading to quicker invasion and fixation.

Intermediate dynamics

In the intermediate regime $\psi \gtrsim 1$ and $m \ll 1$ (again ensuring slow migration and a suitable coarse-grained description), there is a crossover between the extinction and competition-dominated dynamics. At fixed migration rate m, this intermediate regime occurs in the range $\ln(1/m) \lesssim K \lesssim \ln(\Omega K/m)$; see Appendix C.2. Furthermore, the metapopulation is partially occupied for $\ln(1/m) \lesssim K \lesssim \ln(\Omega/m)$ corresponding to $1 < \psi < \Omega - 1$. These bounds are illustrated by the vertical lines in Fig. C.2.

When $\psi \gtrsim 1$, migration and deme extinction occur on the timescale τ_E. In the long run, deme recolonisations and extinctions balance each other, yielding a dynamical equilibrium consisting of $\Omega_{\mathrm{occ}} = \Omega(1 - 1/\psi)$ occupied demes and $\Omega - \Omega_{\mathrm{occ}}$ empty demes; see Fig. 5.3. In this regime, we therefore have a three-state coarse-grained description of the dynamical equilibrium consisting of a random mixture of empty demes, and occupied W and M demes; see Fig. 5.2(b). The metapopulation may, in fact, be fully occupied at its equilibrium in the intermediate regime, with occasional deme extinctions which are quickly recolonised, differentiating it from the competition-dominated regime. After a

mean time $\theta_{\text{int}}^{\text{G}}$ the metapopulation reaches the dynamical equilibrium consisting of a fraction $1 - \Omega_{\text{occ}}/\Omega = 1/\psi$ of empty demes, and the remaining demes are all of either type M or W with probability ϕ_{int}^{G} and $1 - \phi_{\text{int}}^{\text{G}}$, respectively. The dynamical equilibrium is thus defined by the quantities ψ, given by Eq. (5.4), and $\phi_{\text{int}}^{\text{G}}$ which is the probability that mutants M take over the $\Omega_{\text{occ}} = \Omega(1 - 1/\psi)$ occupied demes, where the unconditional mean fixation time is given by $\theta_{\text{int}}^{\text{G}}$. These quantities are derived and discussed in Appendix C.2 for a metapopulation on an arbitrary regular lattice consisting initially of a single M deme; see Eq. (C.2) and Fig. C.2

5.3 Time-varying environments

We now investigate the impact of EV implemented through a time-varying carrying capacity, $K(t)$ as in Eq. (2.22) driven by the DMN $\xi(t) \in \{-1, 1\}$; see Fig. 5.6. Moreover, we are particularly concerned with population bottlenecks, arising when the deme size is drastically reduced, as discussed in Ch. 2.3.2. When $\nu \lesssim 1$, the deme size n tracks $K(t)$ and experiences a bottleneck whenever the carrying capacity switches from K_+ to K_-, as seen throughout previous chapters and in Fig. 5.6(a,right) (Wienand et al., 2017, 2018). Therefore, this setup captures the joint effect of EV, DF, and migration on the metapopulation dynamics, where we have justified that each of these elements is typically present in natural biological populations in Ch. 1. We assume that $K_+ \gg 1$ such that, in the mild environment the deme size is large and therefore subject to weak DF. In what follows, we distinguish between weak bottlenecks, where $\psi(m, K_-) \gg 1$ and deme extinction is negligible, and strong bottlenecks, where $\psi(m, K_-) < 1$ and deme extinctions dominate.

Weak bottlenecks: $\psi(m, K_-) \gg 1$

In the case of $\psi(m, K_-) \gg 1$, each deme on the metapopulation is subjected to a weak bottleneck at an average frequency $\nu/2$ when $\nu \lesssim 1$; see Fig. 5.6(a,top). The condition $\psi(m, K_-) \approx me^{K_-} \gg 1$ ensures that deme extinction can be neglected, with metapopulation dynamics dominated by M/W competition. The metapopulation fate can therefore be captured by a two-state coarse-grained description similar to that of Ch. 5.2. Now with a time-varying environment, the deme size, and hence number of migrating cells, varies with $K(t)$. It is therefore useful to introduce environmental state dependent counterparts to $\langle N \rangle$ defined in Eq. (2.28) which capture the long-term average deme size dependent on the environmental state $\xi = \pm 1$ and switching rate ν, denoted $\mathcal{N}_\xi(\nu) \equiv \mathcal{N}_\pm(\nu)$.

We first discuss the metapopulation fate in the limit of slow and fast environmental switching, which strongly resembles the same limiting regimes considered in the simple example of Ch. 2.3.2, and then return to the above case of weak bottlenecks with $\nu \lesssim 1$.

When the environment varies very slowly, $\nu \ll 1$, the carrying capacity remains at its initial value, i.e. $K(t) = K_+$ or $K(t) = K_-$ each with a probability $1/2$, until invasions lead to the fixation of W or M, and thus $\mathcal{N}_\pm(\nu) = K_\pm$. In other words, the time between switches is longer than the fixation time in each environment such that

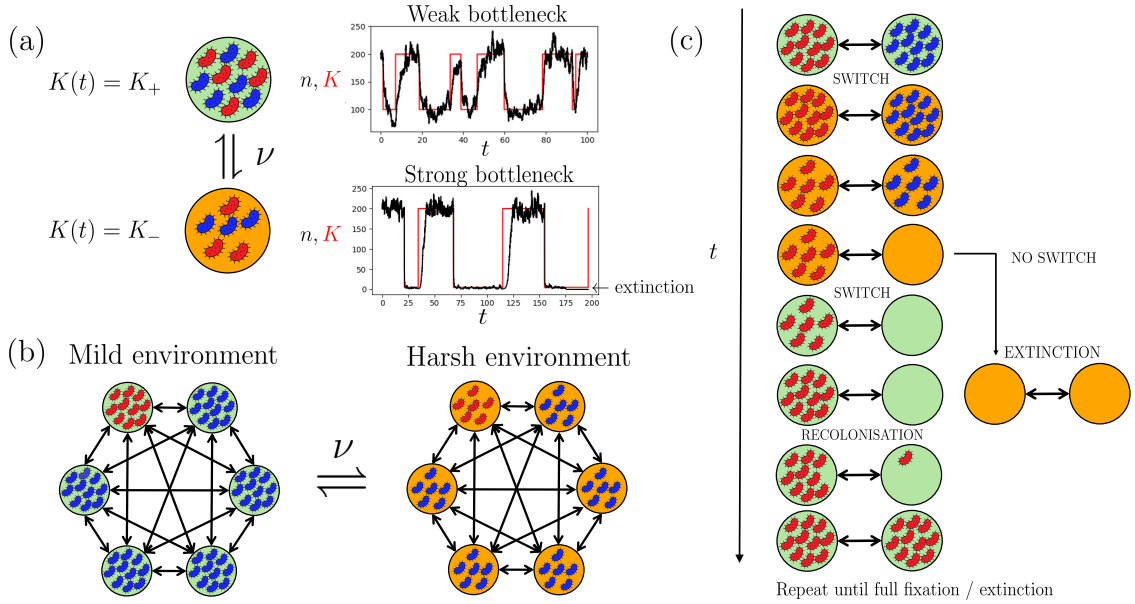

Figure 5.6: (a) Left: single deme in time-switching environment. The carrying capacity $K(t)$ encodes environmental variability by switching between $K = K_+$ (mild environment, green / light) and $K(t) = K_- < K_+$ (harsh environment, orange / dark) at symmetric rate ν (see also Appendix C.5). Communities are larger in the mild environment. When $K(t)$ switches at an intermediate rate, each deme experiences bottlenecks at an average frequency $\nu/2$. Right: n and K against time in the intermediate switching regime where the size n of a deme undergoes bottlenecks. Parameters are: $K_+ = 200$, $\nu = 0.05$ and $K_- = 100$ (top) and $K_- = 5$ (bottom). The bottlenecks are weak when $\psi(m, K_-) \gg 1$ (top, right) where deme extinction is unlikely. When $\psi(m, K_-) < 1$, there are strong bottlenecks and each deme can go extinct in the harsh environment (bottom, right). (b) Clique metapopulation with $\Omega = 6$ connected demes (double arrows). All demes have the same time-switching carrying capacity $K(t)$ encoding environmental variability across the metapopulation, with each deme in the same environmental state. (c) Example evolution across two nearest-neighbour demes in a switching environment subject to strong bottlenecks in the intermediate switching regime; see text. Starting in the mild environment where $K = K_+$, the carrying capacity switches to K_- (harsh environment) after $t \sim 1/\nu$. Following the $K_+ \to K_-$ switch, each deme size decreases and each subpopulation is subject to strong demographic fluctuations and hence prone to extinction. In the absence of recolonisation of empty demes, effective only in the mild state, all demes go extinct. If there is a switch back to the mild environment $K_- \to K_+$ prior to total extinction, empty demes can be rescued by migration and recolonised by incoming W or M cells from neighbouring demes. In the sketch, an empty deme is recolonised by a mutant in the mild environment and becomes an M deme. The cycle continues until the entire metapopulation consists of only W or M demes, or metapopulation extinction.

$\nu \max(\theta^{\mathrm{G}}(m, K_+), \theta^{\mathrm{G}}(m, K_-)) < 1$, where $\theta^{\mathrm{G}}(m, K)$ is given by Eq. (5.14). In the slow switching regime, the M fixation probability and MFT on a metapopulation spatially arranged as a regular graph G are respectively denoted by Φ_0^{G} and Θ_0^{G}. The quantities are obtained by averaging their static counterparts defined in Eq. (5.14) over the stationary distribution of K, yielding

$$\begin{aligned} \Phi_0^{\mathrm{G}}(m, K_\pm) &= \Phi_0(K_\pm) = \frac{1}{2}\left[\phi(K_+) + \phi(K_-)\right], \\ \Theta_0^{\mathrm{G}}(m, K_\pm) &= \frac{1}{2}\left[\theta^{\mathrm{G}}(m, K_+) + \theta^{\mathrm{G}}(m, K_-)\right]. \end{aligned} \tag{5.15}$$

When the environment varies very quickly, $\nu \gg 1$, the DMN self averages before fixation from invasions can occur, and the carrying capacity of each deme rapidly reaches the effective value $\mathcal{K}$ with $\mathcal{N}_\pm(\infty) \to \mathcal{K}$ (Wienand et al., 2017, 2018; Taitelbaum et al., 2020); see Ch. 2.3.2. In this fast switching regime, the M fixation probability and MFT on a metapopulation spatially arranged as a regular graph G, respectively denoted by Φ_∞^{G} and $\Theta_\infty^{\mathrm{G}}$, are obtained by replacing K with $\mathcal{K}$ in Eq. (5.14), yielding

$$\begin{aligned} \Phi_\infty^{\mathrm{G}}(m, \mathcal{K}) &= \Phi_\infty(\mathcal{K}) = \phi(\mathcal{K}), \\ \Theta_\infty^{\mathrm{G}}(m, K_\pm) &= \theta^{\mathrm{G}}(m, \mathcal{K}). \end{aligned} \tag{5.16}$$

From these expressions and Eq. (5.14), we notice the fixation probability in the regime of slow and fast switching is independent of the migration rate and spatial structure: $\Phi_0^{\mathrm{G}} = \Phi_0$ and $\Phi_\infty^{\mathrm{G}} = \Phi_\infty$. However, the metapopulation MFT depends explicitly on the migration rate m and G, with $\Theta_0^{\mathrm{G}} \sim 1/m$ and $\Theta_\infty^{\mathrm{G}} \sim 1/m$. Outside of these limiting regimes, the metapopulation dynamics are far richer. Under intermediate switching rate, when $\nu \lesssim 1$, the coupling of DF and EV plays a key role. Cell migration depends on the deme size that varies with the environmental state, and so the metapopulation dynamics cannot be mapped onto those of a suitable static counterpart as in the limiting regimes. The M/W competition characterising the intermediate switching regime dynamics can be described by the coarse-grained representation of Ch. 5.2 generalised to a time-varying environment following Ch. 4.2.2 and Wienand et al. (2017, 2018). Here, we analyse the influence of ν and m on the M fixation probability, $\Phi_i^{\mathrm{G}}(\nu, m)$, and MFT, $\Theta_i^{\mathrm{G}}(\nu, m)$, in a metapopulation consisting of i mutants demes and $\Omega - i$ W-demes spatially arranged as a regular graph G. To this end, we consider a birth-death process for the number $i = 0, \ldots, \Omega$ of M demes. As in Ch. 5.2, we assume that there is initially a single M deme ($i = 1$). The effective rates for increase or decrease in the number of M demes, $\mathcal{T}_{i,\xi}^{\pm}$, depend on the expected number of migrating cells, which in turn depends on the deme size that is now a time-varying quantity driven by Eq. (2.22). In a time-varying environment, the expected number of migrants from a deme, mn, is approximated by $m\mathcal{N}_\xi(\nu)$, where the the deme size in each environmental state can be approximated by using the conditional PDMP distributions defined by Eq. (2.26) to obtain

$$\mathcal{N}_\xi(\nu) = \int_{K_-}^{K_+} n p_{\xi,\nu/s}(n)\, \mathrm{d}n.$$

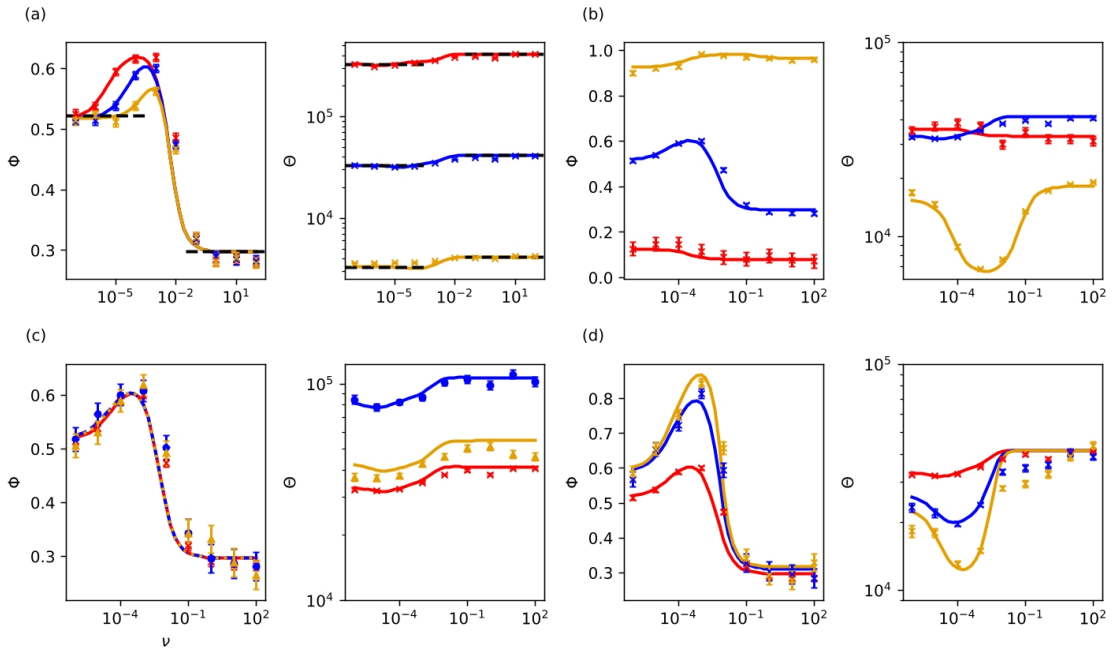

Figure 5.7: Fixation probability Φ^{G} and mean fixation time Θ^{G} against switching rate ν for various parameters. Each panel shows Φ^{G} against ν (left) and Θ^{G} against ν (right). Markers show simulation results and lines are predictions of Eq. (5.22). (a,b) $\Phi^{\mathrm{clique}}(\nu)$ and $\Theta^{\mathrm{clique}}(\nu)$ for a clique metapopulation and different values of m in (a) and s in (b). (a) $m = 10^{-5}$ (red), $m = 10^{-4}$ (blue), $m = 10^{-3}$ (yellow), and $s = 0.01$. (b) $s = 10^{-3}$ (red), $s = 10^{-2}$ (blue), $s = 10^{-1}$ (yellow), and $m = 10^{-4}$. Dashed black lines are guides to the eye showing $\Phi_{0,\infty}$ in (a,left) and $\Theta_{0,\infty}$ in (a,right); see text. Other parameters are $\Omega = 16$, $K_+ = 200$, and $K_- = 20$. (c) $\Phi^{\mathrm{G}}(\nu)$ and $\Theta^{\mathrm{G}}(\nu)$ for clique (red, crosses), cycle (blue, circles), and grid (yellow, triangles). Other parameters are $\Omega = 16$, $K_+ = 200$, $K_- = 20$, $s = 0.01$, $m = 10^{-4}$. (d) $\Phi^{\mathrm{clique}}(\nu)$ and $\Theta^{\mathrm{clique}}(\nu)$ for a clique metapopulation with $K_+ = 200$ (red), $K_+ = 500$ (blue), and $K_+ = 1000$ (yellow). Deviations occur for Θ with $K_+ = 1000$ since the slow-migration condition is not satisfied in the mild environment. Other parameters are $\Omega = 16$, $K_- = 20$, and $s = 0.01$, $m = 10^{-4}$. In all examples, there is initially a single M deme and $\Omega - 1$ others of type W; see text.

Additionally, and as in Ch. 2.3.2 and Wienand et al. (2017, 2018), the switching rate has been rescaled, $\nu \to \nu/s$, by the timescale of the deme fixation dynamics where there are an average of $\mathcal{O}(\nu/s)$ switches on the deme fixation timescale. As in static environments (see Eq. (5.11)) the transition rates $\mathcal{T}^{\pm}_{i,\xi}$ depend on the spatial structure, via $E_{\mathrm{G}}(i)/q_{\mathrm{G}}$, and on the probability $\rho_{M/W,\xi}(\nu)$ that an M/W migrant invades a W/M deme in the environment ξ. Putting everything together, this yields the effective transition rates

$$\begin{aligned}\mathcal{T}^{+}_{i,\xi}(\nu, m, \mathrm{G}) &= m\mathcal{N}_{\xi}(\nu)\frac{E_{\mathrm{G}}(i)}{q_{\mathrm{G}}}\rho_{M,\xi}(\nu),\\ \mathcal{T}^{-}_{i,\xi}(\nu, m, \mathrm{G}) &= m\mathcal{N}_{\xi}(\nu)\frac{E_{\mathrm{G}}(i)}{q_{\mathrm{G}}}\rho_{W,\xi}(\nu),\end{aligned} \tag{5.17}$$

where, by analogy with Eq. (5.10), we have introduced

$$\begin{aligned}\rho_{M,\xi}(\nu) &\equiv \frac{s}{1+s}\frac{1}{1-(1+s)^{-\mathcal{N}_{\xi}(\nu)}},\\ \rho_{W,\xi}(\nu) &\equiv \frac{s}{(1+s)^{\mathcal{N}_{\xi}(\nu)}}\frac{1}{1-(1+s)^{-\mathcal{N}_{\xi}(\nu)}}.\end{aligned} \tag{5.18}$$

With Eq. (5.17), by dropping all explicit dependence of the transition rates except on i and ξ, we obtain the M fixation probability starting from the environmental state ξ with i mutant demes on a graph G, denoted by $\Phi^{\mathrm{G}}_{i,\xi}(\nu, m, K_{\pm})$, as the solution of the ν-dependent first-step analysis equation (Gardiner, 2009; Ashcroft et al., 2014)

$$\left[\mathcal{T}^{+}_{i,\xi} + \mathcal{T}^{-}_{i,\xi} + \nu\right]\Phi^{\mathrm{G}}_{i,\xi} = \mathcal{T}^{+}_{i,\xi}\Phi^{\mathrm{G}}_{i+1,\xi} + \mathcal{T}^{-}_{i,\xi}\Phi^{\mathrm{G}}_{i-1,\xi} + \nu\Phi^{\mathrm{G}}_{i,-\xi}, \tag{5.19}$$

subject to the boundary conditions $\Phi^{\mathrm{G}}_{0,\xi} = 0$ and $\Phi^{\mathrm{G}}_{\Omega,\xi} = 1$. The metapopulation MFT in the environmental state ξ, denoted by $\Theta^{\mathrm{G}}_{i,\xi}$, similarly satisfies

$$\left[\mathcal{T}^{+}_{i,\xi} + \mathcal{T}^{-}_{i,\xi} + \nu\right]\Theta^{\mathrm{G}}_{i,\xi} = 1 + \mathcal{T}^{+}_{i,\xi}\Theta^{\mathrm{G}}_{i+1,\xi} + \mathcal{T}^{-}_{i,\xi}\Theta^{\mathrm{G}}_{i-1,\xi} + \nu\Theta^{\mathrm{G}}_{i,-\xi}, \tag{5.20}$$

with boundary conditions $\Theta^{\mathrm{G}}_{0,\xi} = \Theta^{\mathrm{G}}_{\Omega,\xi} = 0$. Eqs. (5.19) and (5.20) generalise Eqs. (5.13) to a time-switching environment, with the last terms on the right-hand side accounting for environmental switching, and coupling $\Phi^{\mathrm{G}}_{i,\xi}$ to $\Phi^{\mathrm{G}}_{i,-\xi}$ and $\Theta^{\mathrm{G}}_{i,\xi}$ to $\Theta^{\mathrm{G}}_{i,-\xi}$. Eqs. (5.19) and (5.20) can be solved numerically using standard methods similarly to Eqs. (4.12) and (4.13) of Ch. 4 since they are entirely equivalent in form. In Ch. 4, we knew exactly the state of the system following an environmental switch through an instantaneous change to the toxin level, unlike the system here where the population size does not change instantaneously after an environmental switch. The analysis here allows us to appropriately capture the average population size reached following an environmental switch $n \approx \mathcal{N}_{\xi}(\nu)$ under weak selection ($s \ll 1$) and slow migration ($m \ll 1$). Therefore, the continuously varying population size on a deme is approximated by assuming the population size switches back and forth between $\mathcal{N}_{\pm}$, making it amenable to the same numerical methods as used to tackle Eqs. (4.12) and (4.13). The M fixation probability $\Phi^{\mathrm{G}}_{i}(\nu)$ and MFT $\Theta^{\mathrm{G}}_{i}(\nu)$ regardless of

ξ are obtained by averaging over the stationary distribution of ξ, yielding

$$\begin{aligned}\Phi_i^{\mathrm{G}}(\nu, m) &= \frac{1}{2}\sum_{\xi} \Phi_{i,\xi}^{\mathrm{G}}(\xi, \nu, m),\\ \Theta_i^{\mathrm{G}}(\nu, m) &= \frac{1}{2}\sum_{\xi} \Theta_{i,\xi}^{\mathrm{G}}(\xi, \nu, m),\end{aligned} \tag{5.21}$$

where we have reinstated the explicit dependence on ν and m. As we specifically consider the initial condition of a single M deme, we set $i = 1$ in Eq. (5.21) and simplify the notation by writing

$$\Phi^{\mathrm{G}}(\nu, m) \equiv \Phi_1^{\mathrm{G}}(\nu, m) \text{ and } \Theta^{\mathrm{G}}(\nu, m) \equiv \Theta_1^{\mathrm{G}}(\nu, m), \tag{5.22}$$

Therefore, Eq. (5.22) gives the M fixation probability and MFT in the combined coarse-grained and PDMP description. In Fig. 5.7, the comparison of the predictions of Eq. (5.22) with the simulation results of the full model on the regular graphs $\mathrm{G} \in \{\text{clique}, \text{cycle}, \text{grid}\}$ shows that Eq. (5.22) captures well the dependence of Φ^{G} and Θ^{G} on ν, m, s and K_+. In particular, Eq. (5.22) reproduces on all G the non-monotonic ν-dependence of Φ^{G} and Θ^{G} (when this feature is present), as well as their behaviour when $\nu \to 0, \infty$ given by Eqs. (5.15) and (5.16).

In stark contrast with the case of static environments, we see that Φ^{G} and Θ^{G} depend on spatial migration. Fig. 5.7(a,left) demonstrates clear differences for $\Phi^{\text{clique}}(\nu, m)$ across m values in the range $\nu \in [10^{-4}, 10^{-1}]$. These deviations, of up to 20%, exceed the error bars and are captured well by Eq. (5.22). In Fig. 5.7(c,left), we notice that both simulation results and predictions of Eq. (5.22) for $\Phi^{\mathrm{G}}(\nu, m)$ differ slightly for $\nu < 10^{-3}$ (though are almost indistinguishable) for each graph G, whereas Fig. 5.7(c,right) shows that Θ^{G} depends on the spatial structure. The explicit dependence of the fixation probability on migration and spatial structure deviates from the case of static environments seen in Fig. 5.5, and is therefore a signature of eco-evolutionary dynamics of the metapopulation in time-varying environments. As shown in Appendix C.3, the correspondence demonstrated in Marrec et al. (2021) between Φ^{G} and the fixation probability of a random walk for the number $i = 0, 1, \ldots, \Omega$ of mutant demes with hopping probabilities independent of m and G, and absorbing states $0, \Omega$, breaks down in time-varying environments. This leads to the dependence of Φ^{G} and Θ^{G} on m and G in time-switching environments.

Another distinctive feature of Φ^{G} and Θ^{G} is their non-monotonic ν-dependence when the other parameters (s, m, $K_\pm$, Ω) are kept fixed. In particular, Fig. 5.7 shows that Φ^{G} may exhibit a sharp peak in the regime of intermediate switching rate, $\nu \in [10^{-4}, 10^{-1}]$, that is well captured by Eq. (5.22). This contrasts directly with the results in a single well-mixed population, as in Ch. 2.3.2 and Wienand et al. (2017, 2018), where the fixation probability varies monotonically with ν; see Fig. 2.2(f). The non-monotonic ν-dependence of Φ^{G} and Θ^{G} is therefore an inherent effect of spatial migration. Intuitively, this behaviour can be understood by first considering the limit of very slow switching, i.e. $\nu \to 0$, and how

the dynamics change as ν is increased. Under very slow switching, the metapopulation is initialised and fixates prior to any environmental switches. Thus, the fixation properties are given by Eq. (5.15). Crucially, the MFT for a system initialised in the K_- state is much larger than that of a system initialised in the K_+ state, since invasions are far less frequent due to the smaller population size. Furthermore, the M fixation probability in the K_- state is lower than that of the K_+ state since, under the smaller population size, DF are amplified and therefore diffusion has a stronger effect than selection. As ν is gradually increased, a point is reached whereby an environmental switch is expected prior to fixation for systems initialised in the harsh state but not for those initialised in the mild state due to the larger MFT in K_-. This switch prior to fixation for systems initialised in the harsh state into the mild state therefore allows for the subsequent fixation of that system to occur faster and with a higher likelihood of M fixation than it would have done continuing in the K_- state. As ν increases further, environmental switches occur prior to fixation in either environmental state, and so this effect is partially lost. Furthermore, the average deme size is a decreasing function of ν (see Fig. 2.2(e) of Ch. 2.3.2 and Wienand et al. (2017, 2018)) meaning that as ν increases further, M fixation becomes less probable and takes longer due to the smaller average deme size. Hence, the best conditions for the fixation of M under weak bottlenecks are for a range of ν in the intermediate regime.

Strong bottlenecks: $\psi(m, K_-) < 1$

In the case of $\psi(m, K_-) < 1$, each deme on the metapopulation is subjected to strong bottlenecks; see Fig. 5.6(a). In the harsh environment $\xi = -1$ ($K = K_-$), the entire metapopulation experiences extinction, in a time $\theta_E(K_-, \Omega)$, denoted θ_E here for conciseness, which is short compared to the fixation timescale. However, in the mild state $\xi = 1$ ($K = K_+$), deme extinction can be neglected and each deme can be regarded as being occupied by either W or M cells. Therefore, the dynamics in the harsh state is dominated by deme extinction, while in the mild environment there is M/W recolonisation and competition. In the realm of strong bottlenecks, EV therefore subjects the metapopulation to periods dominated in turn by deme extinction and M/W recolonisation and competition, yielding complex dynamical scenarios whose analysis is difficult. However, we can gain valuable insight by considering first the limits of $\nu \ll 1$ and $\nu \gg 1$, and then the case of intermediate switching where $\nu \lesssim 1$.

As in the weak bottleneck case, when the environment varies very slowly, $\nu \ll 1$, the environment remains at its initial value for long periods, that is $K = K_\pm$ if $\xi(0) = \pm 1$ each with a probability 1/2. On the one hand, if initially $\xi = -1$ (harsh environment) then $K = K_-$ and each deme is prone to extinction after a mean time $\tau_E(K_-)$, which eventually leads to the collapse of the metapopulation after a time $\theta_E \approx e^{K_-} \ln(\Omega)/K_-$ when $\Omega \gg 1$ and $K_- \gg 1$; see Eq. (2.6) and Fig. 5.8(a). On the other hand, if the environment is initialised with $\xi = 1$ (mild conditions), $n \approx K_+$ and there is M/W competition characterised by the fixation of M with a probability $\phi(K_+)$ approaching 1 when $K_+ s \gg 1$; see Eq. (5.14) and Fig. 5.8(b). As a result, when $\nu \ll 1$ and $K_+ s \gg 1$, there are two equally likely outcomes illustrated in Fig. 5.8(a,b): either the extinction of

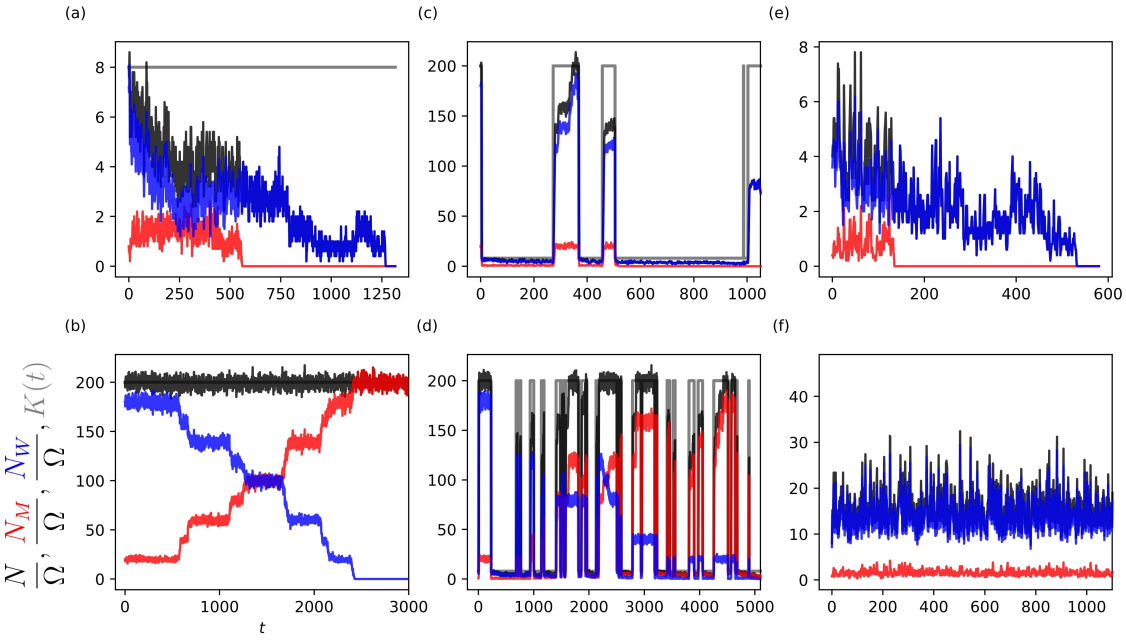

Figure 5.8: Typical single realisations of N/Ω (black), N_M/Ω (red), N_W/Ω (blue), and $K(t)$ (grey) against time for different values of K_- and ν. (a,b): Here, $\nu = 10^{-4}$ and $K_- = 8$. In (a), $K = K_-$ at $t = 0$ and M and then W quickly go extinct. In (b), $K = K_+$ at $t = 0$ and M fixates the population while W goes extinct. (c,d): Here, $\nu = 10^{-2}$ and $K_- = 8$. In (c), mutants survive the first few bottlenecks but their abundance is low leading to the fixation of W and removal of M after four bottlenecks ($t \gtrsim 1000$). In (d), mutants survive the first bottlenecks and spread in the mild state where they recolonise and invade demes. They are eventually able to fixate the population. (e,f): Here, $\nu = 10$, and $K_- = 4$ in (e) and $K_- = 10$ in (f). $K(t)$ switches very frequently and is not shown for clarity. In (e), the deme size is $n \approx 2K_- = 8$ and the dynamics is dominated by deme extinction leading to the rapid extinction of the metapopulation. In (e), the deme size is $n \approx 2K_- = 20$ and there is M/W competition that leads to fixation of M and extinction of W after a typical time $t \sim \theta^{\text{clique}}(2K_-) \gtrsim 10^4$ (not shown). Similar results are obtained on other regular graphs G; see text. Other parameters are $\Omega = 10$, $s = 0.1$, $m = 10^{-4}$, and $K_+ = 200$. In all panels, initially there is a single M deme and $\Omega - 1$ demes occupied by W.

the metapopulation in a mean time θ_E as in Fig. 5.8(a), or the fixation of M after a mean time $\theta^{\mathrm{G}}(K_+)$ as in Fig. 5.8(b).

Under fast environmental switching, when $\nu \gg 1$, the carrying capacity self-averages (see Ch. 2.3.2) and takes the effective value $\mathcal{K}$, with $n \approx \mathcal{K}$ after $t \sim 1$ for $\mathcal{K} \gg 1$ (Wienand et al., 2017, 2018). Since $\mathcal{K} \approx 2K_-$ when $K_+ \gg K_-$, if $\psi(m, 2K_-) < 1$ the dynamics is characterised by the extinction of individual demes after a mean time $\tau_E(2K_-)$, followed by extinction of the entire metapopulation after a mean time $\theta_E(\Omega, 2K_-)$; see Fig. 5.8(e). However, if $\psi(m, 2K_-) \gg 1$, the dynamics is characterised by M/W competition and fixation after a mean time $\theta^{\mathrm{G}}(2K_-)$, as illustrated by Fig. 5.8(f). For $2K_-s \gg 1$, selection dominates and M is likely to fixate, while for $2K_-s \ll 1$, selection is weak and DF are strong allowing diffusion to dominate and lead to likely W fixation.

In slowly and rapidly changing environments under sufficient selective advantage s, regardless of the spatial structure, the metapopulation subject to strong bottlenecks is therefore always at risk of either complete extinction or of being taken over by mutants.

In the intermediate switching regime, $\nu \lesssim 1$ with $\psi(m, K_-) < 1$, the metapopulation experiences strong bottlenecks (since the population size evolves on a timescale $\sim \mathcal{O}(1)$), interspersed by periods of recovery which can prevent metapopulation extinction for extended periods of time. In the harsh environmental state ($K = K_-$), the dynamics is dominated by deme extinction, while in the mild state ($K = K_+ \gg K_-$), there is recolonisation of empty demes that rapidly become either W or M demes occupied at $n \approx K_+$, followed by invasions and M/W competition. In order to prevent metapopulation extinction, the mean time spent in the harsh environmental state must be shorter than the metapopulation MET in the harsh environment, i.e. $1/\nu < \theta_E$. Hence, when $\nu \lesssim 1$ and $\nu\theta_E > 1$, the metapopulation is unlikely to go extinct and transiently consists of a mixture of empty demes and M/W demes before either M or W fixates the remaining occupied demes. In this regime, mutants are likely to be removed from the metapopulation when there is an initially small fraction of them; see Fig. 5.8(c). This is because the extinction of demes is indiscriminate on deme type (i.e. M or W), and therefore it is more likely for a small number of M demes to reach extinction prior to the extinction of the large number of W demes making up the remainder of the metapopulation. At each strong bottleneck, there is then a finite probability of causing all M demes to reach extinction before switching to the mild environment, where surviving mutants can invade W demes and recolonise empty demes. In a scenario illustrated by Fig. 5.8(c), there are periods of duration $\sim 1/\nu$ during which the number of mutants remains low and prone to extinction when $K = K_-$, followed by periods in K_+ where the number of M demes increases (due to M/W competition). Each bottleneck can therefore be seen as an attempt to remove M demes, whereas the switches from $K_- \to K_+$ allows the metapopulation to be recolonised and the mutants to recover somewhat. This cycle repeats itself until M demes are entirely removed after sufficiently many bottlenecks. Following this process, the metapopulation consists of a fluctuating number of W demes and empty demes. This scenario is the most likely to occur when the initial fraction of M demes is small. Another possible outcome, illustrated

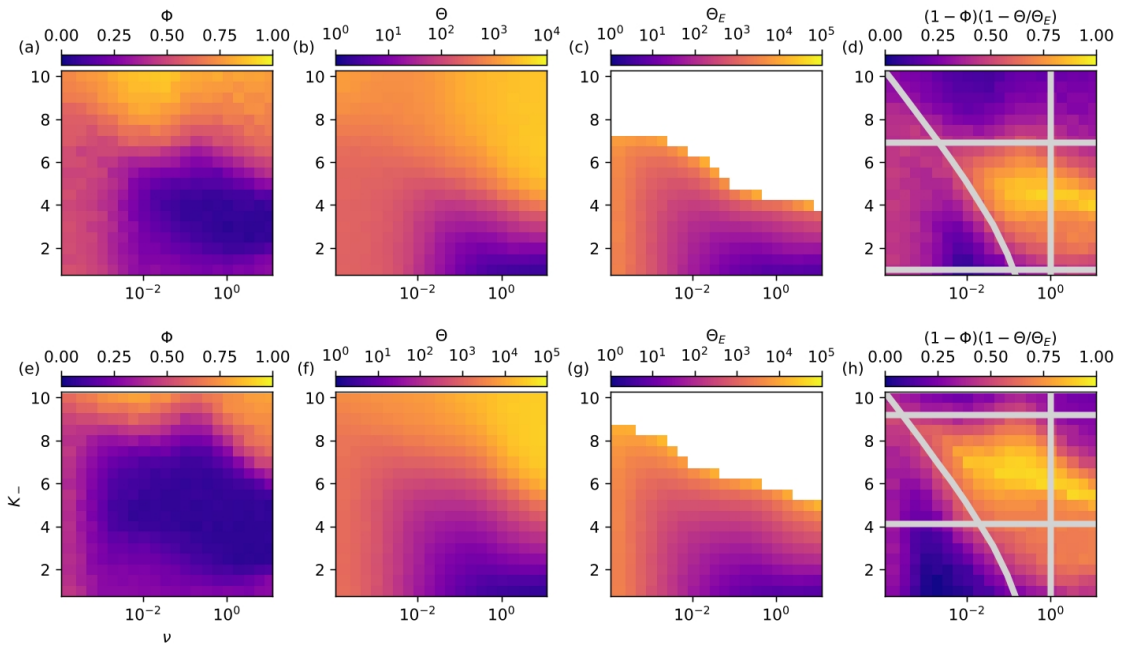

Figure 5.9: Near-optimal condition for the idealised treatment strategy. (ν, K_-) heatmaps of Φ, Θ, Θ_E and $(1-\Phi)(1-\Theta/\Theta_E)$ for a clique metapopulation. The migration rate is $m = 10^{-3}$ in (a-d) and $m = 10^{-4}$ in (e-h). White space in panels (c) and (g) indicate where at least one realisation for those parameters did not reach extinction by $t = 10^5$, i.e. $\Theta_E \sim 10^5$ or larger. Grey lines in panels (d) and (h) show the near-optimal conditions for the idealised treatment strategy: $\psi(m, K_-) < 1$ below the top horizontal line, $mK_+\theta_E > 1$ above the bottom horizontal line, and $\nu\theta_E > 1$ above the curved line, while the vertical line indicates where $\nu < 1$ and θ_E from Eq. (5.9). The near-optimal treatment conditions is the yellowish cloud at the centre of the area enclosed by these lines. Similar results are obtained on other regular graphs G; see text and Fig. C.3. Other parameters $\Omega = 16$, $s = 0.1$, and $K_+ = 200$. In all panels, initially there is a single M deme and $\Omega - 1$ demes occupied by W.

by Fig. 5.8(d), occurs when mutants surviving the harsh conditions invade and are successful in recolonising many demes in the mild environment. Mutants can thus significantly increase the number of M demes, exceeding that of W demes. In this case, bottlenecks can be seen as attempt to remove W demes, and the most likely outcome is the removal of W demes. The metapopulation eventually consists of a fluctuating number of empty demes and mutant demes, as illustrated by Fig. 5.8(d). The results of Fig. 5.8 have been obtained for cliques, but the same qualitative behaviour is expected for any regular graphs G, with the spatial structure affecting the the long-term fraction of occupied demes and therefore the probability of removal of mutants at each bottleneck. However, phenomena operated by extinction are mostly independent of G and m, as illustrated in Fig. C.3 of Appendix C.4.

A hypothetical idealised treatment strategy. In this intermediate switching regime, the metapopulation is likely to avoid extinction in the harsh environment if $\nu\theta_E \gtrsim 1$. Moreover, when $mK_+\theta_E \gtrsim 1$ then deme recolonisations occur sufficiently quickly in the mild environment to prevent the accumulation of extinct demes and eventual metapopulation

extinction. Hence, the metapopulation is likely to avoid extinction when $\nu\theta_E > 1$ and $mK_+\theta_E > 1$ and either W or M can be entirely removed, with respective probabilities Φ and $1-\Phi$, after a mean time Θ, whereas the metapopulation MET in the time-varying environment, Θ_E, occurs on a much longer timescale ($\Theta_E \gg \Theta$). As an application, we consider a hypothetical idealised treatment strategy to efficiently remove unwanted mutants from an otherwise healthy system by controlling the environmental conditions via the parameters K_- and ν. By the nature of how mutants arise in microbial populations, they are initially rare. In this context, M cells are interpreted as the unwanted mutants that have a selective advantage over W cells composing an organism, here represented by the metapopulation consisting initially of $\Omega-1$ demes of type W and a single M deme. In a healthy host, cells replicate in a controlled, self-regulating manner. Mutations may lead to the loss of this self-regulation of cell replication, and such mutant cells replicate rapidly. These cells are cancerous and, due to the nature of mutations, are initially rare. Thus these initial conditions are relevant, even for smaller systems. If allowed to proliferate, cancer cells will outcompete the slower-growing healthy cells, leading to a growing tumour. Therefore, in this motivating context, we should like to remove these more aggressive cells to leave healthy cells behind while not eliminating healthy cells. The idealised treatment strategy consists of finding the optimal environmental conditions to remove M cells and minimise the risk of extinction of the entire metapopulation. This corresponds to determining the range of K_- and ν for which Φ and Θ/Θ_E are minimal. According to the above discussion, the near-optimal conditions for this idealised treatment strategy on a regular graph G are

$$\psi(m, K_-) < 1, \quad \nu \lesssim 1, \quad \nu\theta_E \gtrsim 1, \quad mK_+\theta_E \gtrsim 1. \tag{5.23}$$

Under these conditions, illustrated in Fig. 5.9, which depend on m but not on the spatial structure G, EV generates successive strong bottlenecks at a frequency ensuring that the mutant type is the most likely to go extinct in a mean time that is much shorter than the metapopulation MET. While determining analytically Φ and Θ/Θ_E satisfying Eq. (5.23) is challenging, this can be done efficiently numerically as illustrated by the heatmaps of Fig. 5.9, and be summarised by maximising the composite quantity $(1-\Phi)\,(1-\Theta/\Theta_E)$, as shown in Fig. 5.9(d,h). In the examples of Fig. 5.9, we find that the near-optimal treatment conditions are $10^{-2} \lesssim \nu \lesssim 1$ and for K_- that changes with m: $K_- \in [1,7]$ for $m = 10^{-3}$ and $K_- \in [4,9]$ for $m = 10^{-4}$. The idealised treatment strategy therefore consists of letting the metapopulation evolve under the near optimal conditions Eq. (5.23), under which it undergoes a series of strong bottlenecks whose expected outcome is the removal of mutants. Once all mutants are removed, as in Fig. 5.8(c), the final course of the treatment consists of keeping the metapopulation in the mild environment (with $K = K_+$), where W cells would spread and finally take over all the demes. In the example of Fig. 5.8(c), this would be achieved by setting $K = K_+$ after $t \gtrsim 1000$. This idealised treatment strategy, illustrated for clique metapopulations in Fig. 5.9, qualitatively holds on regular graphs G, with small influence of the spatial structure on the shape of the heatmap when m is kept fixed, as seen by comparing Figs. 5.9(e-h) and C.3. We note that the yellow regions that

appears for $\nu > 1$ in Fig. 5.9(d,h) are not due to bottlenecks. Instead , these appear as the EV self-averages and the effective carrying capacity reproduces the dynamics found in the intermediate regime discussed briefly in Ch. 5.2 and elaborated on in Appendix C.2.

5.4 Discussion, generalisations, and robustness

Here, I discuss the main results by critically reviewing the assumptions made and outline possible generalisations. I have studied the eco-evolutionary dynamics of a metapopulation consisting of Ω identical demes with the same carrying capacity K, containing wild-type W and mutant M cells, that are connected by slow migration and arranged as regular circulation graphs. While the approach holds for any regular graph, I have specifically considered the examples of cliques (island model), cycles, and square grids (with periodic boundaries). This has allowed us to consider the impact of various graph structures on the metapopulation dynamics. I have analysed the metapopulation dynamics in a static environment where K is constant, and in a time-varying environment where K switches endlessly between K_- and $K_+ > K_-$ at a rate ν; see Eq. (2.22). In static environments, the deme size fluctuates about K and the metapopulation dynamics is characterised by either M/W competition (when $\psi \gg 1$), or by deme extinction (when $\psi < 1$). We have used suitable coarse-grained descriptions to analytically characterise the fate of the population in those regimes; see Fig. 5.5. When, as here, the metapopulation is spatially arranged on circulation graphs, the circulation theorem (Lieberman et al., 2005; Marrec et al., 2021) guarantees that the fixation probability in the competition-dominated regime is independent of the migration rate and the spatial structure. I have also devised a coarse-grained three-state description of the dynamical equilibrium in the intermediate regime (where $\psi \gtrsim 1$) where in the long run there is a mixture of occupied demes of type W or M and empty demes; see Appendix C.2.

In time-varying environments, when K switches neither too quickly nor too slowly, each deme is subject to bottlenecks that can be weak when K_- is large enough to ensure $\psi(m, K_-) \gg 1$. Deme extinction can be neglected in the weak bottleneck regime, and I have combined a coarse-grained description with a PDMP approximation to characterise the M/W competition in time-varying environments in the absence of deme extinction. This has allowed me to show that weak bottlenecks lead to a *non-monotonic* dependence of the mutant fixation probability Φ^{G} and mean fixation time Θ^{G} on the switching rate ν, with an explicit dependence on the migration rate, whereas the spatial structure has an unnoticeable effect on Φ^{G}, regardless of spatial correlations, but influences Θ^{G}. This is in direct contrast with the behaviour of a well-mixed population; see Ch. 2.3.2 and Wienand et al. (2017, 2018). When demes are subject to strong bottlenecks, metapopulation extinction is possible, and sometimes a likely outcome under slow and fast switching ($\nu \ll 1$ and $\nu \gg 1$), whereas the overall extinction can be avoided for long periods under intermediate switching, when M/W competition and deme extinction dynamics are coupled. As a hypothetical application, I have considered an idealised treatment strategy for the rapid removal of the mutant conditioned on minimising the risk of overall extinction.

The coarse-grained descriptions adopted in the static and dynamic environments track the dynamics of the number of M demes, which, in the case of the clique and cycle, is a single unbreakable cluster of M demes. This requires starting from such a cluster, where here we assumed the natural initial condition of a single M deme. Under these considerations, the number of active edges connecting W and M demes in cliques and cycles is known exactly, making these graphs particularly amenable to detailed analysis. It is also possible to capture the number of active edges exactly for other starting configurations of these graphs (e.g. two or more neighbouring M demes) provided that the unbreakable structure of the cluster of M demes is preserved at all times $t \geq 0$. For the sake of concreteness and simplicity, we have focused on a class of regular circulation graphs. In two dimensions, spatial correlations between demes are more complex, and the coarse-grained description of the M/W competition dynamics on a grid has required approximations of the number of active edges; see Appendix C.4. A similar approximation is expected to hold on hypercubic lattices (with periodic boundaries). These considerations on the role of the initial condition and spatial structure do not matter when the metapopulation dynamics is dominated by the extinction of demes since these occur randomly across the metapopulation. As a consequence, the "idealised treatment strategy" based on the dynamic coupling of competition and deme extinction to remove a targeted and initially rare strain is expected to hold on more complex structures, including generic connected graphs.

In this work, I have focussed on the biologically relevant regime of slow migration, which is well known to increase the population fragmentation and hence influences its evolution and diversity (S. Wright, 1943; Slatkin, 1981). Here, the assumption of slow migration is crucial for the coarse-grained description of the metapopulation dynamics, and the values considered in our examples, $m \in [10^{-5}, 10^{-2}]$, are comparable with those used in microfluidic experimental setups (Keymer et al., 2006). For $m \gg 1$, the behaviour of a single well-mixed population is recovered; see Ch. 2.3.2 and Wienand et al. (2017). For intermediate m, the dynamics is characterised by coarsening, i.e. the slow growth of domain sizes over time (Krapivsky et al., 2010; Täuber, 2014). For the sake of simplicity and without loss of generality, we have assumed that migration occurs without any directional preference and with the same rate for M and W. These assumptions can be relaxed and the coarse-grained description be readily generalised to the case of directional and type-specific migration (Marrec, 2023), yielding the same qualitative behaviour discussed here for circulation graphs. We note however that asymmetric directional migration significantly affects the evolutionary dynamics on non-circulation graphs, like the star, where the asymmetry can lead to either an amplification or suppression of the mutant fixation probability (Lieberman et al., 2005; Marrec et al., 2021; Abbara & Bitbol, 2023; Abbara et al., 2024; Moawad et al., 2024). It would be interesting to study the evolution on these non-circulation graphs in time-varying environments in the case of symmetric and directional migration. For computational tractability, I have chiefly considered metapopulations consisting of 16 demes of size ranging between 1 and 200, which are much smaller systems than most realistic microbial communities. However, we note that with microfluidic devices and single-cell techniques, it is possible to perform spatially structured experiments

with 10 to 100 cells per microhabitat patch, which are conditions close to those used in our model (Keymer et al., 2006; Hsu et al., 2019; Totlani et al., 2020). Moreover, *in-vivo* host-associated metapopulations are often fragmented into a limited number of relatively small demes, e.g. $\Omega \approx 25$ and $K \approx 1000$ in mouse lymph nodes (Ganchua et al., 2020; Van den Broeck et al., 2020; van Tatenhove-Pel et al., 2021; Fruet et al., 2024).

The analysis of this chapter therefore furthers the understanding of the impact of spatial structure, migration, and DF on the spread of a mutant strain subject to EV. Under this EV, I have identified and characterised various dynamical scenarios which display non-trivial dependencies on the environmental switching rate and migration rate of the cells. Crucially, this behaviour does not occur in the cases of a static environment or a well-mixed population, and thus directly stems from the interplay between EV and spatial structure. I have also demonstrated how EV coupled to DF on a spatially structured population can be utilised in novel ways to achieve desired evolutionary outcomes, here being the efficient removal of an unwanted mutant.

Chapter 6

Conclusions

This thesis contributes to the growing body of literature investigating the impact of environmental variability on the evolution of biological systems, particularly in the case of microbial communities. Here, I have focussed in particular on competition between two species, competing for a common pool of resources which is tacitly assumed to be continuously replenished. In considering the full stochastic birth and death dynamics of these systems, I have investigated the likelihood that one of the species takes over the population, with the other going extinct, unable to return. Throughout, one key common aspect of the models developed is the use of a time-varying carrying capacity to introduce environmental variability to the population. The carrying capacity changes with instantaneous switches between two values, one large and one small, mimicking the sharp transitions that can occur in microbial environments (Wahl et al., 2002; Brockhurst, 2007; Patwa & Wahl, 2010; Shade et al., 2012; Stegen et al., 2012; Coates et al., 2018). Furthermore, it is common to introduce environmental variability in this way in laboratory experiments (Acar et al., 2008; Sanchez & Gore, 2013; G. Lambert & Kussell, 2014; Rodríguez-Verdugo et al., 2019; Abdul-Rahman et al., 2021; Nguyen et al., 2021; Shibasaki et al., 2021). This variability leads to changes in the population size which, in turn, controls the strength of demographic fluctuations in the population, impacting its subsequent evolution. Therefore environmental variability and demographic fluctuations are coupled via the time-varying population size that modulates the amplitude of the demographic fluctuations. In this way, I have coupled environmental variability to the evolutionary dynamics of the systems considered, which is a key feature of the work of this thesis. Across these models, I have found that environmental variability generally impacts the likelihood of species fixation, long-lived species coexistence, the time required for species fixation, as well as the composition of the population under long-lived coexistence. Furthermore, I have investigated the dynamics through both extensive stochastic simulations and the development of novel analytical tools, thus allowing for a comprehensive understanding of the systems considered.

In Ch. 3, I considered two distinct models of cooperative AMR with competing resistant and sensitive species, motivated by the growing problem of AMR evolution in clinical in-

fections (O'Neill, 2016). If allowed to evolve under no environmental variability, we saw that resistant cells are likely to remain in the population for long times, which is undesired in the context of our motivating example. I then considered the case of a fixed volume population in which the nutrient concentration varied in time. Under this scenario, I uncovered a *resistance-eradication mechanism* that comes about due to the environmental variability and the transients it induces, occurring when the rate of environmental change is comparable to that of the relaxation of the evolutionary dynamics ($\nu \sim s$). By computational means, I showed that this mechanism allows for a fast eradication of resistant cells, and argued that it holds also for large microbial communities, comparable to those used in laboratory experiments ($N > 10^6$). This makes apparent the importance of considering environmental variability in such systems of interest: though the model considered is quite abstracted from reality, the eradication of resistant cells is an issue of key importance to society today, and this only arises under the consideration of environmental variability. Furthermore, I characterise the behaviour more generally across the parameter space considered, determining environmental conditions whereby species coexist for long times without fixation and those where the resistant species fixate the population. Since this work has been undertaken, Hernández-Navarro, Distefano, et al. (2024) have developed a more realistic extension of the model to a metapopulation structure, where a similar resistance-eradication mechanism remains but is enhanced compared to a single well-mixed population, particularly under slow cell migration.

Following this case of a constant volume and varying nutrient concentration, I also considered the scenario whereby the volume of the population varies in time, with the nutrient concentration of the population held constant. Under this form of EV, the long-time eco-evolutionary dynamics were similarly difficult to predict compared to the case of a constant environment: in the presence of EV, long-lived coexistence of the strains is possible even when fast fixation is likely, and there can be early fixation of a strain even when long-lived coexistence is expected. By computing the fixation-coexistence diagrams of the system through simulations, I determined the environmental conditions separating areas of the diagrams where fixation of one strain is most likely from areas where long-lived coexistence of both species is most likely. These findings were then rationalised by devising an analytical approach, built on the combination of suitable quenched and annealed averaging procedures in different regimes of environmental variability, thus reproducing qualitatively and quantitatively the diagrams and fixation-coexistence properties obtained from simulations. Furthermore, this accurately captured the behaviour of the probability of long-lived coexistence and of fixation conditioned on fast fixation with varying switching rate and cooperation threshold. Importantly in the context of modelling the evolution of AMR, the findings allowed for the identification of the most favourable environmental conditions for the *early eradication of AMR*. However, unlike in the previous model, there does not exist a general resistance-eradication mechanism which can remove resistant cells regardless of cooperation threshold.

The results of Ch. 4 demonstrated the impact of twofold environmental variability. In this

model, resistant and sensitive species competed subject to a time-varying carrying capacity, as before, and a time-varying toxin level. Under harsh conditions, the level of toxin is high and resources are scarce, while environmental conditions are mild when the level of toxin is low and resources are abundant. The toxin-level being in its high or low level state determined if the resistant or sensitive species was selected for, respectively. When the environment is static, there is no long-lived coexistence since one species dominates and rapidly fixates the population. However, I showed that under sufficiently fast and strong variability in the toxin level, the long-lived coexistence of resistant and sensitive cells emerged where it crucially was not possible under a static environment. I computationally and analytically obtained the fixation-coexistence phase diagrams of this system, allowing for the precise identification of the environmental conditions under which species coexistence is almost certain for extended periods, and the phases where one species dominates, as well as the crossover regimes where both coexistence and fixation are possible, but not guaranteed. I found that, while variability in the toxin level can promote coexistence, resource variability can strongly inhibit it. This carrying capacity switching lead to population bottlenecks responsible for large demographic fluctuations which promoted fast fixation, with the effect being amplified for stronger bottlenecks. More generally, the influence of the population size distribution on the fixation-coexistence phase diagram was characterised completely. Finally, I determined how the make-up of the coexistence phase and average abundance of each strain depended on the rates of environmental change. In summary, in this chapter I determined the circumstances in which environmental variability, together with demographic fluctuations, favours or hinders the long-lived coexistence of competing species, and how it affects the fraction and abundance of each strain in the community. This work hence contributes to further elucidate the role of environmental variability and demographic fluctuations on the maintenance of biodiversity in complex ecosystems, demonstrating that the details of how an environmental attribute (e.g. nutrient or toxin level) impacts species can determine whether or not coexistence is promoted or hindered by variability in this attribute.

The problem of how microbial communities evolve subject to environmental variability is vital when considering the issue of AMR, so that the effectiveness of treatments can be maximised, while minimising their harmful effects. In considering the models of Chs. 3 and 4, I have shown that EV can have qualitative effects on the population evolution, either promoting or jeopardising lasting species coexistence. Furthermore, I have shown that specific choices of the EV can promote a given desired evolutionary outcome in a population; for example the intermediate bottlenecks in the first model of Ch. 3 leading to the resistance-eradication mechanism. This work paves the way for several possible applications, for instance, in microbial experiments with controlled environmental conditions (Wahl et al., 2002; Brockhurst, 2007; Acar et al., 2008; Patwa & Wahl, 2010; Shade et al., 2012; Stegen et al., 2012; Sanchez & Gore, 2013; G. Lambert & Kussell, 2014; Coates et al., 2018; Rodríguez-Verdugo et al., 2019; Abdul-Rahman et al., 2021; Nguyen et al., 2021; Shibasaki et al., 2021), which might shed light on new possible treatments against AMR in real-world clinical infections.

In Ch. 5, I considered how a time-varying capacity impacts the ability of a mutant with a selective advantage to take over a spatially structured metapopulation of wild-type individuals, where migration between demes on the metapopulation is slow. Using coarse-grained approaches, I first demonstrated that under no environmental variability there are two key regimes of behaviour, with a crossover regime between them. I characterised analytically and using stochastic simulations a regime dominated by deme extinction, one dominated by the competition between the mutants and wild-type cells, and the crossover regime combining local competition and extinction.

In time-varying environments, various qualitatively different dynamical scenarios arise and environmental variability can significantly influence the evolution of the metapopulation. When the rate of switching is neither too slow nor too fast, demes experience bottlenecks and the population is prone to fluctuations or extinction. When the time-varying carrying capacity remains large and bottlenecks are weak, deme extinction is negligible. The dynamics is thus dominated by the competition between wild-type cells and mutants to invade and take over demes, and eventually the population, which I characterised by adapting the coarse-grained description used in the competition-dominated regime of the constant environment. In this approach, I accurately determined the fixation probability and mean fixation time of metapopulations under weak bottlenecks and showed that these quantities can vary non-monotonically with the environmental switching rate, an effect caused by the spatial structure of the population which is not present in well-mixed populations (Wienand et al., 2017, 2018). I found that in the regime of weak bottlenecks, the mutant fixation probability on regular circulation graphs depends on the migration rate, which is in stark contrast with what happens in static environments (Lieberman et al., 2005; Marrec et al., 2021), while the spatial structure has a small but essentially unnoticeable effect. These elements combined therefore demonstrated the importance of realistic models for microbial evolution: if one were to presume that the robust results of Wienand et al. (2017, 2018) and Lieberman et al. (2005) and Marrec et al. (2021) hold jointly, the novel behaviour uncovered here is missed. Furthermore, when the carrying capacity is small under harsh conditions, bottlenecks are strong and there is a dynamical coupling of strain competition in the mild environmental state and deme extinction in the harsh environment. In this case, various scenarios arose, among which I identified a mechanism, expected to hold on any regular graph, driven by environmental variability and fluctuations to efficiently eradicate one strain.

As a hypothetical application, I thus proposed an idealised treatment to remove the mutant, assumed to be unwanted and favoured by selection. I showed that when each deme is subject to strong bottlenecks at intermediate switching rates the mutant can be efficiently removed by demographic fluctuations arising in the harsh environment without exposing the entire population to a risk of rapid extinction. I thus determined the near-optimal conditions on the switching rate and bottleneck strength for this idealised treatment and found that these are qualitatively the same on other graphs. In summary, this analysis sheds further light on the influence of the spatial structure, migration, and fluctuations on

the spread of a mutant strain in time-varying environments. I have identified and characterised various dynamical regimes, displaying a complex dependence on the switching and migration rates and shown that environmental variability and fluctuations can be utilised to achieve desired evolutionary outcomes like the efficient removal of an unwanted mutant. While having made several simplifying assumptions, allowing for analytical progress, many of these can be relaxed without affecting the results or the methodology. The approach holds for arbitrary regular graphs and can be generalised to more complex spatial settings. The model studied therefore has numerous potential applications. For instance, it mirrors the *in vitro* evolution of a mutant across an array of micro-fluidic devices, where cells migrate between "microhabitat patches" either via microchannels or pipette, with bottlenecks implemented via a strict control of the nutrient level in each device (Keymer et al., 2006; Hsu et al., 2019; Totlani et al., 2020).

In summary, this thesis demonstrates the generally non-trivial and often significant impact of environmental variability through a coupling with population-level dynamics on several models of biological interest. We have motivated the importance of EV by its ubiquity in natural populations, and shown that its inclusion in the models considered can significantly alter the evolutionary dynamics of the population. Furthermore, in each of the models I have envisaged a particular evolutionary outcome which is preferred: the removal of resistant cells or unwanted mutants. I have obtained specific conditions on the environmental variability where these evolutionary outcomes are promoted. This research therefore suggests the importance of considering EV in order to capture the dynamics of natural populations, allowing for the uncovering of novel dynamical population behaviours which do not appear if EV is neglected, some of which may be of clinical relevance.

Furthermore, this research naturally leads to several other potentially fruitful avenues of research. Firstly, the behaviour of multi-species (> 2) communities with complex interaction networks subject to EV is of great interest, particularly with reference to biodiversity and coexistence. While their study would require the development of new tools, as much of the work here is focussed on two-species populations, this work paves the way for a complete understanding of such systems and may serve as a baseline for comparison. Additionally, the effect of the EV considered here has primarily been in the carrying capacity of the population. This has allowed for a large amount of analytical progress through the use of tools already developed, but we need not restrict ourselves to this case. This was seen in Ch. 4 where EV impacts the birth rates of species in addition to the effect on carrying capacity. Therefore, modelling EV as a DMN for analytical convenience, but considering various different ways in which this may directly impact the species, would allow for a far broader understanding of the impact of EV on population evolution. This could be applied, for example, to the models of Ch. 3, where we note that a constant replenishment of antimicrobial at constant concentration regardless of environmental state is assumed. An interesting approach for future work therefore may include investigating how these populations evolve when no drug is administered in the mild environmental state, and therefore the harsh environment displays the combined effect of a nutrient

shock and antimicrobial. Furthermore, in all models considered in this thesis we have neglected mutations and further adaptation on the timescale of the dynamics investigated. Developments investigating the effect of EV on adaptive populations, both theoretical and experimental, have been made (Mateu et al., 2021; Raatz & Traulsen, 2023; Izutsu et al., 2024), but generally their dynamics remain poorly understood. This is a particularly relevant problem as it relates to the evolution of antimicrobial tolerance, a key pathway to the evolution of AMR (Levin-Reisman et al., 2017; Lewis & Shan, 2017). Finally, the work of Ch. 5 can be extended to consider asymmetric migration and various non-circulation graphs. While analytically convenient, circulation graphs may not represent the most biologically plausible model of a microbial community, for example in the digestive tract where migration is particularly asymmetric (Labavić et al., 2022). It would be interesting to investigate how asymmetries in migration both in species and direction, together with EV, on general graph structures, can affect the evolutionary dynamics of the population. Moreover, I have proposed these future developments with the relatively simple case of a mutant and wild-type species competing for shared resources in mind. Models with more complex interactions between species may be developed on spatial structures subject to EV, leading to novel behaviours as in Hernández-Navarro, Distefano, et al. (2024). These future frontiers will help to elucidate further the impact of EV on natural populations, with potentially major implications for clinical settings and our understanding of evolutionary dynamics as a whole.

Appendix A

Additional material for Chapter 3

A.1 Derivations for the Moran process

Here, we derive the exact results for the fixation probability and mean fixation time in a constant environment in a Moran process and detail how their approximations are obtained.

A.1.1 Fixation probability

The effective Moran transition rates are $\widetilde{T}_R^+ = T_R^+ T_S^- / N$ and $\widetilde{T}_R^- = T_R^- T_S^+ / N$ (see Ch. 2.2.2), which read

$$\begin{aligned} \widetilde{T}_R^+ (N_R, N) &= \frac{(1-s) \cdot N_R(N-N_R)/K}{1 - a\theta\,[N_{\text{th}} - N_R] + (a\theta\,[N_{\text{th}} - N_R] - s) N_R/N}, \\ \widetilde{T}_R^- (N_R, N) &= \frac{(1 - a\theta\,[N_{\text{th}} - N_R]) \cdot (N-N_R) N_R/K}{1 - a\theta\,[N_{\text{th}} - N_R] + (a\theta\,[N_{\text{th}} - N_R] - s) N_R/N}. \end{aligned} \tag{A.1}$$

In the above transition rates, the constant carrying capacity K and total population size coincide, as is required in the Moran process, and we therefore set $N = K$ in the transition rates (A.1). The expression for $\gamma\,(N_R, N)$ under these dynamics is then given by

$$\gamma\,(N_R) = \frac{1 - aH}{1 - s},$$

which depends on the abundance (relative or absolute here are equivalent as this environment is constant) of R relative to the cooperation threshold. Substituting γ in the general exact solution of Eq. (2.20) we get

$$\phi(N_R^0, N) = \begin{cases} 0 & \text{if } N_R^0 = 0, \\ \frac{1 + \sum_{k=1}^{N_R^0 - 1} \left(\frac{1-a}{1-s}\right)^k}{1 + \sum_{k=1}^{N_{\text{th}}-1} \left(\frac{1-a}{1-s}\right)^k + \left(\frac{1-a}{1-s}\right)^{N_{\text{th}}-1} \sum_{k=1}^{N-N_{\text{th}}} \left(\frac{1}{1-s}\right)^k} & \text{if } 1 \le N_R^0 \le N_{\text{th}}, \\ \frac{1 + \sum_{k=1}^{N_{\text{th}}-1} \left(\frac{1-a}{1-s}\right)^k + \left(\frac{1-a}{1-s}\right)^{N_{\text{th}}-1} \sum_{k=1}^{N_R^0 - N_{\text{th}}} \left(\frac{1}{1-s}\right)^k}{1 + \sum_{k=1}^{N_{\text{th}}-1} \left(\frac{1-a}{1-s}\right)^k + \left(\frac{1-a}{1-s}\right)^{N_{\text{th}}-1} \sum_{k=1}^{N-N_{\text{th}}} \left(\frac{1}{1-s}\right)^k} & \text{if } N_{\text{th}} < N_R^0 \le N. \end{cases}$$

Making use of the formula for the sum of a finite geometric progression, this becomes

$$\phi(N_R^0, N) = \begin{cases} \frac{1-\left(\frac{1-a}{1-s}\right)^{N_R^0}}{1-\left(\frac{1-a}{1-s}\right)^{N_{\text{th}}}+\frac{a-s}{s(1-a)}\left(\frac{1-a}{1-s}\right)^{N_{\text{th}}}\left[\left(\frac{1}{1-s}\right)^{N-N_{\text{th}}}-1\right]} & 0 \leq N_R^0 \leq N_{\text{th}} \\ \frac{1-\left(\frac{1-a}{1-s}\right)^{N_{\text{th}}}+\frac{a-s}{s(1-a)}\left(\frac{1-a}{1-s}\right)^{N_{\text{th}}}\left[\left(\frac{1}{1-s}\right)^{N_R^0-N_{\text{th}}}-1\right]}{1-\left(\frac{1-a}{1-s}\right)^{N_{\text{th}}}+\frac{a-s}{s(1-a)}\left(\frac{1-a}{1-s}\right)^{N_{\text{th}}}\left[\left(\frac{1}{1-s}\right)^{N-N_{\text{th}}}-1\right]} & N_{\text{th}} < N_R^0 \leq 1. \end{cases}$$

Finally, the fixation probability of R can be written as

$$\phi\left(N_R^0, N, N_{\text{th}}, s, a\right) = \frac{1-\left(\frac{1-a}{1-s}\right)^{\frac{\left(N_R^0+N_{\text{th}}\right)-\left|N_R^0-N_{\text{th}}\right|}{2}}+\frac{a-s}{s(1-a)}\left(\frac{1-a}{1-s}\right)^{N_{\text{th}}}\left[\left(\frac{1}{1-s}\right)^{\frac{\left(N_R^0-N_{\text{th}}\right)+\left|N_R^0-N_{\text{th}}\right|}{2}}-1\right]}{1-\left(\frac{1-a}{1-s}\right)^{N_{\text{th}}}+\frac{a-s}{s(1-a)}\left(\frac{1-a}{1-s}\right)^{N_{\text{th}}}\left[\left(\frac{1}{1-s}\right)^{N-N_{\text{th}}}-1\right]}. \tag{A.2}$$

By setting $N_R^0 = N_{\text{th}}$, $N = K$, and assuming $(1-a)^{N_{\text{th}}} \ll (1-s)^{N_{\text{th}}}$ and $(1-s)^K \ll (1-s)^{N_{\text{th}}}$ in the above equation, we retrieve our approximate result.

A.1.2 Mean fixation time

The exact expression for the mean fixation time given the above Moran rates is incredibly complex and we do not consider it explicitly here. Instead, we make use of the fact that for the MFT at fixed total population N, we have $\tau_N\left(N_R^0|N_{\text{th}}, s, a, N\right) \approx \tau_N\left(N_R^0 = N_{\text{th}}|N_{\text{th}}, s, a, N\right)$ as in Ch. 3.2, and so we focus on the case $N_R^0 = N_{\text{th}} \equiv Nx_{\text{th}}$ to simplify Eq. (2.19). Note that, in this case, the last double summation has powers of $\gamma = (1-a)/(1-s) < 1$, while the first double summation also has additional summands with high powers of $\gamma = 1/(1-s) > 1$. Hence, the last double summation is negligible with respect to the first one. Furthermore, if we split the inner summation of the first double summation at $n = N_{\text{th}}$ we obtain

$$\tau_N\left(N_R^0\right) \approx \tau_N\left(N_{\text{th}}\right) \approx \phi_N\left(N_{\text{th}}\right) \sum_{k=N_{\text{th}}}^{N-1} \left(\sum_{n=1}^{N_{\text{th}}-1} \frac{\prod_{m=n+1}^{k} \gamma\left(m/N\right)}{\widetilde{T}_R^+\left(n/N\right)} + \sum_{n=N_{\text{th}}}^{k} \frac{\prod_{m=n+1}^{k} \gamma\left(m/N\right)}{\widetilde{T}_R^+\left(n/N\right)} \right).$$

According to the definition of the rates in Ch. 3.2, each summand reads

$$\frac{\prod_{m=n+1}^{k}\gamma\left(m/N\right)}{\widetilde{T}_{R}^{+}\left(n/N\right)}=\frac{(1-a)^{\left[\frac{\left(N_{\mathrm{th}}-1+k\right)-\left|N_{\mathrm{th}}-1-k\right|}{2}-\frac{\left(N_{\mathrm{th}}-1+n\right)-\left|N_{\mathrm{th}}-1-n\right|}{2}\right]}}{(1-s)^{k-n}}\times\left(\frac{\frac{1-s}{N-n}+\frac{1-a\cdot\theta\left(N_{\mathrm{th}}-n\right)}{n}}{1-s}\right),$$

and thus,

$$\tau_{N}(N_{\mathrm{th}})\approx\frac{\phi_{N}(N_{\mathrm{th}})}{1-s}\sum_{k=N_{\mathrm{th}}}^{N-1}\left[\left(\frac{1}{1-s}\right)^{k}\left((1-a)^{N_{\mathrm{th}}-1}\sum_{n=1}^{N_{\mathrm{th}}-1}\left(\frac{1-s}{1-a}\right)^{n}\times\left(\frac{1-s}{N-n}+\frac{1-a}{n}\right)+\sum_{n=N_{\mathrm{th}}}^{k}(1-s)^{n}\left(\frac{1-s}{N-n}+\frac{1}{n}\right)\right)\right]$$

We observe that the first summation over n in the previous equation is independent of k, and therefore we can take it out as a common factor. Regarding the second summation over n, note that only those sums with the highest upper index k are significant because they are weighted by the prefactor $(1-s)^{-k}\gg 1$; furthermore, note that the summands' magnitude rapidly decreases with n. By combining these two features, we note that we can substitute the upper index of the summation k by $N-1$ without incurring a significant error, making the summation independent of k, and taking it out as a common factor as well. Hence, we can now compute the remaining summation over k as a geometric progression. The above considerations yield

$$\tau_{N}(N_{\mathrm{th}})\approx\phi_{N}(N_{\mathrm{th}})\frac{\left(\frac{1}{1-s}\right)^{N-N_{\mathrm{th}}}-1}{s(1-s)^{N_{\mathrm{th}}}}\left((1-a)^{N_{\mathrm{th}}-1}\sum_{n=1}^{N_{\mathrm{th}}-1}\left(\frac{1-s}{1-a}\right)^{n}\times\left[\frac{1-s}{N-n}+\frac{1-a}{n}\right]+\sum_{n=N_{\mathrm{th}}}^{N-1}(1-s)^{n}\left[\frac{1-s}{N-n}+\frac{1}{n}\right]\right)$$

In the first summation over n, each summand is weighted by an exponentially increasing factor $\left(\frac{1-s}{1-a}\right)^{n}\gg 1$. Hence, only the last terms with the highest n are significant. For these summands, we have $n\lesssim N_{\mathrm{th}}$, and the fractions $\frac{1-s}{N-n}$ and $\frac{1-a}{n}$ evolve very slowly with n compared to the exponential factor. Therefore, we can approximate n in the previous fractions by N_{th}, and take them as a common factor out of the summation without introducing significant error. As for the second summation, we can also substitute n by N_{th} in the fractions and take them out as a common factor. In this case, the rationale is that the summands with the lowest n (which corresponds to $n\gtrsim N_{\mathrm{th}}$) are the only significant terms due to the factor $(1-s)^{n}\ll 1$. Finally, we can compute the two remaining geometric series over n, and simplify the expression to that of Eq. (3.6).

Appendix B

Additional material for Chapter 4

B.1 Fitness-switching coexistence: amplitude of variations and timescale

The selection strength s does not only shape the dynamics of the composition (see Eq. (4.4)) but it also determines the amplitude of the T-EV fluctuations, i.e. its variance, which is linked to stronger coexistence in the fast-switching regime; see Ch. 4.2. To show this, we first consider the normalised fitness of the resistant subpopulation

$$\frac{f_R}{\overline{f}} = \frac{1}{x + (1-x)\exp(\xi_T s)}.$$

Since we here focus on how s may shape coexistence through the toxin level fluctuation size, and coexistence dominates in the fast toxin-switching regime, we assume $\nu_T \gg 1$. As discussed in Ch. 4.2.1, in the fast-switching regime, the per capita growth rate (normalised fitness) of strain R averaged over the stationary distribution of ξ_T reads

$$\left\langle \frac{f_R}{\overline{f}} \right\rangle = \frac{1-\delta_T}{2} \frac{1}{x + (1-x)\exp(-s)} + \frac{1+\delta_T}{2} \frac{1}{x + (1-x)\exp(s)}.$$

To derive its variance, we also have to compute the average of its square as

$$\left\langle \left(\frac{f_R}{\overline{f}} \right)^2 \right\rangle = \frac{1-\delta_T}{2} \frac{1}{(x + (1-x)\exp(-s))^2} + \frac{1+\delta_T}{2} \frac{1}{(x + (1-x)\exp(s))^2}.$$

Combining both, we obtain the variance of the normalised resistant fitness due to the environmental fluctuations in the toxin level

$$\begin{aligned} \mathrm{Var}\left(\frac{f_R}{\overline{f}} \right) &= \left\langle \left(\frac{f_R}{\overline{f}} \right)^2 \right\rangle - \left\langle \frac{f_R}{\overline{f}} \right\rangle^2 \\ &= \frac{(1-\delta_T^2)}{4} \left(\frac{(\exp(2s)-1)(1-x)}{(x + (1-x)\exp(s))(1 + x(\exp(s)-1))} \right)^2. \end{aligned}$$

A similar analysis for the sensitive strain, which has a normalised fitness $\exp(\xi_T s)$ times that of the resistant strain, provides

$$\mathrm{Var}\left(\frac{f_S}{\overline{f}}\right) = \frac{(1-\delta_T^2)}{4}\left(\frac{(\exp(2s)-1)x}{(x+(1-x)\exp(s))(1+x(\exp(s)-1))}\right)^2.$$

In both cases, we conclude that the variance (arising from the T-EV) indeed increases with the selection strength s. Therefore, s does shape the strength of coexistence.

Note that the amplitude of the fluctuations of the carrying capacity K-EV (at no bias $\delta_K = 0$, for simplicity) increases with γ. In conclusion, and as discussed in Ch. 4.3.2 and Fig. 4.5, the EV can either promote coexistence (T-EV) or jeopardise it (K-EV), and both parameters s and γ determine long-lived coexistence.

To discuss the coexistence timescale, we consider the small s regime by expanding the numerator and denominator of the right-hand-side of Eq. (4.6) to order $\mathcal{O}(s^2)$, which yields

$$\begin{aligned}\dot{x} &\approx \frac{x(1-x)}{2}\left[\frac{(1+\delta_T)(1-(1+s+s^2/2))}{x+(1-x)(1+s+s^2/2)} + \frac{(1-\delta_T)(1-(1-s+s^2/2))}{x+(1-x)(1-s+s^2/2)}\right] \\ &\approx -s^2 x(1-x)\left[x-\left(\frac{1}{2}-\frac{\delta_T}{s}\right)\right] = -s^2 x(1-x)\left[x-x^*\right],\end{aligned} \tag{B.1}$$

where $x^* = \frac{1}{2} - \frac{\delta_T}{s}$ is the coexistence equilibrium under $s \ll 1$. The equilibrium x^* is physical (and stable) only when $-\frac{s}{2} < \delta_T < \frac{s}{2}$; i.e. only in the special case of almost symmetric switching ($\delta_T = \mathcal{O}(s)$ or smaller). From Eq. (B.1), the coexistence equilibrium is approached slowly, with a relaxation time on the order of $\sim 1/s^2$; thus, taking into account demographic noise, the expected fixation time is $\tau \sim e^{\langle N\rangle s^2}$ when $\langle N\rangle s^2 \gg 1$ (Assaf & Mobilia, 2010; Mobilia & Assaf, 2010; Assaf & Meerson, 2017).

B.2 Quasi-stationary probability density of composition under coexistence

The joint stationary probability density function of the x-PDMP is labelled by $\rho_\pm(x) \equiv \rho(x, \xi_T = \pm)$, and satisfies (Horsthemke & Lefever, 1984; Bena, 2006; Ridolfi et al., 2011)

$$\partial_t \rho_\pm = -\partial_x(\dot{x}_\pm \rho_\pm) - \nu_\pm \rho_\pm + \nu_\mp \rho_\mp, \tag{B.2}$$

where $\dot{x}_\pm \equiv x(1-x)(1-e^{\pm s})/[x+(1-x)e^{\pm s}]$, and the marginal stationary probability density function of the x-PDMP defined by Eq. (4.4) is $\rho(x) \equiv \rho_+(x) + \rho_-(x)$.

Following Horsthemke and Lefever (1984) and Ridolfi et al. (2011), from Eq. (B.2), we can define $J_\pm = \dot{x}_\pm \rho_\pm + \int_0^x (\nu_\pm \rho_\pm - \nu_\mp \rho_\mp)\, \mathrm{d}x'$ as the probability flux of the system, and then rewrite Eq. (B.2) as $\partial_t \rho_\pm = -\partial_x J_\pm$. Note that by definition the x-PDMP ignores DF, hence $x = 0, 1$ states cannot be reached. We thus set probability flux at the boundaries to zero as natural boundary conditions (BCs) (Gardiner, 2009). Since we want to derive

the stationary joint probability density function $\rho\,(t \to \infty)$ under zero-current BCs, we use $\rho = \rho_+ + \rho_-$ and take $\partial_t \rho = -\partial_x (J_+ + J_-) = 0$. In this case, we obtain $J_+ + J_- = 0$, where the flux boundary conditions set the integration constant to 0. From this relation we can find that $\rho_\pm = \frac{-\dot{x}_\mp \rho_\mp}{\dot{x}_\pm}$. It is useful to introduce the auxiliary variable $q \equiv \rho_+ - \rho_-$, and write $J_+ + J_- = 0$ as $\dot{x}_+ \frac{\rho+q}{2} + \dot{x}_- \frac{\rho-q}{2} = 0$. After rearranging for q we can substitute this into our expression for $\rho_\pm$ to find $\rho_\pm = \frac{\rho \pm q}{2} = \frac{\pm \dot{x}_\mp}{\dot{x}_- - \dot{x}_+} \rho$. The equation for the PDMP density of the resistant fraction x at quasi-stationary coexistence then reads

$$\partial_x \left(\frac{\dot{x}_- \dot{x}_+}{\dot{x}_- - \dot{x}_+} \rho \right) + \frac{\dot{x}_- \dot{x}_+}{\dot{x}_- - \dot{x}_+} \rho \left(\frac{\nu_+}{\dot{x}_+} + \frac{\nu_-}{\dot{x}_-} \right) = 0.$$

Multiplying by -1, rearranging, and integrating, leads to

$$\ln \left(\frac{\rho}{\frac{1}{-\dot{x}_+} + \frac{1}{\dot{x}_-}} \right) - \ln (C) = \int^x \left(\frac{\nu_+}{-\dot{x}_+} - \frac{\nu_-}{\dot{x}_-} \right) \, \mathrm{d}x', \tag{B.3}$$

where C is an integration constant, and

$$\frac{1}{-\dot{x}_+} = \frac{\frac{e^s}{x} + \frac{1}{1-x}}{e^s - 1} \quad \text{and} \quad \frac{1}{\dot{x}_-} = \frac{\frac{1}{x} + \frac{e^s}{1-x}}{e^s - 1},$$

see Eq. (4.4) with $\xi_T = \pm 1$. Eq. (B.3) yields

$$\ln \left(\frac{\rho}{C \frac{e^s+1}{e^s-1} \frac{1}{x(1-x)}} \right) = \frac{\nu_+ \left(e^s \ln (x) - \ln (1-x) \right) - \nu_- \left(\ln (x) - e^s \ln (1-x) \right)}{e^s - 1},$$

and the normalised x-PDMP stationary probability density function then becomes

$$\rho = \frac{\Gamma (\lambda + \mu)}{\Gamma (\lambda) \Gamma (\mu)} x^{\lambda - 1} (1-x)^{\mu - 1}, \tag{B.4}$$

which corresponds to the well-known *beta distribution* with

$$\lambda \equiv \frac{\nu_+ e^s - \nu_-}{e^s - 1} \quad \text{and} \quad \mu \equiv \frac{\nu_- e^s - \nu_+}{e^s - 1}.$$

Under the change of variables $\nu_\pm = \nu_T \, (1 \mp \delta_T)$, and after some algebra, the exponents read

$$\lambda = \nu_T \left(1 - \delta_T \coth \left(\frac{s}{2} \right) \right) \quad \text{and} \quad \mu = \nu_T \left(1 + \delta_T \coth \left(\frac{s}{2} \right) \right),$$

giving the probability density Eq. (B.4) in terms of the environmental parameters and the selection bias. Fig. B.1 shows the predictions of Eq. (B.4) and its excellent match with simulation data.

As mentioned in Ch. 4.4.1, a complementary characterisation of the coexistence phase is provided by the modal value, denoted by $\hat{x}$, of the probability density function of the x-PDMP, derived in Eq. (B.4). As the x-PDMP density is a beta distribution, its modal value is

$$\hat{x} = \frac{\lambda - 1}{\lambda + \mu - 2} = \frac{1}{2} \left(1 - \frac{\nu_T}{\nu_T - 1} \delta_T \coth \left(\frac{s}{2} \right) \right). \tag{B.5}$$

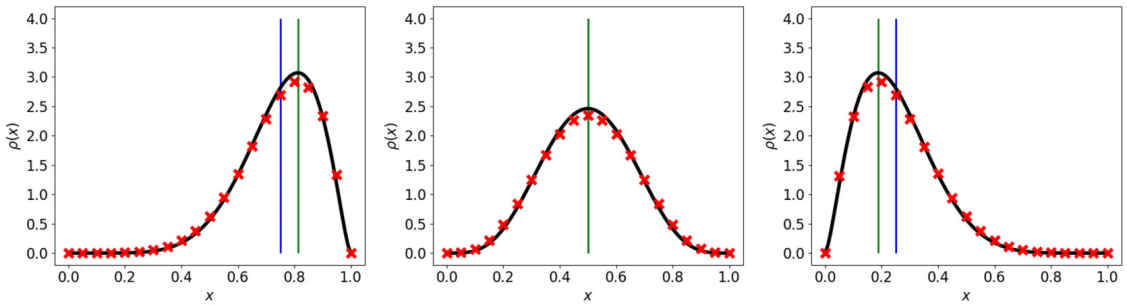

Figure B.1: Predictions of x-PDMP stationary density $\rho(x)$ against x for $\delta_T \in \{-0.5, 0.0, 0.5\}$ from left to right. Theoretical predictions (solid lines) from Eq. (B.4) are in excellent agreement with simulation results ($\times$). Blue vertical line shows predicted mean x^* from Eq. (4.7) and green vertical line shows predicted mode $\hat{x}$ from Eq. (B.5). Parameters used are $s = 10$, $\nu_T = 5$, and fixed $K_0 = 100$. Simulation results have been averaged over 10^3 realisations.

Note that the x-PDMP distribution is unimodal only for $\lambda, \mu > 1$, i.e. $\nu_T(1 - |\delta_T|) > 1$. However, we use $\hat{x}$ only as an analytical proxy for the expected value of x in the coexistence and fixation-coexistence crossover regions (coexistence probability $0 < \eta \leq 1$), which coincide with the unimodal regime. For pure coexistence $\eta \to 1$, observed at $\nu_T \to \infty$ and $\delta_T \neq \pm 1$, the modal $\hat{x}$ value reduces to the mean field expression x^* of Eq. (4.7). As shown in Fig. B.2, the modal value $\hat{x}$ approximates the unconditional expected R fraction $\langle x \rangle$ (red crosses) in the regime $\nu_T > 1/(1 - |\delta_T|)$, where there is a non-zero coexistence probability ($0 < \eta < 1$). This therefore captures more accurately the value of x actually observed when coexistence occurs for $0 < \eta < 1$, where the distribution becomes increasingly biased towards $x = 0$ or $x = 1$ for $\delta_T \neq 0$ as ν_T decreases, as can be seen by consideration of Eq. (B.4). This is ignored in the mean of the coexistence state x^*, which is independent of ν_T.

In the fixation regime where $\nu_T < 1/(1 - |\delta_T|)$, we find a higher (lower) fixation probability for the resistant strain than for the sensitive one when δ_T is negative (positive), with the fraction of R (hence ϕ) approaching one (Fig. B.2, left) or zero (Fig. B.2, right) when $\nu_T \approx 1$. The rationale is that, for very small ν_T, the strain that fixates is set by the initial toxin state, as we expect no toxin switches before fixation has occurred; the probability to start at $\xi_T = \pm 1$ is $(1 \pm \delta_T)/2$. When ν_T is increased further the system experiences both environmental states, and the the toxin bias δ_T sets which strain is more likely to fixate. For larger $\nu_T > 1/(1 - |\delta_T|)$, coexistence takes over as the result of the self-averaging of the transition rates over the stationary ξ_T distribution.

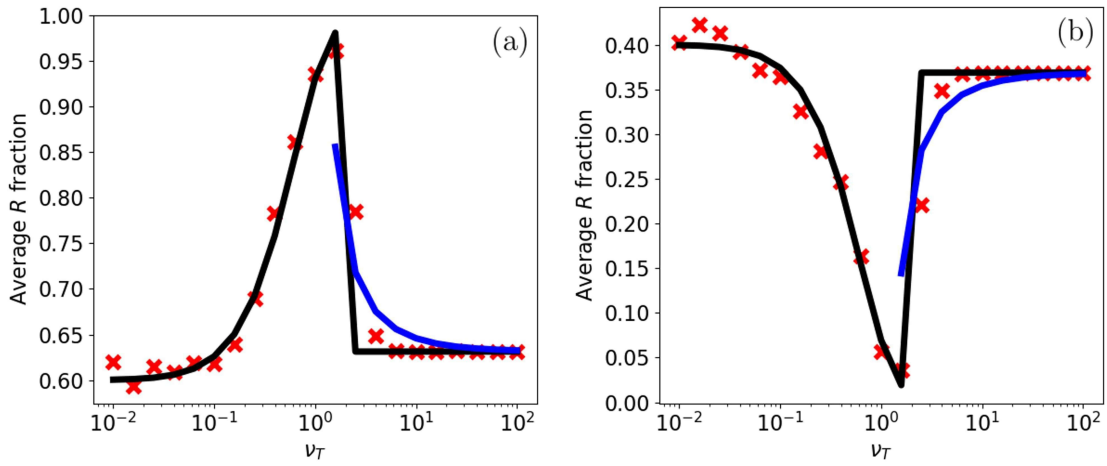

Figure B.2: Average R fraction unconditional on coexistence against ν_T for $\delta_T \in \{-0.2, 0.2\}$ from left to right. Black line $\langle x \rangle$ from Eq. (4.18), blue line from $\hat{x}$ of Eq. (B.5), and simulation results ($\times$). Simulation results obtained from a "horizontal cut" at fixed δ_T of Fig. 4.6, where we now count the overall fraction of R (no longer conditioned to coexistence). There is a non-trivial dependence on ν_T, matching that which is seen in Fig. 4.7(b) where we find peaks of fixation / extinction. Other parameters are: $K_0 = 500$, $\gamma = 0.5$, $\nu_K = 10$, $\delta_K = 0.0$, and $s = 2$.

B.3 Coexistence under time-varying carrying capacity and final fixation

In Fig. 4.4(a-c) we find that the region of coexistence grows when ν_K is increased. This behaviour is expected for an effective population size that would increase with ν_K, as suggested by the MFT that increase with the population size (Fig. 4.2(c)). However, this seems at odds the average population size $\langle N \rangle$ decreasing with ν_K as shown by Fig. 2.2(e). A more suitable characterisation of the influence of ν_K on coexistence phase is thus provided by the modal value $\hat{N}$ of the N-PDMP QPSD, given by Eq. (4.17). Indeed, Fig. B.3 illustrates that $\hat{N}$, unlike $\langle N \rangle$, increases with ν_K for $\delta_K < \gamma$ in line with the results reported in Fig. 4.4(a-c).

For a complete characterisation of the coexistence regime we now briefly discuss the final state that is attained after after a long transient ensuring that a large fluctuation drives the system from the long-lived metastable coexistence to one of the two absorbing states where a single strain takes over the entire population (Assaf & Mobilia, 2010; Mobilia & Assaf, 2010). Fig. B.4 illustrates the full fixation outcome diagram (under no K-EV for simplicity), even in the phase of long-lived coexistence. Fixation in this regime is determined by the sign of δ_T, with a sharp transition at $\delta_T = 0$. This is because fixation occurs most likely in the absorbing state closest to the coexistence equilibrium x^* given by Eq. (4.7): here, the toxin bias eventually imposes the fixation of S ($\delta_T > 0$) or R ($\delta_T < 0$).

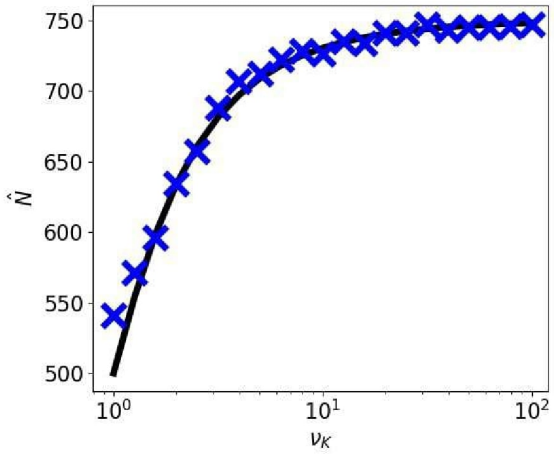

Figure B.3: Modal value $\hat{N}$ of the probability density function Eq. (2.27) against ν_K using Eq. (4.17) (solid line) and points from simulations averaged over 10^2 realisations ($\times$) obtained by tracking the modal value of the QPSD. Parameters used are $K_0 = 1000$, $\gamma = 0.5$, $\delta_K = 0.0$, $\nu_T = 10.0$, $\delta_T = 0.0$. As discussed in Ch. 4.3.2, we find that for $\delta_K < \gamma$ there is an increase of $\hat{N}$ with ν_K up to $\mathcal{K} = 750$ (fast-switching limit), thus allowing for a greater range of δ_T values that give coexistence.

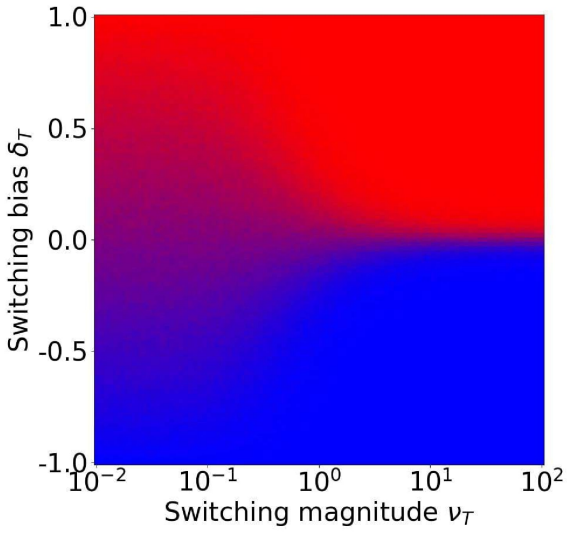

Figure B.4: Fixation in coexistence region. The system fixates within the coexistence region at time $t \approx 400 = 8\langle N \rangle$ in the most extreme case. The corresponding fixation-coexistence diagram is given by Fig. 4.3(b). Parameters used: $K_0 = 50$, $\gamma = 0.0$ (no K-EV), and $s = 1.0$. Colour coding is the same as in Fig. 4.3.

B.4 Fully correlated and anti-correlated environmental variability

In the case of fully correlated/anti-correlated T-EV and K-EV, environmental variability is no longer twofold since we have $\xi \equiv \xi_T$ and $\xi_K = \xi$ (fully correlated EV) or $\xi_K = -\xi$ (fully anti-correlated EV). The switching carrying capacity can thus be written as

$$K(t) = K_0[1 + \widetilde{\gamma}\xi(t)],$$

where $\widetilde{\gamma} = \gamma$ in the fully correlated case, and $\widetilde{\gamma} = -\gamma$ when T-EV and K-EV are fully anti-correlated. For instance, this implies that, in the correlated case, the environmental state $\xi = +1$ corresponds to $f_s = e^s > 1$ and $K = K_+$ (low toxin level, abundant resources), while $\xi = -1$ is associated with $f_S = e^{-s} < 1$ and $K = K_-$ (high toxin level, scarce resources). As said, under fully correlated/anti-correlated T/K-EV, environmental variability is no longer twofold: ξ simultaneously drives the level of toxin and the abundance of resources. Hence, we can characterise the effect of fully correlated/anti-correlated EV in terms of $\nu \equiv \nu_T$ and $\delta \equiv \delta_T$, and the fully anti-correlated case is related to completely correlated EV via $\widetilde{\gamma} \to -\widetilde{\gamma}$. An example of fully-anticorrelated EV modelled in terms of a dichotomous process driving the level of toxins and resources in the context of competitive exclusion is considered in Shibasaki et al. (2021).

Fig. B.5 shows the comparison between the uncorrelated T-EV and K-EV studied in the main text (top row), and the fully correlated (middle row) and fully anti-correlated (bottom row) cases reported here, all under $K_0 = 1000$ and $\gamma = 0.9$, and for different selection strengths $s \in \{0.2, 2, 20\}$ (left to right columns). For the uncorrelated case, the parameters of K-EV are independent from those of T-EV parameters, and are here chosen to be $(\nu_K, \delta_K) = (10^{-4}, 0)$, i.e. unbiased slow-switching K-EV (similar to the example of Fig. 4.4(a)).

Since the fully correlated and anti-correlated cases (middle and bottom rows) are mirror images through the horizontal axis (symmetric with respect to $\delta_T = 0$) and under a red-blue colour change, we focus on the correlated case only (middle row). For this case, $\widetilde{\gamma} = \gamma = 0.9$, with $\xi_K = \xi_T \equiv \xi$, $\nu_K = \nu_T$, and $\delta_K = \delta_T$. In the fully correlated case, we observe that both the blue (resistant fixation) and the bright green (coexistence) regions shift upwards (to higher toxin level biases δ_T) as the selection strength increases (from left to right column). We can understand this phenomenon in light of the T-correlated K-EV fluctuations. This is, since $\delta_K = \delta_T$, a lower value of δ_T in the diagrams implies longer cumulative periods in the harsh toxin level, but also in the low carrying capacity environment. Therefore, lower δ_T provides the selective advantage to resistant strain at the same time that it shrinks the total population. DF being stronger in smaller populations, correlated T-EV and K-EV thus provide higher R fixation probability (blue region shifted up), as well as lower coexistence probability (green region shifted up). Moreover, since total population increases with the bias towards positive carrying (here $\delta_K = \delta_T$) (see Ch. 4.3.1) the MFT thus increases with δ_T (see Fig. 4.2(c)), and the coexistence probability

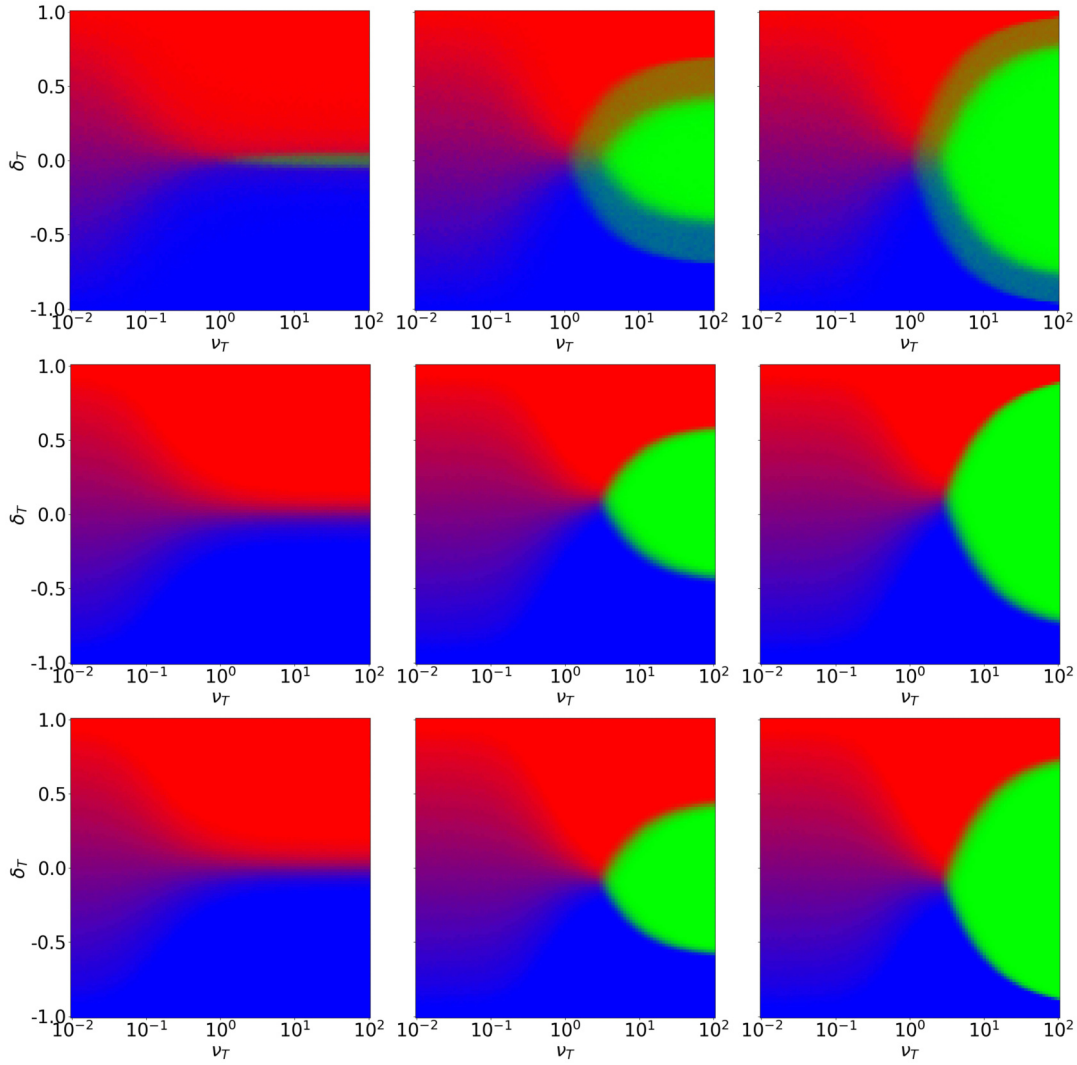

Figure B.5: Top to bottom: uncorrelated, fully correlated and fully anticorrelated case heatmap plots from 10^3 realisations with $\gamma = 0.9$ (correlated: $\widetilde{\gamma} = 0.9$, anticorrelated: $\widetilde{\gamma} = -0.9$). Left to right we have $s \in \{0.2, 2, 20\}$ and use $K_0 = 1000$. In the uncorrelated case we have $\nu_K = 0.0001$ and $\delta_K = 0.0$. Considering the correlated case, in the coexistence region, for $\delta \to +1$ and fast-switching $\nu \gtrsim 1$ the effective carrying capacity increases. Therefore, we see the coexistence region extended further towards $\delta = 1$. For $\delta \to -1$ and $\nu \gtrsim 1$ we find the converse where the effective carrying capacity decreases and thus the coexistence region shrinks away from $\delta = -1$. A similar logic applies to the anticorrelated case; see text. Colour coding is the same as in Fig. 4.3.

thus shifts upwards. The magnitude of the upwards shift in the correlated case, is small but increases with selection strength s that increases the amplitude of the T-EV fluctuations.

In summary, we obtain the same qualitative results for fully correlated/anti-correlated T/K-EV as when $\xi_{T/K}$ are independent (uncorrelated environmental noise, twofold EV), with some minor quantitative differences, as shown in Fig. B.5 and discussed above. We conclude that the similar behaviour observed for uncorrelated and (anti-)correlated T/K-EV indicates that our findings are robust against the detailed model specifications: the results are expected to be valid for the general case of twofold environmental variability where T/K-EV are neither completely independent nor fully correlated/anti-correlated.

Appendix C

Additional material for Chapter 5

C.1 Further details on the model

In this section, we provide further details on the model by discussing the master equation encoding its individual-based dynamics, and give further details of the size distribution of a single deme under the effect of migration.

C.1.1 Master equation

As discussed in Ch. 5.1, the individual-based model is a continuous-time multivariate Markov process defined by the reaction and transition rates Eq. (5.1) and (5.2). The intra and inter-deme dynamics is encoded in a master equation for the probability $P(\{n_W, n_M\}, \xi, t)$ that at time t the metapopulation is in the environmental state ξ and configuration $\{n_W, n_M\} \equiv (\dots, n_W(x), n_M(x), \dots)$, where $n_{W/M}(x)$ denotes the number of cells of type W/M in deme $x = 1, \dots, \Omega$. The master equation (ME) for the metapopulation dynamics subject to environmental switching on a regular graph G of degree (or number of nearest neighbours) q_G reads (van Kampen, 1992; Gardiner, 2009)

$$\begin{aligned}\frac{\partial P(\{n_W, n_M\}, \xi, t)}{\partial t} = &\sum_{x=1}^{\Omega} \sum_{\alpha} \Big\{ \left(\mathbb{E}_\alpha^-(x) - 1\right) T_\alpha^-(x) P(\{n_W, n_M\}, \xi, t) \\ &+ \left(\mathbb{E}_\alpha^+(x) - 1\right) T_\alpha^+(x) P(\{n_W, n_M\}, \xi, t) \\ &+ \frac{1}{2} \sum_{y \text{ n.n. } x} \Big[\left(\mathbb{E}_\alpha^+(y)\mathbb{E}_\alpha^-(x) - 1\right) T_\alpha^{m,\mathrm{G}}(x) P(\{n_W, n_M\}, \xi, t) \\ &+ \left(\mathbb{E}_\alpha^+(x)\mathbb{E}_\alpha^-(y) - 1\right) T_\alpha^{m,\mathrm{G}}(y) P(\{n_W, n_M\}, \xi, t) \Big] \Big\} \\ &+ \nu \left[P(\{n_W, n_M\}, -\xi, t) - P(\{n_W, n_M\}, \xi, t) \right],\end{aligned} \tag{C.1}$$

where y n.n. x denotes the sum over the q_G neighbours y of the deme x and $P(\dots) = 0$ for any of $n_M(x) < 0$ and $n_W(x) < 0$. The shift operators $\mathbb{E}_\alpha^\pm(x)$ act on a general function $f(\dots, n_W(x) \pm 1, n_M(x) \dots, \xi, t)$ by raising or decreasing by one the number of cells of type α in deme x. For example, $\mathbb{E}_W^\pm(x) f(\dots, n_W(x), n_M(x) \dots, \xi, t) = f(\dots, n_W(x) \pm$

$1, n_M(x)\ldots,\xi,t)$ and $\mathbb{E}_M^{\pm}(x)f(\ldots,n_W(x),n_M(x)\ldots,\xi,t) = f(\ldots,n_W(x),n_M(x)\pm 1\ldots,\xi,t)$. The first and second lines on the right-hand-side of Eq. (C.1) encodes the intra-deme birth-death dynamics, the third and fourth lines represent the inter-deme dynamics via inward and outward migration, and the last line accounts for symmetric random environmental switching. Here, the ME has specifically been formulated in the presence of environmental switching, but its static-environment counterpart is readily obtained from C.1 by setting $\nu = 0$ and replacing $K(t)$ by a constant carrying capacity K. This yields the ME for $P(\{n_W, n_M\}, t)$ that is the probability to find the metapopulation in a given state $\{n_W, n_M\}$ at time t (with no environmental dependence). Moreover, by setting $\Omega = 1$ and $m = 0$ in Eq. (C.1), the second and third lines on the right-hand side cancel, we obtain the ME encoding the intra-deme dynamics of a single isolated deme (Wienand et al., 2017, 2018).

While the ME of Eq. (C.1) holds for any regular graphs G, in our examples we consider specifically the regular circulation graphs $\mathrm{G} = \{\mathrm{clique}, \mathrm{cycle}, \mathrm{grid}\}$. The space-dependent individual-based dynamics encoded in the ME has been simulated using the Monte Carlo method described in Ch. D.2. It is worth noting that demographic fluctuations eventually lead to the extinction of the entire metapopulation, in all regimes. However, this phenomenon occurs after a time growing dramatically with the system size as seen in Ch. 5.2, and it can generally not be observed in sufficiently large metapopulations for $\psi \gg 1$, see Fig. 5.5(e) (Lande et al., 1998).

C.1.2 Eco-evolutionary dynamics of a single deme with migration

In Ch. 2.3.2, we saw that $p_\xi(\nu, n)$ and $p(\nu, n)$ give a PDMP description of the quasi-stationary distribution of the size of an isolated deme ($m = 0$) and capture the behaviour qualitatively well. However, we have not yet asserted whether or not this remains the case for a single deme under migration. In fact, the n-PDMP stationary densities given by Eqs. (2.26) and (2.27) are still a valid approximations of the long-time size distribution of n in the presence of migration as considered here. As shown in Fig. C.1, the influence of migration on the distribution of the deme size is essentially unnoticeable, and its main features are therefore still well captured by Eq. (2.26) and Eq. (2.27).

Intuitively, this can be understood by noticing that the spatial structures considered here are circulation graphs, yielding the same inward and outward migration flow at each deme, and each deme has the same carrying capacity. As a consequence, the average number of cells per deme is expected to be independent of migration. The latter remains well captured by $p_\pm(\nu, n)$ and $p(\nu, n)$ on all spatial structures considered here, as seen in Fig. C.1.

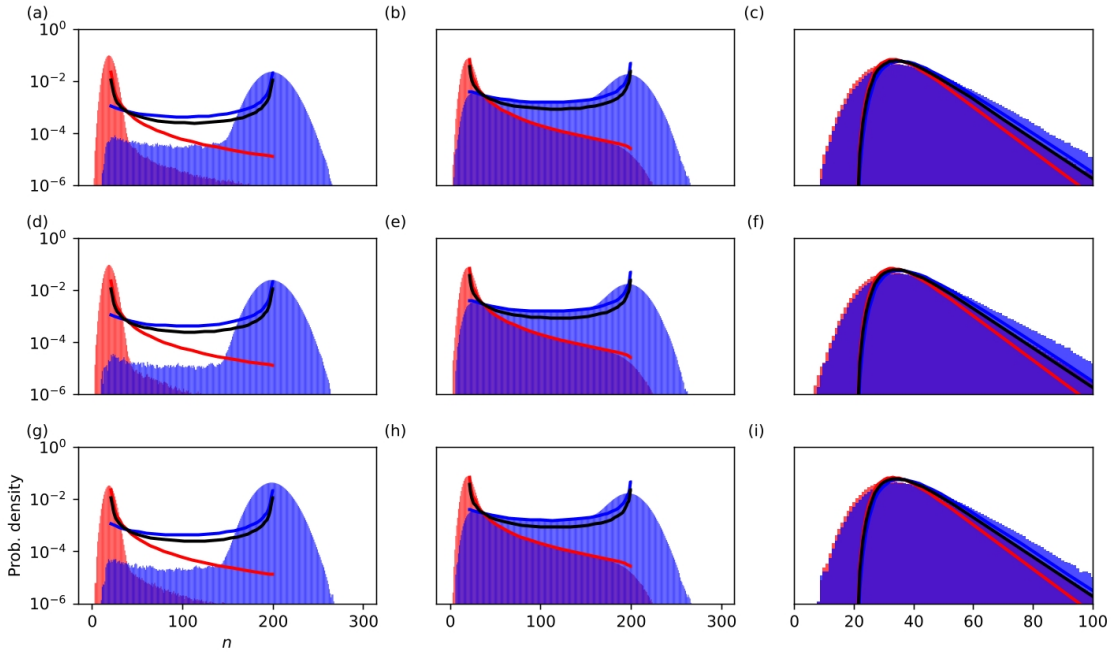

Figure C.1: Quasi-stationary population size distribution of a deme (n-QPSD) distribution for various parameters and its n-PDMP approximation by Eqs. (2.26) and (2.27). Red and blue bars show data for the n-QPSD conditioned on $K(t) = K_-$ and $K(t) = K_+$, respectively. Red, blue, and black solid lines are the n-PDMP stationary densities $p_-(\nu, n)$, $p_+(\nu, n)$, and $p(\nu, n)$, respectively, given by Eqs. (2.26) and (2.27). (a-c) are for clique, (d-f) for cycle, and (g-i) for grid metapopulations. We have $\nu = 10^{-3}$ in (a,d,g), $\nu = 10^{-1}$ in (b,e,h), and $\nu = 10^{2}$ in (c,f,i). Other parameters are $\Omega = 16$, $m = 10^{-3}$, $K_+ = 200$, and $K_- = 20$. All represent a single realisation tracked until $t = 10^5$.

C.2 Further details on the intermediate dynamics in static environments

In this section, we provide further details about the analysis of the intermediate dynamics in static environments; see Ch. 5.2. In the intermediate regime, a metapopulation experiences some deme extinctions, but does not quickly reach total metapopulation extinction, instead surviving for long times. The wild-type and mutant cells compete on the metapopulation which may be only partially occupied, consisting of M, W, and empty demes. Here, we consider intermediate metapopulation dynamics on a regular graph G, obtaining the explicit results $\phi_{\text{int}}^{\text{G}}$ and $\theta_{\text{int}}^{\text{G}}$ for $\text{G} \in \{\text{clique}, \text{cycle}, \text{grid}\}$ reported in Fig. C.2 when the metapopulation initially consists of a single M deme and $\Omega - 1$ demes occupied by W. This region is concretely defined for values of ψ such that $1 < \psi < K\Omega$ for $\Omega \gg 1$, where the lower bound is obtained from ensuring that $\Omega_{\text{occ}} = 1$ from Eq. (5.6) and the upper bound is obtained by considering the point where every individual is expected to migrate on the timescale of deme extinction. Using that $\psi \approx me^K$ for $K \gg 1$, we obtain the condition $\ln(1/m) \lesssim K \lesssim \ln(\Omega K/m)$.

The intermediate regime is characterised by M/W competition and deme extinction. Therefore, in addition to invasions, a W deme may become an M deme through extinction followed by a recolonisation, i.e. $W \to \emptyset \to M$, where $\emptyset$ indicates an extinct deme. Similarly, an M-deme can be changed into a W-deme via $M \to \emptyset \to W$. We assume that there is initially a single M deme in the metapopulation (and $\Omega - 1$ demes of type W). With a probability p_{surv} (see below), the initial M deme survives the short transient as the metapopulation reaches the dynamical equilibrium and the number of number of M demes $i = 0, 1, \ldots, \Omega_{\text{occ}}$ grows and shrinks through invasions and extinction-recolonisation events. We assume that immediately $\Omega_E = \Omega/\psi$ demes go extinct, so that the metapopulation quickly reaches its equilibrium occupancy $\Omega_{\text{occ}} = \Omega\,(1 - 1/\psi)$. In this dynamical equilibrium, a W deme can become an M deme via $W \to \emptyset$ (W deme extinction) at rate $r_{\text{ext},W}$ followed by $\emptyset \to M$ (recolonisation by M) at rate $r_{\text{rec},M}^{\text{G}}$. The overall extinction-recolonisation reaction $W \to \emptyset \to M$ thus occurs at rate $1/(1/r_{\text{ext},W} + 1/r_{\text{rec},M}^{\text{G}})$. Here, the rate of W deme extinction is $r_{\text{ext},W} = (\Omega_{\text{occ}} - i)/\tau_E$ and τ_E is given by Eq. (2.6). We proceed similarly for the extinction of an M deme and its recolonisation into a W deme according to $M \to \emptyset \to W$. Taking also into account the rate of invasion, see Eq. (5.11), the size i of the M-cluster on a regular graph G varies according to the transition rates

$$\widetilde{T}_i^{+}(m, \text{G}, K) = mK \frac{\widetilde{E}_{\text{G}}(i)}{q_{\text{G}}} \left[\rho_M + \frac{1}{\psi - 1} \frac{q_{\text{G}}}{\Omega} \frac{i(\Omega_{\text{occ}} - i)}{\widetilde{E}_{\text{G}}(i)} \right],$$

$$\widetilde{T}_i^{-}(m, \text{G}, K) = mK \frac{\widetilde{E}_{\text{G}}(i)}{q_{\text{G}}} \left[\rho_W + \frac{1}{\psi - 1} \frac{q_{\text{G}}}{\Omega} \frac{i(\Omega_{\text{occ}} - i)}{\widetilde{E}_{\text{G}}(i)} \right].$$

It is important to note that the $\widetilde{E}_{\text{G}}(i)$ in these expressions explicitly represent the number of active edges between M and W on the metapopulation given i mutant demes, taking into account the presence of extinct demes. Therefore, their expressions for a given graph

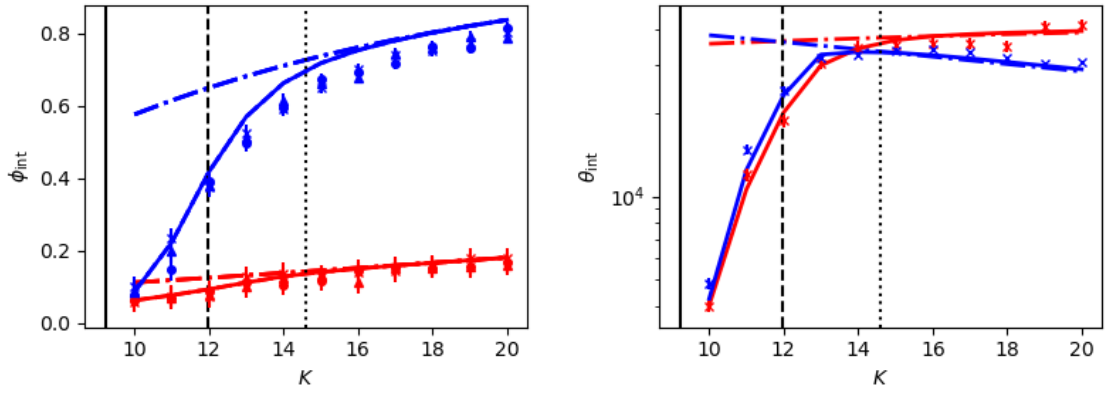

Figure C.2: ϕ_{int} vs. K for $s = 0.1$ (blue) and $s = 0.01$ (red) on clique (solid lines / crosses), cycle (dashed lines / circles), and a grid (dotted lines / triangles). The different symbols and lines are almost indistinguishable. θ_{int} vs. K for the same parameters for a clique metapopulation. The vertical solid and dashed line indicate the boundaries of the region where the number of occupied demes $\Omega_{\text{occ}} \in [1, \Omega - 1]$, see text. The dotted line indicates where $\psi = \Omega K$, i.e. every individual migrates in the time required for an independent deme extinction. Markers show simulation results, solid lines are predictions of Eq. (C.2), and dash-dot lines are predictions of Eq. (5.14). Other parameters are $m = 10^{-4}$ and $\Omega = 16$.

structure G generally differ from those considered in Ch. 5.2 denoted $E_{\text{G}}(i)$. With these rates, we find the first-step analysis equations for the probability $\phi^{\text{G}}_{\text{int},i}$ that the dynamical equilibrium comprising an initial M-cluster of size i consists only of occupied M demes after a mean time $\theta^{\text{G}}_{\text{int},i}$ given by

$$
\begin{aligned}
(\widetilde{T}^+_i + \widetilde{T}^-_i)\phi^{\text{G}}_{\text{int},i} &= \widetilde{T}^+_i \phi^{\text{G}}_{\text{int},i+1} + \widetilde{T}^-_i \phi^{\text{G}}_{\text{int},i-1}, \\
(\widetilde{T}^+_i + \widetilde{T}^-_i)\theta^{\text{G}}_{\text{int},i} &= 1 + \widetilde{T}^+_i \theta^{\text{G}}_{\text{int},i+1} + \widetilde{T}^-_i \theta^{\text{G}}_{\text{int},i-1}.
\end{aligned}
$$

These equations are subject to the boundary conditions $\phi^{\text{G}}_{\text{int},0} = 0, \phi^{\text{G}}_{\text{int},\Omega_{\text{occ}}} = 1$ and $\theta^{\text{G}}_{\text{int},0} = \theta^{\text{G}}_{\text{int},\Omega_{\text{occ}}} = 0$. We can solve these as they exactly resemble the first-step equations of the Moran process (see Ch. 2.2.2) and thus have $\phi^{\text{G}}_{\text{int}} \equiv p_{\text{surv}} \phi^{\text{G}}_{\text{int},1}$ and $\theta^{\text{G}}_{\text{int}} \equiv p_{\text{surv}} \theta^{\text{G}}_{\text{int},1} + (1 - p_{\text{surv}})\tau_E$. The factor $p_{\text{surv}} = \frac{\Omega_{\text{occ}}}{\Omega} = 1 - 1/\psi$ is the probability that the initial M deme reaches the dynamical equilibrium, while the contribution $(1 - p_{\text{surv}})\tau_E$ to $\theta^{\text{G}}_{\text{int}}$ accounts for the probability that the initial M deme goes extinct in a mean time τ_E (given by Eq. (2.6)) before reaching the equilibrium. The final expressions of $\phi^{\text{G}}_{\text{int}}$ and $\theta^{\text{G}}_{\text{int}}$ thus read

$$
\begin{aligned}
\phi^{\text{G}}_{\text{int}} &= p_{\text{surv}} \frac{1}{1 + \sum_{k=1}^{\Omega_{\text{occ}}-1} \prod_{m=1}^{k} \widetilde{\gamma}(m)}, \\
\theta^{\text{G}}_{\text{int}} &= \phi^{\text{G}}_{\text{int}} \sum_{k=1}^{\Omega_{\text{occ}}-1} \sum_{n=1}^{k} \frac{\prod_{m=n+1}^{k} \widetilde{\gamma}(m)}{\widetilde{T}^+_n} + (1 - p_{\text{surv}})\tau_E,
\end{aligned}
\tag{C.2}
$$

where

$$
\widetilde{\gamma}_{\text{G}}(i) \equiv \frac{\rho_W + \frac{1}{\psi - 1} \frac{q_{\text{G}}}{\Omega} \frac{i(\Omega_{\text{occ}} - i)}{\widetilde{E}_{\text{G}}(i)}}{\rho_M + \frac{1}{\psi - 1} \frac{q_{\text{G}}}{\Omega} \frac{i(\Omega_{\text{occ}} - i)}{\widetilde{E}_{\text{G}}(i)}},
\tag{C.3}
$$

and the upper limit of the first sum in $\phi_{\text{int}}^{\text{G}}$ and $\theta_{\text{int}}^{\text{G}}$ is rounded to the nearest integer. We find that $\phi_{\text{int}}^{\text{G}}$ depends on the migration rate m, carrying capacity K, and the spatial structure G via $\widetilde{\gamma}_{\text{G}}$ and Ω_{occ}. In the case of the clique, $\widetilde{E}_{\text{G}}(i) \approx i(\Omega_{\text{occ}} - i)$, and therefore for $\Omega \gg 1$ the expression of Eq. (C.3) simplifies to

$$\widetilde{\gamma}_{\text{clique}}(i) \equiv \widetilde{\gamma}_{\text{clique}} = \frac{\rho_W + \frac{1}{\psi-1}}{\rho_M + \frac{1}{\psi-1}}.$$

We notice that for all graphs G, the expressions of Eq. (C.2) coincide with those of Eq. (5.14) of the competition-dominated regime, with $\widetilde{\gamma}_G(i) \overset{\psi \gg 1}{\longrightarrow} \gamma = \rho_W/\rho_M$. In Fig. C.2, we find that the predictions of Eq. (C.2) are in good agreement with simulation results for all spatial structures G. Moreover, we notice that the spatial dependence of $\phi_{\text{int}}^{\text{G}}$ and $\theta_{\text{int}}^{\text{G}}$ is barely noticeably.

C.3 Breakdown of the circulation theorem under weak bottlenecks

In this section, we discuss in further detail the dependence of the fixation probability $\Phi^{\text{G}}(\nu, m)$ on the migration rate m and spatial structure G of the metapopulation in time-switching environments under weak bottlenecks.

In static environments, where K is constant, a generalisation of the circulation theorem guarantees that the fixation probability is independent on the migration rate and spatial structure of the metapopulation arranged on a circulation graph, see Eq. (5.14). This results from a correspondence between the fixation probability and the number of M demes performing a biased random walk on $\{0, \dots, \Omega\}$ with a bias that is independent of m and G (Marrec et al., 2021).

In time-switching environments under weak bottlenecks (deme extinction is negligible) the correspondence is between the fixation $\Phi^{\text{G}}(\nu, m)$ and the random walk (with absorbing boundaries) on $\{0, \dots, \Omega\} \times \{-1, 1\}$ for the number of fully mutant demes in the environmental state $\xi = \pm 1$. As a consequence, $\Phi^{\text{G}}(\nu, m)$ is the probability of absorption in the state Ω. In this setting, defining the state of the random walk by (i, ξ), where $i = 0, 1, \dots, \Omega$, the random walk moves to the right $(i \to i+1)$ with a probability $r(i, \xi)$, to the left $(i \to i-1)$ with a probability $\ell(i, \xi)$, or switches environment $(\xi \to -\xi)$ with probability $\epsilon(i, \xi)$, where

$$\begin{aligned}
r(i,\xi) &= \frac{m\mathcal{N}_\xi(\nu)\frac{E_{\text{G}}(i)}{q_{\text{G}}}\rho_{M,\xi}(\nu)}{m\mathcal{N}_\xi(\nu)\frac{E_{\text{G}}(i)}{q_{\text{G}}}\rho_{M,\xi}(\nu) + m\mathcal{N}_\xi(\nu)\frac{E_{\text{G}}(i)}{q_{\text{G}}}\rho_{W,\xi}(\nu) + \nu}, \\
\ell(i,\xi) &= \frac{m\mathcal{N}_\xi(\nu)\frac{E_{\text{G}}(i)}{q_{\text{G}}}\rho_{W,\xi}(\nu)}{m\mathcal{N}_\xi(\nu)\frac{E_{\text{G}}(i)}{q_{\text{G}}}\rho_{M,\xi}(\nu) + m\mathcal{N}_\xi(\nu)\frac{E_{\text{G}}(i)}{q_{\text{G}}}\rho_{W,\xi}(\nu) + \nu}, \\
\epsilon(i,\xi) &= \frac{\nu}{m\mathcal{N}_\xi(\nu)\frac{E_{\text{G}}(i)}{q_{\text{G}}}\rho_{M,\xi}(\nu) + m\mathcal{N}_\xi(\nu)\frac{E_{\text{G}}(i)}{q_{\text{G}}}\rho_{W,\xi}(\nu) + \nu}.
\end{aligned} \tag{C.4}$$

$\Phi^{\mathrm{G}}(\nu, m)$ thus coincides with the probability that the random walk defined by Eq. (C.4) gets absorbed in the state $i = \Omega$. Unlike the case of the competition-dominated regime under the static environment, the fixation probability here typically depends on all parameters, including the migration rate. For the fixation probability to remain unchanged under parameter changes requires strict conditions. This can be seen by assuming that for a parameter set S_1 the probabilities $r_1(i,\xi)$, $\ell_1(i,\xi)$, and $\epsilon_1(i,\xi)$ define the random walk corresponding to the fixation probability $\Phi^{\mathrm{G}}_{i,\xi}$. We therefore have

$$\Phi^{\mathrm{G}}_{i,\xi} = r_1(i,\xi)\Phi^{\mathrm{G}}_{i+1,\xi} + \ell_1(i,\xi)\Phi^{\mathrm{G}}_{i-1,\xi} + \epsilon_1(i,\xi)\Phi^{\mathrm{G}}_{i,-\xi}.$$

We can also assume that under another set of parameters, say S_2, $\Phi^{\mathrm{G}}_{i,\xi}$ remains unchanged for all i and ξ with a corresponding random walk defined by the probabilities $r_2(i,\xi)$, $\ell_2(i,\xi)$, and $\epsilon_2(i,\xi)$, such that

$$\Phi^{\mathrm{G}}_{i,\xi} = r_2(i,\xi)\Phi^{\mathrm{G}}_{i+1,\xi} + \ell_2(i,\xi)\Phi^{\mathrm{G}}_{i-1,\xi} + \epsilon_2(i,\xi)\Phi^{\mathrm{G}}_{i,-\xi}.$$

Subtracting the second equation from the first, and using conservation of probability, we find that

$$(r_1(i,\xi) - r_2(i,\xi))(\Phi^{\mathrm{G}}_{i+1,\xi} - \Phi^{\mathrm{G}}_{i,-\xi}) + (\ell_1(i,\xi) - \ell_2(i,\xi))(\Phi^{\mathrm{G}}_{i-1,\xi} - \Phi^{\mathrm{G}}_{i,-\xi}) = 0. \tag{C.5}$$

The cases of $\Phi^{\mathrm{G}}_{i+1,\xi} - \Phi^{\mathrm{G}}_{i,-\xi} = 0$ and $\Phi^{\mathrm{G}}_{i-1,\xi} - \Phi^{\mathrm{G}}_{i,-\xi} = 0$ imply that the fixation probability of all transient states is identical, and therefore we neglect this unphysical case. Defining $\Delta r(i,\xi) = r_1(i,\xi) - r_2(i,\xi)$ and $\Delta\ell(i,\xi) = \ell_1(i,\xi) - \ell_2(i,\xi)$, Eq. (C.5) yields

$$\Delta r(i,\xi) = \frac{\Phi^{\mathrm{G}}_{i+1,\xi} - \Phi^{\mathrm{G}}_{i,-\xi}}{\Phi^{\mathrm{G}}_{i,-\xi} - \Phi^{\mathrm{G}}_{i-1,\xi}}\Delta\ell(i,\xi). \tag{C.6}$$

For each of the $2(\Omega-2)$ transient states we therefore have a constraint given by Eq. (C.6). However, $\Delta r(i,\xi)$ and $\Delta\ell(i,\xi)$ are controlled by $|S_1| = |S_2| = p$ degrees of freedom (system parameters) where $p \ll 2(\Omega-2)$. Therefore, the system is overdetermined and Eq. (C.6) is only generally satisfied across all (i,ξ) for the trivial solution $\Delta r(i,\xi) = \Delta\ell(i,\xi) = 0$, i.e. $S_1 = S_2$. This implies that in time-fluctuating environments the fixation probability $\Phi^{\mathrm{G}}(\nu, m)$ is expected to depend on m and G.

Interestingly however, Fig. 5.7(c) illustrates the almost unnoticeable dependence of $\Phi^{\mathrm{G}}(\nu, m)$ on the specific spatial structure. This is due to the overall similar impact of the factor $E_{\mathrm{G}}(i)/q_G$ for the various graphs. While differences arise when m varies at fixed ν due to large variations in the timescales of the competition dynamics (significantly more invasions when $K = K_+$ than when $K = K_-$), varying spatial structure produces small changes in these timescales, and as such leads to almost unnoticeable changes in Φ.

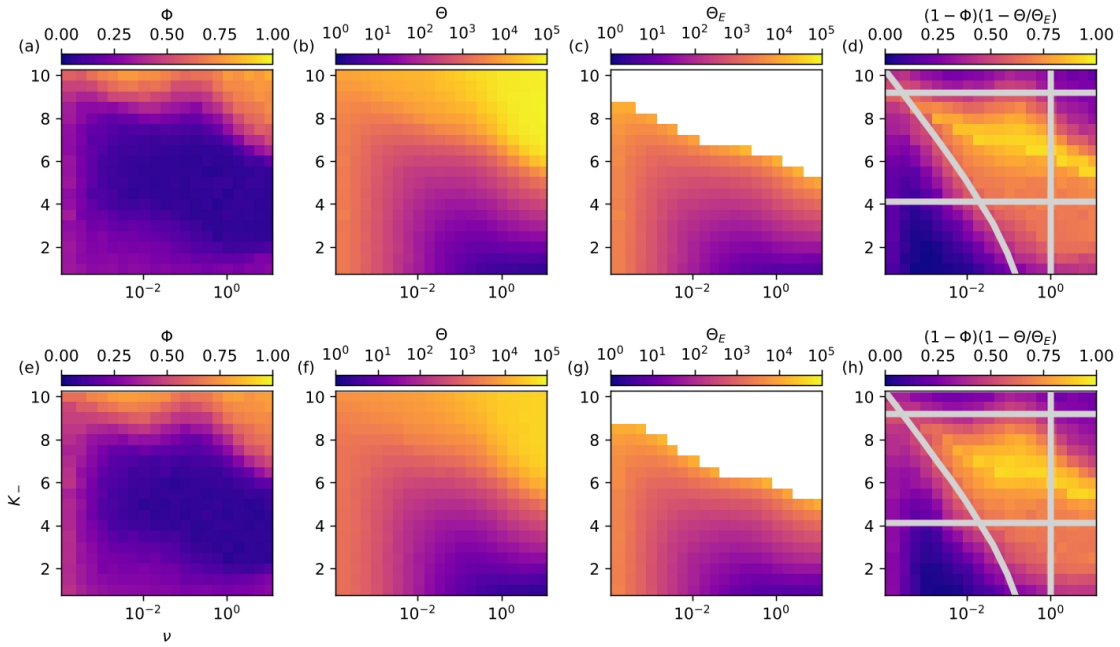

Figure C.3: Near-optimal condition for the idealised treatment strategy on a cycle and grid metapopulation. (ν, K_-) heatmaps of Φ, Θ, Θ_E and $(1-\Phi)(1-\Theta/\Theta_E)$ for the cycle (a-d) and grid (e-h) metapopulations, see Appendix C.4. White space in panels (c) and (g) indicate the region of the parameter where at least one realisation for those parameters did not reach extinction by $t = 10^5$. Grey lines in panels (d) and (h) show the near-optimal conditions for the idealised treatment strategy: $\psi(m, K_-) < 1$ below the top horizontal line, $mK_+\theta_E > 1$ above the bottom horizontal line, and $\nu\theta_E > 1$ above the curved line, while the vertical line indicates where $\nu < 1$ and θ_E from Eq. (5.9). The near-optimal treatment conditions is the yellowish cloud at the centre of the area enclosed by these lines. Other parameters are $\Omega = 16$, $m = 10^{-4}$, $s = 0.1$, and $K_+ = 200$. In all panels, initially there is a single M deme and $\Omega - 1$ demes occupied by W.

C.4 The influence of spatial structure under strong bottlenecks

In Figs. 5.5(a,c) and 5.7(c), we have found that the spatial structure has a barely noticeable influence on the fixation probability and mean fixation time when the carrying capacity is constant and in time-varying environments in the regime of weak bottlenecks. Fig. C.3 shows the heatmaps on a cycle and a grid metapopulation for the "idealised treatment strategy" proposed in Ch. 5.3, which are almost identical. This is in accord with Eqs. (5.23) predicting that the same migration rate yields the same near optimal conditions for the heatmaps of metapopulation on any regular graph, here a cycle and a grid. Simulation results confirm spatial structure is only responsible for minor quantitative changes in the region of the heatmaps corresponding to the near-optimal "treatment conditions". This stems from the removal scenario characterising the idealised treatment strategy being due to deme extinction which is mostly independent of G and m.

C.5 Asymmetric environmental switching

For the sake of simplicity and clarity, we have focused on symmetric environmental switching. In this section, we relax this assumption and outline how the results of the paper can be generalised to the case when there is an environmental bias, i.e. when there is a different average time spent in the states $\xi = \pm 1$, as introduced in Ch. 2.3.1.

In the realm of the coarse-grained description, the regime of weak bottlenecks dominated by the W/M competition can be characterised by the M fixation probability $\Phi^{\mathrm{G}}(\nu, \delta, m)$ and unconditional mean fixation time $\Theta^{\mathrm{G}}(\nu, \delta, m)$ by Eq. (5.22) obtained by solving the first-step analysis equations Eq. (5.19) and Eq. (5.20) with the transition rates Eq. (5.17) and Eq. (5.18) obtained using $\mathcal{N}_\xi(\nu, \delta)$ averaged over Eq. (2.26), i.e. $\mathcal{N}_\xi(\nu, \delta) = \int n p_\xi(\nu, \delta, n) \mathrm{d}n$. The results of Fig. C.4 for a cycle metapopulation show that the predictions coarse-grained description based on the PDMP approximation Eq. (2.26)

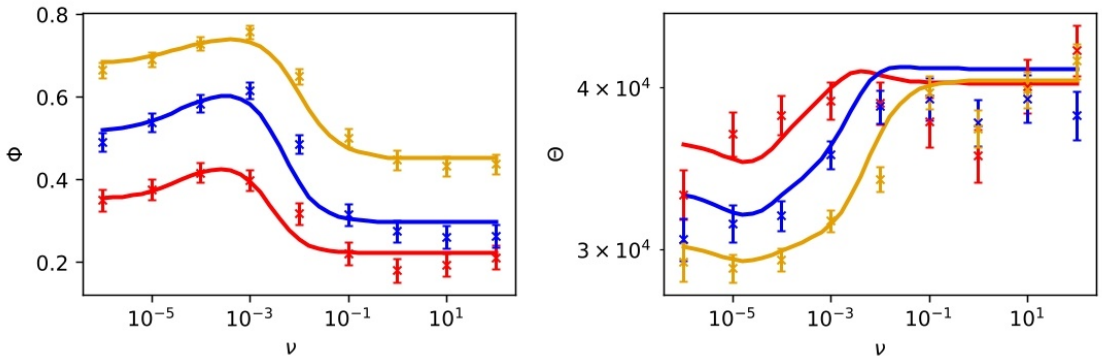

Figure C.4: Fixation probability Φ^{G} and mean fixation time Θ^{G} against switching rate ν for different values of δ. Red, blue, and yellow represent $\delta = -0.5$, $\delta = 0.0$, and $\delta = 0.5$, respectively. Markers show simulation results and lines are predictions of Eq. (5.22). Other parameters are $\Omega = 16$, $s = 0.01$, $m = 10^{-4}$, $K_+ = 200$, and $K_- = 20$.

are in good agreement with simulation results. $\Phi^{\mathrm{G}}(\nu,\delta,m)$ and $\Theta^{\mathrm{G}}(\nu,\delta,m)$ are again found to exhibit a non-monotonic dependence on ν, with extrema in the range of intermediate ν. The main effect of δ is to increase the M fixation probability and reduce the mean fixation time when $\delta > 0$, which is intuitive since this corresponds to a bias towards the mild state favouring the fixation of M.

The regime of strong bottlenecks is dominated by the interplay between M/W competition in the mild state ($K = K_+$) and deme extinction in the harsh environmental state ($K = K_-$), occurring in time $\theta_E \equiv \theta_E(K_-,\Omega)$. In this regime, the near-optimal conditions for the removal of the mutant strain can be obtained as under symmetric switching (given by Eq. (5.23)) and read

$$\begin{aligned} &\psi(m,K_-) < 1,\ \nu(1\pm\delta) \lesssim 1, \\ &\nu(1+\delta)\theta_E \gtrsim 1,\ mK_+\theta_E\frac{1+\delta}{1-\delta} \gtrsim 1, \end{aligned} \tag{C.7}$$

which, as Eq. (5.23), are conditions depending on m but not on the spatial structure G. The main differences from Eq. (5.23) are in the conditions $\theta_E\nu_- = \theta_E\nu(1+\delta) \gtrsim 1$ and $mK_+\theta_E\frac{\nu_-}{\nu_+} = mK_+\theta_E\frac{1+\delta}{1-\delta} \gtrsim 1$. The first of these changes ensures that a switch occurs before the metapopulation MET in the harsh environment, θ_E. The second ensures there are enough recolonisations in the mild environment to maintain the metapopulation given the minimum switching rate required to prevent extinction in the harsh environment, i.e. rearranging $\theta_E\nu_- \gtrsim 1$ gives $\nu \gtrsim 1/(\theta_E(1+\delta))$ and for sufficient recolonisations we require $mK_+/\nu_+ \equiv mK_+/(\nu(1-\delta)) \gtrsim 1$, where we substitute our expression for ν. Since θ_E is independent of δ, we expect that the conditions Eq. (C.7) define a region in the parameter space that is similar to that obtained under symmetric switching, shifted towards higher (lower) values of ν and K_- when $\delta < 0$ ($\delta > 0$). This picture is confirmed by the heatmaps of Fig. C.5.

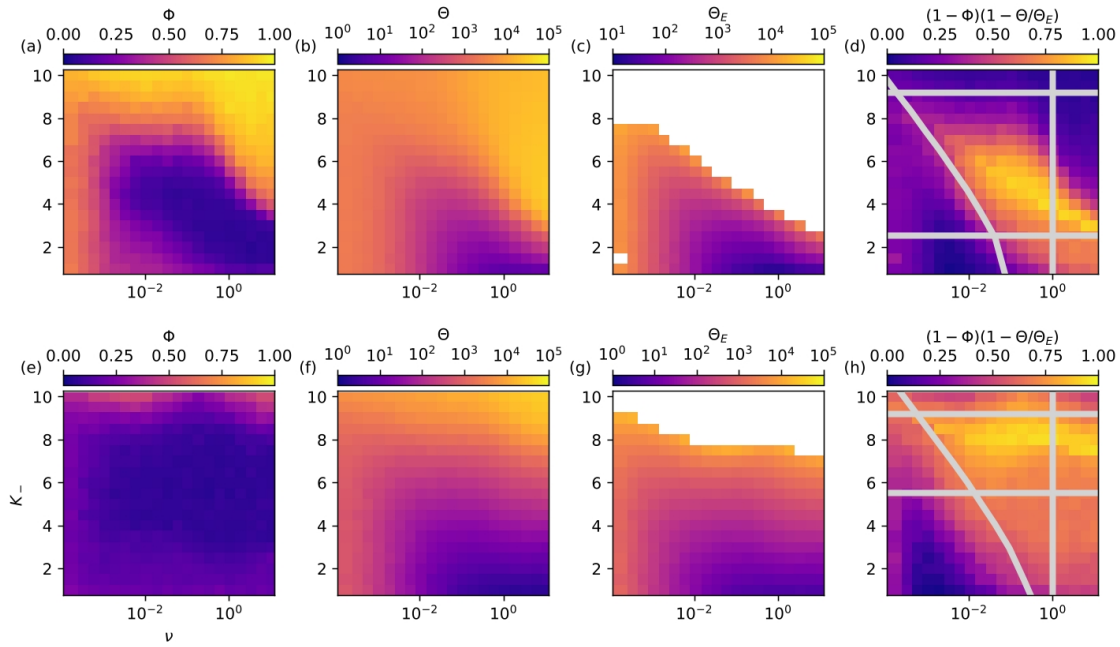

Figure C.5: Near-optimal condition for the idealised treatment strategy on the clique metapopulation. (ν, K_-) heatmaps of Φ, Θ, Θ_E and $(1-\Phi)(1-\Theta/\Theta_E)$ for the $\delta = 0.5$ (a-d) and $\delta = -0.5$ (e-h) metapopulations, see Appendix C.5. White space in panels (c) and (g) indicate the region of the parameter where at least one realisation for those parameters did not reach extinction by $t = 10^5$. Grey lines in panels (d) and (h) show the near-optimal conditions for the idealised treatment strategy in the asymmetric environment: $\psi(m, K_-) < 1$ below the top horizontal line, $mK_+\theta_E\frac{1+\delta}{1-\delta} > 1$ above the bottom horizontal line, and $\nu(1+\delta)\theta_E > 1$ above the curved line, while the vertical line indicates where $\nu < 1$ and θ_E from Eq. (5.9). The near-optimal treatment conditions is the yellowish cloud at the centre of the area enclosed by these lines. Other parameters are $\Omega = 16$, $m = 10^{-4}$, $s = 0.1$, and $K_+ = 200$. In all panels, initially there is a single M deme and $\Omega - 1$ demes occupied by W.

Appendix D

Computational methods

To complement the theoretical work developed in this thesis, I additionally carry out computational simulations of the models investigated. This allows for a confirmation of the accuracy of any analytical results found, a test of the limits of the approximations made to see where they no longer hold, and for investigation of the behaviour of the systems beyond the limits of the analytical tools developed here. Here, I will explain the simulation methods used in this thesis, while the algorithms applied to each specific model can be found in the corresponding paper. Error bars on data points from simulations are calculated using the standard error on the mean from the many stochastic realisations for the point. Note, however, that across the entire thesis typical error bars are found to be small and almost coincide with the markers. Therefore, for the sake of readability, error bars are only displayed where they are clearly visible and are otherwise omitted from figures.

D.1 Next reaction method

In Chs. 2, 3, and 4, I utilise the next reaction method, introduced in Gibson and Bruck (2000). This is an efficient method used to simulate stochastic realisations of a systems in a way that correctly reproduces the statistical properties of that system. It works as follows (adapted from a description laid out in Anderson (2007)):

1. Initialise the system, setting the number of individuals of each species, the environmental state, and the time $t = 0$.
2. Calculate the rates for each of the M possible events, $\mathbf{a} = \{a_1, ..., a_M\}$.
3. Draw M independent random numbers from a uniform distribution on $(0, 1)$, labelled $\mathbf{r} = \{r_1, ..., r_M\}$.
4. For each event $k \in \{1, ..., M\}$, set $T_k = \frac{1}{a_k} \ln\left(\frac{1}{r_k}\right)$ giving $\mathbf{T} = \{T_1, ..., T_M\}$.
5. Set $t = \min(\mathbf{T})$. Label the event with minimum T_k out of the M possible events as μ and its time T_μ.

6. Carry out the changes corresponding to event μ, updating the number of individuals of each species or changing the environmental state.

7. Recalculate the rates for all of the possible events following these changes and label these new rates $\overline{\mathbf{a}} = \{\overline{a}_1, ..., \overline{a}_M\}$.

8. For each event $k \neq \mu$, set $T_k = \frac{a_k}{\overline{a}_k}(T_k - t) + t$.

9. For event $k = \mu$, draw r from a uniform distribution on $(0, 1)$, and set $T_\mu = \frac{1}{\overline{a}_\mu} \ln\left(\frac{1}{r}\right) + t$.

10. Set $\mathbf{a} = \overline{\mathbf{a}}$.

11. Loop back to step 5 or quit.

This algorithm is beneficial to use over other stochastic algorithms as, after the initial computationally expensive step to draw M independent random numbers, each following loop of the algorithm only requires one new random number to be generated. For simulations with many individuals that run for long periods, this provides a considerable boost to computational efficiency over other popular algorithms which require two random numbers to be generated at every loop, the Gillespie algorithm being a prime example (Gillespie, 1976, 1977).

D.2 Discrete-time Monte Carlo method

In Ch. 5, I utilise the discrete-time Monte Carlo method to simulate evolution on a metapopulation. To recap from their brief introduction in Ch. 1, a metapopulation is a spatially structured community, consisting of several subpopulations where individuals interact, see Fig. 1.3. Furthermore, the individuals may migrate between neighbouring subpopulations. Here I use a discrete-time Monte Carlo method, an approximate method, where here I set the discrete time interval $\Delta t = 1$. It works as follows:

1. Initialise the system, setting the number of individuals of each species on each subpopulation, the environmental state, and the time $t = 0$.

2. Calculate the rates for each of the M possible event, $\mathbf{a} = \{a_1, ..., a_M\}$.

3. Calculate the total rate for any event to occur in the system, denoted $A = \sum_{k=1}^{M} a_k$.

4. Set the total number of reactions to occur in the next discrete time interval Δt to be $N = \text{round}\,(A\Delta t)$, such that the timescale of the simulation is consistent with the theoretical model considered, i.e. we expect $A\Delta t$ reactions from a system with reaction rate A in a time Δt.

5. Draw N random numbers from a uniform distribution on $(0, 1)$, labelled $\mathbf{r} = \{r_1, ..., r_N\}$.

6. Sequentially for each random number $r_k \in \mathbf{r}$, calculate Ar_k, find n such that $\sum_{i=1}^{n} a_i > Ar_k$, perform the reaction n, update each event rate in $\mathbf{a}$, and update the total rate sum $A = \sum_{k=1}^{M} a_k$.

7. Increment t by Δt.

8. Loop back to step 4 or quit.

It should be noted that, unlike in a typical discrete-time Monte Carlo method, the rates are updated after every event and not after each time interval. This is necessary in the systems considered to prevent negative population sizes as subpopulations may contain few individuals. This means that, in terms of computational efficiency, there is little improvement here over the next reaction method. However, the discrete-time Monte Carlo method is conceptually simpler and therefore easier to implement in computer code, particularly when working with complex systems involving spatial structure and a changing environment.

References

Abbara, A., & Bitbol, A.-F. (2023). Frequent asymmetric migrations suppress natural selection in spatially structured populations. *PNAS Nexus*, *2*(11), pgad392. https://doi.org/10.1093/pnasnexus/pgad392

Abbara, A., Pagani, L., García-Pareja, C., & Bitbol, A.-F. (2024). Mutant fate in spatially structured populations on graphs: Connecting models to experiments. *PLOS Comput. Biol.*, *20*(9), e1012424. https://doi.org/10.1371/journal.pcbi.1012424

Abdul-Rahman, F., Tranchina, D., & Gresham, D. (2021). Fluctuating environments maintain genetic diversity through neutral fitness effects and balancing selection. *Mol. Biol. Evol.*, *38*(10), 4362–4375. https://doi.org/10.1093/molbev/msab173

Acar, M., Mettetal, J. T., & van Oudenaarden, A. (2008). Stochastic switching as a survival strategy in fluctuating environments. *Nat. Genet.*, *40*(4), 471–475. https://doi.org/10.1038/ng.110

Allee, W. C., & Bowen, E. S. (1932). Studies in animal aggregations: Mass protection against colloidal silver among goldfishes. *J. Exp. Zool.*, *61*(2), 185–207. https://doi.org/10.1002/jez.1400610202

Allen, L. J. S. (2003). *An Introduction to Stochastic Processes with Applications to Biology* (1st ed.). Pearson Education.

Allen, L. J. S. (2007). *An introduction to mathematical biology*. Pearson Prentice Hall.

Allen, R. J., & Waclaw, B. (2018). Bacterial growth: A statistical physicist's guide. *Rep. Prog. Phys.*, *82*(1), 016601. https://doi.org/10.1088/1361-6633/aae546

Anderson, D. F. (2007). A modified next reaction method for simulating chemical systems with time dependent propensities and delays. *J. Chem. Phys.*, *127*(21), 214107. https://doi.org/10.1063/1.2799998

Andersson, D. I., Patin, S. M., Nilsson, A. I., & Kugelberg, E. (2007). The biological cost of antibiotic resistance. In R. A. Bonomo & M. Tolmasky (Eds.), *Enzyme-mediated resistance to antibiotics: Mechanisms, dissemination, and prospects for inhibition* (pp. 339–348). ASM Press. https://doi.org/10.1128/9781555815615.ch21

Antal, T., & Scheuring, I. (2006). Fixation of Strategies for an Evolutionary Game in Finite Populations. *Bull. Math. Biol.*, *68*(8), 1923–1944. https://doi.org/10.1007/s11538-006-9061-4

Ashcroft, P., Altrock, P. M., & Galla, T. (2014). Fixation in finite populations evolving in fluctuating environments. *J. R. Soc. Interface*, *11*(100), 20140663. https://doi.org/10.1098/rsif.2014.0663

Asker, M., Hernández-Navarro, L., Rucklidge, A. M., & Mobilia, M. (2023). Coexistence of Competing Microbial Strains under Twofold Environmental Variability and Demographic Fluctuations. *New J. Phys.*, *25*(12), 123010. https://doi.org/10.1088/1367-2630/ad0d36

Asker, M., Swailem, M., Täuber, U. C., & Mobilia, M. (2025, April). *Fixation and extinction in time-fluctuating spatially structured metapopulations* [arXiv preprint]. https://doi.org/10.48550/arXiv.2504.08433

Assaf, M., & Meerson, B. (2017). WKB theory of large deviations in stochastic populations. *J. Phys. A: Math. Theor.*, *50*, 263001. https://doi.org/10.1088/1751-8121/aa669a

Assaf, M., & Mobilia, M. (2010). Large fluctuations and fixation in evolutionary games. *J. Stat. Mech.*, *2010*(09), P09009. https://doi.org/10.1088/1742-5468/2010/09/P09009

Assaf, M., & Mobilia, M. (2011). Fixation of a deleterious allele under mutation pressure and finite selection intensity. *J. Theor. Biol.*, *275*(1), 93. https://doi.org/10.1016/j.jtbi.2011.01.025

Assaf, M., Roberts, E., Luthey-Schulten, Z., & Goldenfeld, N. (2013). Extrinsic noise driven phenotype switching in a self-regulating gene. *Phys. Rev. Lett.*, *111*, 058102. https://doi.org/10.1103/PhysRevLett.111.058102

Assaf, M., & Meerson, B. (2010). Extinction of metastable stochastic populations. *Phys. Rev. E*, *81*(2), 021116. https://doi.org/10.1103/PhysRevE.81.021116

Assaf, M., Mobilia, M., & Roberts, E. (2013). Cooperation dilemma in finite populations under fluctuating environments. *Phys. Rev. Lett.*, *111*(23), 238101. https://doi.org/10.1103/PhysRevLett.111.238101

Balaban, N. Q., Merrin, J., Chait, R., Kowalik, L., & Leibler, S. (2004). Bacterial Persistence as a Phenotypic Switch. *Science*, *305*(5690), 1622–1625. https://doi.org/10.1126/science.1099390

Barabás, G., D'Andrea, R., & Stump, S. M. (2018). Chesson's coexistence theory. *Ecol. Monogr.*, *88*, 1. https://doi.org/10.1002/ecm.1302

Barrick, J. E., Yu, D. S., Yoon, S. H., Jeong, H., Oh, T. K., Schneider, D., Lenski, R. E., & Kim, J. F. (2009). Genome evolution and adaptation in a long-term experiment with Escherichia coli. *Nature*, *461*(7268), 1243–1247. https://doi.org/10.1038/nature08480

Barton, N. H. (1993). The probability of fixation of a favoured allele in a subdivided population. *Genet. Res.*, *62*(2), 149–157. https://doi.org/10.1017/S0016672300031748

Bena, I. (2006). Dichotomous Markov Noise: Exact results for out-of-Equilibrium systems. *Int. J. Mod. Phys. B*, *20*, 2825. https://doi.org/10.1142/S0217979206034881

Bernatová, S., Samek, O., Pilát, Z., Šerý, M., Ježek, J., Jákl, P., Šiler, M., Krzyžánek, V., Zemánek, P., Holá, V., Dvořáčková, M., & Růžička, F. (2013). Following the Mechanisms of Bacteriostatic versus Bactericidal Action Using Raman Spectroscopy. *Molecules*, *18*(11), 13188–13199. https://doi.org/10.3390/molecules181113188

Berry, R. J. (1964). The Evolution of an Island Population of the House Mouse. *Evolution*, *18*(3), 468–483. https://doi.org/10.2307/2406357

Bhat, A. S. (2025). A stochastic field theory for the evolution of quantitative traits in finite populations. *Theor. Popul. Biol.*, *161*, 1–12. https://doi.org/10.1016/j.tpb.2024.10.003

Bhat, A. S., & Guttal, V. (2025). Eco-Evolutionary Dynamics for Finite Populations and the Noise-Induced Reversal of Selection. *Am. Nat.*, *205*(1), 1–19. https://doi.org/10.1086/733196

Blythe, R. A., & McKane, A. J. (2007). Stochastic models of evolution in genetics, ecology and linguistics. *J. Stat. Mech: Theory Exp.*, *2007*(07), P07018–P07018. https://doi.org/10.1088/1742-5468/2007/07/P07018

Bottery, M. J., Pitchford, J. W., & Friman, V. P. (2021). Ecology and evolution of antimicrobial resistance in bacterial communities. *ISME J.*, *15*(4), 939–948. https://doi.org/10.1038/s41396-020-00832-7

Bottery, M. J., Wood, A. J., & Brockhurst, M. A. (2016). Selective conditions for a multidrug resistance plasmid depend on the sociality of antibiotic resistance. *Antimicrob. Agents Chemother.*, *60*(4), 2524–2527. https://doi.org/10.1128/aac.02441-15

Bradshaw, A. D. (1965, January). Evolutionary Significance of Phenotypic Plasticity in Plants. In *Advances in Genetics* (pp. 115–155, Vol. 13). Academic Press. https://doi.org/10.1016/S0065-2660(08)60048-6

Brand, A., Allen, L., Altman, M., Hlava, M., & Scott, J. (2015). Beyond authorship: Attribution, contribution, collaboration, and credit. *Learn. Publ.*, *28*(2), 151–155. https://doi.org/10.1087/20150211

Brockhurst, M. A. (2007). Population Bottlenecks Promote Cooperation in Bacterial Biofilms. *PLOS ONE*, *2*(7), e634. https://doi.org/10.1371/journal.pone.0000634

Brook, I. (2004). β-Lactamase-producing bacteria in mixed infections. *Clin. Microbiol. Infect.*, *10*(9), 777–784. https://doi.org/10.1111/j.1198-743X.2004.00962.x

Brook, I. (2009). The role of beta-lactamase-producing-bacteria in mixed infections. *BMC Infect. Dis.*, *9*, 1–4. https://doi.org/10.1186/1471-2334-9-202

Burch, C. L., & Chao, L. (1999). Evolution by small steps and rugged landscapes in the RNA virus ϕ6. *Genetics*, *151*(3), 921–927. https://doi.org/10.1093/genetics/151.3.921

Canetti, G. (1956). Dynamic aspects of the pathology and bacteriology of tuberculous lesions. *Am. Rev. Tuberc. Pulm. Dis.*, *74*(2–2), 13–21.

Caporaso, J. G., Lauber, C. L., Costello, E. K., Berg-Lyons, D., Gonzalez, A., Stombaugh, J., Knights, D., Gajer, P., Ravel, J., Fierer, N., Gordon, J. I., & Knight, R. (2011). Moving pictures of the human microbiome. *Genome Biol.*, *12*, R50. https://doi.org/10.1186/gb-2011-12-5-r50

Chakraborty, P. P., Nemzer, L. R., & Kassen, R. (2023). Experimental evidence that network topology can accelerate the spread of beneficial mutations. *Evol. Lett.*, *7*(6), 447–456. https://doi.org/10.1093/evlett/qrad047

Chesson, P. (1994). Multispecies competition in variable environments. *Theor. Popul. Biol.*, *45*(3), 227–276. https://doi.org/10.1006/tpbi.1994.1013

Chesson, P. (2000a). General theory of competitive coexistence in spatially-varying environments. *Theor. Popul. Biol.*, *58*, 211. https://doi.org/10.1006/tpbi.2000.1486

Chesson, P. (2000b). Mechanisms of maintenance of species diversity. *Annu. Rev. Ecol. Syst*, *31*, 343. https://doi.org/10.1146/annurev.ecolsys.31.1.343

Chesson, P. (1978). Predator-Prey Theory and Variability. *Annu. Rev. Ecol. Syst.*, *9*, 323–347.

Chesson, P., & Warner, R. R. (1981). Environmental Variability Promotes Coexistence in Lottery Competitive Systems. *Am. Nat.*, *117*(6), 923–943. https://doi.org/10.1086/283778

Chotibut, T., & Nelson, D. R. (2015). Evolutionary dynamics with fluctuating population sizes and strong mutualism. *Phys. Rev. E*, *92*(2), 022718. https://doi.org/10.1103/PhysRevE.92.022718

Cignarella, F., Cantoni, C., Ghezzi, L., Salter, A., Dorsett, Y., Chen, L., Phillips, D., Weinstock, G. M., Fontana, L., Cross, A. H., Zhou, Y., & Piccio, L. (2018). Intermittent fasting confers protection in CNS autoimmunity by altering the gut microbiota. *Cell Metab.*, *27*, 1222–1235. https://doi.org/10.1016/j.cmet.2018.05.006

Coates, J., Park, B. R., Le, D., Şimşek, E., Chaudhry, W., & Kim, M. (2018). Antibiotic-induced population fluctuations and stochastic clearance of bacteria. *eLife*, *7*, e32976. https://doi.org/10.7554/eLife.32976

Constable, G. W. A., & McKane, A. J. (2014). Population genetics on islands connected by an arbitrary network: An analytic approach. *J. Theor. Biol.*, *358*, 149–165. https://doi.org/10.1016/j.jtbi.2014.05.033

Constable, G. W. A., Rogers, T., McKane, A. J., & Tarnita, C. E. (2016). Demographic noise can reverse the direction of deterministic selection. *Proc. Natl. Acad. Sci. U.S.A.*, *113*(32). https://doi.org/10.1073/pnas.1603693113

Contois, D. E. (1959). Kinetics of Bacterial Growth: Relationship between Population Density and Specific Growth Rate of Continuous Cultures. *Microbiology*, *21*(1), 40–50. https://doi.org/10.1099/00221287-21-1-40

Cremer, J., Meilbinger, A., & Frey, E. (2011). Evolutionary and population dynamics: A coupled approach. *Phys. Rev. E*, *84*, 051921. https://doi.org/10.1103/PhysRevE.84.051921

Cremer, J., Reichenbach, T., & Frey, E. (2009). The edge of neutral evolution in social dilemmas. *New J. Phys.*, *11*(9), 093029. https://doi.org/10.1088/1367-2630/11/9/093029

Crow, J. F., & Kimura, M. (1970). *An introduction to population genetics theory*. Pearson Education.

Dadgostar, P. (2019). Antimicrobial Resistance: Implications and Costs. *Infect. Drug Resist.*, *12*, 3903–3910. https://doi.org/10.2147/IDR.S234610

Danino, M., & Shnerb, N. M. (2018). Fixation and absorption in a fluctuating environment. *J. Theor. Biol.*, *441*, 84–92. https://doi.org/10.1016/j.jtbi.2018.01.004

Davies, J. (1994). Inactivation of antibiotics and the dissemination of resistance genes. *Science*, *264*(5157), 375–382. https://doi.org/10.1126/science.8153624

Davis, M. H. A. (1984). Piecewise-Deterministic Markov Processes: A General Class of Non-Diffusion Stochastic Models. *J. R. Stat. Soc. Ser. B Methodol.*, *46*(3), 353–388. https://doi.org/10.1111/j.2517-6161.1984.tb01308.x

DeLong, J. P., & Cressler, C. E. (2023). Stochasticity directs adaptive evolution toward nonequilibrium evolutionary attractors. *Ecology*, *104*(1), e3873. https://doi.org/10.1002/ecy.3873

Diz-Pita, É., & Otero-Espinar, M. V. (2021). Predator–Prey Models: A Review of Some Recent Advances. *Mathematics*, *9*(15), 1783. https://doi.org/10.3390/math9151783

Eliopoulos, G. M., Cosgrove, S. E., & Carmeli, Y. (2003). The Impact of Antimicrobial Resistance on Health and Economic Outcomes. *Clin. Infect. Dis.*, *36*(11), 1433–1437. https://doi.org/10.1086/375081

Ellner, S. P., Snyder, R. E., Adler, P. B., & Hooker, G. (2019). An expanded modern coexistence theory for empirical applications. *Ecol. Lett.*, *22*, 3. https://doi.org/10.1111/ele.13159

Engel, P., & Moran, N. A. (2013). The gut microbiota of insects–diversity in structure and function. *FEMS Microbiol. Rev.*, *37*(5), 699–735. https://doi.org/10.1111/1574-6976.12025

Engering, A., Hogerwerf, L., & Slingenbergh, J. (2013). Pathogen–host–environment interplay and disease emergence. *Emerg. Microbes Infect.*, *2*(1), 1–7. https://doi.org/10.1038/emi.2013.5

Ewens, W. J. (2004). *Mathematical population genetics*. Springer, New York, USA.

Feldman, W. E. (1976). Concentrations of bacteria in cerebrospinal fluid of patients with bacterial meningitis. *J. Pediatr.*, *88*(4), 549–552. https://doi.org/10.1016/S0022-3476(76)80003-0

Feller, W. (1951, January). Diffusion Processes in Genetics. In *Proceedings of the Second Berkeley Symposium on Mathematical Statistics and Probability* (pp. 227–247, Vol. 2). University of California Press. https://doi.org/10.1525/9780520411586-018

Feller, W. (1939). Die Grundlagen der Volterraschen Theorie des Kampfes ums Dasein in wahrscheinlichkeitstheoretischer Behandlung. *Acta Biotheor.*, *5*(1), 11–40. https://doi.org/10.1007/BF01602932

Fisher, R. A. (1930). *The genetical theory of natural selection*. Clarendon Press.

Frank, S. A., & Slatkin, M. (1990). Evolution in a Variable Environment. *Am. Nat.*, *136*(2), 244–260. https://doi.org/10.1086/285094

Fruet, C., Müller, E. L., Loverdo, C., & Bitbol, A.-F. (2024, September). *Spatial structure facilitates evolutionary rescue by cost-free drug resistance* [arXiv preprint]. https://doi.org/10.48550/arXiv.2409.07377

Fuhrer, T., Fischer, E., & Sauer, U. (2005). Experimental Identification and Quantification of Glucose Metabolism in Seven Bacterial Species. *J. Bacteriol.*, *187*(5), 1581–1590. https://doi.org/10.1128/jb.187.5.1581-1590.2005

Fux, C. A., Costerton, J. W., Stewart, P. S., & Stoodley, P. (2005). Survival strategies of infectious biofilms. *Trends Microbiol.*, *13*(1), 34–40. https://doi.org/10.1016/j.tim.2004.11.010

Gaál, B., Pitchford, J. W., & Wood, A. J. (2010). Exact results for the evolution of stochastic switching in variable asymmetric environments. *Genetics*, *184*(4), 1113–1119. https://doi.org/10.1534/genetics.109.113431

Ganchua, S. K. C., White, A. G., Klein, E. C., & Flynn, J. L. (2020). Lymph nodes – The neglected battlefield in tuberculosis. *PLOS Pathog.*, *16*(8), e1008632. https://doi.org/10.1371/journal.ppat.1008632

Gardiner, C. W. (2009). *Stochastic methods*. Springer, USA.

Garud, N. R., Good, B. H., Hallatschek, O., & Pollard, K. S. (2019). Evolutionary dynamics of bacteria in the gut microbiome within and across hosts. *PLOS Biol.*, *17*(1), e3000102. https://doi.org/10.1371/journal.pbio.3000102

Ghoul, M., & Mitri, S. (2016). The Ecology and Evolution of Microbial Competition. *Trends Microbiol.*, *24*(10), 833–845. https://doi.org/10.1016/j.tim.2016.06.011

Gibson, M. A., & Bruck, J. (2000). Efficient Exact Stochastic Simulation of Chemical Systems with Many Species and Many Channels. *J. Phys. Chem. A*, *104*(9), 1876–1889. https://doi.org/10.1021/jp993732q

Gillespie, D. T. (1976). A general method for numerically simulating the stochastic time evolution of coupled chemical reactions. *J. Comput. Phys.*, *22*(4), 403–434. https://doi.org/10.1016/0021-9991(76)90041-3

Gillespie, D. T. (1977). Exact stochastic simulation of coupled chemical reactions. *J. Phys. Chem.*, *81*(25), 2340–2361. https://doi.org/10.1021/j100540a008

Goldenfeld, N. (1992). *Lectures on phase transitions and the renormalization group*. CRC Press.

Good, B. H., McDonald, M. J., Barrick, J. E., Lenski, R. E., & Desai, M. M. (2017). The dynamics of molecular evolution over 60,000 generations. *Nature*, *551*(7678), 45–50. https://doi.org/10.1038/nature24287

Gothwal, R., & Shashidhar, T. (2015). Antibiotic pollution in the environment: A review. *Clean–Soil Air Water*, *43*(4), 479–489. https://doi.org/10.1002/clen.201300989

Grilli, J. (2020). Macroecological laws describe variation and diversity in microbial communities. *Nat. Commun.*, *11*, 4743. https://doi.org/10.1038/s41467-020-18529-y

Habets, M. G. J. L., Rozen, D. E., Hoekstra, R. F., & de Visser, J. A. G. M. (2006). The effect of population structure on the adaptive radiation of microbial populations evolving in spatially structured environments. *Ecol. Lett.*, *9*(9), 1041–1048. https://doi.org/10.1111/j.1461-0248.2006.00955.x

Haldane, J. B. S. (1927). A mathematical theory of natural and artificial selection, part V: Selection and mutation. *Math. Proc. Camb. Philos. Soc.*, *23*(7), 838–844. https://doi.org/10.1017/S0305004100015644

Hanski, I. (1999). *Metapopulation ecology*. Oxford University Press, New York, USA.

Hauert, C., Chen, Y.-T., & Imhof, L. A. (2014). Fixation Times in Deme Structured, Finite Populations with Rare Migration. *J. Stat. Phys.*, *156*(4), 739–759. https://doi.org/10.1007/s10955-014-1022-y

He, Q., Mobilia, M., & Täuber, U. C. (2011). Coexistence in the two-dimensional May-Leonard model with random rates. *Eur. Phys. J. B*, *82*, 97. https://doi.org/10.1140/epjb/e2011-20259-x

Hengge-Aronis, R. (1993). Survival of hunger and stress: The role of rpoS in early stationary phase gene regulation in E. Coli. *Cell*, *72*(2), 165–168. https://doi.org/10.1016/0092-8674(93)90655-A

Hernández-Navarro, L., Asker, M., & Mobilia, M. (2024). Eco-evolutionary dynamics of cooperative antimicrobial resistance in a population of fluctuating volume and size. *J. Phys. Math. Theor.*, *57*(26), 265003. https://doi.org/10.1088/1751-8121/ad4ad6

Hernández-Navarro, L., Asker, M., Rucklidge, A. M., & Mobilia, M. (2023). Coupled environmental and demographic fluctuations shape the evolution of cooperative antimicrobial resistance. *J. R. Soc. Interface*, *20*(208), 20230393. https://doi.org/10.1098/rsif.2023.0393

Hernández-Navarro, L., Distefano, K., Täuber, U. C., & Mobilia, M. (2024, December). *Slow spatial migration can help eradicate cooperative antimicrobial resistance in time-varying environments* [arXiv Preprint]. https://doi.org/10.1101/2024.12.30.630406

Hidalgo, J., Suweis, S., & Maritan, A. (2017). Species coexistence in a neutral dynamics with environmental noise. *J. Theor. Biol.*, *413*, 1–10. https://doi.org/10.1016/j.jtbi.2016.11.002

Himeoka, Y., & Mitarai, N. (2020). Dynamics of bacterial populations under the feast-famine cycles. *Phys. Rev. Res.*, *2*(1), 013372. https://doi.org/10.1103/PhysRevResearch.2.013372

Hofbauer, J., & Sigmund, K. (1998). *Evolutionary games and population dynamics*. Cambridge University Press.

Hoffmann, A. A., & Sgrò, C. M. (2011). Climate change and evolutionary adaptation. *Nature*, *470*(7335), 479–485. https://doi.org/10.1038/nature09670

Hooper, D. U., Chapin III, F. S., Ewel, J. J., Hector, A., Inchausti, P., Lavorel, S., Lawton, J. H., Lodge, D. M., Loreau, M., Naeem, S., Schmid, B., Setälä, H., Symstad, A. J., Vandermeer, J., & Wardle, D. A. (2005). Effects of Biodiversity on Ecosystem Functioning: A Consensus of Current Knowledge. *Ecol. Monogr.*, *75*(1), 3–35. https://doi.org/10.1890/04-0922

Horsthemke, W., & Lefever, R. (1984). *Noise-induced transitions*. Springer, Berlin.

Houchmandzadeh, B. (2015). Fluctuation driven fixation of cooperative behavior. *Biosystems*, *127*, 60–66. https://doi.org/10.1016/j.biosystems.2014.11.006

Houchmandzadeh, B., & Vallade, M. (2012). Selection for altruism through random drift in variable size populations. *BMC Evol. Biol.*, *12*(1), 61. https://doi.org/10.1186/1471-2148-12-61

Hsu, R. H., Clark, R. L., Tan, J. W., Ahn, J. C., Gupta, S., Romero, P. A., & Venturelli, O. S. (2019). Microbial Interaction Network Inference in Microfluidic Droplets. *Cell Syst.*, *9*(3), 229–242.e4. https://doi.org/10.1016/j.cels.2019.06.008

Hu, J., Amor, D. R., Barbier, M., Bunin, G., & Gore, J. (2022). Emergent phases of ecological diversity and dynamics mapped in microcosms. *Science*, *378*, 85. https://doi.org/10.1126/science.abm7841

Hufton, P. G., Lin, Y. T., Galla, T., & McKane, A. J. (2016). Intrinsic noise in systems with switching environments. *Phys. Rev. E*, *93*(5), 052119. https://doi.org/10.1103/PhysRevE.93.052119

Hughes, D., & Andersson, D. I. (2012). Selection of resistance at lethal and non-lethal antibiotic concentrations. *Curr. Opin. Microbiol.*, *15*(5), 555–560. https://doi.org/10.1016/j.mib.2012.07.005

Izutsu, M., Lake, D. M., Matson, Z. W. D., Dodson, J. P., & Lenski, R. E. (2024). Effects of periodic bottlenecks on the dynamics of adaptive evolution in microbial populations. *Microbiology*, *170*(9), 001494. https://doi.org/10.1099/mic.0.001494

Jakiela, S., Kaminski, T. S., Cybulski, O., Weibel, D. B., & Garstecki, P. (2013). Bacterial growth and adaptation in microdroplet chemostats. *Angew. Chem. Int. Ed.*, *52*(34), 8908–8911. https://doi.org/10.1002/anie.201301524

James, T. W. (1961). Continuous Culture of Microorganisms. *Annu. Rev. Microbiol.*, *15*, 27–46. https://doi.org/10.1146/annurev.mi.15.100161.000331

Johnston, R. F., & Selander, R. K. (1964). House Sparrows: Rapid Evolution of Races in North America. *Science*, *144*(3618), 548–550. https://doi.org/10.1126/science.144.3618.548

Joshi, J., & Guttal, V. (2018). Demographic noise and cost of greenbeard can facilitate greenbeard cooperation. *Evolution*, *72*(12), 2595–2607. https://doi.org/10.1111/evo.13615

Kalyuzhny, M., Kadmon, R., & Shnerb, N. M. (2015). A neutral theory with environmental stochasticity explains static and dynamic properties of ecological communities. *Ecol. Lett.*, *18*(6), 572–580. https://doi.org/10.1111/ele.12439

Kettlewell, B. (1973, August). *The evolution of melanism*. Oxford University Press.

Keymer, J. E., Galajda, P., Muldoon, C., Park, S., & Austin, R. H. (2006). Bacterial metapopulations in nanofabricated landscapes. *Proc. Natl. Acad. Sci. U.S.A.*, *103*(46), 17290–17295. https://doi.org/10.1073/pnas.0607971103

Kimura, M., & Weiss, G. H. (1964). The Stepping Stone Model of Population Structure and the Decrease of Genetic Correlation with Distance. *Genetics*, *49*(4), 561–576. https://doi.org/10.1093/genetics/49.4.561

Krapivsky, P. L., Redner, S., & Ben-Naim, E. (2010). *A kinetic view of statistical physics*. Cambridge University Press, Cambridge, USA.

Kreger, J., Brown, D., Komarova, N. L., Wodarz, D., & Pritchard, J. (2023). The role of migration in mutant dynamics in fragmented populations. *J. Evol. Biol.*, *36*, 444. https://doi.org/10.1111/jeb.14131

Kryazhimskiy, S., Rice, D. P., & Desai, M. M. (2012). Population subdivision and adaptation in asexual populations of Saccharomyces cerevisiae. *Evolution*, *66*, 1931. https://doi.org/10.1111/j.1558-5646.2011.01569.x

Kussell, E., & Leibler, S. (2005). Phenotypic Diversity, Population Growth, and Information in Fluctuating Environments. *Science*, *309*(5743), 2075–2078. https://doi.org/10.1126/science.1114383

Labavić, D., Loverdo, C., & Bitbol, A.-F. (2022). Hydrodynamic flow and concentration gradients in the gut enhance neutral bacterial diversity. *Proc. Natl. Acad. Sci. U.S.A.*, *119*(1), e2108671119. https://doi.org/10.1073/pnas.2108671119

Lambert, A. (2006). Probability of fixation under weak selection: A branching process unifying approach. *Theor. Popul. Biol.*, *69*(4), 419–441. https://doi.org/10.1016/j.tpb.2006.01.002

Lambert, G., & Kussell, E. (2014). Memory and fintess optimization of bacteria under fluctuating environments. *PLOS Genet.*, *10*(9), e1004556. https://doi.org/10.1371/journal.pgen.1004556

Lande, R., Engen, S., Sæther, B.-E., & Saether, B.-E. (1998). Extinction Times in Finite Metapopulation Models with Stochastic Local Dynamics. *Oikos*, *83*(2), 383. https://doi.org/10.2307/3546853

Leibold, M. A., Urban, M. C., De Meester, L., Klausmeier, C. A., & Vanoverbeke, J. (2019). Regional neutrality evolves through local adaptive niche evolution. *Proc. Natl. Acad. Sci. U.S.A.*, *116*, 2612. https://doi.org/10.1073/pnas.1808615116

Lenski, R. E., Rose, M. R., Simpson, S. C., & Tadler, S. C. (1991). Long-Term Experimental Evolution in Escherichia coli. I. Adaptation and Divergence During 2,000 Generations. *Am. Nat.*, *138*(6), 1315–1341. https://doi.org/10.1086/285289

Levin-Reisman, I., Ronin, I., Gefen, O., Braniss, I., Shoresh, N., & Balaban, N. Q. (2017). Antibiotic tolerance facilitates the evolution of resistance. *Science*, *355*(6327), 826–830. https://doi.org/10.1126/science.aaj2191

Levins, R. (1969). Some demographic and genetic consequences of environmental heterogeneity for biological control. *Bull. Entomol. Soc. Am.*, *15*, 237. https://doi.org/10.1093/besa/15.3.237

Levins, R. (1966). The strategy of model building in population biology. *Am. Sci.*, *54*(4), 421–431.

Levins, R. (1968). *Evolution in changing environments: Some theoretical explorations*. Princeton University Press.

Lewis, K., & Shan, Y. (2017). Why tolerance invites resistance. *Science*, *355*(6327), 796–796. https://doi.org/10.1126/science.aam7926

Lewontin, R. C. (1955). The effects of population density and composition on viability in drosophila melanogaster. *Evolution*, *9*(1), 27–41. https://doi.org/10.1111/j.1558-5646.1955.tb01511.x

Lewontin, R. C. (Ed.). (1968). *Population Biology and Evolution: Proceedings of the International Symposium Sponsored by Syracuse University and the New York State Science and Technology Foundation, June 7-9, 1967, Syracuse, New York*. Syracuse University Press.

Lieberman, E., Hauert, C., & Nowak, M. A. (2005). Evolutionary dynamics on graphs. *Nature*, *433*(7023), 312–316. https://doi.org/10.1038/nature03204

Lin, W.-H., & Kussell, E. (2016). Complex interplay of physiology and selection in the emergence of antibiotic resistance. *Curr. Biol.*, *26*, 1486. https://doi.org/10.1016/j.cub.2016.04.015

Lin, Y. T., Kim, H., & Doering, C. R. (2012). Features of Fast Living: On the Weak Selection for Longevity in Degenerate Birth-Death Processes. *J. Stat. Phys.*, *148*(4), 647–663. https://doi.org/10.1007/s10955-012-0479-9

Lindsey, H. A., Gallie, J., Taylor, S., & Kerr, B. (2013). Evolutionary rescue from extinction is contingent on a lower rate of environmental change. *Nature*, *494*, 463. https://doi.org/10.1038/nature11879

Lopatkin, A. J., Meredith, H. R., Srimani, J. K., Pfeiffer, C., Durrett, R., & You, L. (2017). Persistence and reversal of plasmid-mediated antibiotic resistance. *Nat. Commun.*, *8*, 1689. https://doi.org/10.1038/s41467-017-01532-1

Lorenzen, K., & Enberg, K. (2002). Density-dependent growth as a key mechanism in the regulation of fish populations: Evidence from among-Population comparisons. *Proc. R. Soc. Lond. B Biol. Sci.*, *269*(1486), 49–54. https://doi.org/10.1098/rspb.2001.1853

Lotka, A. J. (1925). *Elements of physical biology*. Williams & Wilkins.

Luria, S. E., & Delbrück, M. (1943). Mutations of bacteria from virus sensitivity to virus resistance. *Genetics*, *28*(6), 491–511. https://doi.org/10.1093/genetics/28.6.491

MacArthur, R. H., & Wilson, E. O. (1967). *The theory of island biogeography* (Vol. 1). Princeton University Press.

Mahrt, N., Tietze, A., Künzel, S., Franzenburg, S., Barbosa, C., Jansen, G., & Schulenburg, H. (2021). Bottleneck size and selection level reproducibly impact evolution of antibiotic resistance. *Nat. Ecol. Evol.*, *5*(9), 1233–1242. https://doi.org/10.1038/s41559-021-01511-2

Marrec, L. (2023, November). *Quantifying the impact of genotype-dependent gene flow on mutation fixation in subdivided populations* [bioRxiv Preprint]. https://doi.org/10.1101/2023.11.29.569213

Marrec, L., & Bitbol, A.-F. (2020). Resist or perish: Fate of a microbial population subjected to a periodic presence of antimicrobial. *PLOS Comput. Biol.*, *16*(4), 1–19. https://doi.org/10.1371/journal.pcbi.1007798

Marrec, L., Lamberti, I., & Bitbol, A.-F. (2021). Toward a Universal Model for Spatially Structured Populations. *Phys. Rev. Lett.*, *127*(21), 218102. https://doi.org/10.1103/PhysRevLett.127.218102

Maruyama, T. (1970). On the fixation probability of mutant genes in a subdivided population. *Genet. Res.*, *15*(2), 221–225. https://doi.org/10.1017/S0016672300001543

Mateu, J. C., Sireci, M., & Muñoz, M. A. (2021). Phenotypic-dependent variability and the emergence of tolerance in bacterial populations. *PLOS Comp. Biol.*, *17*(9), e1009417. https://doi.org/10.1371/journal.pcbi.1009417

Melbinger, A., Cremer, J., & Frey, E. (2010). Evolutionary game theory in growing populations. *Phys. Rev. Lett.*, *105*(17), 178101. https://doi.org/10.1103/physrevlett.105.178101

Melbinger, A., Cremer, J., & Frey, E. (2015). The emergence of cooperation from a single mutant during microbial life cycles. *J. R. Soc. Interface*, *12*(108), 20150171. https://doi.org/10.1098/rsif.2015.0171

Melnyk, A. H., Wong, A., & Kassen, R. (2015). The fitness costs of antibiotic resistance mutations. *Evol. Appl.*, *8*(3), 273–283. https://doi.org/10.1111/eva.12196

Meredith, H. R., Srimani, J. K., Lee, A. J., Lopatkin, A. J., & You, L. (2015). Collective antibiotic tolerance: Mechanisms, dynamics and intervention. *Nat. Chem. Biol.*, *11*(3), 182–188. https://doi.org/10.1038/nchembio.1754

Merritt, J., & Kuehn, S. (2018). Frequency- and amplitude-dependent microbial population dynamics during cycles of feast and famine. *Phys. Rev. Lett.*, *121*, 098101. https://doi.org/10.1103/PhysRevLett.121.098101

Metropolis, N., & Ulam, S. (1949). The Monte Carlo Method. *J. Am. Stat. Assoc.*, *44*(247), 335–341. https://doi.org/10.1080/01621459.1949.10483310

Meyer, I., & Shnerb, N. M. (2020). Evolutionary dynamics in fluctuating environment. *Phys. Rev. Res.*, *2*(2), 023308. https://doi.org/10.1103/PhysRevResearch.2.023308

Meyer, I., Steinmetz, B., & Shnerb, N. M. (2021). *Species coexistence and temporal environmental fluctuations: A quantitative comparison between stochastic and seasonal variations* [bioRxiv preprint]. https://doi.org/10.1101/2021.04.20.440706

Meyer, I., Taitelbaum, A., Assaf, M., & Shnerb, N. M. (2023). *Emergence of a novel phase in population and community dynamics due to fat-tailed environmental correlations* [arXiv preprint]. https://doi.org/10.48550/arXiv.2311.08825

Moawad, A., Abbara, A., & Bitbol, A.-F. (2024). Evolution of cooperation in deme-structured populations on graphs. *Phys. Rev. E*, *109*(2), 024307. https://doi.org/10.1103/PhysRevE.109.024307

Mobilia, M. (2023). Polarization and consensus in a voter model under time-fluctuating influences. *Physics*, *5*, 517. https://doi.org/10.3390/physics5020037

Mobilia, M., & Assaf, M. (2010). Fixation in evolutionary games under non-vanishing selection. *EPL*, *91*, 10002. https://doi.org/10.1209/0295-5075/91/10002

Mollison, D. (1977). Spatial Contact Models for Ecological and Epidemic Spread. *J. R. Stat. Soc. Ser. B Methodol.*, *39*(3), 283–326. https://doi.org/10.1111/j.2517-6161.1977.tb01627.x

Mollison, D. (1991). Dependence of epidemic and population velocities on basic parameters. *Math. Biosci.*, *107*(2), 255–287. https://doi.org/10.1016/0025-5564(91)90009-8

Moran, P. A. P. (1958). Random processes in genetics. *Math. Proc. Camb. Philos. Soc.*, *54*(1), 60–71. https://doi.org/10.1017/s0305004100033193

Moran, P. A. P. (1962). *The Statistical Processes of Evolutionary Theory*. Oxford, UK: Clarendon.

Murray, C. J. L., Ikuta, K. S., Sharara, F., Swetschinski, L., Robles Aguilar, G., Gray, A., Han, C., Bisignano, C., Rao, P., Wool, E., Johnson, S. C., Browne, A. J., Chipeta, M. G., Fell, F., Hackett, S., Haines-Woodhouse, G., Kashef Hamadani,

B. H., Kumaran, E. A. P., McManigal, B., ... Naghavi, M. (2022). Global burden of bacterial antimicrobial resistance in 2019: A systematic analysis. *The Lancet*, *399*(10325), 629–655. https://doi.org/10.1016/S0140-6736(21)02724-0

Murugan, A., Husain, K., Rust, M. J., Hepler, C., Bass, J., Pietsch, J. M. J., Swain, P. S., Jena, S. G., Toettcher, J. E., Chakraborty, A. K., Sprenger, K. G., Mora, T., Walczak, A. M., Rivoire, O., Wang, S., Wood, K. B., Skanata, A., Kussell, E., Ranganathan, R., ... Goldenfeld, N. (2021). Roadmap on biology in time varying environments. *Phys. Biol.*, *18*, 041502. https://doi.org/10.1088/1478-3975/abde8d

Nahum, J. R., Godfrey-Smith, P., Harding, B. N., Marcus, J. H., Carlson-Stevermer, J., & Kerr, B. (2015). A tortoise-hare pattern seen in adapting structured and unstructured populations suggests a rugged fitness landscape in bacteria. *Proc. Natl. Acad. Sci. U.S.A.*, *112*, 7530. https://doi.org/10.1073/pnas.1410631112

Nannipieri, P., Ascher, J., Ceccherini, M. T., Landi, L., Pietramellara, G., & Renella, G. (2017). Microbial diversity and soil functions. *Eur. J. Soil Sci.*, *68*(1), 12–26. https://doi.org/10.1111/ejss.4_12398

Nemeth, J., Oesch, G., & Kuster, S. P. (2015). Bacteriostatic versus bactericidal antibiotics for patients with serious bacterial infections: Systematic review and meta-analysis. *J. Antimicrob. Chemother.*, *70*(2), 382–395. https://doi.org/10.1093/jac/dku379

Nguyen, T., Lara-Gutiérrez, J., & Stocker, R. (2021). Environmental fluctuations and their effects on microbial communities, populations and individuals. *FEMS Microbiol. Rev.*, *45*, fuaa068. https://doi.org/10.1093/femsre/fuaa068

Nishimori, H., & Ortiz, G. (2010, December). *Elements of phase transitions and critical phenomena*. Oxford University Press.

Novick, A., & Szilard, L. (1950). Description of the Chemostat. *Science*, *112*(2920), 715–716. https://doi.org/10.1126/science.112.2920.715

O'Malley, R. E. (2014). Asymptotic Approximations. In *Historical Developments in Singular Perturbations* (pp. 27–51). Springer International Publishing. https://doi.org/10.1007/978-3-319-11924-3_2

O'Neill, J. (2016). *Tackling drug-resistant infections globally: Final report and recommendations* (Report). Government of the United Kingdom.

Pai, A., Tanouchi, Y., & You, L. (2012). Optimality and robustness in quorum sensing (QS)-mediated regulation of a costly public good enzyme. *Proc. Natl. Acad. Sci. U.S.A.*, *109*(48), 19810–19815. https://doi.org/10.1073/pnas.1211072109

Palaci, M., Dietze, R., Hadad, D. J., Ribeiro, F. K. C., Peres, R. L., Vinhas, S. A., Maciel, E. L. N., Valle Dettoni, V., Horter, L., Boom, W. H., et al. (2007). Cavitary disease and quantitative sputum bacillary load in cases of pulmonary tuberculosis. *J. Clin. Microbiol.*, *45*(12), 4064–4066. https://doi.org/10.1128/jcm.01780-07

Pankey, G. A., & Sabath, L. D. (2004). Clinical Relevance of Bacteriostatic versus Bactericidal Mechanisms of Action in the Treatment of Gram-Positive Bacterial Infections. *Clin. Infect. Dis.*, *38*(6), 864–870. https://doi.org/10.1086/381972

Parsons, T. L., & Quince, C. (2007a). Fixation in haploid populations exhibiting density dependence I: The non-neutral case. *Theor. Popul. Biol.*, *72*(1), 121–135. https://doi.org/10.1016/j.tpb.2006.11.004

Parsons, T. L., & Quince, C. (2007b). Fixation in haploid populations exhibiting density dependence II: The quasi-neutral case. *Theor. Popul. Biol.*, *72*(4), 468–479. https://doi.org/10.1016/j.tpb.2007.04.002

Parsons, T. L., Quince, C., & Plotkin, J. B. (2010). Some consequences of demographic stochasticity in population genetics. *Genetics*, *185*(4), 1345–1354. https://doi.org/10.1534/genetics.110.115030

Patwa, Z., & Wahl, L. M. (2008). The fixation probability of beneficial mutations. *J. R. Soc. Interface*, *5*(28), 1279–1289. https://doi.org/10.1098/rsif.2008.0248

Patwa, Z., & Wahl, L. M. (2010). Adaptation Rates of Lytic Viruses Depend Critically on Whether Host Cells Survive the Bottleneck. *Evolution*, *64*(4), 1166–1172. https://doi.org/10.1111/j.1558-5646.2009.00887.x

Pelletier, F., Garant, D., & Hendry, A. P. (2009). Eco-evolutionary dynamics. *Philos. Trans. R. Soc. B Biol. Sci.*, *364*(1523), 1483–1489. https://doi.org/10.1098/rstb.2009.0027

Pimentel, D. (1968). Population Regulation and Genetic Feedback. *Science*, *159*(3822), 1432–1437. https://doi.org/10.1126/science.159.3822.1432

Pinsky, M. L. (2019). Species coexistence through competition and rapid evolution. *Proc. Natl. Acad. Sci. U.S.A.*, *116*, 2407. https://doi.org/10.1073/pnas.1822091116

Pinsky, M. A., & Karlin, S. (2011). *An introduction to stochastic modeling*. Elsevier.

Poole, K. (2007). Efflux pumps as antimicrobial resistance mechanisms. *Ann. Med.*, *39*(3), 162–176. https://doi.org/10.1080/07853890701195262

Raatz, M., & Traulsen, A. (2023). Promoting extinction or minimizing growth? The impact of treatment on trait trajectories in evolving populations. *Evolution*, *77*(6), 1408–1421. https://doi.org/10.1093/evolut/qpad042

Raymond, F., Ouameur, A. A., Déraspe, M., Iqbal, N., Gingras, H., Dridi, B., Leprohon, P., Plante, P.-L., Giroux, R., Bérubé, È., Frenette, J., Boudreau, D. K., Simard, J.-L., Chabot, I., Domingo, M.-C., Trottier, S., Boissinot, M., Huletsky, A., Roy, P. H., … Corbeil, J. (2016). The initial state of the human gut microbiome determines its reshaping by antibiotics. *ISME J.*, *10*, 707. https://doi.org/10.1038/ismej.2015.148

Reichenbach, T., Mobilia, M., & Frey, E. (2007). Mobility promotes and jeopardizes biodiversity in rock–paper–scissors games. *Nature*, *448*, 1046. https://doi.org/10.1038/nature06095

Rescan, M., Grulois, D., Ortega-Aboud, E., & Chevin, L.-M. (2020). Phenotypic memory drives population growth and extinction risk in a noisy environment. *Nat. Ecol. Evol.*, *4*(2), 193–201. https://doi.org/10.1038/s41559-019-1089-6

Ridolfi, L., D'Odorico, P., & Laio, F. (2011). *Noise-induced phenomena in the environmental sciences*. Cambridge Univeristy Press.

Riley, K. F., Hobson, M. P., & Bence, S. J. (2006). *Mathematical methods for physics and engineering: A comprehensive guide*. Cambridge University Press.

Rodríguez-Verdugo, A., Vulin, C., & Ackermann, M. (2019). The rate of environmental fluctuations shapes ecological dynamics in a two-species microbial system. *Ecol. Lett.*, *22*(5), 838–846. https://doi.org/10.1111/ele.13241

Rogers, T., & McKane, A. J. (2015). Modes of competition and the fitness of evolved populations. *Phys. Rev. E*, *92*(3), 032708. https://doi.org/10.1103/PhysRevE.92.032708

San Millan, A., & Maclean, R. C. (2017). Fitness costs of plasmids: A limit to plasmid transmission. *Microbiol. Spectr.*, *5*(5), 5–5. https://doi.org/10.1128/microbiolspec.MTBP-0016-2017

Sanchez, A., & Gore, J. (2013). Feedback between population and evolutionary dynamics determines the fate of social microbial populations. *PLOS Biol.*, *11*(4), e1001547. https://doi.org/10.1371/journal.pbio.1001547

Shade, A., Peter, H., Allison, S., Baho, D., Berga, M., Buergmann, H., Huber, D., Langenheder, S., Lennon, J., Martiny, J., Matulich, K., Schmidt, T., & H, J. (2012). Fundamentals of microbial community resistance and resilience. *Front. Microbiol.*, *3*(417), 1–15. https://doi.org/10.3389/fmicb.2012.00417

Shahid, M., Sobia, F., Singh, A., Malik, A., Khan, H. M., Jonas, D., & Hawkey, P. M. (2009). Beta-lactams and beta-lactamase-inhibitors in current-or potential-clinical practice: A comprehensive update. *Crit. Rev. Microbiol.*, *35*(2), 81–108. https://doi.org/0.1080/10408410902733979

She, J.-J., Liu, W.-X., Ding, X.-M., Guo, G., Han, J., Shi, F.-Y., Lau, H. C.-H., Ding, C.-G., Xue, W.-J., Shi, W., Liu, G.-X., Zhang, Z., Hu, C.-H., Chen, Y., Wong, C. C., & Yu, J. (2024). Defining the biogeographical map and potential bacterial translocation of microbiome in human surface organs. *Nat. Commun.*, *15*, 427. https://doi.org/10.1038/s41467-024-44720-6

Shibasaki, S., Mobilia, M., & Mitri, S. (2021). Exclusion of the fittest predicts microbial community diversity in fluctuating environments. *J. R. Soc. Interface*, *18*(183), 20210613. https://doi.org/10.1098/rsif.2021.0613

Slatkin, M. (1981). Fixation Probabilities and Fixation Times in a Subdivided Population. *Evolution*, *35*(3), 477–488. https://doi.org/10.2307/2408196

Smith, J. M., & Price, G. R. (1973). The Logic of Animal Conflict. *Nature*, *246*(5427), 15–18. https://doi.org/10.1038/246015a0

Smith, J. M. (1982). *Evolution and the theory of games*. Cambridge University Press.

Smith, M. R., & Wood Jr, W. B. (1956). An experimental analysis of the curative action of penicillin in acute bacterial infections: III. The effect of suppuration upon the antibacterial action of the drug. *J. Exp. Med.*, *103*(4), 509–522. https://doi.org/10.1084/jem.103.4.509

Smits, S. A., Leach, J., Sonnenburg, E. D., Gonzalez, C. G., Lichtman, J. S., Reid, G., Knight, R., Manjurano, A., Changalucha, J., Elias, J. E., Dominguez-Bello, M. G., & Sonnenburg, J. L. (2017). Seasonal cycling in the gut microbiome of the Hadza hunter-gatherers of Tanzania. *Science*, *357*, 802–805. https://doi.org/10.1126/science.aan4834

Soto, S. M. (2013). Role of efflux pumps in the antibiotic resistance of bacteria embedded in a biofilm. *Virulence*, *4*(3), 223–229. https://doi.org/10.4161/viru.23724

Srinivasan, S., & Kjelleberg, S. (1998). Cycles of famine and feast: The starvation and outgrowth strategies of a marine Vibrio. *J. Biosci.*, *23*, 501–511. https://doi.org/10.1007/BF02936144

Stegen, J. C., Lin, X., Konopka, A. E., & Fredrickson, J. K. (2012). Stochastic and deterministic assembly processes in subsurface microbial communities. *ISME J.*, *6*, 1653–1664. https://doi.org/10.1038/ismej.2012.22

Sun, G.-Q. (2016). Mathematical modeling of population dynamics with Allee effect. *Nonlinear Dyn.*, *85*(1), 1–12. https://doi.org/10.1007/s11071-016-2671-y

Szczesny, B., Mobilia, M., & Rucklidge, A. M. (2014). Characterization of spiraling patterns in spatial rock-paper-scissors games. *Phys. Rev. E*, *90*, 032704. https://doi.org/10.1103/PhysRevE.90.032704

Taitelbaum, A., West, R., Assaf, M., & Mobilia, M. (2020). Population Dynamics in a Changing Environment: Random versus Periodic Switching. *Phys. Rev. Lett.*, *125*(4), 048105. https://doi.org/10.1103/PhysRevLett.125.048105

Taitelbaum, A., West, R., Mobilia, M., & Assaf, M. (2023). Evolutionary dynamics in a varying environment: Continuous versus discrete noise. *Phys. Rev. Res.*, *5*(2), L022004. https://doi.org/10.1103/PhysRevResearch.5.L022004

Täuber, U. C. (2014). *Critical dynamics*. Cambridge University Press, Cambridge, USA.

Tenaillon, O., Barrick, J. E., Ribeck, N., Deatherage, D. E., Blanchard, J. L., Dasgupta, A., Wu, G. C., Wielgoss, S., Cruveiller, S., Médigue, C., Schneider, D., & Lenski, R. E. (2016). Tempo and mode of genome evolution in a 50,000-generation experiment. *Nature*, *536*(7615), 165–170. https://doi.org/10.1038/nature18959

Thattai, M., & Van Oudenaarden, A. (2004). Stochastic gene expression in fluctuating environments. *Genetics*, *167*, 523. https://doi.org/10.1534/genetics.167.1.523

Totlani, K., Hurkmans, J.-W., Van Gulik, W. M., Kreutzer, M. T., & Van Steijn, V. (2020). Scalable microfluidic droplet on-demand generator for non-steady operation of droplet-based assays. *Lab. Chip*, *20*(8), 1398–1409. https://doi.org/10.1039/C9LC01103J

Traulsen, A., Claussen, J. C., & Hauert, C. (2005). Coevolutionary dynamics: From finite to infinite populations. *Phys. Rev. Lett.*, *95*(23), 238701. https://doi.org/10.1103/PhysRevLett.95.238701

Traulsen, A., & Haeurt, C. (2009). Stochastic evolutionary game dynamics. *Rev. Nonlinear Dyn. Complex.*, 25–61. https://doi.org/10.1002/9783527628001.ch2

Travisano, M., Mongold, J. A., Bennett, A. F., & Lenski, R. E. (1995). Experimental tests of the roles of adaptation, chance, and history in evolution. *Science*, *267*(5194), 87–90. https://doi.org/10.1126/science.7809610

Travisano, M., Vasi, F., & Lenski, R. E. (1995). Long-term experimental evolution in escherichia coli. III. Variation among replicate populations in correlated responses to novel environments. *Evolution*, *49*(1), 189–200. https://doi.org/10.1111/j.1558-5646.1995.tb05970.x

Tutt, J. W. (1896). *British moths*. G. Routledge.

Uecker, H., & Hermisson, J. (2011). On the fixation process of a beneficial mutation in a variable environment. *Genetics*, *188*(4), 915–930. https://doi.org/10.1534/genetics.110.124297

van Kampen, N. G. (1992). *Stochastic processes in physics and chemistry*. North-Holland, Amsterdam.

van Tatenhove-Pel, R. J., Rijavec, T., Lapanje, A., van Swam, I., Zwering, E., Hernandez-Valdes, J. A., Kuipers, O. P., Picioreanu, C., Teusink, B., & Bachmann, H. (2021). Microbial competition reduces metabolic interaction distances to the low μm-Range. *ISME J.*, *15*(3), 688–701. https://doi.org/10.1038/s41396-020-00806-9

Van den Bergh, B., Swings, T., Fauvart, M., & Michiels, J. (2018). Experimental Design, Population Dynamics, and Diversity in Microbial Experimental Evolution. *Microbiol. Mol. Biol. Rev.*, *82*(3), e00008–18. https://doi.org/10.1128/MMBR.00008-18

Van den Broeck, W., Derore, A., & Simoens, P. (2020). Anatomy and nomenclature of murine lymph nodes: Descriptive study and nomenclatory standardization in BALB/cAnNCrl mice. *J. Immunol. Methods*, *312*(1–2), 12–19. https://doi.org/10.1016/j.jim.2006.01.022

van der Horst, M. A., Schuurmans, J. M., Smid, M. C., Koenders, B. B., & ter Kuile, B. H. (2011). De novo acquisition of resistance to three antibiotics by Escherichia coli. *Microb. Drug Resist.*, *17*(2), 141–147. https://doi.org/10.1089/mdr.2010.0101

Vega, N. M., & Gore, J. (2014). Collective antibiotic resistance: Mechanisms and implications. *Curr. Opin. Microbiol.*, *21*, 28–34. https://doi.org/10.1016/j.mib.2014.09.003

Volterra, V. (1926). Fluctuations in the abundance of a species considered mathematically. *Nature*, *118*(2972), 558–560. https://doi.org/10.1038/118558a0

Wahl, L. M., Gerrish, P. J., & Saika-Voivod, I. (2002). Evaluating the Impact of Population Bottlenecks in Experimental Evolution. *Genetics*, *162*(2), 961–971. https://doi.org/10.1093/genetics/162.2.961

Wang, G., Su, Q., Wang, L., & Plotkin, J. B. (2023). Reproductive variance can drive behavioral dynamics. *Proc. Natl. Acad. Sci. U.S.A.*, *120*, e216218120. https://doi.org/10.1073/pnas.2216218120

West, J., Adler, F., Gallaher, J., Strobl, M., Brady-Nicholls, R., Brown, J., Roberson-Tessi, M., Kim, E., Noble, R., Viossat, Y., Basanta, D., & Anderson, A. R. A. (2023). A survey of open questions in adaptive therapy: Bridging mathematics and clinical translation. *eLife*, *12*, e84263. https://doi.org/10.7554/eLife.84263

West, R., & Shnerb, N. M. (2022). Quantitative characteristics of stabilizing and equalizing mechanisms. *Am. Nat.*, *88*, E160. https://doi.org/10.1086/720665

Whitlock, M. C. (2003). Fixation probability and time in subdivided populations. *Genetics*, *164*, 767. https://doi.org/10.1093/genetics/164.2.767

Widder, S., Allen, R. J., Pfeiffer, T., Curtis, T. P., Wiuf, C., Sloan, W. T., Cordero, O. X., Brown, S. P., Momeni, B., Shou, W., Kettle, H., Flint, H. J., Haas, A. F.,

Laroche, B., Kreft, J.-U., Rainey, P. B., Freilich, S., Schuster, S., Milferstedt, K., ... Soyer, O. S. (2016). Challenges in microbial ecology: Building predictive understanding of community function and dynamics. *ISME J.*, *10*, 2557–2568. https://doi.org/10.1038/ismej.2016.45

Wienand, K., Frey, E., & Mobilia, M. (2017). Evolution of a Fluctuating Population in a Randomly Switching Environment. *Phys. Rev. Lett.*, *119*(15), 158301. https://doi.org/10.1103/PhysRevLett.119.158301

Wienand, K., Frey, E., & Mobilia, M. (2018). Eco-evolutionary dynamics of a population with randomly switching carrying capacity. *J. R. Soc. Interface*, *15*(145), 20180343. https://doi.org/10.1098/rsif.2018.0343

Wild, G., & Traulsen, A. (2007). The different limits of weak selection and the evolutionary dynamics of finite populations. *J. Theor. Biol.*, *247*(2), 382–390. https://doi.org/10.1016/j.jtbi.2007.03.015

Wright, G. D. (2005). Bacterial resistance to antibiotics: Enzymatic degradation and modification. *Adv. Drug Deliv. Rev.*, *57*(10), 1451–1470. https://doi.org/10.1016/j.addr.2005.04.002

Wright, S. (1931). Evolution in Mendelian Populations. *Genetics*, *16*(2), 97. https://doi.org/10.1093/genetics/16.2.97

Wright, S. (1943). Isolation by distance. *Genetics*, *28*(2), 114–138. https://doi.org/10.1093/genetics/28.2.114

Wright, S. (1949). Population Structure in Evolution. *Proc. Am. Philos. Soc.*, *93*(6), 471–478.

Xue, B. K., & Leibler, S. (2017). Bet hedging against demographic fluctuations. *Phys. Rev. Lett.*, *119*, 108103. https://doi.org/10.1103/PhysRevLett.119.108103

Yagoobi, S., & Traulsen, A. (2021). Fixation probabilities in network structured metapopulations. *Sci. Rep.*, *11*(1), 17979. https://doi.org/10.1038/s41598-021-97187-6

Yoshida, T., Jones, L. E., Ellner, S. P., Fussmann, G. F., & Hairston, N. G. (2003). Rapid evolution drives ecological dynamics in a predator–prey system. *Nature*, *424*(6946), 303–306. https://doi.org/10.1038/nature01767

Yurtsev, E. A., Chao, H. X., Datta, M. S., Artemova, T., & Gore, J. (2013). Bacterial cheating drives the population dynamics of cooperative antibiotic resistance plasmids. *Mol. Syst. Biol.*, *9*, 683. https://doi.org/10.1038/msb.2013.39